UAB
Universitat Autònoma de Barcelona

Department of Cellular Biology, Physiology and Immunology
Universitat Autònoma de Barcelona

Protein Subunit Vaccine Development for COVID-19 and Syphilis

Carlos Ávila Nieto

Doctoral Thesis in Advanced Immunology,
by Universitat Autònoma de Barcelona,

2023

Thesis Directors:

Jorge Carrillo Molina, PhD

Julià Blanco Arbués, PhD

Group of Immunology (IGG) and Cell Virology and Immunology
(VIC), at the AIDS Research Institute (IrsiCaixa)

UAB
Universitat Autònoma
de Barcelona

IrsiCaixa
Institut de Recerca de la Sida

Unió Europea
Fons social europeu
L'FSE inverteix en el teu futur
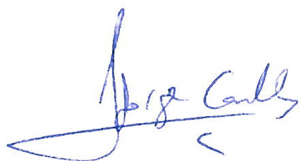
Generalitat de Catalunya
Departament d'Empresa i Coneixement
Secretaria d'Universitats i Recerca

El Dr. Jorge Carrillo Molina investigador del Institut de Receca de la SIDA (IRSICaixa) y el Dr. Julià Blanco Arbués, investigador del Institute d'Investigació en Ciències de la Salut Germans Trias I Pujol (IGTP) y professor de la Universitat de VIC-Universitat Centrar de Catalunya,

Hacen constar,

Que el trabajo experimental y la redacción de la Tesis doctoral titulada "Protein Subunit Vaccine Development for COVID-19 and Syphilis", ha sido realizada por Carlos Ávila Nieto bajo su dirección y consideran que es apto para ser presenteda y optar al título de Doctor en Inmunología Avanzada por la Universitat Autònoma de Barcelona.

Haciendo constancia de ello mediante la firma de este documento en Badalona a 18 de Septiembre de 2023.

Jorge Carrillo Molina   Julià Blanco Arbués

A mis padres, a mi familia

- Papá, Mamá, ¿qué es eso?
¿Y cómo funciona? ¿Y por qué?

La curiosidad

TABLE OF CONTENTS

ABBREVIATIONS

ICU	Intensive Care Unit
2019-nCoV	2019 Novel Coronavirus
SARS-CoV-2	Severe Acute Respiratory Syndrome Coronavirus 2
COVID-19	Coronavirus Disease 2019
WHO	World Health Organization
IFR	Infection Fatality Rate
CFR	Case Fatality Rate
Ro	Reproduction Number
CoVs	Coronaviruses
SARS-Cov	Severe Acute Respiratory Syndrome Coronavirus
MERS-CoV	Middle East Respiratory Syndrome Coronavirus
HCoVs	Human Coronaviruses
SARS	Severe Acute Respiratory Syndrome
MERS	Middle East Respiratory Syndrome
RBD	Receptor Binding Domain
+ssRNA	Positive-Sense Single-Stranded RNA
ORF	Open Reading Frame
S	Spike protein
M	Membrane protein
E	Envelope protein
N	Nucleocapsid protein
RNP	Ribonucleoprotein
RTC	Replication-Transcription Complex
VLP	Virus-Like Particle
aa	Amino Acids
FP	Fusion Peptide

HR	Heptapeptide Repeat
ACE2	Angiotensin-Converting Enzyme 2
TMPRSS2	Transmembrane Protease Serine 2
GISAID	Initiative on Sharing All Influenza Data
PANGOLIN	Phylogenetic Assignment of Named Global Outbreak Lineages
VOC	Variant of Concern
VOI	Variant of Interest
VUM	Variant Under Monitoring
ECDC	European Centre of Disease Prevention and Control
PAMP	Pathogen-Associated Molecular Patterns
DAMP	Damage-Associated Molecular Pattern
PRR	Patter Recognition Receptor
DC	Dendritic cell
NK	Natural Killer
ILC	Innate Lymphoid Cell
TLR	Toll-Like Receptor
RIG-I	Retinoic Acid Inducible gene I
RLR	RIG-I Like Receptors
NLR	Nucleotide-binding oligomerization domain-Like Receptor
CLR	C-type Lectin Receptors
dsRNA	double-strand RNA
MDA5	Melanoma Differentiation-Associated gene 5
LGP2	Laboratory of Genetics and Physiology 2
IFN	Interferon
SIRS	Systemic Inflammatory Response Syndrome
ARDS	Acute Respiratory Distress Syndrome
MHC	Major Histocompatibility Complex
APC	Antigen Presenting-Cell
LN	Lymph Node

Tfh	T follicular helper cell
Th1	T helper type 1
PBMC	Peripheral Blood Mononuclear Cell
BCR	B-Cell Receptor
GC	Germinal Center
ADCC	Antibody Dependent Cellular Cytotoxicity
ADCP	Antibody Dependent Cellular Phagocytosis
MVA	Moddified Vaccina Virus Ankara
IND	Investigational New Drug Application
FDA	US Food and Drug Administration
EMA	Europe Medicines Agency
BLA	Biologics License Application
EUA	Emergency Use Authorization
EUL	Emergency Use Listing
EU	European Union
HIV	Human Immunodeficiency Virus
OD	Optical Density
GSH	Golden Syrian Hamster
AU	Arbitrary Unit
CT	Cycle Threshold
FDR	False Discovery Rate
SEM	Standard Errors of the Means
gRNA	Genomic RNA
IHC	Immunohistochemistry
TPA	*Treponema pallidum* subespecie *pallidum*
MSM	Men who have Sex with Men
OMP	Outer Membrane Protein
OM	Outer Membrane
IM	Inner Membrane
LPS	Lipopolysaccharide

PMN	Polymorphonuclear cells
Tpr	Treponema Pallidum Repeat family protein
DTH	Delayed Type Hypersensitivity
MOSP	Major Outer Sheath Protein
MoRF	Molecular Recognition Feature
CRP	cAMP Receptor Protein
TROMP	Treponema Rare Outer Membrane Protein
LysM	Lysin Motif
MIDAS	Metal Ion-Dependent Adhesion Site
vWA	von Willebrand Factor Type A
POTRA	Polypeptide Transport-Associated
polyG	Guanosine homopolymer
IPTG	Isopropyl-β-D-1-thiogalactopyranoside
IMAC	Immubolized-Metal Affinity Chromatography
TEV	Tobacco Etch Virus
BSA	Bovine Serum Albumin
CAS	Casein
HSA	Human Serum Albumin

FOREWORD

Since Edward Jenner vaccine discovery, vaccines have demonstrated to be one of the most potent tools for infectious disease control and eradication. Vaccines have evolved concurrently with the technological progresses and several vaccines platforms have been created to face different pathogens. Specifically, in the current work we chose subunit protein platform for the development of vaccines against two pathogens, SARS-CoV-2 and *Treponema pallidum* subsp. *pallidum*, which are the causative agents of COVID-19 and syphilis, respectively. Although a common strategy has been followed in both cases, different technical solutions were needed to adapt the strategy to each pathogen considering their differences. As consequence, both works are presented separately to facilitate the reading. However, four common objectives for SARS_CoV-2 and *Treponema pallidum* subsp. *pallidum* vaccines development can be defined: (1) antigen selection and design, (2) antigen production and purification, (3) antigen characterization and, (4) immunogenicity and efficacy evaluation. Throughout this thesis, these four objectives were accommodated to satisfy each pathogen vaccine demands and recapitulated in a final section in which conclusions from both pathogens work were contrasted.

The present thesis was made from 2018 to 2023 and initially it was conceived as a syphilis vaccine project. Nonetheless, in 2020 COVID-19 pandemic was declared and our research focused on the development of a COVID-19 vaccine. After that, the syphilis project was resumed. Thus, the knowledge acquired during SARS-CoV-2 and *Treponema pallidum* subsp. *pallidum* work have been helpful to each other. Overall, the current research highlights the versatility of vaccine technology, and specifically protein-subunit platform, to give response to different pathogens and infectious diseases.

Dr. Jorge Carrillo and Dr. Julià Blanco

SUMMARY

Throughout history, the human species has been challenged by different pathogens. Althought the immune system is highly effective protecting us from their infection, in some cases it fails, and we fall sick. Nowadays, modern medicine has vaccines to fight pathogens, which are considered one of the most successful achievements for infectious disease control and eradication. Thus, in the present work we use protein-subunit platform for the development of two vaccines against two pathogens: SARS-CoV-2 and *Treponema pallidum* subsp. *pallidum*, with a totally different approach.

SARS-CoV-2 is the etiologic agent of the recent COVID-19 pandemic. Specifically, SARS-CoV-2 infection begins with the interaction between the viral Spike and the ACE2 protein on the host cell surface. The Spike protein, and more specially its RBD domain, is one of the main targets of cellular and humoral immunity. Since both responses have been related with a disease improvement, most current vaccines against SARS-CoV-2 are based on the entire Spike or RBD. However, the Spike used in some of these vaccines (S-2P) still shows some structural instability, which can affect its yield and antigenicity. Thus, we explored different structural stabilization approaches of Spike and evaluated their immunogenicity and prophylactic capability against SARS-CoV-2 infection in K18-hACE2 mice and golden Syrian hamsters. Overall, we found a set of mutations that increased recombinant protein yield and showed higher efficacy than S-2P at protecting from severe disease in animal models.

Treponema pallidum subsp. *pallidum* causes syphilis, a venereal disease. Despite syphilis is an old known disease and it is easily treated with penicillin; the number of cases has been rising in the last decades. Thus, current medical measures are not enough for its control and a syphilis vaccine could be pivotal. However, syphilis vaccine has been elusive despite several attempts. *Treponema pallidum* is characterized by a paucity of surface proteins and multiple immune evasion mechanisms. To overcome these issues, we hypothesized that a syphilis vaccine should include a wide outer membrane protein repertoire. Here, we selected and produced a set of proteins, as well as evaluated their immunogenicity in mice. Results showed that a multiple protein preparation induced antigen-specific antibodies with capacity of blocking the binding of recombinant proteins to host proteins of the extracellular matrix.

RESUMEN

A lo largo de los años, la especie humana se ha visto azotada por diferentes enfermedades infecciosas. En este sentido, las vacunas han sido cruciales para el control y la eradicación de estas, considerandose uno de los hitos de la medicina moderna. En el trabajo expuesto se han desarrollado dos vacunas basadas en subunidades contra SARS-CoV-2 y *Treponema pallidum* subsp. *pallidum*.

SARS-CoV-2 es el agente etiológico de la COVID-19. La infección por SARS-CoV-2 se da con la unión de la Spike viral a la proteína ACE2 en la superficie celular. La proteína Spike, y más concretamente su dominio RBD, son diana de la respuesta immune celular y humoral. Dado que esta respuesta se ha relacionado con un mejor pronóstico de la enfermedad, la mayoría de vacunas contra SARS-CoV-2 se basan en la Spike o el RBD. Sin embargo, algunas vacunas contienen una forma mutada de la Spike (S-2P) que presenta cierto grado de inestabilidad estructural y que afecta a su expressión e immunogenicidad. Es por ello que en esta tesis se exploran nuevas aproximaciones de estabilización de la proteína Spike y sus efectos en la immunogenicidad y la eficacia contra la infección por SARS-CoV-2 en ratones K18-hACE2 y hámsters sirios. En conclusión, se describieron un conjunto de mutaciones de la Spike que mejoraron tanto la producción como la protección frente a la enfermedad severa en comparación con la S-2P.

Treponema pallidum subsp. *pallidum* es el patógeno causante de la sífilis, una enfermedad venérea. A pesar de que la sífilis no es una enfermedad nueva y tiene fácil tratamiento, el número de casos ha incrementado en las últimas décadas. Así pues, las medidas sanitarias actuales no han sido capaces de evitar su propagación y una vacuna sería determinante para su control. Sin embargo, la vacuna contra la sífilis permanece esquiva y enfrenta algunos desafíos. Concretamente *T. pallidum* se caracteriza por una baja densidad antigénica en su superficie y consta de varios mecanismos de evasión inmune. En este trabajo, hipotetizamos que una vacuna contra la sífilis debería incluir un amplio repertorio de proteínas de membrana externa. Es por ello por lo que se seleccionaron y produjeron un conjunto de proteínas y se evaluó su inmunogenicidad en ratones. Como conlusión las proteínas evaluadas produjeron anticuerpos específicos que además tenían la capacidad de bloquear la unión de las proteínas recombinantes a proteínas de la matriz extracelular.

RESUM

Al llarg de la història, l'espècie humana s'ha vist sacsejada per diferents malalties infeccioses. Tot i que el sistema immune és altament efectiu protegint-nos d'infeccions, a vegades falla, i emmalaltim. La medicina moderna ha utilitzat les vacunes per lluitar contra patògens, ja que són un dels major acompliments pel control i l'erradicació de les malalties infeccioses. En aquest treball, utilitzem una plataforma basada en proteïna/subunitat per desenvolupar dues vacunes, una contra SARS-CoV-2 i una altra contra *Treponema pallidum* subsp. *pallidum.*

SARS-CoV-2 és l'agent etiològic de la recent pandèmia de la COVID-19. Específicament, la infecció per SARS-CoV-2 comença amb la interacció entre la Spike viral i la proteïna ACE2 de la superfície de la cèl·lula. La proteïna Spike, i més específicament el seu domini RBD, és una de les principals dianes de la immunitat cel·lular i humoral. Com que les dues respostes s'han relacionat amb el millorament de la malaltia, la majoria de les vacunes actuals contra la COVID-19 estan basades en la Spike o el domini RBD. Tot i així, la Spike que s'ha utilitzat en algunes d'aquestes vacunes (S-2P) encara mostra certa inestabilitat estructural, la qual pot afectar a la seva producció i antigenicitat. Per tant, hem explorat diferents estratègies d'estabilització estructural de la Spike i hem avaluat la seva immunogenicitat i capacitat profilàctica contra la infecció pel SARS-CoV-2 en ratolins K18-hACE2 i hàmsters Siris. En resum, hem identificat un conjunt de mutacions que augmenten la producció de proteïna i milloren la capacitat protectora contra la malaltia greu en models animals, comparat amb la S-2P.

Treponema pallidum subsp. *pallidum* produeix sífilis, una malaltia venèria. Tot i que la sífilis no és una malaltia nova i es pot tractar fàcilment amb penicil·lina, el número de casos ha augmentat en les últimes dècades. Com que les mesures mèdiques actuals no han sigut capaces d'evitar la seva propagació, vacuna podria ser determinant pel seu control. Desafortunadament, la vacuna contra sífilis sembla presentar algunes dificultats. Concretament, T. *pallidum* es caracteritza per una baixa densitat antigènica en la seva superfície, i presenta múltiples mecanismes d'evasió immune. En aquest treball, hem hipotetitzat que una vacuna contra sífilis hauria d'incloure un ampli repertori de proteïnes de la membrana externa. Per a aquesta raó, es van seleccionar, produir, i avaluar la seva immunogenicitat en ratolins. En resum, el conjunt de proteïnes avaluades van produir anticossos específics que són capaços de bloquejar la unió de les proteïnes recombinants a les proteïnes de la matriu extracel·lular.

COVID-19

INTRODUCTION

1.COVID-19 Pandemic

In December 2019, several cases of pneumonia of unknown origin emerged in Wuhan, Hubei, China[1]. Most of the cases were associated with exposure in the Huanan Seafood Wholesale market from Wuhan[2]. The pneumonia outbreak was related with a high number of patient admission into intensive care unit (ICU)[3]. The increase in the number of new cases and the spread outside Wuhan pointed to an infectious origin[4]. On January 7th of 2020 a new coronavirus was identified as the causative microbial agent of the new pneumonia outbreak[5]. The new virus was firstly named "2019 novel coronavirus" (2019-nCoV) and lately "Severe Acute Respiratory Syndrome Coronavirus 2" (SARS-CoV-2) by the International Committee on Taxonomy of Viruses[6]. Thus, the new emergent respiratory illness became known as "Coronavirus disease 2019" (COVID-19). At the end of January 2020, the first cases out of China were reported in Thailand, Japan, and the Republic of Korea, with a total of 282 confirmed cases and six deaths[7]. COVID-19 rapidly spread to other parts of the world and moreover the number of deceases increased concerningly. In one month, COVID-19 outbreak affected 26 countries with 75.748 confirmed cases and 2.229 associated deaths[7]. In view of the alarming level of spread and severity, the World Health Organization (WHO) declares COVID-19 as a pandemic on 11 March 2020, becoming the first one since the 1918 flu pandemic. To date, over 770 million confirmed COVID-19 cases and over 6.9 million deaths have been reported globally[7].

1.1. COVID-19 Disease and Global Impact

COVID-19 is a respiratory disease with mild to moderate symptoms in most cases (80%) and an incubation period of 2-14 days[8,9]. Main symptoms include fever, headache, muscle weakness, tiredness, shortness of breath and, loss of taste and smell; which can be managed easily from home[8]. However, severe COVID-19 infection can also occur with serious symptoms like breathing difficulty, chest pain or pressure, and loss of speech or movement; which require medical attention and even hospitalization. COVID-19 respiratory symptoms can finally complicate in those severe cases and cause respiratory failure with consequent death[8]. Different risk factors have been associated with severe and critical COVID-19 development,such as older age and previous existing health problems like obesity,

heart diseases, cancer, pulmonary illness and, immunodeficiencies among others[10,11].

In epidemiology three statistical measures are used to model how a disease affect population; the infection fatality rate (IFR), the case fatality rate (CFR) and the reproduction number (Ro). CFR is defined as the proportion of infected cases which end up on death from total cases, while IFR represents the expected death among infected individuals. CFR and IFR are considered equal when all the infection cases are well diagnosed and recorded. Thus, estimated fatality rate of COVID-19 depends so much on location and varies from the beginning to the outgoing pandemic[12]. Finally, Ros indicate the number of people who get infected from one carrier during their infectious period. If Ro is greater than 1 the infectious is more contagious and difficult to control, while if Ro is smaller than 1 the infection spreads less and eventually disappear. As well as fatality rate, Ro also varied during COVID-19 pandemic depending on the circulating SARS-CoV-2 variant. Considering this epidemiologic parameters, SARS-CoV-2 is characterized by a higher transmissibility rate (Ro: 2.53-6.72) than other coronaviruses (CoVs), such as Severe Acute Respiratoy Syndrome Coronavirus (SARS-CoV) (Ro:2.3-3.7) and Middle East Respiratory Syndrome Coronavirus (MERS-CoV) (Ro: 0.8-1.3)[13,14]. This Ro can be even higher in the case of SARS-CoV-2 Omicron variants, with an average Ro of 8.2[15]. Contrary to Ro, SARS-CoV-2 CFR (1.83-6.3%) is lower than SARS-CoV (11%) and MERS-CoV (34.3%)[14]. Awfully, SARS-CoV-2 CFR increases drastically in association with risk factors; for example, CFR in patients over 65 years old reaches 16.9%- 24%[16], while in case of cancer arises 25-37%[17]. COVID-19 pandemic was defined by these epidemiological parameters, but also by the number of hospitalizations associated with the infection. This value varies from one country to another, and also from the beginning of the pandemic to date. In general terms, SARS-CoV-2 is associated with a high number of hospitalizations which increase in presence of risk factors[18].

COVID-19 pandemic has involved a huge impact to the world not only in public health, but also at economic and social levels. The high Ro and CFR, as well as the high numbers of hospitalizations associated with SARS-CoV-2 infections, led to the health system saturation in most countries. To face SARS-CoV-2 rapid spreading, the governments around the world were forced to declared the state of emergency, which changed people life until now. State of emergency in some countries, such

as Spain, included lockdown measures and stopping all the activity, which directly influenced on economy. A global decrease on Gross Domestic Product have been reported during pandemic, which added to the increase in expenditure to deal with medical needs; resulted on an economic recession scenario[19]. Several people lost their jobs, particularly those relate to non-essential services[20]. Education and public health access, as well as other essential services were compromised[21,22]. The social distance and the security measures have also affected relationship among people[23]. There was an increase in mental health problems like post-traumatic stress disorder, anxiety, depression, and other symptoms of distress[20,24]. Hence, in order to recover public health, economy, and social normality, there was a global urgency in developing a vaccine against SARS-CoV-2 to control COVID-19 pandemic. The design of an effective vaccine begins with understanding the biology of the pathogen, as well as, the immune response during infection.

1.2. SARS-CoV-2

SARS-CoV-2 belongs to Coronaviridae family, which included two subfamilies: *Letovirinae* and *Orthocoronavirinae.* The later one is the most diverse with four genera *Alphacoronaviruses, Betacoronaviruses, Gammacoronaviruses* and *Deltacoronaviruses*[25]. Besides SARS-CoV-2, betacoronaviruses includes other human coronaviruses (HCoVs) as HCoV-OC43, HCoV-HKU1, SARS-CoV and MERS-CoV; whereas human coronaviruses HCov-229E and HCoV-NL63 are alpha-coronaviruses. In contrast with SARS-CoV, SARS-CoV-2 and MERS-CoV, the other HCoVs (HCoV-OC43, HCoV-HKU1, HCoV-229E, and HCoV-NL64) cause harmless infections[26]. CoVs are both, animal and human pathogens[27–30]. *Alphacoronaviruses* and *Betacoronaviruses* include only mammalian CoVS, while the other two genera include CoVs that affect predominantly birds[31] (**Fig.1**).

Sequencing analysis has shown that SARS-CoV-2 is related to SARS-CoV and MERS-CoV, with a 79% and 50% identity, respectively[5]. Both, SARS-CoV and MERS-CoV, were also responsible of two relevant respiratory diseases in the 20th century. SARS-CoV emerged in China in 2002 and caused Severe Acute Respiratory Syndrome (SARS) epidemic with 8.422 reported infections and 916 deaths until its containment in 2004[32]. MERS-CoV appeared in Saudi Arabia in 2012 and it is the etiological agent of Middle East Respiratory Syndrome (MERS), an endemic disease with 2600 cases and 935 associated deaths [33].
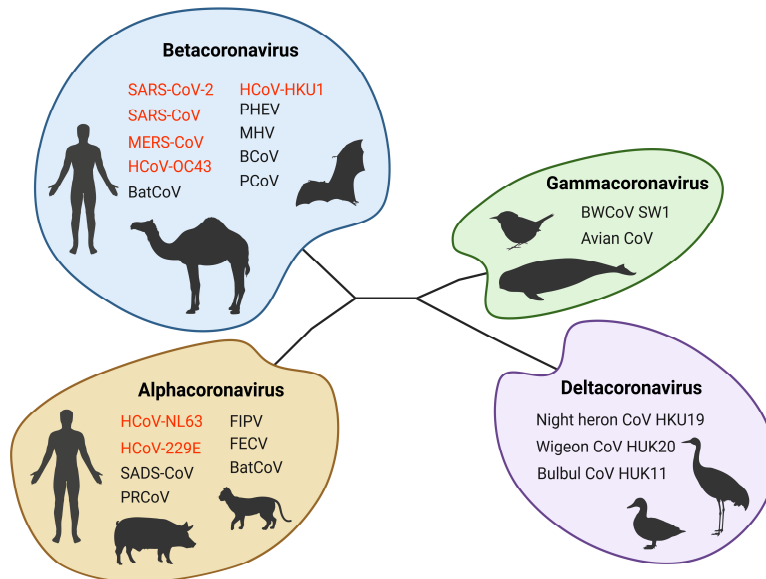
Figure 1. **Phylogenetic tree of SARS-CoV-2**. Schematic representation of the four *Orthocoronavirinae* genera, pointing their evolutionary connection and their animal hosts. Human coronaviruses are highlighting in red. Adapted under CC BY 4.0 License from Singh et al.[31]

Phylogenetic studies have shown that all HCoVs have a zoonotic origin[34]. While HCoV-HKU1 and HCoV-OC43 are considered to be originated from rodents; HCoV-229E, HCoV-NL63, SARS-CoV and, MERS derived from bat CoVs[34,35]. Multiple theories have been considered in relation to SARS-CoV-2 origin, including laboratory escape scenario[36]. However, scientific evidences pointed to a bat origin, since sequencing analysis showed an 88% identity among SARS-CoV-2 and two bat-derived SARS-like CoVs: bat-SL-CoVZC45 and bat-SL-CoVZC21[5]. Notably, Zhou et al. reported the bat coronavirus RaTG13 as the more closely related coronavirus with a 96.2% identity[37]. However, similarity in the genome region of the Receptor binding domain (RBD) of SARS-CoV-2 with the RBD of RaTG13 was below 90%, indicating a less close relationship among two viruses[38]. Interestingly, high RBD similarity has been found in CoVs isolated from pangolins, such as PCoV-GD (96.8%)[38]. Thus, it has been proposed pangolins as an intermediate host, since interspecies transmissions have been previously described for other HCoVs, such as MERS[39]. Moreover, multiple recombinant events have been identified in SARS-CoV-2 genome[40] which could suggest that recombination between bats and pangolins CoVs might happened in another animal host and then jumps to humans[31]. Even when the direct progenitor for SARS-CoV-2 is still not discovered, all phylogenetic studies point to a zoonotic origin.

Genome

SARS-CoV-2 is an enveloped virus with a positive-sense single-stranded RNA (+ssRNA) genome of ~ 30 kb. SARS-CoV-2 genome shows similar architecture to other CoVs[41] (**Fig. 2A**). The RNA genome of CoVs have a 5′-cap and a 3′-poly(A) tail, like most eukaryotic mRNA, which allow their recognition by the host translation machinery[42]. SARS-CoV-2 genome contains 14 open reading frames (ORFs) and encode for a total of 31 proteins divided into: 16 non-structural proteins (nsp1-16), 4 structural proteins, and 11 accessory proteins[43]. The non-structural proteins are encoded by ORF1a (nsp1-nsp11) and ORF1b (nsp12-nsp16) genes, which represent two-thirds of the viral RNA genome. The structural proteins include the Spike (S), Membrane (M), Envelope (E) and Nucleocapsid (N) proteins which are encoded by the S, M, E, and N genes, respectively. Finally, the ORF3a, ORF3b, ORF3c, ORF3d, ORF6, ORF7a, ORF7b, ORF8, ORF9b, ORF9c and ORF10 genes encode accessory proteins. Non-structural proteins ORFs start at the 5′-end, while structural and accessory proteins ORFs are grouped in the 3′-end[43]. Both, non-structural and structural proteins are common elements among CoVs, contrary to accessory proteins which are not shared by all CoVs[44]. Indeed, ORF8 and ORF10 gene are unique for SARS-CoV-2[43,45]. Accessory proteins have diverse function related with viral pathogenesis, such as immune evasion and alteration of apoptosis and mitochondrial function[43]. Non-structural proteins are involved in viral replication, transcription and translation, and also viral pathogenesis during infection through countering the antiviral response[46,47].

Molecular Structure

SARS-CoV-2 virions have a spherical shape with an average diameter of 108 ± 8 nm[48]. The viral RNA is tightly associated with the N proteins and surrounded by a lipid bilayer derived from the host cell. The viral envelope is formed by the M, E, and S viral proteins embedded in the lipid bilayer (**Fig. 2B**).

The N protein is a multifunctional protein that binds to viral RNA and it is involved in the formation of ribonucleoprotein (RNP) complex, which adopt a helical conformation[49]. The packing of RNP complex into the new virions occurs via the interaction between the N protein with the M protein[50]. Furthermore, the N protein interact with a protein subunit of the viral replication-transcription complex (RTC) allowing the correct RNA assembly into the RTC machinery [51].
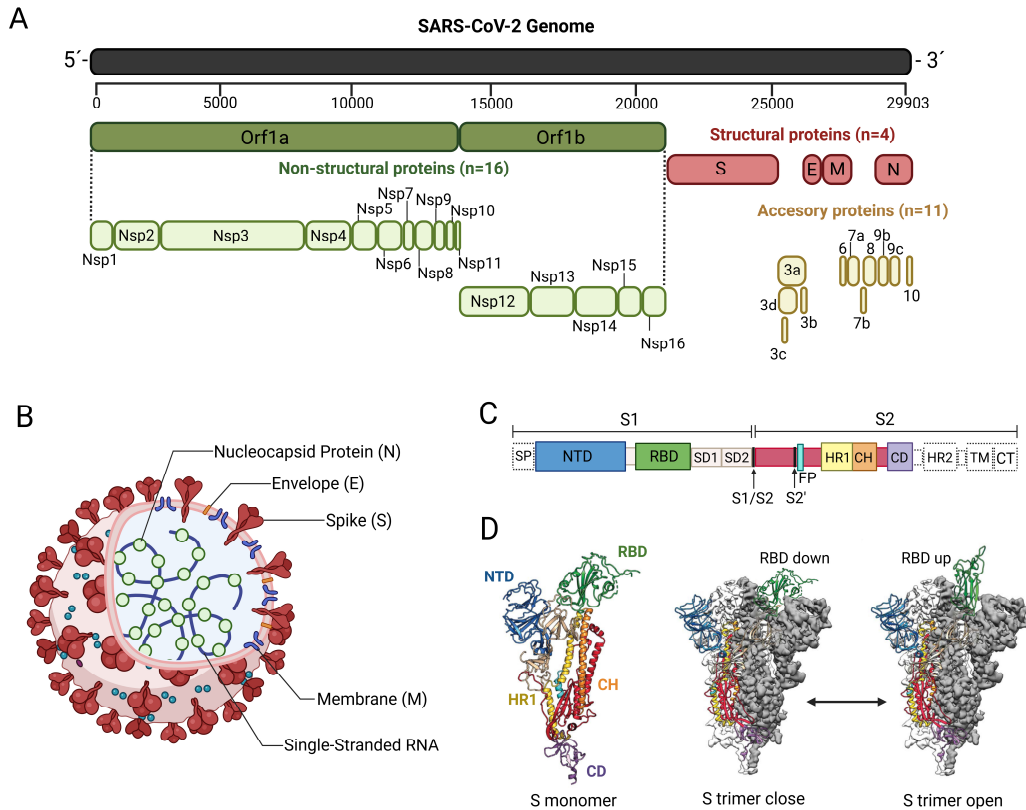
Figure 2. SARS-CoV-2 Structure. (A) SARS.CoV-2 genome organization. SARS-CoV-2 contains 16 non-structural proteins (nsp) and 11 accessory proteins involve in several processes during viral cycle. Viral architecture is composed by four structural proteins, nucleocapsid (N), spike (S), membrane (M), and envelope (E). **(B)** SARS-CoV-2 viral envelope consists of spherical lipid bilayer crossed by M, E, and S proteins that encloses the viral single-stranded RNA bound to N proteins. **(C)** Schematic of S protein primary structure pointing the S1 and S2 subunits and their respective domains. SP, signal peptide; NTD, N-terminal domain; RBD, receptor binding domain; SD1, subdomain 1; SD2, subdomain 2, S1/S2, S1/S2 protease cleavage site; S2′, S2′ protease cleavage site; FP, fusion peptide; HR1, heptad repeat 1; CH, central helix; CD, connector domain; HR2, heptad repeat 2; TM, transmembrane domain; CT, cytoplasmic tail. **(D)** SARS-CoV-2 S monomer and trimer structure. S trimer is shown in its prefusion conformation and in two different states, close (RBD down) and open (RBD up). Each S domain is represented in color according to (c). Those domains in white are not shown. The S structure is from Wrapp et al.[61] under CC BY 4.0 License.

The M protein is the most abundant structural protein which drives the assembly of new virions into the host cells[42]. Oligomerization of new CoVs occurs at the Golgi-endoplasmic reticulum membrane, where the M protein accumulates and recruits S, N and E proteins[52]. Those interactions promote membrane curvature and finally the formation of new virions[53].

The E protein is an integral membrane protein that join to M protein to form the viral envelope. Thus, most E proteins localize in the Golgi-endosplasmic reticulum where participates in virion assembly. Interaction between E protein and M protein is sufficient for the production and release of virus-like particles (VLPs)[54]. Moreover, the E protein is involved in maturation and release of virus particles through its hydrophobic transmembrane domain, since the alteration of this domain affect excretion of virus particles but not virus assembly[55].

The S protein is a glycosylated type I membrane protein (single transmembrane helix with the amino-terminal domain oriented to the outer media), which assembles into homotrimers and it is presented on the viral surface. The S glycoprotein mediates cell receptor attachment and viral and cell host membrane fusion[56]. In some CoVs, this structural protein has been reported to also mediate the fusion between infected cell and adjacent cells, allowing virus spreading by syncytia formation[57]. Thus, coronavirus life cycle and infectivity strongly depend on S protein. Furthermore, S protein was identified as the most significant immune target in HCoVs, such as SARS-CoV[58]. Hence, at the beginning of the pandemic, scientific research focused on the characterization of the SARS-CoV-2 S glycoprotein.

SARS-CoV-2 S protein has a size of 180-200 kDa with a total length of 1273 amino acids (aa). Each monomer consists of two subunits, S1 and S2. The S1 subunit (14-685 aa) comprises the N-terminal segment (14-685 aa) and include the RBD (319-541 aa). Whereas, S2 subunit (686-1273 aa) encompasses the fusion peptide (FP) (788-806 aa), heptapeptide repeat sequence 1 (HR1) (912-984 aa), heptapeptide repeat sequence 2 (HR2) (116-1213 aa), transmembrane domain (1213-1237 aa) and the cytoplasm domain (1237-1273 aa)[59] (**Fig.2C**). While S1 is involved in the binding to the host cell receptor through the RBD, the S2 subunit is responsible for viral fusion and entry[60]. Both SARS-CoV and SARS-CoV-2 S glycoproteins bind to the angiotensin-converting enzyme 2 (ACE2) receptor to gain cell entry[60]; although, the affinity of SARS-CoV-2 S protein for ACE2 is 10 to 20-fold higher[61]. Since RBD is the region involved in this binding, it constitutes a major target of neutralizing antibodies[62]. The S trimer exists in a prefusion conformation and undergoes structure rearrangement upon ACE2 binding, leading to a post-fusion conformation[61,63]. According to Cryo-EM microscopy, the prefusion conformation of SARS-CoV-2 S protein can switch between an open (RBD exposed, "up") and close (RBD not exposed, "down") state[61] (**Fig.2D**). Since in the close state S does

not expose any RBD, this is considered an inactive conformation unable to interact with the host cell receptor[64]. The RBD motility is conserved among other related beta-CoVs such as SARS-CoV and MERS-CoV, which suggest that SARS-CoV-2 S glycoprotein might also pivots between one RBD "up" and three RBDs "up", being the last one the most unstable conformations[61,64,65]. Moreover, RBD-ACE2 binding is flexible showing different RBD angles in "up" conformation[63,66], which may affect epitope exposure and antibody access.

Viral Cycle and Infection

SARS-CoV-2 infection begins with the specific binding of the S protein to the ACE2 receptor (**Fig.3A**). Besides ACE2 expression, SARS-CoV-2 infection also requires the surface co-expression of the transmembrane protease serine 2 (TMPRSS2)[60]. The S2 subunit contain an internal cleavage site, known as S2′ site, which is structural constraint in S pre-fusion state[67]. ACE2 binding triggers S2′ site exposure which is catalyzed by the cellular TMPRSS2[68]. This cleavage uncouples both S1 and S2 subunits, and the S protein undergoes conformational changes, in which S2 subunit is elongated and the FP inserts into the cell membrane forming a fusion pore that allow the viral genome to enter into the cell[69] (**Fig.3B**). Thus, ACE2 and TMPRSS2 co-expression mostly determine viral tropism. However, although SARS-CoV-2 has greater preference for TMPRSS2, other serine proteases can contribute to fusion process[70–72]. As well as other HCoVs, SARS-CoV-2 can also be internalized via clathrin-mediated endocytosis[73] and S2 site can be cleaved by endosomal cathepsins to activate the membrane fusion process[74].

Once the viral RNA genome is inside the cytoplasm, it recruits the cellular translation machinery and encodes two polyproteins Pp1a and Pp1b[75] (**Fig.3C**). These two polyproteins are processed by viral proteases into nsp1-nsp16, and some of them assemble to form the RTC[76]. The viral RNA genome serves as template for RTC to synthesize a full-length RNA copy and several subgenomic mRNAs, which are used to produce structural and accessory proteins[77] (**Fig.3D**). Replication and transcription occur within double membrane replication organelles that are formed during early infection[78]. Structural proteins translocate to endoplasmic reticulum-Golgi compartments where nucleocapsid protein and newly viral RNA are assembled (**Fig.3E**), forming new virions into vesicular compartments that are finally secreted by exocytosis[77,79] (**Fig.3F and G**). During cellular trafficking, S protein priming is performed by host furin protease. Contrary to SARS-CoV, SARS-CoV-2

S incorporates a furin cleavage site among S1 and S2 subunits (S1/S2 site)[80]. S priming enhances SARS-CoV-2 infectivity, as long as favors RBD "up" state[81] and mutation of furin cleavage site was demonstrated to result in decreased pathogenesis *in vivo*[82].
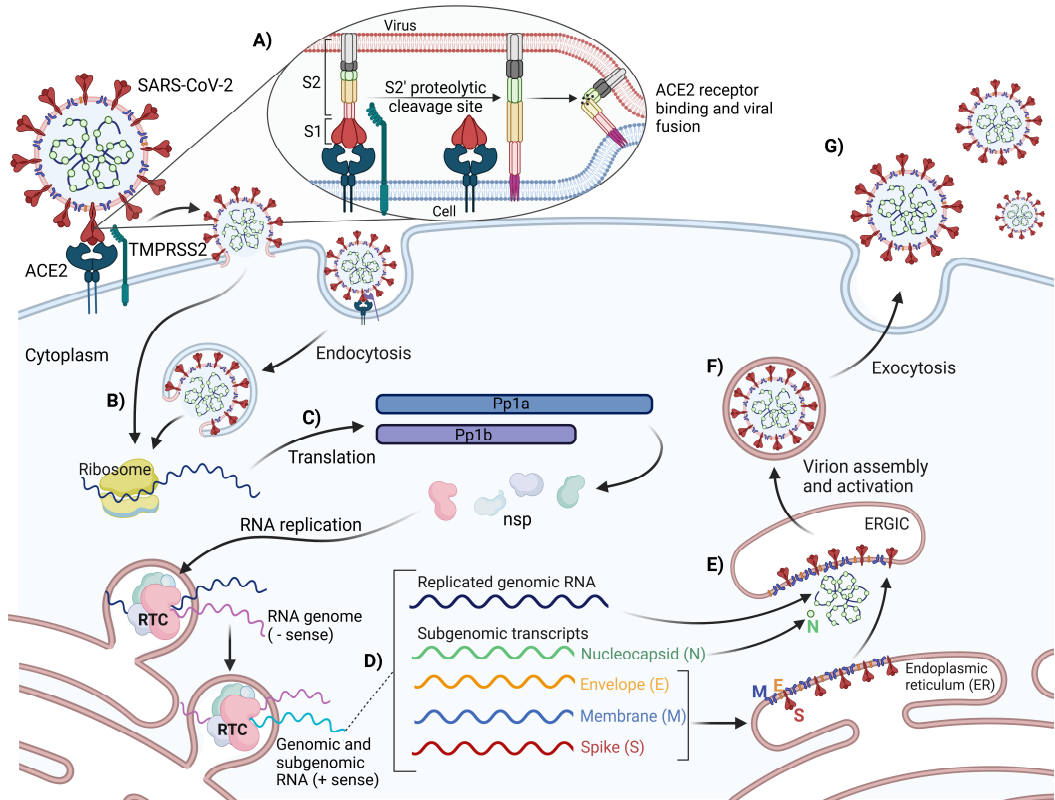
Figure 3. SARS-CoV-2 viral cycle. (A) SARS-CoV-2 infects cell after S binding to ACE2 receptor. This binding promotes structural changes in the S protein with subsequent fusion peptide (FP) exposition. **(B)** After FP insertion into the cell membrane the viral genome is dropped into cytoplasm. SARS-CoV-2 also can enter by clathrin-mediated endocytosis. **(C)** Two primary protein transcripts are translated and processed into non-structural proteins (nsp) that combine to form viral replication-transcription complex (RTC). **(D)** Viral RTC leads RNA replication and subgenomic RNAs production which translates into structural proteins. **(E)** Viral RNA copy and structural proteins assemble into new virions in endoplasmic reticulum-Golgi intermediate compartment (ERGIC). **(F)** During assembly, SARS-CoV-2 virions are activated by furin cleavage. **(G)** Finally, mature virions release by exocytosis. Adapted under CC BY 4.0 License from Lebeau[79].

SARS-CoV-2 Mutagenesis and Variants

In general, CoVs have a low mutation rate (~10^{-6} per site per cycle) since they present a proofreading exoribonuclease[83]. However, natural selection can still occur fixing mutations that benefit viral survival. Remarkably, antigenic drift is a variation mechanism which affects specifically genes that code for viral antigens targeted by

the immune response. Thus, new emergent virus variants can escape from prior immune responses[84]. Antigenic drift has been described in HCoVs; for example, the mutation D480A/G in the RBD of SARS-CoV became dominant during 2003/2004 epidemic and triggered resistance to previous neutralizing antibodies[85]. Since the beginning of the pandemic, SARS-CoV-2 genome has been worldwide sequenced and tracked, allowing surveillance of new mutations that might affect virus pathogenicity.

Actually, there are millions of SARS-CoV-2 whole genome sequences available and published by the Global Initiative on Sharing All Influenza Data (GISAID) (https://covariants.org/). SARS-CoV-2 genetic lineages have been named following the Phylogenetic Assignment of Named Global Outbreak Lineages (PANGOLIN) or Pango nomenclature; or the WHO nomenclature based on Greek alphabet assignment. A large amount of difference sequences has been reported with the consequent description of several SARS-CoV-2 variants with diverse epidemiological characteristics. This made necessary to categorized variants in three groups attending to their risk to public health: Variant of Concern (VOC), Variant of Interest (VOI) and Variant Under Monitoring (VUM), from more to less health impact[86]. Among them, VOCs have received special attention, since they are described as variants with an increase in transmissibility and virulence, and/or decrease in the effectiveness of the public health, social and therapeutics measures. A total of five SARS-CoV-2 VOCs have been recognized by the WHO; Alpha (B.1.1.7, Pango nomenclature), Beta (B.1.351), Gamma (P.1), Delta (B.1.617.2) and Omicron (B.1.1.529)[86] (**Table.1**). Omicron is considered the last current circulating variant family, while the other four have been de-escalated because they are no longer circulating or no remain any problem for public health. To date, multiple mutation events have been reported on S protein. Interestingly, some of these mutations are kept among VOCs and a large number of them affect the RBD (**Table.1**) with different implications, such as higher affinity for ACE2 receptor and resistance to neutralizing antibodies[87,88]. Those mutations had also an impact on variants transmissibility, showing a faster spreading, and severity, increasing the number of hospitalization cases. Alarmingly, all VOCs excepting Alpha, reduce the efficacy of available therapeutic treatments and vaccines[87,88]. This highlight the importance of a continuous update of vaccines and therapies research in this field.

WHO n.	Pango n.	S mutations	Detection Date	De-escalated Date	Impact on transmissibility	Impact on immunity	Impact on severity
Alpha	B.1.1.7	H69del, V70del, Y144del, **N501Y**, A570D, **D614G**, **P681H**, T716I, S982A, D1118H	September 2020	September 2021	Increased	Similar	Increased
Beta	B.1.351	L18F, D80A, D215G, LAL242-244del, R246I, **K417N**, **E484K**, **N501Y**, **D614G**, **A701V**	September 2020	March 2022	Increased	Increased	Increased
Gamma	P.1	L18F, T20N, P26S, D138Y, R190S, **K417T**, **E484K**, **N501Y**, **D614G**, **H655Y**, T1027I	January 2021	March 2022	Increased	Increased	Increased
Delta	B.1.617.2	T19R, V70F, T95I, E156del, F157del, R158G, A222V, W258L, **K417N**, **L452R**, **T478K**, **D614G**, **P681R**, D950N	October 2020	June 2020	Increased	Increased	Increased
Omicron	B.1.1.529 + descendant sublineages	A67V, H69del, V70del, T95I, G142del, V143del, Y144del, Y145D, N211del, L212I, **G339D**, **S371L**, **S373P**, **S375F**, **K417N**, **N440K**, **G446S**, **S447N**, **T478K**, **E484A**, **Q493R**, **G496S**, **W498R**, **N501Y**, **Y505H**, T547K, **D614G**, H655Y, N679K, P681H, N764K, D796Y, N856K, Q964H, N969K, L981F	November 2021	March 2023	Increased	Increased	Decreased

Table 1. SARS-CoV-2 Variants of Concerns (VOCs). WHO and Pango nomenclature (n.) of the five SARS-CoV-2 VoCs are indicated. Spike mutations are pointed in bold and those locate in RBD are marked in red. Impact on transmissibility, immunity, and severity is described regarding prior variants. Impact on immunity refers to immune escape to SARS-CoV-2 treatments, vaccines and neutralizing antibodies from convalescents individuals. del: deletion. This table was made according to European Centre for Disease Prevention and Control (ECDC).

43

2. Immune Response Upon SARS-CoV-2 Infection

SARS-CoV-2 is transmitted by respiratory fluids that contain virus and contact with mucous membranes. Infection begins in upper respiratory tract and gradually descends to lower respiratory tract. Thus, viral load is higher in nasopharynx during early infection and greater in sputum at late infection[89]. In the upper respiratory tract, SARS-CoV-2 infect epithelial and secretory goblet cells, while in lower respiratory part, it infects epithelial cells and type II pneumocytes[90]. These cells co-express the ACE2 receptor and the TMPRSS2 protease[90]. Although, the respiratory system is the major target of SARS-CoV-2, ACE2 expression is ubiquitous and infection of other cells and tissues have been reported, such as enterocytes, vascular endothelial cells, and epithelial cells from the distal tube[91]. Accordingly, cardiovascular, gastrointestinal, and kidney injury have been described as complications in severe COVID-19 cases[92–94]. Moreover, subclinical multi-organ symptoms have also been reported in non-severe and recovered COVID-19 patients[95]. Thus, COVID-19 prognosis will depend on pulmonary injury and multi-organ affection[96], which are directly influenced by the capacity of the immune system to control and clear SARS-CoV-2 infection.

2.1. Innate Immunity

The innate immune response is the first line of defense against SARS-CoV-2 infection. During early infection, viral products (pathogen-associated molecular patterns, PAMPs), as well as products from cell damage (damage-associated molecular patterns, DAMPs) are recognized by patter recognition receptors (PRRs). PRRs are expressed mainly in innate immune cells, including macrophages, monocytes, dendritic cells (DCs), neutrophils, natural killers (NKs) and innate lymphoid cells (ILCs); but also, in non-immune cells, such as epithelia cells[97]. PRRs include Toll-like receptors (TLRs), retinoic acid-inducible gene I (RIG-I)-like receptors (RLRs), nucleotide-binding oligomerization domain-like receptors (NLRs) and, C-type lectin receptors (CLRs) subfamilies[98]. Recognition of PAMPs or DAMPs by these receptors induces an inflammatory response through activation of innate immune cells, which produce pro-inflammatory cytokines and chemokines, and also trigger cell death programs on infected cells[98].

SARS-CoV-2 structural proteins and viral RNA are the main target of PRRs. Specifically, TLRs are integral membrane sensors and play a main role during SARS-CoV-2 replication and viral trafficking. Several studies reported that the S, M, and E proteins induce inflammation via TLR2 signaling[99–101]. Additionally, S1 subunit initiates a pro-inflammatory cascade by interacting with TLR4[102], while TLR3 and TLR7/TLR8 may be activated by SARS-COV-2 derived double-strand RNA (dsRNA) intermediates during viral replication in endosomes[103,104].

Cytosolic viral RNAs are recognized by RLRs, which include RIG-I, melanoma differentiation-associated gene 5 (MDA5) and laboratory of genetics and physiology 2 (LGP2) receptors. Stimulation of RLRs trigger the expression of interferon (IFN) genes. While little is known about LGP2 ligand, RIG-I senses 5′-triphosphorilated ssRNA and MDA5 binds to long dsRNA. Thus, both RIG-I and MDA5 are suggested to recognize genomic and subgenomic RNA intermediate products from SARS-CoV-2 replication and transcription. Indeed, the lack of MDA5, LGP2 and RIG-I reduces IFNs production and the pro-inflammatory response upon infection[105,106]. Besides that, RIG-I has been reported to hamper SARS-CoV-2 replication in an IFN-independent manner, through binding to viral RNA and blocking attachment to the viral RTC[107].

Like RLRs, NLRs are also intracellular cytosolic sensor. NLRs includes 23 members involved in the recognition of bacterial derived-PAMPs or in inflammasome assembling[108]. From this last group, NLRP3 is one of the best characterized. Upon different stimuli, NLRP3 oligomerized and form the inflammasome complex. This complex triggers the cleavage of pro-caspase-1 to caspase 1, which catalyze the activation of pro-IL-1β and pro-IL-18 inflammatory cytokines; as well as Gasdermin D cleavage which promotes pyroptosis[109]. Several PAMPs from SARS-CoV-2, including viral ssRNA, ORF3a accessory protein and, N protein, stimulate NLRP3 activation[110–112].

Pro-inflammatory cytokines and chemokines produced by PRRs signaling (e.g. TNF, IFN, IL-1β, IL-6, CCL2, and MIP-1α) in response to SARS-CoV-2, induce local vasodilation and immune cell recruitment, such as monocytes and neutrophils; and lately, lymphocytes. Cytokines also activate macrophages, DCs and NK cells, which boost viral clearance and antigenic processing/presentation. Moreover, cytokines can induce systemic fever and trigger the acute-phase response. Hence, in infected

tissues innate response creates an antiviral environment which limit viral replication and spread, providing time to adaptive response development (**Fig.4A**). Interestingly, in some patients, the innate immune response controls SARS-CoV-2 infection without stimulating adaptive immunity[113]. Nevertheless, innate immune responses and pro-inflammatory cytokines persistence at high levels is related to severe COVID-19[114,115] (**Fig.4B**). SARS-CoV-2 is able to evade innate immune response by reducing the expression of IFNs levels[116–118], delaying the development of the adaptive immune response, and promoting a pro-inflammatory cytokines dysregulation[119]. According to Karki et al., TNF and IFN-γ signaling induce inflammatory programmed cell death (PANoptosis) during COVID-19, which promote a cytokine storm development[120]. Thus, a positive loop is created among PANoptosis and cytokine storm, which finally cause a cytokine shock with systemic inflammatory response syndrome (SIRS) and acute respiratory distress syndrome (ARDS), both common in severe COVID-19[120].
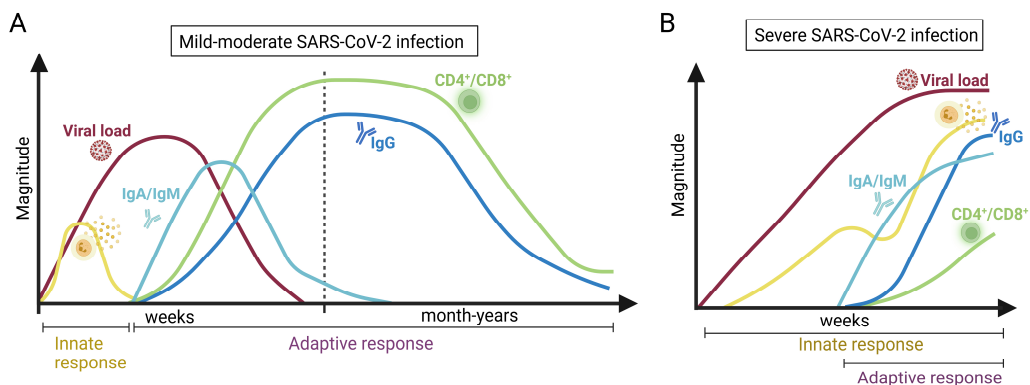
Figure 4. Immune response during SARS-CoV-2 infection. Simplified representation of the innate and adaptive immune response kinetics under **(A)** mild-moderate and **(B)** severe or fatal COVID-19. Dash line marks COVID19 recovery and the evolution of the immune response beyond time after healing. Yellow line represented the innate immune response, red line showed the viral load, blue lines represented the humoral response and green line displayed the cellular response.

2.2. Adaptive Immunity

The development of a proper SARS-CoV-2 specific-adaptive immune response is associated with the resolution of average COVID-19 cases. This aim to the important role of adaptive response during SARS-CoV-2 infection and its understanding to the effective vaccine development. Adaptive immunity has two main branches, the cellular and the humoral response.

Cellular Response

Adaptive cellular response includes CD4^{+} and CD8^{+} T cells populations. The generation of a specific cellular response against SARS-CoV-2 require antigen presentation in the context of Major Histocompatibility Complex (MHC) class I (for CD8^{+} T cells) and class II (for CD4^{+} T cells)[121,122]. Contrary to MHC-I, which is expressed by almost all nucleated cells, the MHC-II is restricted to antigen-presenting-cells (APCs); which include macrophages, DCs, and B cells. Particularly, DCs play a major role in the development of adaptive immune responses. Resident DCs from respiratory tract capture SARS-CoV-2 antigens and migrate to proximal draining lymph nodes (LNs) where present these antigens to CD8^{+} and CD4^{+} T cells. The recognition of MHC/antigen complexes by T cells and concomitant co-stimulatory signals, trigger its activation, proliferation and migration to the site of infection[123].

Both CD4^{+} and CD8^{+} T cells are involved in the anti-SARS-CoV-2 immune response[124,125]. During SARS-CoV-2 infection, the CD4^{+} T cell repertoire is activated against almost all viral proteins and the magnitude of the response correlates with the level of expression of each protein[125]. S, M and N proteins are the major targets of CD4^{+} T cells response[125] in both convalescent and acute SARS-CoV-2 infected individuals[124]. SARS-CoV-2 specific CD4^{+} T cells can be detected as early as 4 days after symptoms onset[124] (**Fig.4A**), and a rapid CD4^{+} T cell response correlates with infection control and mild COVID-19[126]. In contrast, late and poor SARS-CoV-2 specific CD4^{+} T cells response is strongly associated with severe disease[126,127](**Fig.4A**). The strong association between CD4^{+} T cells and disease prognosis lie in their multiple functions during SARS-CoV-2 infection. Thus, CD4^{+} follicular helper T cells (Tfh) are critical in the development of B-cell and long-term humoral responses against SARS-CoV-2[124,127]. In addition, IFN-γ-, IL-2-, and TNF-producing T helper type 1 cells (Th1) play a major role in the immune responses to SARS-CoV-2[124,127] by mediating direct antiviral functions, recruiting monocytes, and boosting CD8^{+} T-cell and macrophage activity.

Regarding CD8^{+} T cells, although their frequencies in SARS-CoV-2 infected subjects are lower than CD4^{+} T cells[125,127], they are still important for viral clearance. Indeed, the magnitude of CD8^{+} T cells in peripheral blood monocular cells (PBMCs) have been associated with better COVID-19 prognosis[124,128]. SARS-CoV-2 specific

CD8^{+} T cells are reactive against multiple viral proteins, including S, N, M and accessory proteins[125,127,129,130].

After viral clearance, T cell response gradually declines, but it still remains detectable up to one year after COVID-19 recovery[131] (**Fig.4A**). SARS-CoV-2 T cell memory persistence have been found independently of COVID-19 severity[132]. However, differences were reported among circulating CD8^{+} and CD4^{+} memory T cells, since long-lasting CD8^{+} T cells were not detectable in some convalescent individuals[133]. Apart from circulating memory T cells, both CD4^{+} and CD8^{+} tissue-resident memory T cells were found in the airway tract and associated LNs[134]. Moreover, different studies reported that despite a slightly decrease, pre-existing SARS-CoV-2 cellular response remains active against new SARS-CoV-2 variants[135,136].

Humoral Response

The humoral immune response is mediated by antigen-specific B cells that produce antibodies after antigen activation via B-cell receptor (BCR)[137,138]. This encounter occurs mainly in secondary lymph tissues, such as LNs. Signaling via BCR triggers gene expression programs, and antigen internalization and processing. Activated B cells migrate to the B-T border of immature follicles into the LNs, where they present the processed antigen to CD4^{+} helper T cells through MHC-II molecules. T cell co-stimulation promotes B cell proliferation and lead differentiation into short-lived extrafollicular plasmablasts. These cells are responsible for early humoral response characterized by low-affinity IgMs, and to a lesser extent IgGs[137,138]. Additionally, after B- and T-cell synapse, B cells start the immunoglobulin class switching process and derive to germinal center (GC) formation[139]. In GC, B cells interacts with CD4^{+} Tfh cells and undergoes immunoglobulin somatic hypermutation[137,138]. This process is coupled to antigen selection that results in an affinity maturation process. By this mechanism, B cells expressing high affinity antibodies are selected and progressively differentiated to long-lived plasma cells or memory B cells. Upon antigen re-exposition, memory B cells rapidly generate antibody-producing plasma blasts or re-enter GC for further maturation and diversification of antibody response[140].

During SARS-CoV-2 infection, antibody seroconversion occurs rapidly between 5-15 days post-symptoms onset (**Fig.4A**). Although classically IgM antibodies precede circulating IgG, in SARS-CoV-2 infection, IgG can be early or simultaneously

detected with IgM during seroconversion[141,142]. Remarkably, IgA antibodies, which are critical in mucosal tissue protection, may appear on days 4-6 post-symptoms onset exceeding IgM titters[143]. While IgG levels progressively increase after infection, reaching a plateau by 3-4 weeks post-symptoms onset and a late progressive decay, IgM and IgA levels begins to decrease from the third-four weeks[141]. Despite this general description, SARS-CoV-2 seroconversion profile and antibodies levels may vary according to COVID-19 clinical severity. Thus, high antibodies titters (including neutralizing ones) have been found in severe COVID-19 patients[144–147]. This elevated humoral response may be connected with extended and high viral antigen exposure in acute COVID-19 cases[148] and consequently humoral response is triggered much longer[149]. Contrarily, asymptomatic patients show the lowest concentration of antibodies[150]. Hence, high antibodies titters are not necessarily related to greater COVID-19 prognosis. Notably, despite higher antibody levels, Tang et al. showed that antibody affinity is lower in deceased than in recovered patients[151]. A poor antibody affinity maturation has been previously reported in elder people[152], which belongs to COVID-19 high-risk population. Thus, humoral response efficacy against SARS-CoV-2 may be more a matter of quality than quantity. After COVID-19 recovery, specific SARS-CoV-2 antibodies are still detectable for long time. Overall, IgM and IgA have a short-life and their levels decline between 1 and 3 months after infection, while IgG peak remains stable up to 6-month post-infection and it experiences a significant decrease between 6-8 month after symptom onset[153–156] (**Fig.4A**). One year after symptom onset, specific IgM and IgA were not detectable in most patients. In contrast, anti-SARS-CoV-2 IgG persists detectable over one year[156–158]. Long-lived antibodies result from the development of a SARS-CoV-2 specific memory B-cell compartment. While antibody levels decrease gently after reaching their peak, circulating memory B cells increased over time and arise their maximum at 3-6 months post-infection[153,158]. In addition, memory B cells remain without significant variation up to one year after infection independently on severity disease[158,159].

Humoral response is directed against both SARS-CoV-2 structural and non-structural proteins[160]. Antibodies against the S, N and E proteins have been detected in COVID-19 patients[161,162], and their levels correlate with COVID-19 prognosis[163]. Both, S1 and S2 subunits are targeted by humoral responses[164], but the RBD into the S1 subunit was found the immunodominant target[62,165].

Remarkably, 90% of neutralizing antibodies target the RBD domain[165], with the remaining 10% directed against other S1 motifs, such as the N-terminal domain[166,167], or the S2 subunit[168,169], and quaternary epitopes involving S-trimer conformation[167]. Consequently, driven by immune pressure, the S protein accumulates several mutations among variants, and most particularly in the RBD[170]. Despite that, it has been demonstrated that humoral response can evolve by somatic hypermutation, antigen selection and affinity maturation, increasing neutralizing potency[171]. This process may overcome SARS-CoV-2 escape mutations[172], rendering to the humoral response the capability to neutralize emerged VOCs[171,173,174]. Neutralizing antibody titters against SARS-CoV-2 show a dynamic pattern similar to the total IgG antibodies. Indeed, anti-RBD and anti-S IgG levels showed a great correlation with neutralization titters[175]. SARS-CoV-2 infected individuals develop a rapid neutralizing response[176,177] with maximum activity in the first month post symptom onset[158,178]. After that, neutralizing activity declines[178,179], but attains a stable plateau by months 4 to 6 post-infection which maintains beyond one year after recovery[158,180]. Particularly, neutralizing titters are higher in severe COVID-19 episodes than mild-symptom cases[181]. The presence of neutralizing antibodies against SARS-CoV-2 correlates with survival, more specially neutralization potency[175]. Additionally, neutralizing antibodies provide protection to re-infection[182,183].

Besides neutralization, other antibody effector functions have also been reported during SARS-CoV-2 viral clearance. Non-neutralizing antibodies can mediate complement activation or interact with Fc-receptors expressed on the surface of immune cells and mediate antibody dependent cellular cytotoxicity (ADCC), and antibody dependent cellular phagocytosis (ADCP). Expression of viral proteins on the surface of infected host cells can be recognized by non-neutralizing antibodies, which triggered NK activation and killing of infected cells by ADCC[184]. While, non-neutralizing antibodies can opsonize viral particles triggering their phagocytosis by macrophages via ADCP. Both effector functions have been described during COVID-19 infection, with similar dynamic trend as neutralizing antibodies[185–188]. Additionally, sera from COVID-19 patients has been reported to activate complement system on the surface of infected cells[185].

3. SARS-CoV-2 Vaccine Development

Prior to SARS-CoV-2 pandemic, no vaccines against CoVs have been approved for use in humans. Since circulating HCoV-HKU1, HCoV-OC43, HCoV-229E, and HCoV-NL63 caused mild-disease, it was not until SARS-CoV and MERS-CoV emergence that coronavirus vaccine research was a priority. During the SARS-CoV outbreak, vaccines were under development and two reached phase I trials[189,190]. However, as virus was eradicated and non-reemergence occured since 2004, SARS-CoV vaccine development was discontinued. Contrary, MERS-CoV has remained being a health problem much longer. Although the majority of MERS-CoV cases concentrate in Middle East and the infection ratio have declined since 2016[191], the vaccine development has maintained active more time and three vaccines have undergone phase 1 trials in the last four years[192–194]. The knowledge acquired through preclinical and clinical studies of SARS-CoV and MERS-CoV vaccines, as well as on the immune response to coronaviruses, was pivotal for the development of current SARS-CoV-2 vaccines.

3.1. From SARS-CoV and MERS-CoV to SARS-CoV-2 Vaccine.

A crucial point in the design of a vaccine is the election of the target antigens that will be presented to the host immune system. Regarding this, since S protein is immunodominant and anti-S humoral response correlates with neutralization activity in SARS-CoV[58,195] and MERS-CoV[196,197] infected individuals, most vaccines against these CoVs were based on this protein. Besides the target antigen selection, the vaccine platform is also critical for the elicitation of protective immune responses. In the last decades, vaccine manufacturing has been benefited from the progress in molecular biology, and several novel vaccine platforms have been improved, such as recombinant viral vectors and nucleic acid vaccines. Moreover, advance in adjuvant research has also helped to increase vaccine immuogenicity. Here, we reviewed the different vaccines platforms which have been used in the context of SARS-CoV and MERS-CoV, and that lately helped to speed up SARS-CoV-2 vaccines development.

Whole inactivated vaccines are based on killed pathogens, such as virions inactivated chemically or by radiation, while the attenuated vaccines include live pathogen but weakened by deleting or mutating pathogenic components[198]. Both

vaccine platforms contain nearly the full antigen repertoire from the original virus and can induce a broad immune response. Additionally, they can be administered using different inoculation routes and thus, they can elicit protection in the pathogen entry site, usually at mucosal level[199]. Preclinical research with inactivated SARS-CoV and MERS-CoV in mice had shown that they can elicited neutralizing antibodies[200–202]. However, some studies reported that inactivated SARS-CoV and MERS-CoV formulations caused eosinophil-related lung pathology upon viral challenge[200,203]. For the generation of live attenuated SARS-CoV and MERS-CoV vaccines, several structural and non-structural proteins were targeted to reduce viral virulence, including the E protein[204,205] and the combination of nsp16 and nsp14 proteins[206–208]. Both attenuation strategies have been shown to provide protection against viral challenge after vaccination. Despite that, safety concerns were associated with live attenuated vaccines, that hampered their progression to clinical trials.

Apart from whole inactivated and live attenuated vaccines, subunit vaccine platform was widely evaluated in SARS-CoV and MERS-CoV. Subunit vaccines consist of isolated antigens (usually proteins) that are produced mostly recombinantly. As a small fragment, subunit vaccines are less immunogenic than whole pathogen, but the use of adjuvants and sequential boosting favor the induction of an effective immune response[209]. SARS-CoV and MERS-CoV subunit vaccines focused mainly on recombinant S protein and more particularly on RBD. Both, monomeric and trimeric S protein were immunogenic and protected upon SARS-CoV challenge in animal models[210–212]. The RBD showed similar results with potent neutralizing antibody induction and protective capacity against SARS-CoV[213–215]. In addition, the S2 subunit, N, and M proteins from SARS-CoV were also analyzed with poorly or no evidence of neutralizing response[216–218]. Considering SARS-CoV previous results, most MERS-CoV protein subunit vaccines were based on the RBD antigen, and showed great immunogenicity and strong neutralizing antibody responses, which can even cross-neutralize different viral strains[219–221]. Besides RBD, the whole S1 subunit, and its N-terminal domain provide protection against MERS-CoV infection in pre-clinal studies[222–224]. Regarding the use of the trimeric S protein as immunogen, the S ectodomain displays high instability, which makes S protein difficult to produce as recombinant protein[65]. In this sense, Pallesen and colleagues described that the incorporation of two proline mutations at positions V1060 and

L1061 stabilized the MERS-CoV trimeric S protein in its prefusion state[65]. Compared with wild-type S, V1060P/L1061P mutant protein (S-2P) showed an increased yield as recombinant protein and higher capability to induce neutralizing antibodies upon immunization. Interestingly, this strategy is translatable to other coronavirus S protein, such as SARS-CoV, HCoV-HUK[65], and recently SARS-CoV-2[225].

To overcome immunogenicity issues associated with subunit vaccines, nanoparticles-based vaccines and viral vector vaccines emerged as increased protein presentation platforms[226]. Nanoparticles include several antigen forms, such as VLPs and bacterial outer membrane vesicles platforms. Specifically, VLPs consist of self-assemble viral particles which contain structural proteins but lack viral genome. Additionally, they can work as heterogenous recombinant proteins carriers. Compared with whole or live-attenuated pathogen, the absence of genomic material makes VLPs safer vaccines. Regarding the use of nanoparticles-based vaccines in coronaviruses, two SARS-CoV VLP vaccines based on hepatitis B virus and influenza particles, which express the S protein on their surface, have demonstrated to be immunogenic and protect against viral infection in preclinical studies[227,228]. Similarly, both chimeric and MERS-CoV VLPs generated using M, E and S proteins had also shown to be effective protecting from MERS-CoV infection[229,230].

Viral vector vaccines consist of modified viruses for encoding antigens of interest. Thus, during vaccination viral genomic material is delivered into the cells through infection and host cells will synthetize and present antigens[231]. Viral vector vaccines can be replicative and non-replicative, and may mimic natural infection inducing strong immune response without adjuvant. However, their manufacture is complicated and they have risk of viral genome integration in infected cells requiring extra safety steps[231]. Moreover, pre-existing vector immunity can limit the immune response to the antigen of interest[232,233]. Notably, the knowledge acquired during SARS-CoV and MERS-CoV viral vector research have been leveraged lately in SARS-CoV-2 vaccine development. Viral vector vaccines in SARS-CoV and MERS-CoV were based mainly on S protein. Several pre-clinical studies have demonstrated that adenoviral vectors are safe and elicit potent immune response and protection upon viral challenge for both coronaviruses[234–238]. Remarkably, one vaccine encompassing a chimpanzee adenoviral vector (ChAdOx1) and the MERS-CoV S protein induced high titers of neutralizing antibodies as well as cell-mediated

immunity[239] and provided protection in three different animals models[240–242]. Given these results, ChAdOx1 MERS-CoV vaccine was tested in humans. This vaccine was safe and well-tolerated by volunteers, and vaccine-elicited immune responses remained detectable in most cases after one-year[193]. Besides adenoviral vectors, a modified vaccinia virus Ankara (MVA) vector expressing SARS-CoV S or MERS-CoV S protein induced neutralizing antibodies and provided protection in different animal models[243,244]. In addition, MERS-MVA vaccine was proved in humans, where it showed to be safe and induced both humoral and cellular immune responses against MERS-CoV[194]. Additional viral vectors have been searched in SARS-CoV and MERS-CoV vaccine development, such as Venezuelan encephalitis equine virus and vesicular stomatitis virus[245,246], but none of them entered clinical phase.

Besides viral vector vaccines, nucleic acid platforms have also been used for coronaviruses vaccine development. Nucleic acid vaccines can be of two types, DNA or RNA which encode antigens of interest. Both use the host cell expression machinery to produce antigens and stimulate the immune system. Nucleic acid platforms show several advantages over other vaccine approaches, such as an ease manufacturability, and the preservation of the antigen native structure and post-translational modifications, since its production occurs in host cells as natural viral infection. However, nucleic acid requires the use of complex delivery vehicles to enhance its cell host uptake[247]. RNA system was not enough refined by the time SARS-CoV and MERS-CoV emerged, so only DNA platform were evaluated. Specifically, Yang et al. demonstrated that a DNA vaccine coding for the SARS-CoV S protein protects mice upon viral challenge[248]. Interestingly, this vaccine was well-tolerated in human, and induced neutralizing antibodies and T-cell responses[190]. DNA vaccine approach was also assayed with MERS-CoV vaccine with similar results. Muthumami and colleagues showed that full-length S protein-based DNA vaccine (GLS-5300) was immunogenic and protected against MERS-CoV infection in different animal models[249]. GLS-5300 vaccine was also tested in humans with promising results, without any vaccine-associated severe event and triggered immune response in most participants[192]. Additionally, MERS-CoV S1 subunit based-DNA vaccine elicited higher IgG titters compared to full-length S-DNA vaccine[250]. Besides the S protein, other structural proteins were evaluated with positive results, including N, M and E proteins[251–254]. Moreover, several studies have reported that heterologous prime-boost regimens enhance the DNA vaccine-induced immune responses compared to the homologous regimen[224,255,256].

3.2. The Global Race for the SARS-CoV-2 Vaccine.

Traditional vaccine development (**Fig.5A**) begins with a discovery phase in which vaccines are designed according to pathogen and infection knowledge, and initial immunogenicity and toxicity are evaluated in pre-clinical studies in animal models[257]. If results are promising, an investigational new drug application (IND) is submitted to regulatory agencies, such as the US Food and Drug Administration (FDA) and/or the Europe Medicines Agency (EMA)[258]. After approval, vaccines enter into clinical trial in humans, which can last up to 5-7 years. There are three consecutive clinical phases and each one has a different purpose[258]. In phase I, vaccine safety and immunization dose are tested in an open-label study with a small group of volunteers. Phase II trials involve a higher number of participants than phase I trials and are designed to confirm absence of vaccine-associated health risk and to perform pharmacokinetic and pharmacodynamic studies, as well as provide preliminary evidences of efficacy in target population[258,259]. Phase III has the main objective of confirming the efficacy of the vaccine in a broader population and evaluate the risk-benefit ratio. This later phase study is usually randomized and double-blind including not only a major number of volunteers, but also more heterogenous groups[258,259]. At the end of this phase, if results report a clear clinical efficacy without adverse events associated, biologics license application (BLA) is registered and reviewed by regulatory agencies, which finally authorize drug/vaccine use in humans[258]. After that, large-scale manufacturing and distribution begins. In some case a phase IV trial is required by competent organisms during commercialization state to confirm long-term effectiveness, as well as a better characterization of adverse effects ratio and new risk-associated which could appear in a large-scale study by years[258].

The SARS-CoV-2 health emergency have changed the traditional timeline for vaccine development moving to an accelerated model which allow to have available vaccines in one year after pandemic began[257] (**Fig.5B**). The knowledge acquired from the SARS-CoV and MERS-CoV vaccine development[257], and the rapid communication of SARS-CoV-2 genome made that SARS-CoV-2 vaccine development started rapidly[260].
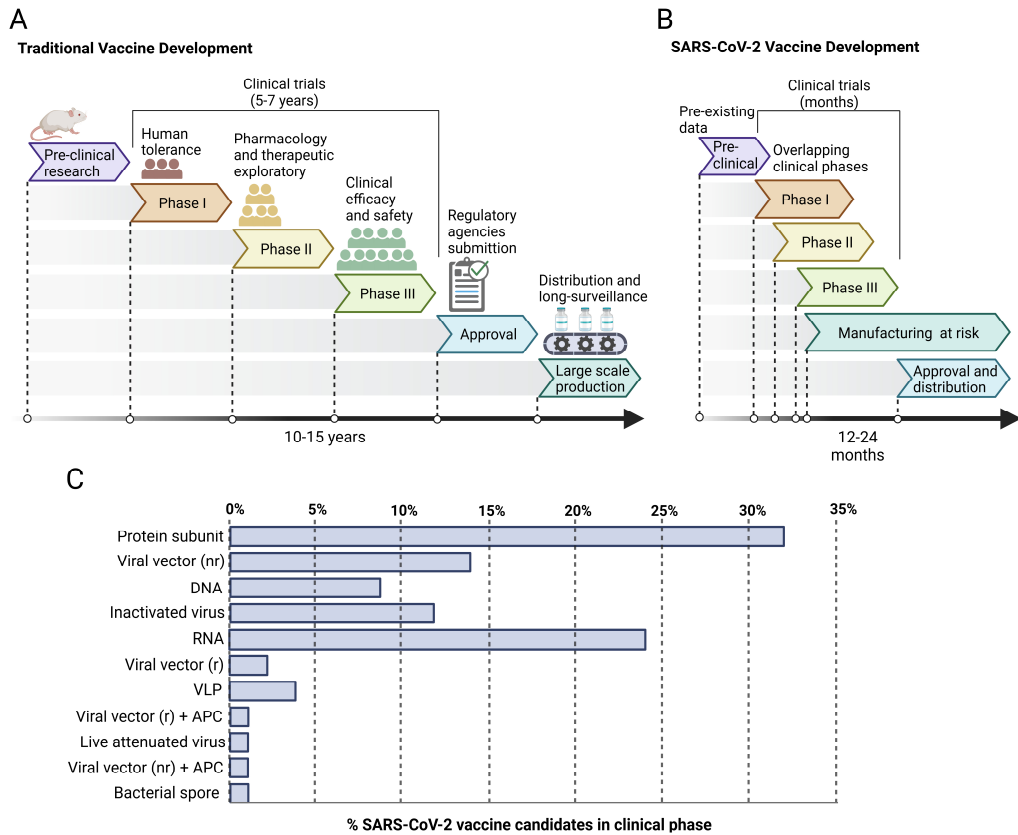
Figure 5. SARS-CoV-2 vaccine development. (A) Schematic diagram of the classical vaccine development pipeline, in which each phase begins after completing prior phases with acceptable results. All the process can take 10-15 years or more. **(B)** Accelerated COVID-19 vaccine development pipeline under the emergency situation of SARS-CoV-2 pandemic. Previous results in SARS-CoV and MERS-CoV shorten pre-clinical phase and clinical trials coincide in time. Furthermore, infrastructure arrangement and manufacturing start before authorization by regulatory medical agencies, assuming cost losses. All this adjustment made possible to develop SARS-CoV-2 vaccines in a record time (12-24 months after pandemic beginning). **(C)** Distribution of the 183 SARS-COV-2 vaccine which have reached clinical phase regarding the type of vaccine employed. According to WHO data at date 30/03/23. VLP = Virus like Particle, nr = non-replicating, r= replicating, and APC (antigen-presenting cell).

As soon as three to four months from the identification of SARS-CoV-2 as the causative agent of COVID-19, several SARS-CoV-2 vaccine candidates entered clinical phase[260]. Moreover, clinical phase followed a different schedule in order to reduce the time, with phase I and phase II trials being overlapped and phase III starting immediately after them or even coinciding with phase II[261]. In the meantime, vaccine manufacturing at large-scale was optimized and even began without results from phase III trials to be ready for a quick commercialization after being licensed[257,261]. Additionally, because of global health emergency, some vaccine

candidates received the Emergency Use Authorization (EUA) by regulatory agencies, which allowed their use in humans before having a formal approval. As results of these actions, SARS-CoV-2 vaccines were available in a record time (12 to 16 months)[261], which has helped to fight COVID-19 pandemic until nowadays, when COVID-19 does not constitute a public health emergency[262].

According to WHO, on March 30 of 2023 more than 300 SARS-CoV-2 vaccine candidates were under development[263]. A total of 183 vaccines based on several different platforms (**Fig.5C**) started clinical development[263], and 50 of them were approved or had emergency authorization use in almost one country[264]. Like SARS-CoV and MERS-CoV vaccines, most SARS-CoV-2 vaccine prototypes target the S protein. Currently, 15 vaccines have been granted Emergency Use Listing (EUL) by the WHO[265] and 8 vaccines are authorized in the European Union (EU) by the EMA, including one designed in Spain[266]. Here, we focused mainly on SARS-CoV-2 vaccines approved in the EU.

Live-Attenuated and Whole Inactivated Vaccines

Nowadays, there are 10 whole inactivated COVID-19 vaccines licensed in at least one country, while none live-attenuated COVID-19 vaccine have been authorized. Notably, a SARS-CoV-2 live-attenuated vaccine produced by Codagenix, known as COVI-VAC entered phase III clinical trial[264]. While results from phase I clinical trial demonstrated that the vaccine was well-tolerated and induced both serum and mucosal antibody responses[267], no data from Phase III have been published yet.

With regard to whole-inactivated vaccines, three received the EUL by WHO (CoronaVac, Covaxin and Covilo) and one by the EMA (VAL2001). All of them consist of 2 doses. Clinical trials have shown that they are safe and immunogenic, inducing antibodies as well as cellular immune responses[268]. Interestingly, the VAL2001 study reported a similar seroconversion ratio than the vector-viral vaccine AZD1222 (ChAdOx1, AztraZeneca), but higher neutralizing titters and a more diverse T cell response against other SARS-CoV-2 proteins beyond the S protein[269]. Covilo elicited lower antibody titters than the mRNA vaccine (BNT162b2) but comparable T cell responses[270]. Authorized whole-inactivated vaccines displayed effectiveness specially against severe COVID-19 and decreasing hospitalization ratio, with and overall efficacy of 75%[271]. However, efficacy ratio decreases with new SARS-CoV-2 variants, such as Covaxin and CoronaVac, which showed a reduction from 83% and 77.8% of efficacy to 59% and 65,2% respectively, against Delta variant[268].

Despite this efficacy decline, Mousa et al. reported that immunization with whole-inactivated vaccine (Covilo) still reduced the ratio of hospitalization compare with unvaccinated patients during Delta variant outbreak[272].

Protein Subunit Vaccines

Several SARS-CoV-2 proteins subunit vaccines have been developed but only one, Nuvaxovid (NVX-CoV2373), has received authorization by both FDA and EMA. Nuvaxovid, also known as Covovax, is produced by Novavax and consist of full-length S protein based on SARS-CoV-2 Wuhan-Hu-1 isolate genome[225]. Stable prefusion S protein was accomplished by mutating the furin cleavage site, as well as, by incorporating two proline substitutions at residues K986P and V987P (S-2P) based on Pallesen et al. research[65]. Protein is expressed and purified as transmembrane protein in insect cells[225]. In a phase 1/2 trial Nuvaxovid demonstrated that a two-dose regimen was sufficient to elicit more levels of antibodies and T cell responses than COVID-19 convalescent patients[273]. Vaccine efficacy was reported to be around 90% against symptomatic COVID-19 illness[274,275]. However, efficacy decreases against new SARS-CoV-2 variants, such as Alpha and Beta variants to 86% and 51%, respectively[274,276]. Despite that, Nuvaxovid still provides protection from severe disease and hospitalization[274,275].

Apart from Nuvaxovid, the EMA licensed recently other two protein subunit vaccines, VidPrevtyn Beta and Bimervax, which were developed in response to new SARS-CoV-2 variants. VidPrevtyn Beta created by Sanofi Pasteur, contains the S protein based on SARS-CoV-2 B.1.351 sequence (Beta variant). It includes the 2 prolines mutation (K986P and V987P) and a T4 foldon trimerization domain[277]. On the contrary, Bimervax, which is produced by the Spanish company HIPRA, consists of a recombinant RBD heterodimer from the B.1.351 (Beta) and B.1.1.7 (Alpha) SARS-CoV-2 variants[278]. Both clinical vaccine developments programs were focused mainly on determining their effectivity as booster vaccine. Heterologous booster with VidPrevtyn Beta was compared with homologous booster with Pfizer-BioNTech vaccine (mRNA) in individual previously vaccinated with 2 doses of Pfizer-BioNtech vaccine. Results showed that neutralizing titters against Omicron BA.1 and D614G SARS-CoV-2 variants were higher in the heterologous than homologous booster group[279]. Additionally, the boosting effect of VidPrevtyn Beta was independent from the primary vaccine administered, since it was also observed after Moderna (mRNA) and adenoviral vector (Astrazeneca and Janssen) vaccination[280].

Similar results were obtained with Bimervax, which induce superior neutralizing antibody response than homologous Pfizer-BioNTech vaccine booster against Beta, Omicron BA.1 and Delta SARS-CoV-2 variants throughout the clinical trial[281]. Additional studies are ongoing to determine whether Bimervax response may depend on the primary vaccine used. According to these results, both vaccines were authorized as a COVID-19 booster vaccine.

Viral Vector Vaccines

Currently, there are eight viral vectors SARS-CoV-2 approved vaccines, but only Vaxzevria (ChAdOx1 nCoV-19 by Oxford/Astrazeneca), Jcovden (Ad26.COV2.S by Janssen), and Convidecia (Ad5-nCoV by CanSinoBio) received EUL by WHO. More specifically, the two first were authorized by EMA, while only Jcovden were approved by FDA.

Vaxzevria is based on a non-replicating chimpanzee adeno vectored vaccine platform (ChAdOx1) previously used with MERS-CoV[242] and updating to encode codon-optimized full-length S protein from SARS-CoV-2. Two doses of ChAdOX1 nCoV-19 elicits both specific neutralizing antibodies and T cells response and show an overall efficacy of 75% in preventing symptomatic COVID-19[282,283]. Analysis of the vaccine efficacy during the SARS-CoV-2 Delta variant wave demonstrated that Vaxzevria remains effective against moderate and severe COVID-19[284]. Despite neutralizing titters decrease against Alpha, Beta, Kappa, and Delta compare to wild type SARS-CoV-2, the antigen-specific T-cell response was conserved against these VOCs[284]. Additionally, although it was reported that Vaxzevria efficacy decreases under 20% against some new SARS-CoV-2 variants like Omicron, a third homologous boost raises efficacy to 61% by increasing the immune response after primary vaccination[285]. Finally, no severe effects were found during clinical trials, but during active vaccination program some countries reported cases of a thrombocytopenia syndrome associated with ChAdOx1 nCov-19 vaccination[286]. Nevertheless, these cases were very rare (<1/10000) and the benefit of vaccination exceeded the risk and Vaxzevria remains authorized[287].

Jcovden consist of a non-replicating human adenoviral vector (Ad26) which delivers pre-fusion stabilized SARS-CoV-2 S protein with a mutated furin cleavage site and two proline substitution (K986P, V987P)[288]. In a preclinical experiment in which Mercado et al. tested seven Ad26 vector expressing different SARS-CoV-2 S

variants, results showed that the vector expressing the S variant with the two proline substitutions (S-2P) elicited the higher level of neutralizing antibodies and provide the maximum protection compared to the other constructs[288]. This vector (Ad26.CoV2.S) entered clinical trials and demonstrated that a single dose regimen was enough to trigger neutralizing antibodies in 96% of volunteers, with slightly antibody titters increment after second dose[289]. T-cell response was also induced in study participants in an age-dependent manner, being great in 18-55 years group[289]. In a phase 3 clinical trial, Jcovden was reported to protect against moderate and severe critical COVID-19 with an efficacy of 66% and 85%, respectively. While neutralizing antibodies responses was reduced against new variants, such as Beta and Omicron, T cell responses were preserved[290,291]. Moreover, although a homologous boost increased vaccine effectiveness against SARS-CoV-2 variants, such as Omicron, this increment was high when a heterologous booster with Pfizer/BioNTech or Moderna was performed (from 29% to 54%)[292]. In general, Ad26.CoV2.S is well tolerated, but as ChAdOX1 nCoV-19, it has also rarely associated-risk of thrombosis with thrombocytopenia syndrome[293].

Nucleic Acid Vaccines

SARS-CoV-2 nucleic acids-based vaccine includes both DNA and mRNA vaccines. Remarkably, nucleic acid vaccines have been licensed by the first time during the COVID-19 pandemic. Only mRNA vaccine has been authorized by the FDA and EMA, which include Comirnaty (Pfizer/BioNTech) and Spikevax (Moderna) vaccines. Both are mRNA vaccines encapsulated into lipid nanoparticles that code for a S-2P prefusion stabilized SARS-CoV-2 S protein.

Spikevax vaccine, also known as mRNA-1273, has an overall efficacy of 94% against COVID-19 after two doses administration[294] and elicits both humoral and cellular responses[295]. Antibodies kinetics was similar to convalescent patients[295] and vaccine protection still remains after 5 months after vaccination, with 93% efficacy against COVID-19 and 98% in preventing severe disease[296]. However, according to Berec et al., vaccine efficacy begins to decline beyond 5 months with a 65% efficacy at 7-8 month after second dose[297]. Additionally, since Spikevax use the S protein sequence from the ancestral SARS-CoV-2 WH-1 strain, the vaccine efficacy varies among SARS-CoV-2 variants. For example, the effectiveness against Delta variant decrease until 57%, and 42% in case of Omicron. Moreover, the avoidance of hospitalization during Omicron infection is about 74%. Nevertheless,

a third boosting dose reverses the decreasing trend and vaccine protection level returns to be maximum[297]. Despite that, as new SARS-CoV-2 variants compromise the mRNA-1273 vaccine effectiveness, new bivalent formulations of this vaccine, which include original S protein plus other S protein according to new variants sequence, have been under evaluation. Several of these adjustments entered clinical trial, but nowadays only mRNA-1273.214 (bivalent Original/Omicron BA.1) and mRNA-1273.222 (bivalent Original/Omicron BA.4-5) have been licensed, since Omicron variant showed the higher number of immune escape mutations. Both bivalent vaccines have demonstrated to induce higher neutralizing titters against Omicron variants than those elicited by the original mRNA-1273 vaccine[298–300].

Comirnaty vaccine, also called BNT162b2, which provides 95% of protection against SARS-CoV-2 according to phase 3 clinical trial following a two-dose regimen[301]. Pfizer/BioNTech vaccine is safe and induces high levels of both neutralizing antibodies and T cell responses than those found in convalescent COVID-19 patients. However, a waning of the immune response has been described among 3 and 6 months after second dose administration, which was associated with a decrease of vaccine efficacy over time[302,303]. Moreover, as well as other vaccines based on early SARS-CoV-2 isolated, Comirnaty efficacy decreases against SARS-CoV-2 variants, especially for Delta and Omicron variants, although this reduction is total or partially reversed by a third vaccine boost[304]. Despite that and similarly to SpikeVax vaccine, new BNT162b2 formulations including S protein sequence from Omicron variants have been developed to face immune scape mutations. Indeed, according to clinical trials, levels of neutralizing titters against Omicron were higher in patients which received bivalent vaccine than those with a fourth boost dose[305,306].

Regarding DNA vaccines, ZyCoV-D has been the first and only DNA-based vaccine licensed against SARS-CoV-2, although exclusively in India. It consists of a pVAX-1 DNA plasmid carrying full-length S protein. Pre-clinical data have showed that this vaccine elicited protective level of neutralizing antibodies and T cell response, as well as being well-tolerated[307]. According to phase 3 clinical trial, three doses of ZyCoV-D vaccine have a 66.6% efficacy against Delta SARS-CoV-2 infection[308].

3.3. SARS-CoV-2 Vaccine Challenges

SARS-CoV-2 vaccines development have been confronting numerous challenges. The first one is connected with the proper definition of vaccine, which works emulating the immune response elicited by natural infection. During SARS-COV-2 infection, both mucosal (secretory IgA) and systemic antibody response (IgG) are induced. Notably, Renegar et al. found that secretory IgAs play a major role protecting upper respiratory tract from influenza infection whereas IgGs prevent pathology in the lower respiratory tract[309]. Similarly, mucosal IgA response is crucial against SARS-CoV-2 as respiratory virus. Since intramuscular or intradermal vaccine administration elicits mainly systemic IgGs, and no secretory IgA response[310], this would leave upper respiratory tract vulnerable to infection. Thus, most SARS-CoV-2 vaccines induced a disease-preventing immune response, but not a sterilizing immunity. Hence, intranasally or orally delivered vaccines may provide local protection and prevent SARS-CoV-2 transmission. Mucosal vaccine administration has previously demonstrated to be effective against gastrointestinal and respiratory infections (e.g. poliovirus, rotavirus, adenovirus, and influenza)[311]. Notably, different vaccine platforms can be adapted to mucosal route[312]. Currently, China and India approved nasal COVID-19 vaccines[313], but whether these vaccines prevent viral transmission more efficiently than previous intramuscular vaccines continue unresolved. Additionally, vaccine-induced immunity has to face the emergence of new SARS-CoV-2 variants, which accumulate several immune scape mutations in the S protein, the antigen used by many current vaccines. Thereby, vaccine efficacy decreases progressively with each new SARS-CoV-2 variant. Moreover, both vaccine-induced immune response and natural immunity to SARS-CoV-2 follow a similar decreasing trend over time. Consequently, vaccine effectiveness against SARS-CoV-2 infection and symptomatic disease decreased concomitantly[314,315]. This waning of the vaccine-induced immune response may also compromise the protection against new viral variants[315]. A booster dose was proposed to face this trouble since it demonstrated to increase the protection levels to those obtained shortly after the second dose. Notably, even COVID-19 has been recently deescalated as an emergency public health, it still continues infecting and requires health surveillance and control[316]. Thus, as seasonal influenza vaccination program, COVID-19 vaccination may become annual including future dominant circulating variants[317]. However, this periodical booster program may create a high

demand of vaccines which bring to shortage in the availability of SARS-CoV-2 vaccines specially in low-income country, which may lead to the appearance and spread of new viral variants.

Nowadays, it remains uncertain how SARS-CoV-2 situation will evolve. Thanks to massive genome sequencing, researches have made a great idea of genetic mutation patterns that occurs in SARS-CoV-2 during pandemic. In this sense, Jaroszewski and colleagues found that genomic variations are restricted over these regions which not compromise structurally the protein function[318]. According to that, in the best of scenario structural constraint may not allow further mutations into the S protein region and future SARS-CoV-2 variants will be not more virulent[319]. Thus, current vaccines and specific treatments may be enough to finally eradicate SARS-CoV-2 over time. However, Amoutzias et al. propose other less promising scenarios regarding evolutionary data along all CoVs and SARS-CoV-2[319]. As the most probable situation, SARS-CoV-2 will continue evolving and giving rise to new variants or new strain with different infectious and immune features. In the worst and less probable of scenarios, SARS-CoV-2 may evolve by recombination with other Sarbecoviruses or Betacoronaviruses in animal reservoirs or humans, leading to a major virulent virus. Despite less probable, several studies pinpoint the ability of recombination among CoVs and the importance of this mechanism in their evolution[320–322]. Since immune cross-reactivity against SARS-CoV-2 have been found in patients infected by other HCoVs[323], the immunity elicited by current SARS-CoV-2 vaccines and natural infection are expected to be enough to deal with future variants or strains. However, as occur with previous SARS-CoV-2 variants (e.g. Delta, Omicron), novel strains could accumulate genetic variations that translate in a reduction of immune response efficacy. Hence, in any of these last scenarios current vaccines and treatments will require a rapid adaptation to new strains using the knowledge acquire during and after SARS-CoV-2 pandemic in the CoVs research field.

HYPOTHESIS AND OBJECTIVES

Hypothesis

Nowadays, it is unknown if SARS-CoV-2 vaccines should be adapted to new SARS-CoV-2 variants or vaccination will be included in seasonal vaccination programs like flu vaccine. However, since periodical administration is being considered by worldwide health organizations, a high demand of current or adapted SARS-CoV-2 vaccines will continue in the near future.

Most current SARS-CoV-2 vaccines consist of the full-length S protein stabilizing in its prefusion conformation by two prolines substitution (K986P and V987P). This double mutation increases protein yield, as well as, immunogenicity in comparison to original S protein. However, S protein with two prolines (S-2P) still retains some structural instability that may hamper their production and immunogenicity[64]. Since RBD is the major target of neutralizing antibodies during natural infection, the major or minor RBD exposure would affect the antigenicity of the full S trimer. Thus, in the present work we hypothesized that new mutation approaches could further stabilized the S trimer, increasing its yield, as well as RBD exposure and, consequently, improve S-trimer immunogenicity of future novel SARS-CoV-2 vaccine formulations.

Objectives

The main aim of this project is to explore the effect of novel S protein-stabilizing mutations on the immunogenicity and prophylactic activity of SARS-COV-2 S trimers.

The specific objectives to fulfill this aim are:

Objective I: To design novel S-stabilizing mutations *in silico*.

Objective II: To evaluate the yield and RBD exposure of produced S trimer-mutants.

Objective III: To produce and purify the selected S trimer mutants.

Objective IV: To evaluate the immunogenicity and efficacy of selected mutated S-trimers in animal models challenged with different SARS-CoV-2 strains.

MATERIAL AND METHODS

1. Recombinant trimeric Spike glycoprotein design and modelling

Unsolved secondary structures of the trimer in closed (PDB: 6VXX) and open (PDB: 6VYB) conformations[324] were reconstructed using SwissModel[325]. Then, all possible single mutations in both conformations were modelled using FoldX[326]. For selecting potential variants, two different approaches were used. First, we computed the Gibbs free energy change ($\Delta\Delta G_{open}$) between the WT and the mutant using the open state as a reference. Negative values indicate introduction of stabilization. Second, comparison of the Gibbs free energy changes upon mutation between the closed ($\Delta\Delta G_{closed}$) and open ($\Delta\Delta G_{open}$) conformations ($\Delta\Delta G$) revealed a set of mutations predicted to strengthen the open conformation (positive values indicate stabilization of the open state). For both approaches, all single mutations predicting beneficial energies (or just slightly neutral/worst values) were addressed by inspecting the three-dimensional models. In this regard, the final selection was based on: i) selection of mutations predicted to increase the stability of the open-conformation using FoldX; ii) selection of mutations predicted to increase the stability of the open-conformation over the closed one using FoldX, iii) selection of mutations creating well-defined intermolecular interactions between the RBD domains (including hydrophobic bonds, π-π interactions and cation-π interactions, ionic bonds, hydrophobic contacts or cavity filling mutations) that would exert a positive impact in the open state or a negative one on the closing motion of the trimer.

2. Recombinant protein production and purification

The design of recombinant Spike glycoprotein is based on the one described by Wrapp[61]. Briefly, the C-terminal end of the extracellular portion of the S glycoprotein was fused to a T4-foldon trimerization domain followed by an 8xHis tag and a strep tag II. The furin cleavage site was removed by mutating it to GSAS. DNA constructs were supplied by GeneART (ThermoFisher Scientific) in a pcDNA3.4 backbone. Proteins were produced by transient transfection using the Expi293 expression system (ThermoFisher Scientific), following the manufacturer instructions. Cell culture supernatants were harvested five days after transfection, clarified by centrifugation (3000xg for 20 minutes) or using Sartoclear Dynamics® Lab V (Sartorius) and filtered at 0.2 μm using Nalgene Rapid-Flow sterile single use vacuum filter units (ThermoFisher Scientific). Equivalent transfection efficiency was obtained for all the tested S variants. Proteins were purified by Immobilized Metal

Affinity Chromatography (IMAC) using the Ni-Sepharose Excel histidine-tagged protein purification resin (Cytiva). Purified proteins where concentrated and buffer exchanged to phosphate buffer saline by ultrafiltration (Merck Millipore) and stored at -80°C until use. Purified proteins were quantified by ELISA. Briefly, Nunc MaxiSorp ELISA plates were coated overnight at 4°C with 100 ng/well of HIS.H8, an anti-6xHis monoclonal antibody, in PBS (ThermoFisher Scientific). The following day, plates were blocked with PBS/1% of bovine serum albumin (BSA, Miltenyi BiotecBiotec) for two hours at room temperature. Commercial His-Spike (Sino Biological) was used as standard, starting at 1µg/ml and eight 1/3 serial dilutions. S variants were prepared in blocking buffer at 1/10 serial dilution for quantification. Samples were incubated overnight at 4°C. After that, plates were washed and incubated for 2 hours at room temperature with rabbit anti-SARS-CoV-2 Spike S2 IgG (SinoBiological) at 1/1000 dilution. Then, the HRP conjugated donkey anti-rabbit IgG (H+L) antibody (Jackson ImmunoResearch) at 1/10000 dilution was used as detection antibody. Plates were revealed with o-Phenylenediamine dihydrochloride (OPD) (Sigma-Aldrich) and stopped using 4N of H_2SO_4 (Sigma- Aldrich). The signal was analyzed as the optical density (OD) at 492 nm with noise correction at 620 nm.

Integrity and purity of purified proteins were analyzed by sodium dodecyl sulfate polyacrylamide gel electrophoresis (SDS-PAGE) and Coomassie G-250 staining (ThermoFisher Scientific).

3. Viral stock isolation and titration

In vivo challenge experiments were performed using Cat01 SARS-CoV-2 D614G and Cat24 SARS-CoV-2 B.1.351 variants. Both SARS-CoV-2 variants were isolated from a nasopharyngeal swab from a COVID-19 patient, as previously described[327,328]. Viral isolates were subsequently grown in Vero E6 cells (ATCC CRL-1586) cultured in Dulbecco's modified Eagle medium (Invitrogen) supplemented with 10% fetal bovine serum (FBS; Invitrogen), 100 U/mL penicillin, 100 µg/mL streptomycin (all from Invitrogen). Genomic sequencing was performed from viral supernatant by using standard ARTIC v3 or v4 based protocols followed by Illumina sequencing (dx.doi.org/10.17504/protocols.io.bhjgj4jw). Raw data analysis was performed by viralrecon pipeline (https://github.com/nf-core/viralrecon) while consensus sequence was called using samtools/ivar at the 75% frequency threshold. SARS-CoV-2 D614G variant (EPI_ISL_510689) and SARS-CoV-2 B.1.351

variant (originally detected in South Africa; EPI_ISL_1663571) sequences were deposited at GISAID. Viral stock was titrated in 10-fold serial dilutions on Vero E6 cells to calculate the TCID50 per mL.

4. In vivo immunization and challenge experiments.

All animal procedures were performed under the approval of the Committee on the Ethics of Animal Experimentation of the IGTP and the authorization of Generalitat de Catalunya (Code: 10965 and 11094). Prophylactic activity of the recombinant S-2P, S-V987H, S-21, and S-29 trimeric proteins and a recombinant monomeric RBD against SARS-CoV-2 D614G (Cat01 isolate) and SARS-CoV-2 B.1.351 (Cat24 isolate) was assessed in B6. Cg-Tg(K18-ACE2)2Prlmn/J (K18-hACE2) mice (stock #034860, Jackson Laboratories) and Golden Syrian hamsters (GHS) (Envigo). The mice colony was maintained by breeding K18-hACE2 hemizygotes with C57BL/6J mice following the instructions of Jackson Laboratory (https://www.jax.org/strain/034860). Mice genotyping was performed according to the protocol 38170: Probe Assay – Tg (K18-ACE2) 2Prlmn QPCR version 2.0 (https://www.jax.org/Protocol?stockNumber=034860&protocolID=38170).The GSH colony was maintained by brother/sister mating. Both mice and GSH colonies were stablished at the Centre for Comparative Medicine and Bioimage (CMCiB).

For the SARS-CoV-2 D614G challenge, 68 K18-hACE2 mice (50%male/50% female, 7-9 weeks old) were distributed in five experimental groups: S-2P (n=16), V987H (n=14), RBD (n=15), infected positive controls (n=19) and unvaccinated/uninfected negative control (n=4). Sixty-eight GSH (were distributed in S-2P, S-V987H, RBD and infected positive controls (n=16/group) and unvaccinated/uninfected negative control (n=4). Mice and GSH from the S-2P, S-V987H and RBD groups were DNA-immunized by electroporation in the quadricep posterior. Forty microgram of plasmid coding for the corresponding immunogens were used. Animals were electroporated using a NEPA21 electroporator and tweezer electrodes (Nepagene). Two (for mice) or four (for GSH) weeks later, DNA-immunized animals received a boosting dose consisting of 15µg of recombinant protein adjuvanted with adjust-Phos (Invivogen) in the hock[329]. Control animals were primed with an empty vector and boosted with PBS+Adjust-Phos. Two weeks (mice) or ten days (GSH) after boosting, animals were intranasally challenged with 1000 (mice) or 10000 (GSH) $TCID_{50}$ of SARS-CoV-2 (Cat01 isolate) and followed up for 7

days. Weight and clinical signs were monitored daily after infection. Four animals for each experimental group, except for uninfected controls, were euthanized before challenge and on days 2, 4 or 7 post infection. Uninfected controls were euthanized on day 7 post-infection and only two mice from groups S-V987H and RBD were euthanized before challenge. However, any animal that showed a reduction of weight higher than 20%, a drastic reduction of mobility or a significant reduction of the response to stimuli were euthanized according to the humane endpoints defined in the supervision protocol. Biological samples were collected after euthanasia, including oropharyngeal swab, nasal turbinate, lung, and brain (only in the case of mice) to determine viral loads and perform histopathological analysis. Blood samples were collected before each immunization and viral challenge, and at euthanasia. Blood was left at room temperature for two hours for clotting and serum was collected after centrifugation (10 minutes at 5000xg) and stored at -80ºC until use.

The SARS-CoV-2 B.1.351 (Beta) VoC challenge was used in two different immunization experiments: (1) S-2P/S-V987H and (2) S-2P/S-21/S-29. For the first experiment group (1) 70 K18-hACE2 mice (50% male-female) were distributed as follows: S-2P (n=21), S-V987H (n=21), infected positive controls (n=16) and unchallenged controls (n=10). Mice from S-2P and S-V987H groups were immunized twice (spaced three weeks between both doses) with 15µg of recombinant protein adjuvanted with AddaVax (Invivogen) in the hock. Control mice received only PBS+AddaVax. Two weeks after the booster, mice from groups S-2P, S-V987H and challenged-controls were inoculated intranasally with 1000 TCID50 of SARS-CoV-2 Beta VoC (Cat24 isolate). For the second immunization experiment group (2) 91 K18-hACE2 mice (balanced female-male ratio, 7-9 weeks old) and 49 GSHs (~50% male-female ratio, 5-7 weeks old) were used. Mice were distributed in five experimental groups: S-2P (n=21), S-21(n=22), S-29 (n=22), unvaccinated and challenged controls (n=16), and uninfected negative controls (n=10). GSHs were distributed in five experimental groups: S-2P (n=11), S-21 (n=11), S-29 (n=11), unvaccinated and challenged controls (n=11), and uninfected negative controls (n=5). Both mice and hamsters from S-2P, S-21, and S-29 groups were immunized with 15 µg of recombinant protein with AddaVaxTM (Invivogen) as adjuvant in the hock Three weeks later, immunized animals were boosted with a second dose of the same formulation. Control animals were primed and boosted with PBS and

AddaVaxTM. Two weeks after boosting, mice were challenged with 1000 TCID50 of SARS-CoV-2 (Cat24 isolate) and followed up for 14 days. GSHs were challenged three weeks after boosting with 10000 TCID50 of SARS-CoV-2 (Cat24 isolate) and followed up for 7 days. After infection, body weight and clinical signs were monitored daily until the end of the experiment. Six mice for each experimental group, except the uninfected controls, were euthanized on days 3 and 6. The remaining mice were followed up until day 14 post-infection. Three and four hamsters from each experimental group, except the uninfected control group, were euthanized on days 2 and 4, respectively. The remaining GSHs were euthanized on day 7 post infection. In both challenge experiments, uninfected control group was euthanized at the end of the experiment. Biological sample collection and prosecution was made as SARS-CoV-2 D614G experiment description.

5. Quantification of anti-S and anti-RBD antibodies by ELISA

IgG antibodies elicited against the Spike and RBD glycoproteins were determined using and in-house ELISA in serum samples obtained from animals before each immunization and before viral challenge. In addition, humoral response was also evaluated in serum samples obtained from animals euthanized on days 2, 4, 7 after viral challenge or after humane endpoint. One half of a Nunc MaxiSorp ELISA plate was coated overnight at 4°C with 50 ng/well of antigen in PBS (Spike or RBD, Sino Biologicals). The other half-plate was incubated only with PBS. Then, the whole plate was blocked using PBS/1% of bovine serum albumin (BSA, Miltenyi Biotech) for two hours at room temperature. Mouse standards were prepared as seven 1/3 dilution of the anti-6xHis antibody HIS.H8 (ThermoFisher Scientific), starting at 1 μg/mL. GSH standard was prepared similarly but using a positive GSH serum with the initial dilution at 1/100. All standards and samples were diluted in blocking buffer. After blocking, 50 μL of each standard or diluted samples were added to the antigen coated and antigen free wells in duplicate and incubated overnight at 4°C. Each plate contained samples from all experimental groups. Plates were run in parallel to reduce inter-assay variability. After sample addition, plates were incubated overnight at 4°C. The HRP conjugated (Fab)2 Goat anti-mouse IgG (Fc specific) (1/20,000), or Goat anti-hamster IgG (H+L) (1/20,000) (all from Jackson ImmunoResearch) were used as detection antibodies for mouse and GSH IgG

determination, respectively. Plates were revealed with o-Phenylenediamine dihydrochloride (OPD) (Sigma-Aldrich) and stopped using 4N of H_2SO_4 (Sigma-Aldrich). The signal was analyzed as the optical density (OD) at 492 nm with noise correction at 620 nm.

The specific signal for each sample was calculated after subtracting the background signal obtained in antigen-free wells. Data is shown as arbitrary units (AU) according to the standard used.

6. Neutralization activity of serum samples

The neutralizing activity of serum samples was determined using Human Immunodeficiency Virus (HIV) reporter pseudoviruses expressing SARS-CoV-2 S protein and Luciferase as described by Pradenas et al[330]. In brief, pseudoviruses were produced by co-transfecting Expi293F cells (ThermoFisher Scientific) with the pNL4-3.Luc.R-.E- (NIH AIDS Reagent Program[331]) and several SARS-CoV-2.SctΔ19 plasmids that code for the Spike glycoprotein of the WH1, Beta, Delta or Omicron variants. A VSV-G plasmid was used for the generation of VSV-G-pseudoviruses that were used as negative control. Transfections were performed using the ExpiFectamine293 Reagent kit (ThermoFisher Scientific). After 48h, supernatants were harvested, filtered at 0.45 µm and frozen at -80ºC until use. Pseudoviruses were titrated on HEK293T cells overexpressing human ACE-2 (HEK293T/hACE2) (Integral Molecular).

Serum samples were inactivated at 56ºC for 60 minutes before use. Inactivated samples were 1/3 serially diluted in cell culture medium (DMEN, 10% fetal bovine serum) (range 1/100–1/24300) before mixing with 200 TCID50 of SARS-CoV-2 derived pseudoviruses and incubated for 1 hour at 37ºC. Then, $2x10^4$ HEK293T/hACE2 cells treated with DEAE-Dextran (Sigma-Aldrich) were added. After 48 hours BriteLite Plus Luciferase reagent (PerkinElmer) was added and the results read in an EnSight Multimode Plate Reader. Data were calculated using a 4-parameters logistic equation in Prism 8.4.3 (GraphPad Software) and showed as normalized ID50 (reciprocal dilution inhibiting 50% of the infection). This assay has been previously validated with a replicative viral inhibition assay[176].

7. Viral Load quantification in oropharyngeal swab and tissue samples

Oropharyngeal swabs and samples from nasal turbinate, lung and brain (only mice) were collected immediately after euthanasia in 1.5 mL Sarstedt tubes containing DMEM media supplemented with penicillin (100 U/mL) and streptomycin (100 μg/mL). Tissue samples were homogenized twice at 25 Hz for 30 sec using a TissueLyser II and a 1.5 mm Tungsten bead (QIAGEN). After centrifugation for 2 min at 2,000xg, supernatants were collected and stored at -80 °C until use.

RNA was isolated using the Viral RNA/Pathogen Nucleic Acid Isolation kit and a KingFisher instrument (ThermoFisher Scientific), or an IndiMag pathogen kit (Indical Bioscience) on a Biosprint 96 workstation (QIAGEN) following manufacturer's instructions.

PCR amplification in mice was based on the 2019-Novel Coronavirus Real-Time RT-PCR Diagnostic Panel guidelines and protocol developed by the American Center for Disease Control and Prevention (tps://www.fda.gov/media/134922/download). Briefly, a 20 μL PCR reaction was set up containing 5 μL of RNA, 1.5 μL of N2 primers and probe (2019-nCov CDC EUA Kit, Integrated DNA Technologies) and 10 μl of GoTaq 1-Step RT-qPCR (Promega, Madison). Thermal cycling was performed at 50ºC for 15 minutes (min) for reverse transcription, followed by 95°C for 2 min and then 45 cycles of 95°C for 10 seconds (s), 56°C for 15s and 72ºC for 30s in the Applied Biosystems 7500 or QuantStudio5 Real-Time PCR instruments (ThermoFisher Scientific). For absolute quantification, a standard curve was built using 1/5 serial dilutions of a SARS-CoV2 plasmid (2019-nCoV_N_Positive Control, 200 copies/μL, Integrated DNA Technologies) and run in parallel in all PCR determinations. The viral load of each sample was determined in triplicate and mean viral load (in copies/mL) was extrapolated from the standard curve and corrected by the corresponding dilution factor.

Mouse *gapdh* gene expression was measured in duplicate for each sample using TaqMan gene expression assay (ThermoFisher Scientific) as amplification control.

SARS-CoV-2 genomic RNA (gRNA) detection in GSH was performed based on RT-PCR described by Corman et al.[332], which was adapted to the AgPath-ID One-Step RT-PCR kit (Life Technologies). This RT-PCR targets a fragment of the envelope protein gene using the following primers (Forward: 5′-ACAGGTACGT TAATAGTTAATAGCGT-3′; Reverse: 5′-ATATTGCAGCAGTACGCACACA-3′) and probe (5′-FAM-ACACTAGCCATCCTTACTGCGCTTCG-TAMRA-3′). Thermal cycling was performed at 55°C for 10 min for reverse transcription, followed by 95°C for 3 min and then 45 cycles of 94°C for 15s, 58°C for 30s. Results are shown as cycle threshold (Cts).

8. Pathology and immunohistochemistry

SARS-CoV-2 NP was detected by immunohistochemistry (IHC) using the rabbit monoclonal antibody 40143-R019 (Sino Biological) at 1:15,000 dilution. For immunolabelling visualization, the EnVision®+ System linked to horseradish peroxidase (HRP, Agilent-Dako) and 3,3′-diaminobenzidine (DAB) were used. The amount of viral antigen in tissues was semi-quantitatively scored as indicated in[333,334]. The following score was used: 0: No antigen detection, 1-low, 2-moderate and 3- high amount of antigen (**Fig.6A**). Nasal turbinate and lung from mice and GSH, and brain from mice were collected on days 0 (before viral challenge), 2, 4, 7 or at clinical endpoint after viral challenge, fixed by immersion in 10% buffered formalin and embedded into paraffin blocks. The histopathological analysis was performed on slides stained with hematoxylin/eosin and examined by optical microscopy. A semi-quantitative scored based on the level of inflammation (0-No lesion; 1-Mild, 2-Moderate or 3-Severe lesion) was established (**Fig.6B**) based on previous classifications[333,334].
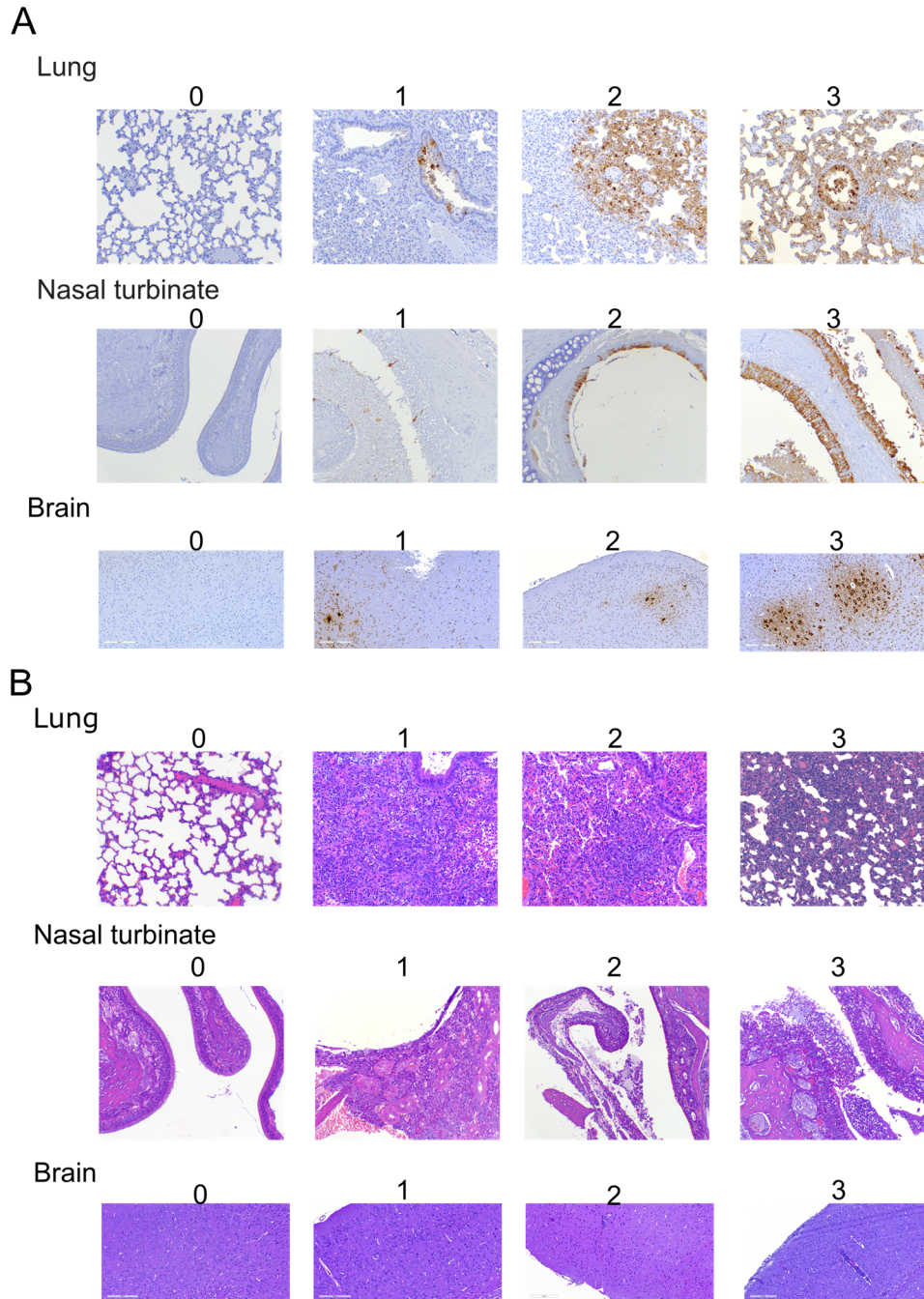
Figure 6. Semi-quantitative histopathologic lesion and immunohistochemistry scoring. Indicated tissues were fixed by immersion in 10% buffered formalin and embedded into paraffin blocks. **(A)** The levels of SARS-CoV-2 nucleoprotein in lung, nasal turbinate and brain slides were determined by immunohistochemistry. Numbers indicate the score assigned to each antigen amount. **(B)** Tissue slides stained with hematoxylin/eosin. Numbers indicate the score assigned to each tissue lesion severity.

9. Statistical analysis

Anti-S and anti-RBD IgG data, as well as neutralizing activity differences among groups at each time point were analyzed using Kruskal-Wallis and Conover's post-hoc tests with multiple comparison correction by using false discovery rate (FDR). Differences among animals within a particular group along time were analyzed using the Friedman test and Conover's post-hoc tests for paired data and corrected for multiple comparison by FDR. Weight variation in SARS-CoV-2 challenged mice over time was analyzed using Kruskal-Wallis corrected by Dunn's test. Severe disease incidence was represented by Kaplan-Meier plots, and Mantel-Cox test was implemented to calculated statistical differences against uninfected group. Levels of SARS-CoV-2 gRNA in tissues were analyzed using Peto & Peto left-censored k sample test corrected by FDR. Histopathology analysis was carried out using Asymptotic Generalized Pearson Chi-Squared test with FDR correction. P values are indicated as follows: * $p<0.05$, ** $p<0.01$, *** $p<0.001$, **** $p<0.0001$, and p values close to statistical significance are shown as number. Statistical analyses were conducted using the R (version 4.1) software environment and GraphPad Prism v8.0.

RESULTS

SECTION I. Immunization with V987H-Stabilized Spike Glycoprotein Protects K18-hACE2 and Golden Syrian Hamster upon SARS-COV-2 Infection

Most SARS-CoV-2 vaccines are based on a mutated version of the Spike glycoprotein (K986P/V987P (S-2P)) with improved stability, yield and immunogenicity. However, S-2P is still produced at low levels. Here, we described a novel V987H mutation that increases by two-fold the production of the recombinant Spike and the exposure of the receptor binding domain (RBD). S-V987H immunogenicity was similar to S-2P in K18-hACE2 mice and golden Syrian hamsters, and superior to a monomeric RBD. Immunization with S-V987H, but not with S-2P or RBD, conferred full protection against severe disease in both animal models after SARS-CoV-2 challenge (D614G and B.1.351 variants). Furthermore, S-V987H immunized K18-hACE2 mice showed a faster tissue viral clearance than RBD- or S-2P-vaccinated animals. Thus, S-V987H protein provides an alternative to S-2P for future SARS-CoV-2 vaccine development.

1.Identification of S Glycoprotein Mutations that Constrain the Motility of RBD

The native SARS-CoV-2 S trimer possess some structural flexibility that affects its stability and immunogenicity[61,335,336]. In addition to pre- and post-fusion S conformations, each RBD displays a dynamic equilibrium between open (up) and closed (down) configurations. In this regard, we aimed to design S variants with a preference for adopting the closed state, and thus, showing limited opening motion and RBD exposure. To this end, we envisioned a computational pipeline involving the three-dimensional modeling of all possible single mutations for both open and closed states, followed by the estimation of changes in their Gibbs free energy ($\Delta\Delta G$) (**Fig.7a**). We focused on all single mutations showing a strong predicted preference for the closed-state ($\Delta\Delta G < -1$ kcal/mol) and among them, only those that clearly generated well-defined interactions (hydrogen bonds, ionic interactions of filling hydrophobic pockets) between the RBDs of the trimer were screened. We selected a total of 11 single mutations (A372W, K386R, G416R, D420R, D420Y, D427I, L517Y, S982F, D985L, V987H, and V987W) (**Fig.7A**). We also included one double

mutation (A372W-D420R) referred as 2M, and a combined quintuple mutation (D198F-G232L-A372W-N394Q-D420R) named 5M. Locations of the selected mutations are represented in **Fig.7B**.
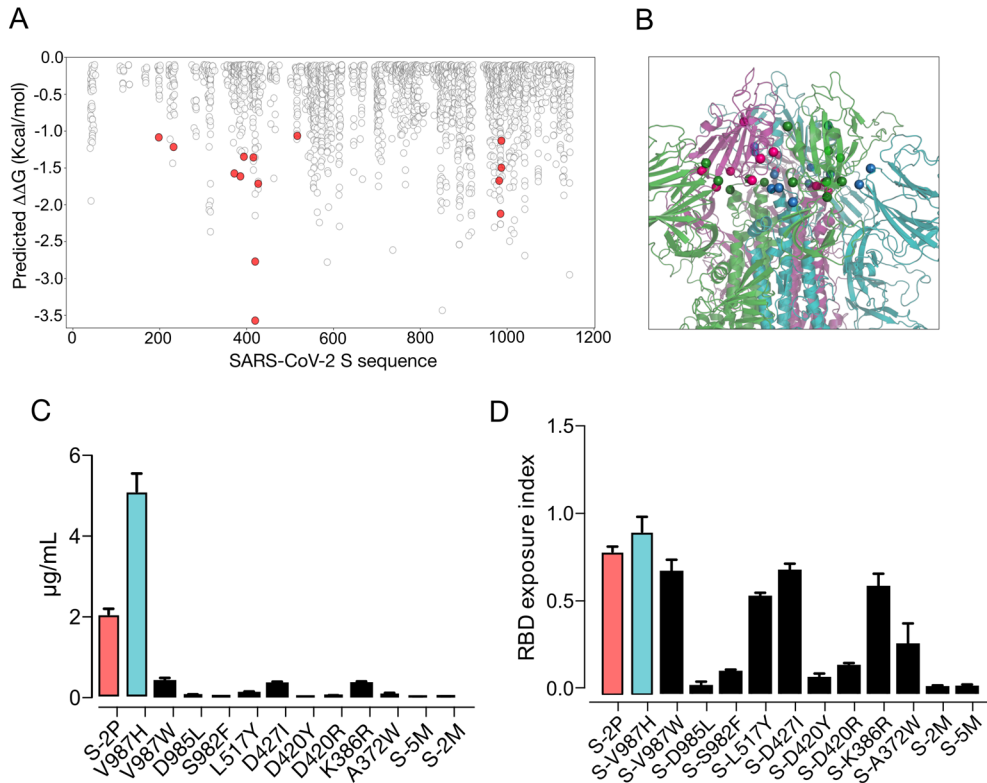

Figure 7. Selection of mutations that stabilized the S glycoprotein in a closed conformation. An *in silico* saturation mutagenesis study was performed for selecting mutations that could stabilize the S glycoprotein in a closed conformation. The production of selected variants and the exposure of the RBD was evaluated by ELISA. **(A)** Saturation mutagenesis of the SARS-CoV-2 S glycoprotein. Mutations selected for experimental characterization (with a favorable predicted ΔΔG < -1 Kcal/mol and showing stabilizing interactions between the RBDs in the closed conformation) are colored depending on the mutant residue. Labeled mutations were selected for experimental characterization. **(B)** Three-dimensional location of the selected mutations (displayed as dots and colored by their belonging monomer) in the closed state of the SARS-CoV-2 S glycoprotein (PDB:6VXX). Mutations are in multiple domains of the S glycoprotein, including NTD, CDT1, CDT2 and HR1-CH region. **(C)** Levels of recombinant S proteins in a 5-day cell culture supernatant of transiently transfected Expi293F cells. Mean plus standard deviation of three experiments are shown. **(D)** RBD exposure index in selected recombinant S proteins. Data are shown as ratio between RBD binding and total protein. Mean plus standard deviation of three experiments are shown. S-2P and S-V987H recombinant proteins are shown in red and blue, respectively.

Recombinant mutant proteins were expressed by transient transfection in Expi293F cells, and their production was evaluated by ELISA (**Fig.7C**). Most variants displayed a substantial decrease in production when compared to the S-2P trimer (**Fig.7C**).

Then, we analyzed the exposure of the RBD by ELISA using a Fc fusion protein containing the extracellular portion of the human ACE2 receptor fused to the human IgG1-Fc domain. The results confirmed that most of the variants were in fact promoting a closed trimer conformation (**Fig.7D**) as it was predicted by our *in silico* pipeline. Moreover, variants associated with a reduced exposure of the RBD also resulted in a very low production. In contrast, the V987H mutation promoted the exposure of the RBD (**Fig.7D**) and showed higher production than the S-2P protein (2.5-fold). Thus, our results suggest that the RBD exposure may be associated with S production levels.

2. S-V987H Trimer Vaccination Protects K18-hACE2 mice from SARS-CoV-2 Infection-Associated Disease.

It has been described that K986P and V987P mutations stabilize and increase the expression and immunogenicity of the Spike glycoprotein[61,336]. Since the V987H mutation improved Spike trimer production and RBD exposure, we evaluated whether it could impact the Spike antigenicity *in vivo.* Thus, we compared the immunogenicity and protective capacity of the recombinant S-2P, S-V987H and RBD (**Fig.8A**) after SARS-CoV-2 D614G challenge in K18-hACE2 mice (**Fig.8B**).

Forty-five K18-hACE2 mice were immunized using a prime-boost immunization strategy (**Fig. 8B**). In addition to S-V987H (n=14), we determined the immunogenicity of S-2P (n=16), and a recombinant monomeric RBD protein (n=15). Mice were first immunized by DNA electroporation with 40 µg of plasmid. Two weeks later, animals were boosted with the corresponding purified recombinant protein (15µg) formulated with aluminum phosphate as adjuvant. Prior to challenge, four mice from S-2P and control groups, two mice from S-V987H and three mice from RBD groups were euthanized to collect tissue samples. Then, 12 vaccinated mice for each group, and 16 unvaccinated controls were intranasally challenged with SARS-CoV-2 D614G (**Fig. 8B**). Four mice (two male/two female) from each group were euthanized on days 2, 4 and 7 (end of the experiment) post-challenge (**Fig.8B**) to analyze the humoral immune responses, viral replication in target organs, and tissue damage. Mice that developed severe SARS-CoV-2 induced disease and/or showed a weight reduction higher than 20% of the initial weight were euthanized before the end of the experiment (day 7) as a humane end point. Four additional unvaccinated mice were used as uninfected controls.
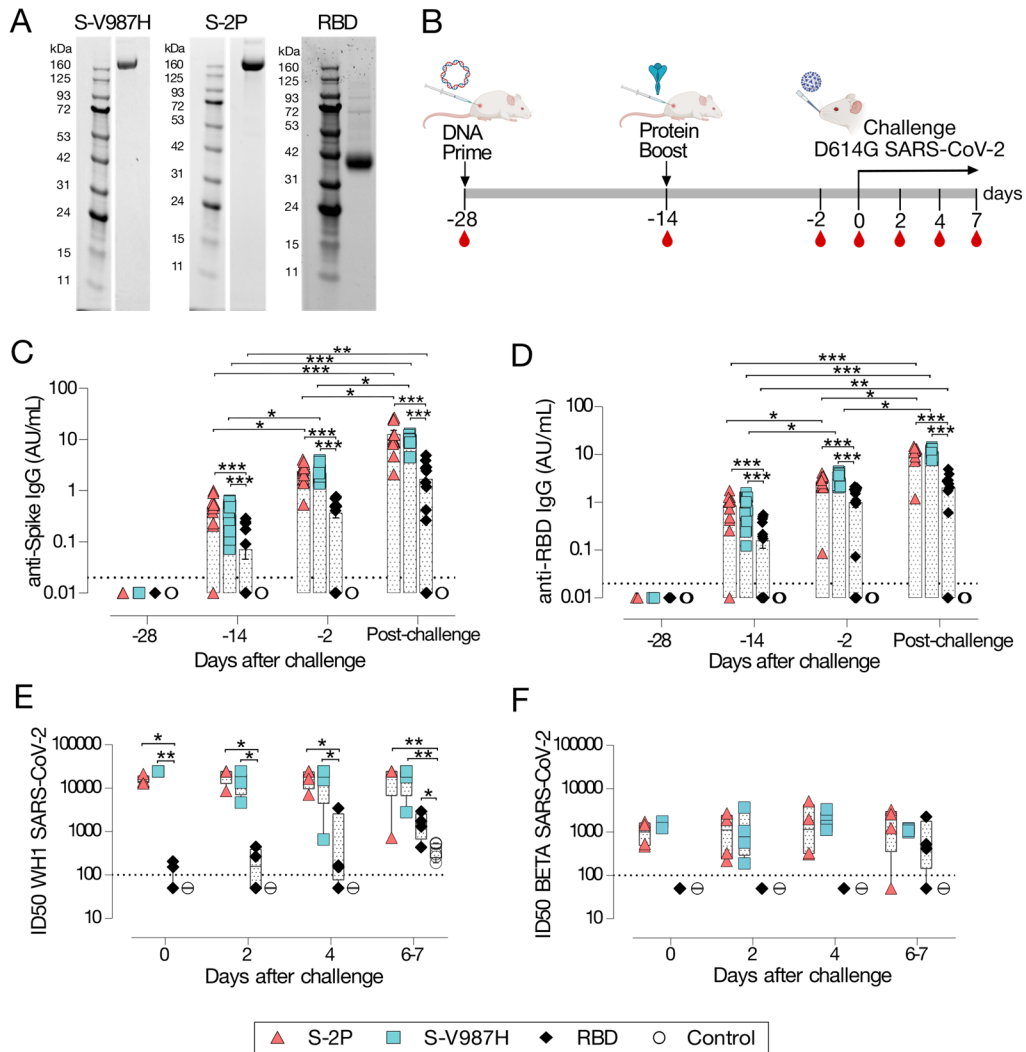
Figure 8. Prophylactic activity of S-V987H immunization and analysis of the humoral response elicited in vaccinated K18-hACE2 mice challenged with the SARS-CoV-2 D614G variant. (A) Purified S-V987H, S-2P, and RBD were analyzed by SDS-PAGE and Coomassie G-250 staining. **(B)** Overview of vaccination strategy and infection timeline. Blood drops indicate collection of biological samples. Red triangles: S-2P group (n= 16). Blue squares: S-V987H group (n= 14). Black diamonds: RBD (n=15). White circles: unvaccinated mice (n=19). **(C)** Kinetics of anti-S IgG and **(C)** anti-RBD IgG in serum samples express as arbitrary units (AU) per mL. **(E)** Levels of neutralizing antibodies against SARS-CoV-2 WH1 and **(F)** SARS-CoV-2 B.1.351 (Beta) variant after viral challenge. Groups in each time point were analyzed using Conover Iman test with multiple comparison correction by FDR. Differences among animals within a particular group along time were analyzed using the Friedman test corrected for multiple comparison using FDR. Mean plus standard errors of the means (SEM) are shown. * p<0.05, ** p<0.01, *** p<0.001.

The humoral responses elicited against the S protein (**Fig.8C**) and the RBD (**Fig.8D**) were evaluated before each immunization (days -28 and -14) and viral challenge (day -2), and in the mice euthanized on days 2, 4 and 7 after infection. At all-time points, mice immunized with S-V987H and S-2P showed similar levels of anti-RBD and anti-Spike IgG antibodies, which were greater than those observed in RBD vaccinated animals ($p<0.001$, Conover-Iman test) (**Fig.8C and D**). For simplification purposes, challenged animals were grouped as a "post-challenge" group (**Fig.8C and D**). The levels of anti-RBD and anti-Spike IgG antibodies in the S-2P and S-V987H groups increased after boost and viral challenge ($p<0.05$, Conover-Iman test) (**Fig. 8C and D**), while mice immunized with RBD only presented increased levels of these antibodies after viral challenge ($p<0.05$, Conover-Iman test), indicating that infection may further boost humoral responses in vaccinated mice (**Fig. 8C and D**).

In addition, we evaluated level of neutralizing antibodies against the Wuhan-Hu-1 (WH1) strain and Beta (B.1.351) variant after SARS-CoV-2 challenge. Both S-2P or S-V987H mice groups developed equivalent titers of neutralizing antibodies against SARS-CoV-2 WH1, but significantly higher than those measured in the RBD immunized group (**Fig.8E**) $p<0.05$, Conover-Iman test). However, only S-2P and S-V987H vaccinated mice had systemic neutralizing activity against the Beta VoC prior to challenge (**Fig.8F**). The progressive increase in the levels of total IgG antibodies and/or neutralizing antibodies observed in both RBD and control-challenged groups after infection (**Fig. 8E and F**) also supports the idea of a boosting of the humoral response after virus challenge.

To assess the ability of each immunogen to prevent SARS-CoV-2 infection-associated disease, we measured weight evolution in all groups as an indicator of disease progression in this model[333]. We identified weight reduction on day 5 post-infection in mice belonging to infected-control and RBD groups, which is opposed to S-2P and S-V987H vaccinated groups ($p<0.05$, Kruskal-Wallis corrected by Dunn's test) (**Fig. 9A**). On day 6 and 7, all animals from the inoculated-control group (n=4), one out of four S-2P vaccinated mice, and two out of four RBD immunized mice had to be euthanized due to disease development (**Fig.9B**); $p<0.05$ compared to control-infected group, Log-rank test) Mice from the S-V987H group did not show clinical signs of disease during the entire experimental procedure ($p<0.01$ compared to control-infected group, Log-rank test) (**Fig.9A and B**).
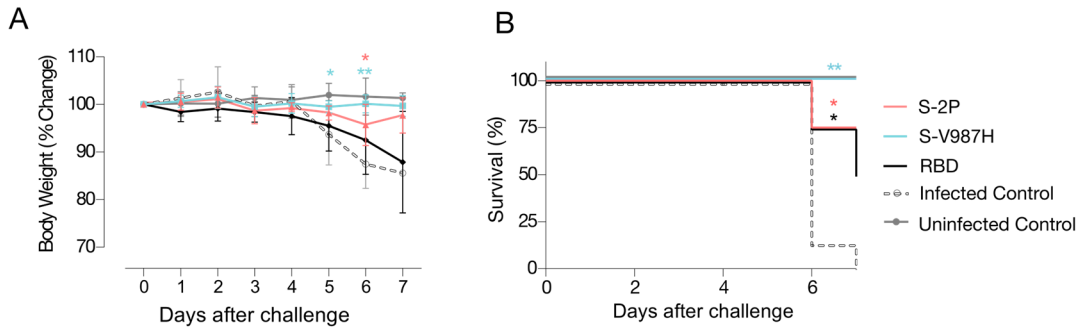
Figure 9. Surveillance of vaccinated K18-hACE2 mice challenged with SARS-CoV-2 D614G. **(A)** Percentage of weight variation in SARS-CoV-2 D614G-infected K18-hACE2 mice over time. Statistical analysis was performed comparing each vaccinated group with the unvaccinated group using KrusKal-Wallis corrected by Dunn's test. **(B)** Kaplan-Meier plot showing the survival rate during the course of the experiment. Statistical analysis was performed against unvaccinated group using Mantel-Cox test. * $p<0.05$, ** $p<0.01$. Red line: S-2P group (n= 16). Blue line: S-V987H group (n= 14). Black line: RBD (n=15). Gray line: unvaccinated/uninfected mice (n=4). White border line: unvaccinated/infected mice (n=19).

In addition to the clinical course, we measured the levels of viral replication by RT-qPCR in four samples (**Fig.10A-D**): oropharyngeal swab, nasal turbinate, lung, and brain. Although the levels of genomic RNA (gRNA) in oropharyngeal swabs decreased in all groups over time, only S-V987H vaccinated mice became undetectable on day 7. On the contrary, S-2P and RBD vaccinated mice remained positive (Fig. 3a, $p<0.05$ Peto & Peto Left-censored k sample test). Similar results were observed in nasal turbinates (**Fig.10B**), where gRNA was lower in S-2P and S-V987H groups compared to control-infected mice or the RBD group on days 6-7 after viral challenge, and the S-V987H group showed the lowest values by day 7. Interestingly, low levels of gRNA were detected in lung and brain from S-V987H immunized mice (lung $p=0.055$, brain $p<0.05$, Peto & Peto Left-censored k sample test) (**Fig.10C and D**), whereas a progressive increase was observed in brains from the infected-control and RBD groups, and in the only S-2P vaccinated mouse that developed disease (**Fig.10C and D**).

To confirm active viral replication, we analyzed N protein levels in tissues by immunohistochemistry (IHC). NP was detected in lung and brain of both control and RBD groups; and in one animal from S-2P group that developed the disease, but not in S-V987H or disease-free S-2P-vaccinated mice after challenge (**Fig.11A**) ($p<0.05$ asymptotic generalized Pearson Chi-Squared test corrected for multiple

comparison using FDR). Low IHC scores were observed in nasal turbinate on days 2 and 4 with no major differences among study groups (**Fig.11A**). Tissue damage was in line with the levels of viral antigens detected by IHC (**Fig.11B**). No tissue damage was observed in lung or brain of mice vaccinated with S-2P and S-V987H, except for the S-2P mouse that became sick (**Fig.11B**). A low lesion score was observed at early time points after challenge in nasal turbinate of all infected mice (**Fig. 11B**).
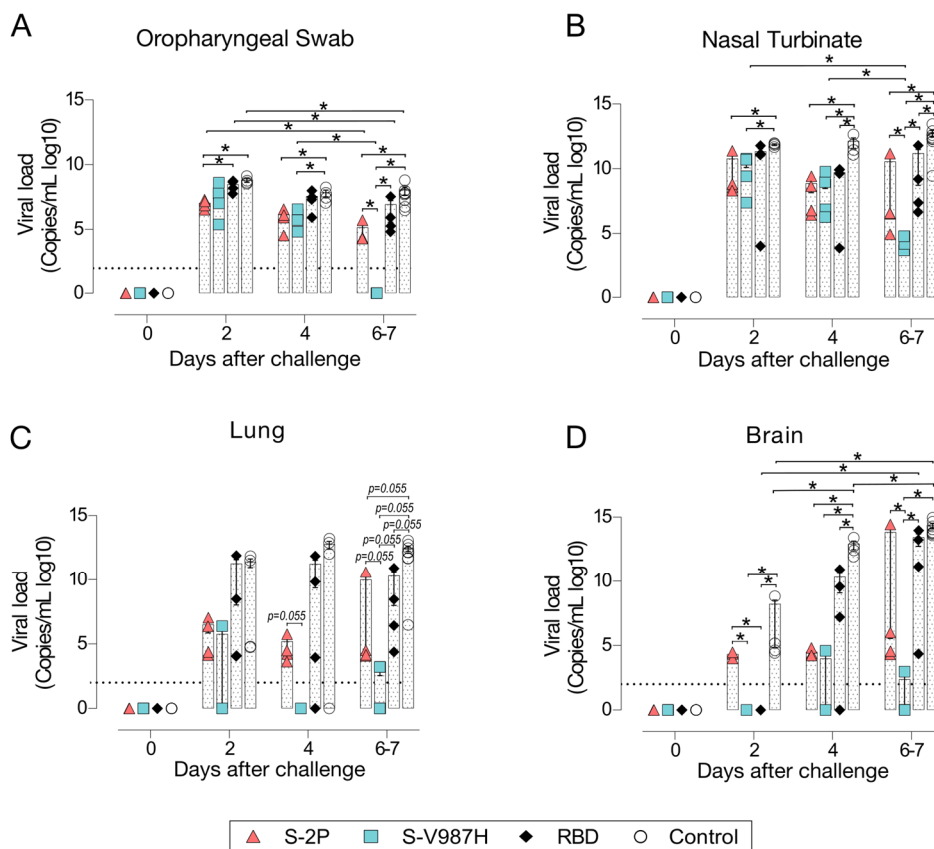
Figure 10. Viral load of tissue samples from SARS-CoV-2 D614G infected K18-hACE2 mice after vaccination. SARS-CoV-2 viral load was analyzed in oropharyngeal swabs, and samples from nasal turbinate, lung, and brain of K18-hACE2 mice upon challenge. Virus distribution and tissue damage were analyzed by histopathology. Levels of SARS-CoV-2 gRNA (expressed as logarithmic of copies/mL) in **(A)** oropharyngeal swabs, **(B)** nasal turbinate, **(C)** lung, and **(D)** brain during infection. Dot line indicates limit of detection (100 copies/mL). Differences between animals were analyzed using Peto & Peto left-censored k sample test, correcting by FDR. * $p < 0.05$. P values proximal to statistical significance are shown as numbers.
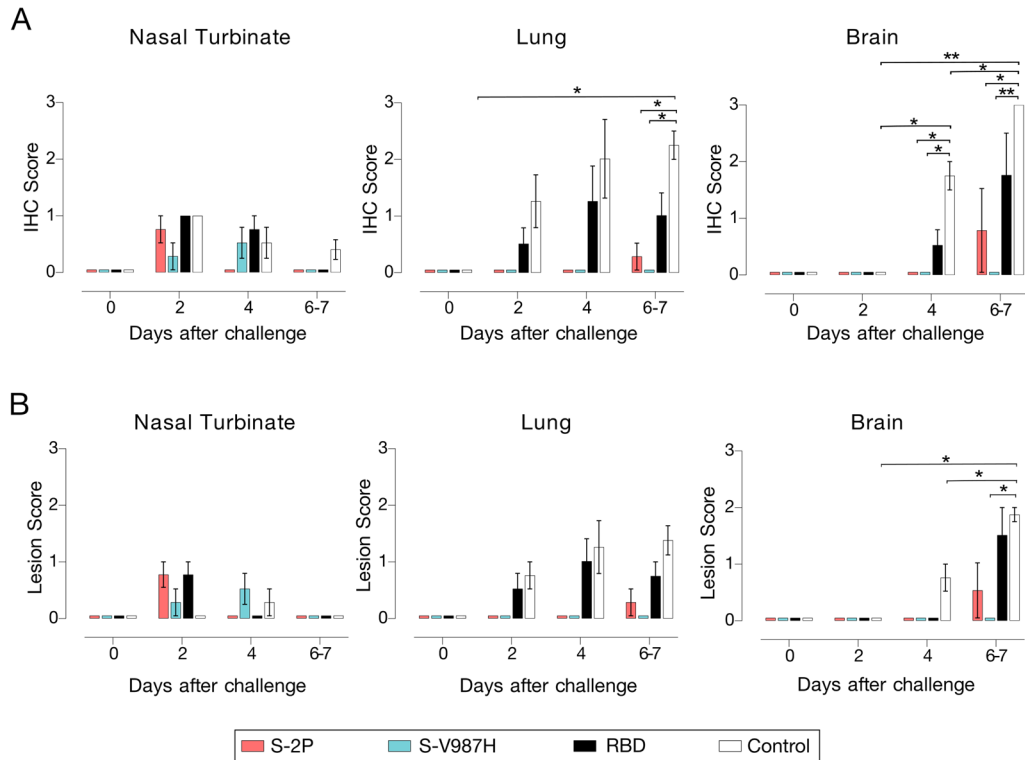
Figure 11. Histopathological analysis of tissue samples from immunized K18-hACE2 mice after challenge with SARS-CoV-2 D614G. Physiological analysis was performed in nasal turbinate, lung, and brain of K18-hACE2 mice upon challenge. Virus distribution and tissue damage were analyzed by histopathology. **(A)** Detection of SARS-CoV-2 N protein in brain, lung, and nasal turbinate by immunohistochemistry. Staining score: (0) no, (1) low, (2) moderate, and (3) high amount of viral antigen. **(B)** Histopathological analysis of nasal turbinate, lung and brain by hematoxylin and eosin staining. Lesion score: (0) no, (1) mild, (2) moderate, and (3) severe lesion. Differences between groups were analyzed using Asymptotic Generalized Pearson Chi-Squared test with FDR correction. * $p < 0.05$, ** $p < 0.01$.

Overall, the immunogenicity of both S-2P and S-V987H trimers was equivalent in K18-hACE2 mice, and greater than the produced by the monomeric RBD immunogen. However, S-V987H vaccination improved mice protection against SARS-CoV-2 D614G variant over the S-2P immunogen, since all mice in S-V987H group were disease free and showed a faster viral clearance in tissues.

3. S-V987H Trimer Vaccination Protects Golden Syrian Hamsters from SARS-CoV-2 infection-associated disease

To confirm the results obtained in the transgenic mouse model, we performed a second experiment using golden Syrian hamster (GSH). Similar to K18-hACE2 mice, GSH were immunized using a prime-boost strategy, and intranasally challenged with SARS-CoV-2 D614G (**Fig.12A**). Animals were monitored until day 7 post-inoculation, since it has been described that animals start spontaneously recovering around a week after viral infection[334,337].

The magnitude of the humoral responses elicited against the S (**Fig.12B**) and the RBD (**Fig.12C**) by both S-2P and S-V987H trimers was similar and greater than those elicited by the RBD immunogen. The levels of anti-RBD and anti-S IgG antibodies increased after each immunization and after viral challenge ($p<0.05$, Friedman test) (**Fig.12B and C**), confirming the results obtained in K18-hACE2 mice. However, unlike mice, infected-control GSHs rapidly developed an anti-S humoral response after challenge, showing similar levels of anti-S and anti-RBD antibodies on day 7 to those observed in animals immunized with the RBD protein (**Fig.12B and C**). When the neutralizing activity of serum samples was analyzed, we observed that GSHs immunized with S-2P or S-V987H proteins neutralized the WH1 variant and, to a lesser extent, the Beta VoC (**Fig.12D and E**). The neutralizing activity against WH1 increased overtime after challenge in all study groups ($p<0.05$, Conover-Iman test). Neutralization of WH1 was also detected in sera from infected control animals by day 4 after challenge, and their titers rapidly increased, becoming similar to the ones observed in S-V987H and RBD groups, and higher than those observed in S-2P vaccinated animals by day 7 ($p<0.05$, Conover-Iman test). Intriguingly, despite all groups showed similar titers of neutralizing antibodies on day 7 after challenge, the levels of anti-RBD and anti-S binding antibodies (**Fig.12B and C**) were higher in the S-2P and S-V987H immunized groups than in infected-controls GSH. These results support that SARS-CoV-2 infection induced a rapid humoral response against SARS-CoV-2 in GSH that may be qualitatively different to the one elicited by immunization.

We then evaluated the clinical course after challenge. Animals in both control and RBD groups showed a progressive weight reduction until day 7 (end of the experiment) indicative of disease progression (% of weight in infected controls=

87.3 ± 3.1; RBD group= 84.4±1.4) (**Fig.12F**). Such weight loss was not observed in S-2P (98.9 ± 1.3) or S-V987H (98.76 ± 2.4) vaccinated GSH (p<0.05 Kruskal-Wallis corrected by Dunn´s test). Thus, both S trimers generated equivalent protection from disease development in vaccinated GSH (**Fig. 12F**).
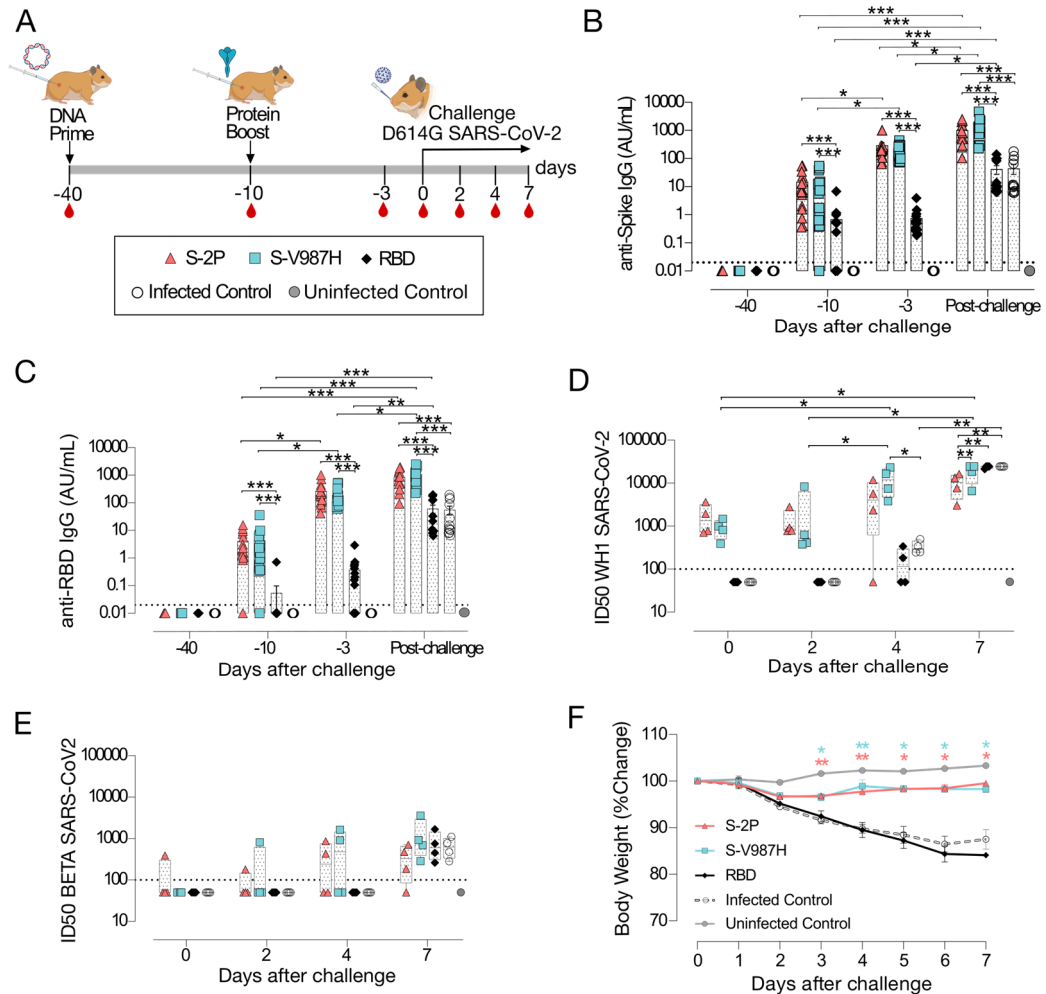
Figure 12. **Prophylactic activity of S-V987H immunization and analysis of the humoral response elicited in vaccinated golden Syrian hamsters challenged with the SARS-CoV-2 D614G variant. (A)** Outline of vaccination strategy and infection timeline. Blood drops indicate collection of biological samples. **(B)** Kinetics of anti-S antibodies and **(C)** anti-RBD antibodies in serum samples. Red triangles: S-2P group (n= 16). Blue squares: S-V987H group (n= 16). Black diamonds: RBD (n=16). White circles: unvaccinated and challenged GSH (n=16). Grey circles: unvaccinated and uninfected GSH (n=4). **(D)** Sera neutralizing activity against SARS-CoV-2 WH1 and **(E)** SARS-CoV-2 B.1.351 (Beta) variants after viral challenge. Antibody levels and neutralizing titters among groups in each time point were analyzed using Conover-Iman test with multiple comparison correction by FDR. Differences among animals within a particular group along time were analyzed using the Friedman test with FDR correction. **(F)** Percentage of weight variation in SARS-CoV-2 D614G-infected GSH over time. Statistical analysis was performed against the unvaccinated group using Krustal-Wallis correcting by Duns test. * p<0.05, ** p<0.01, *** p<0.001.

The presence of SARS-CoV-2 was determined by RT-qPCR in oropharyngeal swabs and respiratory tissue samples (nasal turbinate and lung). Brain was not evaluated in GSHs since SARS-CoV-2 does not affect the brain in this animal model [338]. Despite the levels of gRNA decreased over time in all analyzed samples, we detected lower gRNA levels in nasal turbinate of both S-2P and S-V987H groups on day 4 compared to the RBD and infected-control groups (Fig. 5; $p<0.05$, Peto & Peto Left-censored k sample test). Remarkably, contrary to the RBD or infected-control groups, gRNA was undetectable on day 7 post-infection in S-2P and S-V987H immunized GSHs (**Fig.13**). No major differences were detected in the levels of gRNA in oropharyngeal swabs among the study groups (**Fig.13**). Interestingly, lower levels of gRNA were detected in lungs of S-2P and S-V987H vaccinated animals than in the RBD and infected-control groups on days 2 and 4 (**Fig.13**).
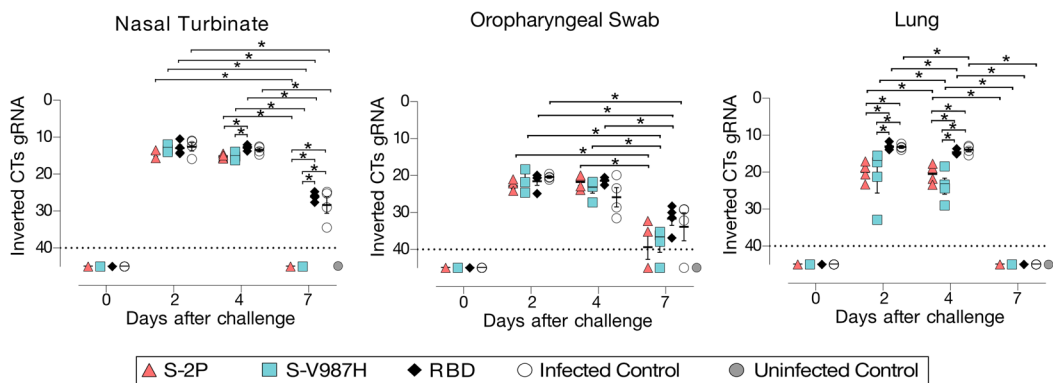
Figure 13. **Viral load on tissue samples from SARS-CoV-2 D614G infected golden Syrian hamsters after vaccination**. SARS-CoV-2 viral load was analyzed in oropharyngeal swabs, and samples from nasal turbinate and lung of infected GSHs. Virus distribution and tissue damage was analyzed by histopathology. Levels of SARS-CoV-2 gRNA, expressed as cycles threshold (CTs), in oropharyngeal swabs, nasal turbinate and lung during infection. Dot line indicates limit of detection (CTs≥40). Differences between groups were analyzed using Peto & Peto left-censored k sample test with FDR correction. * p<0.05.

Viral RNA detection results were in line with the levels of N protein detection by IHC (**Fig.14A**). No major differences in N protein levels were observed among study groups at any time points in nasal turbinate, becoming undetectable by day 7 (**Fig.14A**) (p<0.05, Asymptotic Generalized Pearson Chi-Squared Test). However, lower NP levels were detected in lungs of both S-2P and S-V987H vaccinated groups when compared with RBD and infected controls on days 2, 4 and 7. Interestingly, N protein was not detected in lungs on day 7 in S-2P and S-V987H

groups (**Fig.14A**). All study groups showed a similar lesion degree in nasal turbinate, which decreased by day 7 after challenge (p<0.05). By contrast, a lower tissue damage was observed in lung from S-V987H (on days 4 and 7) and in S-2P (on day 7) groups compared to RBD and infected control groups (p<0.05) (**Fig.14B**).

Overall, our results showed that the immunogenicity and protective efficacy of both S-2P and S-V987H trimers are equivalent in GSHs, and higher than the one conferred by RBD vaccination.
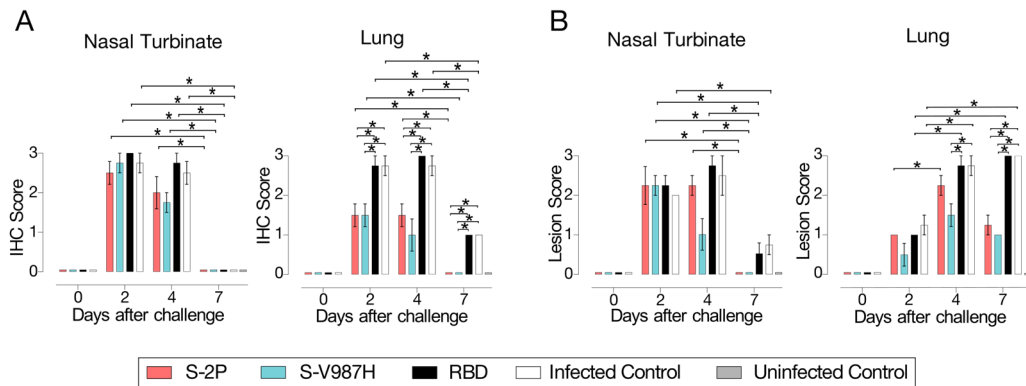
Figure 14. Histopathological analysis of tissues samples from vaccinated golden Syrian hamsters challenged with SARS-CoV-2 D614G. (A) Detection of SARS-CoV-2 N protein in lung and nasal turbinate by immunohistochemistry. Staining score: (0) no, (1) low, (2) moderate, and (3) high amount of viral antigen. **(B)** Histopathologic analysis of nasal turbinate and lung by hematoxylin and eosin staining. Lesion score: (0) no, (1) mild, (2) moderate, and (3) severe lesion. Differences between groups were analyzed by the Asymptotic Generalized Pearson Chi-Squared test corrected using FDR. * p<0.05.

4. S-V987H Vaccination Protects K18-hACE2 Mice from SARS-CoV-2 Beta Variant Challenge.

From the beginning of the COVID-19 pandemic, several SARS-CoV-2 VoC have emerged. These VoC have shown different transmissibility, pathogenic potential and resistance to antibodies previously elicited by vaccination or natural infection[339]. The results described above have shown that S-V987H-vaccinated animals were protected from COVID-19 development after SARS-CoV-2 D614G strain challenge. Additionally, vaccinated animals showed low sera neutralizing activity against the SARS-CoV-2 Beta variant. Since the Beta VoC is one of the most resistant to antibodies elicited by natural infection and the currently available vaccines[180], and also induces severe disease in K18-hACE2 mice[340], we evaluated whether the immune responses induced by S-V987H could protect against disease development

after challenge with the SARS-CoV-2 Beta variant. Thus, we immunized twenty-one K18-hACE2 mice with S-V987H or S-2P, using AddVax as adjuvant in this homologous prime-boost experiment (**Fig.15A**). Unvaccinated mice were used as negative (n=10) and positive (n=16) controls of infection. Two weeks after receiving the protein boost, mice were challenged with the SARS-CoV-2 Beta variant (Fig.15). Six mice from each challenged group were euthanized on days 3 (n=6) and 6 (n=6) after infection. The remaining animals were euthanized on day 14 after challenge, excepting those mice that developed severe disease after day 3 (10 in the infected-control group and one in the S-2P group) that were euthanized before day 14 following the humane endpoints of the protocol and analyzed separately.
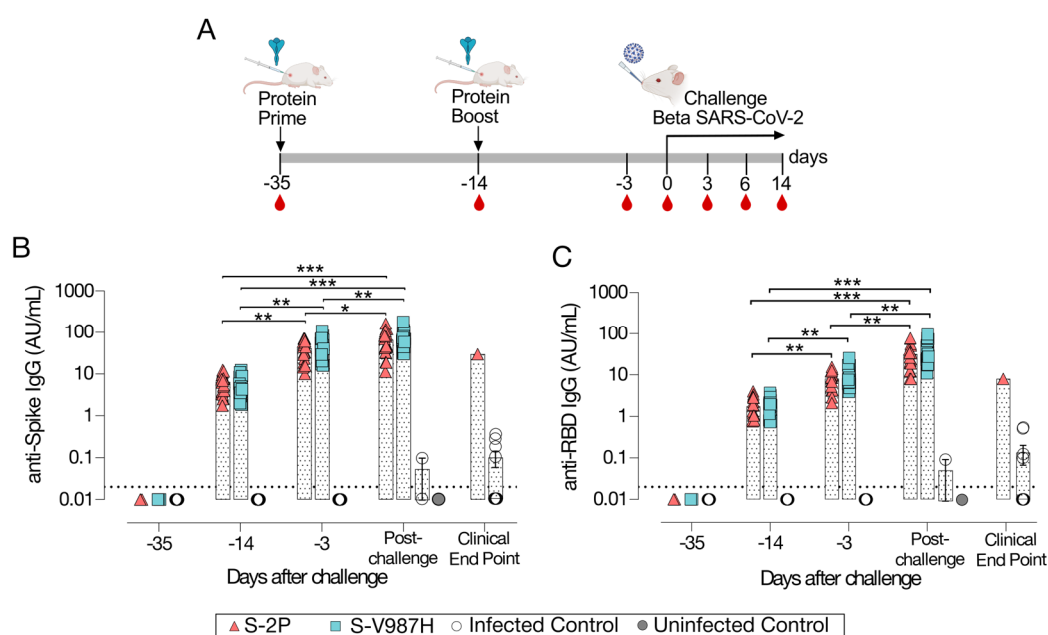
Figure 15. Humoral response elicited in vaccinated K18-hACE2 mice challenged with the SARS-CoV-2 B.1.351 (Beta) variant (A). K18-hACE2 mice were immunized twice with S-V987H (n=21) or S-2P (n=21), adjuvanted with AddaVax. Then, mice were challenged with the SARS-CoV-2 B.1.351 VoC. Two control groups were established: unvaccinated-challenge mice (n=16) and unvaccinated-uninfected mice (n=10). Blood drops indicate collection of biological samples. **(B)** Kinetics of anti-S antibodies and **(C)** anti-RBD antibodies in serum samples. Red triangles: S-2P group. Blue square: S-V987H. White circle: unvaccinated-challenge mice. Grey circles: uninfected mices. Groups in each time point were analyzed using Conover-Iman test with multiple comparison correction by FDR. Differences among animals within a particular group along time were analyzed using Friedman test with FDR correction. *p<0.05, **p<0.01, *** p<0.001, **** p<0.0001. Mean plus standard errors of the means (SEM) are shown.

Of note, both S-2P and S-V987H recombinant proteins induced similar levels of IgG antibodies against the S and the RBD, which increased after each boost and after viral challenge ($p<0.05$, Conover-Iman test) (**Fig.15B and C**). Interestingly, three days

after challenge, S-V987H immunized mice showed higher sera neutralizing activity against the WH1 (n=6; 15376±9203) (**Fig.16A**), and the Delta VoC (n=6; 7750±8403) (**Fig.16C**) than mice immunized with the S-2P (n=6; WH1: 2913±3524; Delta: 1505±4773) (WH1: $p<0.01$; Delta: $p=0.055$; Conover-Iman test). Neutralizing activity against the Beta VoC increased after challenge ($p<0.05$, Conover-Iman test) (**Fig.16B**). In addition, we identified an increasing trend in sera neutralizing activity against Omicron over time ($p=0.055$, Conover-Iman test) (**Fig.16D**). These differences suggest that the humoral responses elicited after S-2P or S-V987H immunization evolved after challenge with the SARS-CoV-2 Beta variant, increasing neutralizing activity against Beta and Omicron VoC, as well as against Delta in the case of the S-2P group. Interestingly, neutralizing activity against the Beta VoC was detected in control-infected mice at clinical endpoint (**Fig.16B**) with little or no cross-neutralization activity with other variants (**Fig.16A,C and D**). No statistical differences in neutralizing activity were observed on days 6 and 14 between S-V987H and S-2P groups for any of four SARS-CoV-2 variants evaluated (**Fig.16A-D**).
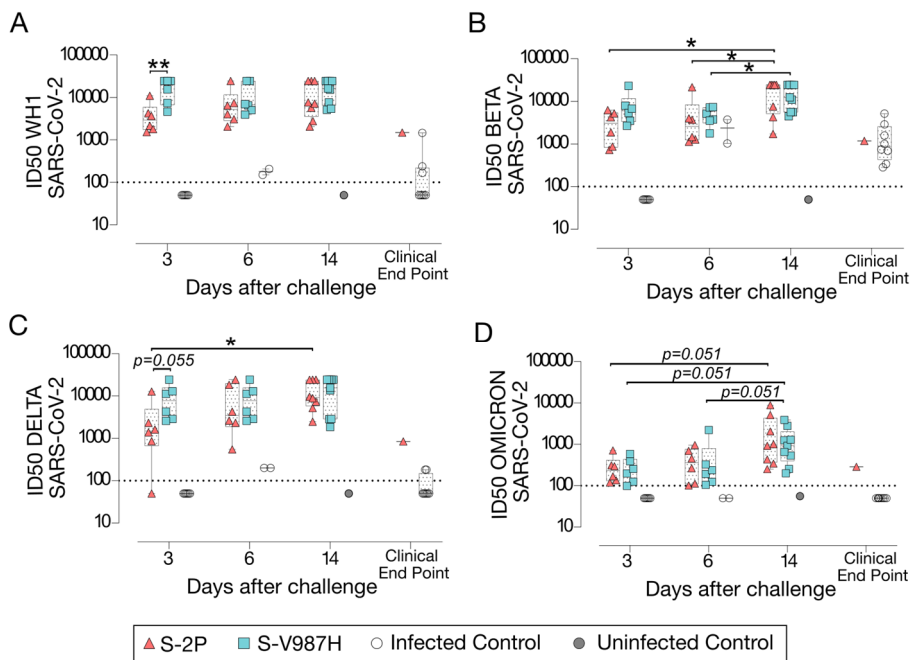
Figure 16. Neutralizing activity of S-V987H in K18-hACE2 mice challenged with the SARS-CoV-2 B.1.351 (Beta) variant. Sera neutralizing titers against **(A)** SARS-CoV-2 WH-1, **(B)** SARS-CoV-2 B.1.351 (Beta), **(C)** SARS-CoV-2 B.1.617.2 (Delta), and **(D)** SARS-CoV-2 B.1.1.529 (Omicron) variants after viral challenge. Groups in each time point were analyzed using Conover-Iman test with multiple comparison correction by FDR. Differences among animals within a particular group along time were analyzed using Friedman test with FDR correction. * p<0.05, ** p<0.01. P values proximal to statistical significance are shown as numbers. Mean plus standard errors of the means (SEM) are shown.

A reduction of body weight associated with disease progression was observed in mice from the infected control group starting on day 2 after challenge compared to mice vaccinated with S-2P and S-V987H (**Fig.17A**) ($p<0.05$, Kruskal-Wallis corrected by Dunn's test). Mice in both Spike-vaccinated groups maintained their weight until day 14 [percentage of weight: S-2P=99±4 (n=9); S-V987H=98±5 (n=9)]. Contrarily to the S-2P and infected control groups, no mice from the S-V987H group (n=9) showed any clinical signs of disease (**Fig.17A and B**) during the experiment (day 14) ($p<0.001$, Long rank test).
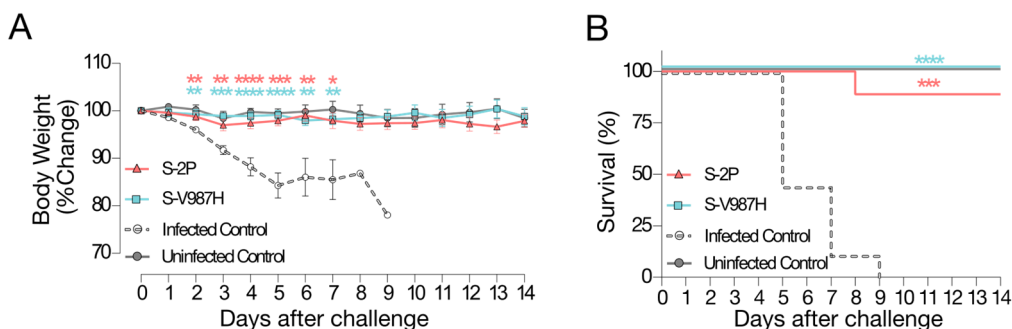
Figure 17. Prophylactic activity of S-V987H in vaccinated K18-hACE2 mice infected with the SARS-CoV-2 B.1.351 (Beta) variant. (A) Percentage of weight variation in SARS-CoV-2 B.1.351 infected K18-hACE2 mice over time. Statistical analysis was performed against the unvaccinated and challenged group using Kruskal-Wallis with Dunn´s test correction. **(B)** Kaplan-Meier plot showing the percentage of SARS-CoV-2-infected animals that were survive at the end of the experiment. Statistical analysis was performed against unvaccinated group using Mantel-Cox test. * $p<0.05$, ** $p<0.01$, *** $p<0.001$, **** $p<0.0001$. Mean plus standard errors of the means (SEM) are shown.

The analysis of viral load in tissues by RT-qPCR showed that both S-2P and S-V987H vaccinated groups had a progressive decrease in gRNA levels in oropharyngeal swabs and lung over time (**Fig.18**) ($p<0.05$; Peto & Peto Left-censored k sample test). Interestingly, the S-V987H group displayed lower viral loads in nasal turbinate than S-2P and infected control animals on day 3, and also in oropharyngeal swab compared to the infected controls (**Fig.18**) ($p<0.05$). However, these differences were not maintained over time and both S-trimer immunized groups showed low but equivalent values of gRNA on day 14 in all analyzed tissues (**Fig.18**). In addition, these groups displayed lower viral load in lung and brain compared to the infected control group at day 3 after challenge (**Fig.18**) ($p<0.05$).
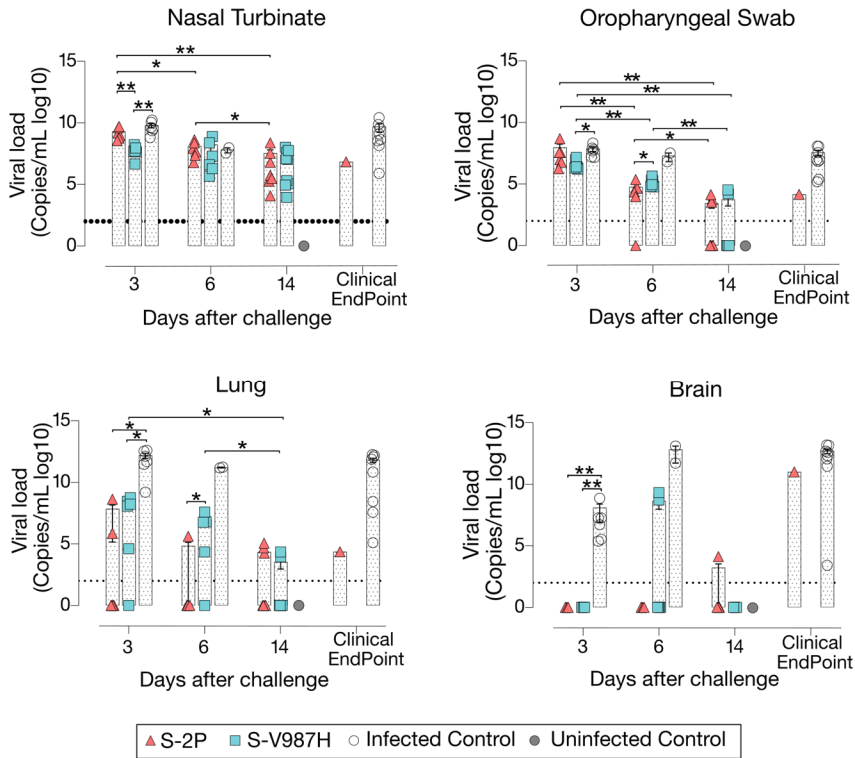
Figure 18. Viral load on tissue samples from SARS-CoV-2 B.1.351 infected K18-hACE2 mice after vaccination. SARS-CoV-2 viral load was analyzed in oropharyngeal swabs, and samples from nasal turbinate, lung and brain of infected K18-hACE2. Levels of SARS-CoV-2 gRNA (expressed as logarithmic of copies/mL) in oropharyngeal swabs, nasal turbinate, lung, and brain during infection. Dot line indicates limit of positivity (100 copies/mL). Differences between groups were analyzed using Peto & Peto left-censored k sample test with FDR correction. * $p<0.05$, ** $p<0.01$.

Remarkably, N protein was hardly detected in lung and brain from S-2P and S-V987H groups by IHC (**Fig.19A**), which was in line with the low levels of gRNA detected in these animals. Despite that, S-2P vaccinated mice showed a higher lesion score in lung at day 14 than the S-V987H group ($p<0.01$; Asymptotic Generalized Pearson Chi-Squared test) (**Fig.19B**), indicating that these mice presented a severe lung damage. Interestingly, both Spike-based immunogens protected from viral dissemination to the brain (**Fig.19**).

To summarize, the immunogenicity of both S-2P and S-V987H trimers was similar in K18-hACE2 SARS-CoV-2 Beta-infected mice, although S-V987H promoted the development of higher serum neutralization, which might explain the increase in protection observed in S-V987H vaccinated animals, compared to the S-2P group.
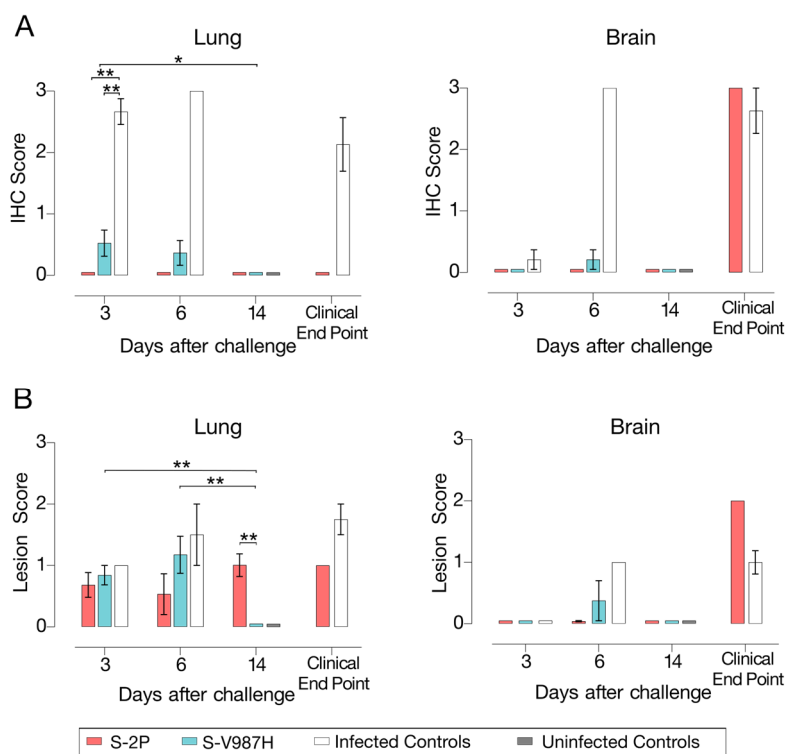
Figure 19. Histopathology analysis of tissue samples from SARS-CoV-2 Beta (B.1.351) challenged K18-hACE2 mice after vaccination. **(A)** Detection of SARS-CoV-2 N protein in brain, lung, and nasal turbinate by immunohistochemistry. Staining score: (0) no, (1) low, (2) moderate, and (3) high amount of viral antigen. **(B)** Histopathological analysis of brain, lung, and nasal turbinate by hematoxylin and eosin staining. Lesion score: (0) no, (1) mild, (2) moderate, and (3) severe lesion. Differences between groups were analyzed using Asymptotic Generalized Pearson Chi-Squared test with FDR correction. * p<0.05, ** p<0.01.

SECTION II. Novel Spike-Stabilized Trimers with Improved Production Protect K18-hACE2 Mice and Golden Syrian Hamsters from SARS-COV-2 Beta Infection

Here we described a novel set of mutations in combination with K986P and V987P (S-2P) identified by molecular modelling and located in the S2 region of the Spike that increase S-2P production up to five-fold. Besides their immunogenicity, the efficacy of two representative S-2P-based mutants, S-29 and S-21, protecting from a heterologous SARS-CoV-2 Beta variant challenge was assayed in K18-hACE2 mice (an animal model of severe SARS-CoV-2 disease) and GSHs (a moderate disease model). S-21 induced higher level of WH1 and Delta variants neutralizing antibodies than S-2P in K18-hACE2 mice three days after challenge. Viral load in nasal turbinate and oropharyngeal samples were reduced in S-21 and S-29 vaccinated mice. Despite that, only the S-29 protein protected 100% of K18-hACE2 mice from severe disease. When GSH were analyzed, all immunized animals were protected from disease development irrespectively of the immunogen they received. Therefore, the higher yield of S-29, as well as its improved immunogenicity and efficacy protecting from the highly pathogenic SARS-CoV-2 Beta variant, pinpoint the S-29 spike mutant as an alternative to the S-2P protein for future SARS-CoV-2 vaccine development.

1. Strategy for S Glycoprotein Stabilization

To increase the S glycoprotein stability and immunogenicity, we followed two different approaches: 1) introduction of point mutations into the S sequence to increase its stabilization (using the open state as a reference structure), and 2) increase of RBD exposure by forcing an open conformation. In this regard, we built a computational pipeline involving the three-dimensional modeling of all possible single mutations in both scenarios (see the Methods section for more details). Moreover, all single mutations that showed a preference for any of these two conditions were visually inspected. Mutations that clearly generated well-defined interactions (e.g. hydrogen bonds, ionic interactions for filling hydrophobic pockets) between different chains of the S trimer were prioritized (**Fig.20A**). S mutants were then produced and their yields and RBD binding were evaluated (**Fig.20B and C**). Based on their production levels, these glycoproteins were classified into three different groups (**Table.2**). Group 1 included those constructs (i.e., S-29 and S-22) that were produced at the highest levels (five-fold compared to the S-2P protein). Group 2 contained S-21, S-24, S-26, S-27, S-30, and S-31, whose production was intermediate (two-fold higher than S-2P). Last, Group 3 included those

S mutants with a protein yield lower than S-2P (S-20, S-23, S-25, S-28, S-32, S-33, S-34, S-35, S-36, S-37, and S-38). Remarkably, all constructs designed to increase RBD exposure were in Group 3, suggesting that those mutations drastically impacted the S stability and/or its production. However, most constructs with an improved production, also showed a better RBD exposure (**Fig.20B and C**).
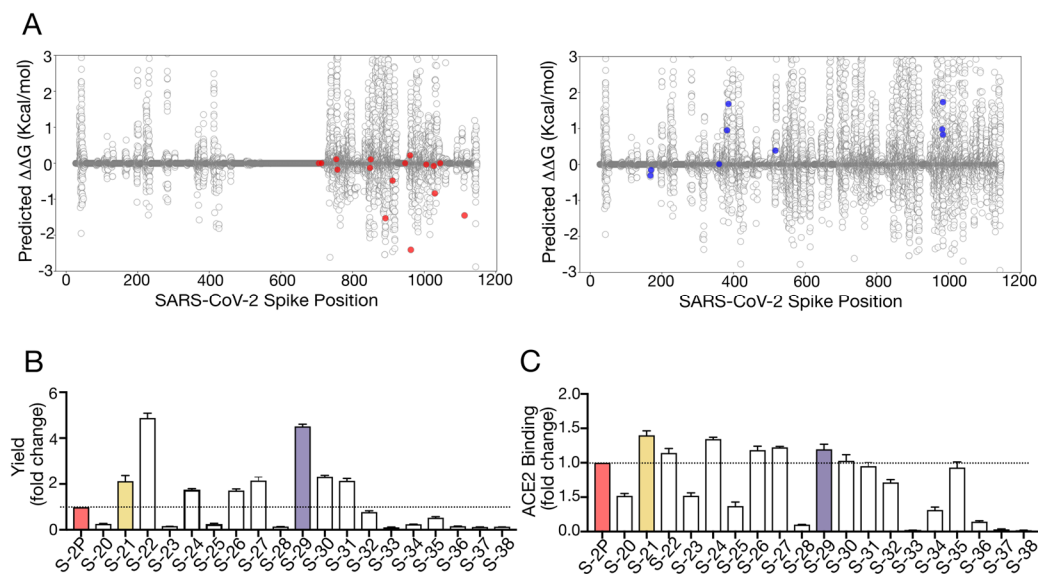
Figure 20. **Selection of mutations that stabilized S glycoproteins. (A)** S stabilizing mutations (red variants, left plot), or amino acids changes that increased RBD exposition (blue variants, right plot) were selected based on energetic filters and visual inspection. Positive energy values indicate stabilization of the open structure versus the closed one. Mutations with neutral (or slightly opposite) energetic trend were included. **(B)** Yields of recombinant S mutants in a five-day cell culture supernatant. Mean plus standard deviation of three experiments are shown. **(C)** RBD exposure index in selected recombinant proteins. Data are shown as ratio between RBD binding and total protein. Mean plus standard deviation of three experiments are shown. S-2P, S-21, and S-29 are shown in red, yellow, and purple, respectively.

Variants S-22 and S-29, with higher expression yield, introduced a positive charge per chain in a local area where the Glu1092 of each chain might cause destabilization. This cluster of Glutamic acid residues facing each other and how the T912R mutation in S-29 might introduce significant stabilization is shown in **Fig.21A**. Similarly, the Q1113R mutant in S-22 placed an arginine next to Glu1092 (**Fig.21B**). Analogous observations can be extracted of most mutants introducing a net charge. We also observed that most mutants increasing RBD exposure, such as S-21, S-24 and S-29, incorporated the S758E mutation. This mutation is in the vicinity of the tip of the closed RBD domain, where two consecutive Aspartic acid residues, Asp427 and Asp428 are located (**Fig.21C**). After modeling the possible positioning of Glu758 (with an initial significant clash with a helix backbone), we speculate that it would be displaced towards the tip of

Group	Construct	Mutations
1	S-22	Q755K, L849K, A892N, K947R, K1045R
1	S-29	S758E, T912R, K947R
2	S-21	A706Q, S758E, L849K, V963E, S1030R, Q1113R
2	S-24	S758E, L849K, V963E
2	S-26	Q755K, C851Q, T961E
2	S-27	A706Q, S1030R, Q1113R
2	S-30	L849K
2	S-31	T961E
3	S-20	A713R, Q755K, C851Q, T912R, T961E, T1027E
3	S-23	A7061, C851Q, T1006W, T1027E, Q1113R
3	S-25	A713R, T912R, T1027E
3	S-28	A706Q, C851Q, T1027E
3	S-32	T1027E
3	S-33	N360R, F168D, Y170D
3	S-34	K386A, D985A
3	S-35	D985A
3	S-36	D985W
3	S-37	L517A, V382A
3	S-38	L517A, V382A, R983A

Table 2. **List of S constructs that incorporate the selected mutations**
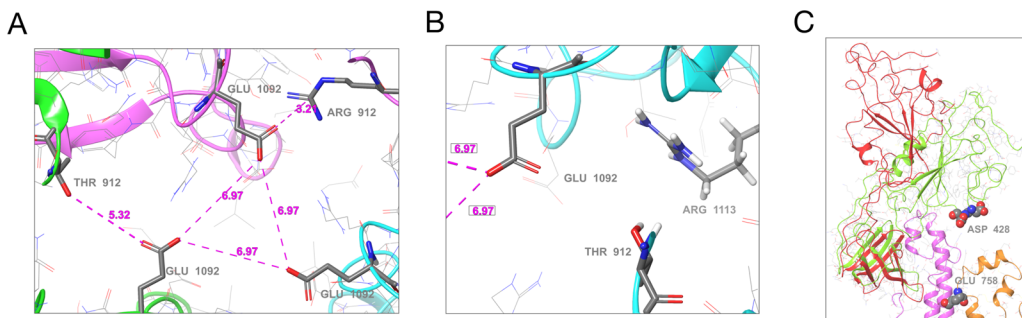
Figure 21. **Structural modelling of stabilizing mutations into S glycoprotein (A)** Presence of a cluster of three Glu residues (one Glu1092 from each chain) that are facing each other in close proximity, with no positive residues nearby. Location of Thr912 is underlined as well. Also notice that one of the three Thr has been mutated to Arg clearly showing a salt bridge interaction with the glutamic acid. **(B)** A detail of the proximity of the 1113 residue, already mutated to Arg, to the Glu1092 cluster. Thr912 is also showed. Structure models were based on 6VXX PDB structure. **(C)** Detail of the RBD opening process and location of some key residues. The red and green ribbons indicate the difference between the open and closed states, underlying the position of the two consecutive aspartic acid residues, Asp428 and Asp427, at the tip of the RBD domain. In orange ribbons the location of the S758E mutation is shown. Notice that the inserted glutamic residue collides with the neighbor helix (pink ribbons). Models generated from the 6VXX (closed) and 6VYB (open) PDB structures.

the RBD domain and destabilize the closed conformation by electrostatic repulsion. Interestingly, S-22 and S-29 constructs share the conservative mutation K947R located in the middle of the heptad repeat 1 (HR1) helix, which could enhance the thermal stability of the protein[341].

2. S-21 and S-29 Vaccination Protects K18-hACE2 Mice from SARS-CoV-2 Induced Disease

To investigate the impact of S mutations on its immunogenicity and capability to protect from SARS-CoV-2-induced disease, we selected two representative S mutants from group 1 (S-29) and 2 (S-21). Then, we performed an immunization study using K18- hACE2 transgenic mice that were subsequently challenged with SARS-CoV-2 B.1.351 (Beta) variant (**Fig.22A**). We used this experimental design for the following reasons: 1) K18-hACE2 transgenic mice develop a severe form of the disease that leads to death[340] unless animals are vaccine-protected; 2) the SARS-CoV-2 Beta variant is partially resistant to antibodies elicited by natural infection or vaccination with immunogens based on the original strain (Wuhan, WH1)[180]; and 3) the SARS-CoV-2 Beta variant is one of the most pathogenic SARS-CoV-2 variants tested in K18-hACE2 transgenic mice[340]. Thus, we established five experimental groups: S-2P (n=21), S-21 (n=22), S-29 (n=22), infected positive controls (n=16), and uninfected negative controls (n=10). Mice from S- 2P, S-21, and S-29 groups were immunized twice, three weeks apart. Animals from both control groups received antigen-free doses. Two weeks after the boost, all animals (except the negative controls) were intranasally challenged with the SARS-CoV-2 Beta variant. Blood and tissue samples were collected after viral challenge on days 3 (n=6), 6 (n=6) and 14 (n=10 for S-21, S-29 and uninfected controls, and n=8 for S-2P) to analyze tissue damage and viral replication (**Fig.22A**). All mice that developed severe disease (one mouse in the S-2P and S-21 groups, and all mice from the positive control group) were euthanized before day 14 following humane endpoints and were analyzed separately. Anti-S (**Fig.22B**) and anti-RBD (**Fig.22C**) IgG humoral responses were evaluated prior to each immunization and viral challenge, and in euthanized animals after infection on days 3, 6, and 14, or due to humane endpoints. Regardless of the immunogen used, all vaccinated animals developed similar anti-S (**Fig.22B**) and anti-RBD (**Fig.22C**) IgG levels, which increased after each immunization and after viral challenge (p<0.01, Conover´s post-hoc test). Since we did not identify significant differences in the humoral responses among vaccinated groups after

challenge we pooled these mice in a single "post-challenge" group to simplify the analysis. Of note, unvaccinated but challenged positive controls elicited low levels of anti-S and anti-RBD IgG antibodies (**Fig.22B and C**) that were detected from day 6 after viral challenge.
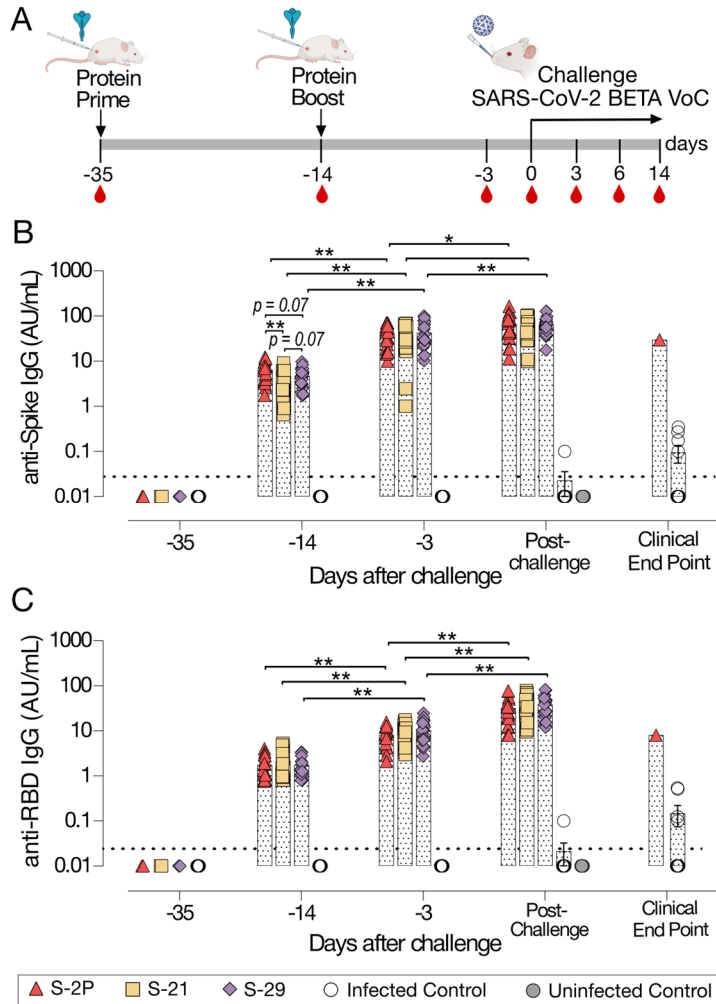
Figure 22. Humoral response elicited by S-21 and S-29 vaccinated K-18 hACE2 mice challenge with SARS-CoV-2 B.1.351 (Beta) variant. (A) Outeline of vaccine strategy and infection. K18-hACE2 mice were immunized twice with S-21 (n=22), S-29 (n=22) or S-2P (n=21), adjuvanted with AddaVax. Mice were challenged with the SARS-CoV-2 B.1.351(Beta) VoC and sacrified at day 3, 6 and 14 to monitor the infection. Two control groups were used: unvaccinated-challenge mice (n=16) and unvaccinated-uninfected mice (n=10). Blood drops indicate collection of biological samples. **(B)** Kinetics of anti-S and **(C)** anti-RBD antibodies in serum samples. Red triangles: S-2P group. Yellow squares: S-21. Purple diamond: S-29. White circles: unvaccinated-challenge mice. Grey circles: unvaccinated-uninfected mice. Groups in each time point were analyzed using Kruskal-Wallis and Conover's post-hoc tests with multiple comparison correction by FDR. Differences among animals within a particular group along time were analyzed using Friedman and Conover's post-hoc test for paired data with FDR correction. * $p<0.05$, ** $p<0.01$, *** $p<0.001$, **** $p<0.0001$. Mean plus standard errors of the means (SEM) are shown.

Sera neutralizing activity against SARS-CoV-2 WH1, Beta, Delta, and Omicron variants was detected in all three vaccinated groups (**Fig.23**). Interestingly, despite having similar levels of anti-RBD IgGs (**Fig.22C**), and a slightly higher levels of anti-S IgG antibodies (**Fig.22B**), S-2P vaccinated mice showed lower sera neutralizing activity against WH1 and Delta variants on day 3 than those immunized with S-21 (**Fig.23A and C**) (WH1 p<0.05; Delta p=0.052, Conover´s post-hoc test). Sera neutralizing activity against Delta and Beta variants increased over time in the S-2P vaccinated group after viral challenge (Beta p<0.05; Delta p=0.052, Conover´s post-hoc test), suggesting that infection boosted the humoral response in these animals. In line, unvaccinated mice developed low sera neutralizing activity against the SARS-CoV-2 Beta variant (**Fig.23B**) with some cross-reactivity with WH1 but limited
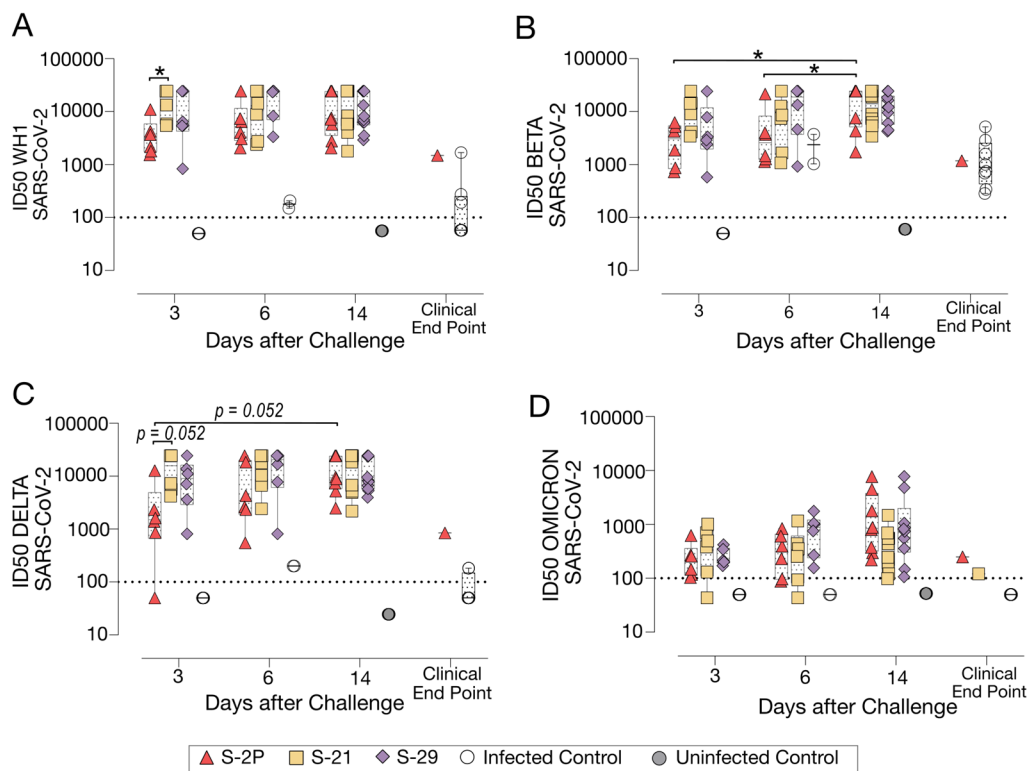
Figure 23. Neutralizing titter of S-21 and S-29 vaccinated K18-hACE2 mice challenged with SARS-CoV-2 Beta variant. Sera neutralizing titers against **(A)** SARS-CoV-2 WH-1, **(B)** SARS-CoV-2 B.1.351 (Beta), **(C)** SARS-CoV-2 B.1.617.2 (Delta), and **(D)** SARS-CoV-2 B.1.1.529 (Omicron) variants after viral challenge. Groups in each time point were analyzed using Kruskal-Wallis and Conover's post-hoc tests with multiple comparison correction by FDR. Differences among animals within a particular group along time were analyzed using Friedman and Conover's post-hoc test for paired data with FDR correction. *p<0.05. P values proximal to statistical significance are shown as numbers. Mean plus standard errors of the means (SEM) are shown.

cross-neutralizing activity against other SARS-CoV-2 variants (**Fig.23A, C and D**) after viral challenge. No boost effect on sera neutralizing activity was detected in S-21- and S-29-immunized mice after challenge, suggesting that the humoral response reached a plateau in these groups.

To determine whether S-2P-, S-21-, and S-29-vaccinated mice were protected against SARS-CoV-2-induced severe disease, we measured body weight evolution (**Fig.24A**), clinical sings, and survival rate after viral challenge (**Fig.24B**). A progressive weight loss was observed in all unvaccinated but challenged mice starting on day 2 post-challenge. These mice developed a severe disease on days 5-9 post-infection and were euthanized following humane endpoints. Conversely, all vaccinated mice (except one S-2P- and one S-21-immunized mice), were disease-free (**Fig.24B**) and did not experience weight loss. All mice belonging to S-29 group were protected from severe disease development (**Fig.24A and B**).
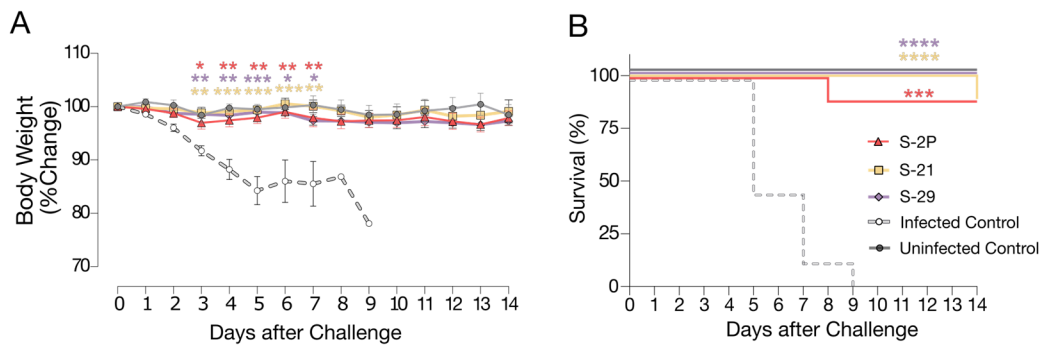
Figure 24. Prophylactic activity of S-21 and S-29 vaccination in K18-hACE2 mice infected with SARS-CoV-B.1.351 (Beta) VoC. (A) Percentage of weight variation in SARS-CoV-2 B.1.351 infected K18-ACE2 mice over time. Statistical analysis was performed against the unvaccinated and challenged group using Kruskal Wallis with Dunn´s post-hoc test. **(B)** Kaplan-Meier plot showing the percentage of SARS-CoV-2-infected animals that were disease-free at the end of the experiment. Statistical analysis was performed against unvaccinated group using Mantel-Cox test. * $p<0.05$, ** $p<0.01$, *** $p<0.001$, **** $p<0.0001$. Mean plus standard errors of the means (SEM) are shown.

The presence of SARS-CoV-2 in oropharyngeal swabs and tissue samples from nasal turbinate, lung, and brain was analyzed by RT-qPCR. All vaccinated mice had significantly lower levels gRNA in lung on day 3 post- inoculation compared to the positive control group ($p<0.05$, Peto & Peto Left-censored k-sample test) (**Fig.25**). Most notably gRNA was scarcely detected in brain of vaccinated mice compared to unvaccinated animals (**Fig.25**). Interestingly, S-21- and S-29- vaccinated mice showed lower viral load in nasal turbinate than S-2P and control groups on day 3,

and S-2P vaccinated mice on day 6 (p<0.05, Peto & Peto Left-censored k- sample test) (**Fig.25**). The lack of differences with the control group on day 6 could be explained due to the small number of unvaccinated mice that reached this timepoint, since the majority had been euthanized on day 5 post-infection (**Fig.24B**). Similarly, S-21 and S-29 groups exhibited lower viral loads in oropharyngeal swabs than unvaccinated mice (S-21 p<0.05; S-29 p=0.066; Peto & Peto Left-censored k-sample test) (**Fig.25**). Generally, gRNA decreased over time in all immunized mice regardless of the analyzed sample, whereas the opposite outcome was observed in mice belonging to the challenged control group, and in those vaccinated mice that developed severe disease (**Fig.25**).
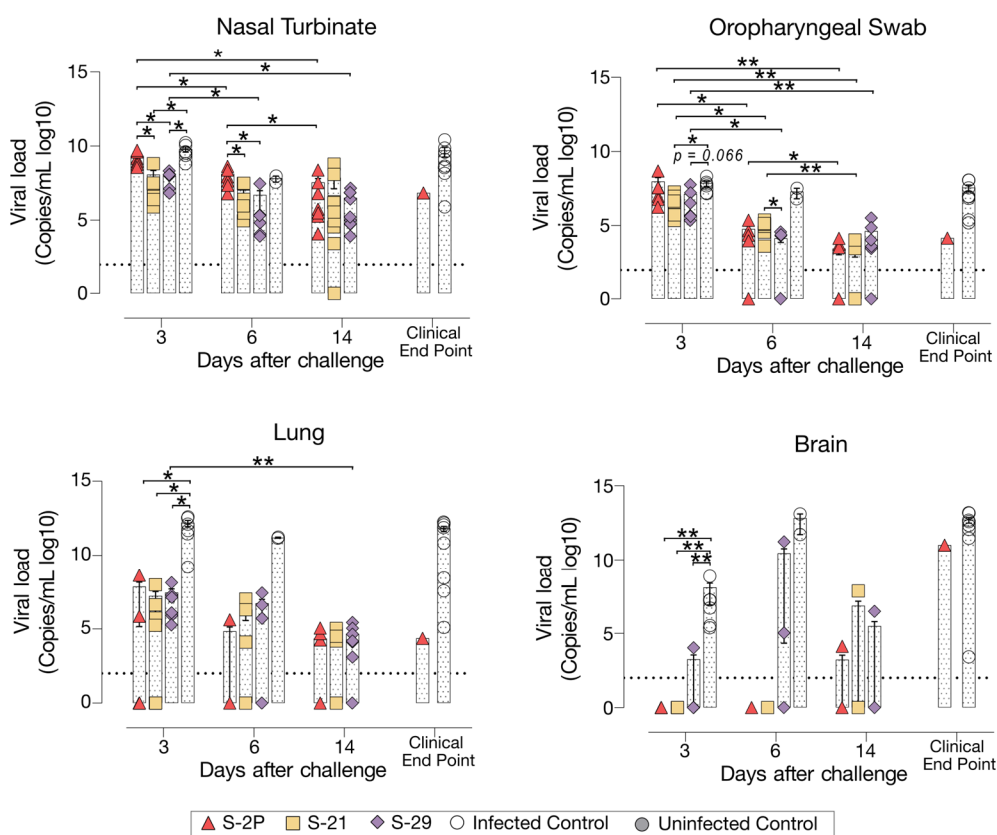
Figure 25. Viral load of biological samples from SARS-CoV-2 B.1.351 infected K18-hACE2 transgenic mice after vaccination. SARS-CoV-2 viral loads were analyzed in oropharyngeal swabs, and samples from nasal turbinate, lung, and brain of infected K18-hACE2 mice. Levels of SARS-CoV-2 gRNA are expressed as logarithmic of copies/mL. Dotted line indicates limit of detection (100 copies/mL). Differences among groups were analyzed using Peto & Peto left-censored k-sample test with FDR correction. * p<0.05, ** p<0.01. P values proximal to statistical significance are shown as numbers.

To confirm active viral replication, N protein levels were analyzed by IHC. N protein was hardly detected in lung and brain samples from S- 2P, S-21 and S-29 groups (**Fig.26A**). These data are in accordance with the viral loads detected in these samples. Despite that, some tissue damage was still detected in the lungs of all vaccinated groups. Remarkably, limited tissue damage was found in the brain of vaccinated mice, except in those animals euthanized due to humane endpoints (**Fig.26B**).
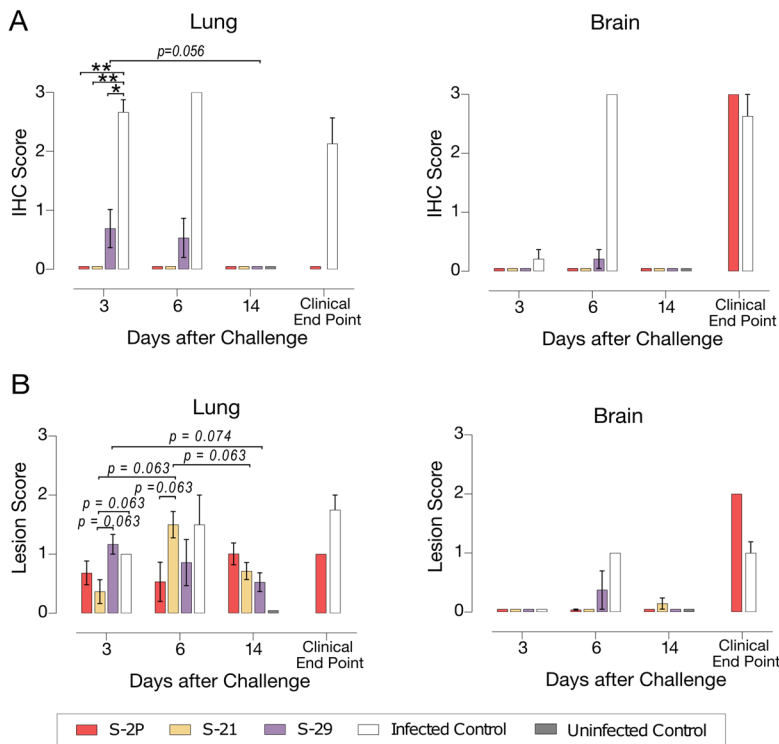
Figure 26. Histopathological analysis of tissues samples from vaccinated K18-hACE2 mice challenged with SARS-CoV-2 B.1.351 VoC. (A) Detection of SARS-CoV-2 N protein in lung and nasal turbinate by immunohistochemistry. Staining score: (0) no, (1) low, (2) moderate, and (3) high amount of viral antigen. **(B)** Histopathologic analysis of nasal turbinate and lung by hematoxylin and eosin staining. Lesion score: (0) no, (1) mild, (2) moderate, and (3) severe lesion. Differences between groups were analyzed by the Asymptotic Generalized Pearson Chi-Squared test corrected using FDR. * $p<0.05$. ** $p<0.01$. P values proximal to statistical significance are shown as numbers.

Overall, S-2P, S-21, and S-29 trimers displayed an equivalent immunogenicity in K18- hACE2 transgenic mice and protected these animals from developing severe disease after SARS-CoV-2 Beta variant challenge. Interestingly, S-21- and S-29-immunized animals had lower viral loads in nasal turbinate than S-2P and infected controls on days 3 and 6 after challenge. Viral loads were also reduced in oropharyngeal swabs of these mice on day 3 compared to infected control groups.

3. S-21 and S-29 Trimer Vaccination Protects Golden Syrian Hamsters from COVID-19 Development

To confirm the results obtained in K18-hACE2 mice, a second immunization and challenge experiment was performed using GSHs with the same immunogens. Unlike K18-hACE2 mice, GSH develop a moderate form of SARS-CoV-2-induced disease, from which they spontaneously recover by day 14 after challenge[334,337]. GSH were immunized following a similar prime/boost strategy to the previously used for K18-hACE2 transgenic mice. Animals were intranasally challenged with the SARS-CoV-2 Beta variant and followed up until day 7 post-challenge (**Fig.27A**), since it has been described that GSH start recovering weight from this day[334,337].
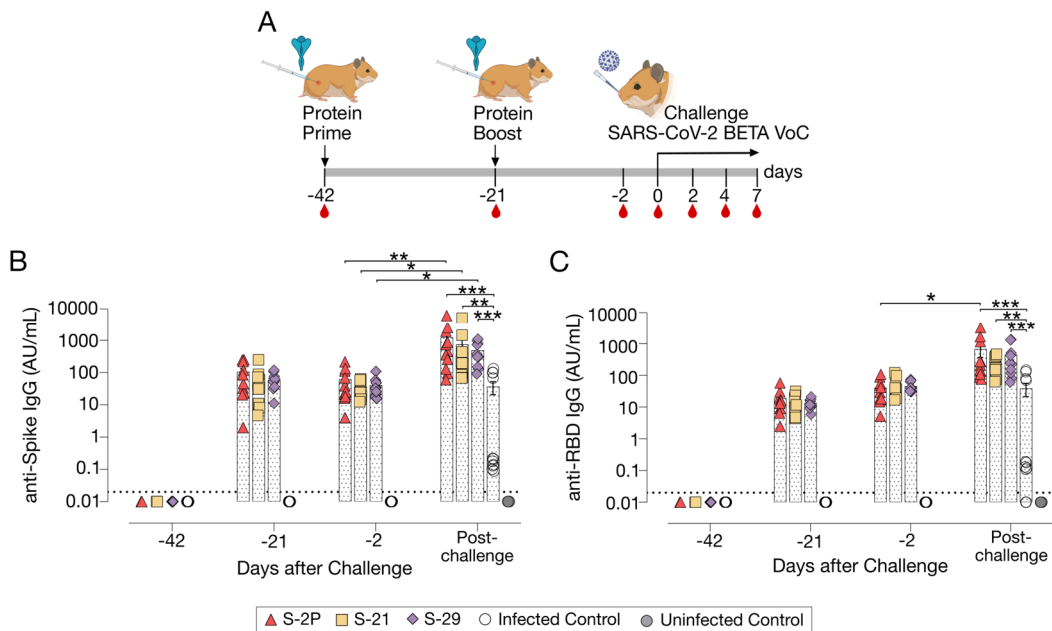
Figure 27. Humoral response of S-21 and S-29 immunized GSHs after challenge with the SARS-CoV-2 B.1.351 (Beta) variant. (A) Overview of immunization strategy and infection timeline. GSH were immunized twice with S-21 (n=11), S-29 (n=11) or S-2P (n=11), adjuvanted with AddaVax. Mice were challenged with the SARS-CoV-2 B.1.351(Beta) VoC and sacrified at day 2, 4 and 7 to monitor the infection. Two control groups were established: unvaccinated-challenged mice (n=11) and unvaccinated-uninfected mice (n=5). Blood drops indicate collection of biological samples. **(B)** Kinetics of anti-S and **(C)** anti-RBD antibodies in serum samples. Red triangles: S-2P group. Yellow squares: S-21. Purple diamond: S-29. White circles: unvaccinated-challenged mice. Grey circles: unvaccinated-uninfected mice. Groups in each time point were analyzed using Kruskal-Wallis and Conover's post-hoc tests with multiple comparison correction by FDR. Differences among animals within a particular group along time were analyzed using the Friedman and Conover's post-hoc tests for paired data with FDR correction. * $p<0.05$, ** $p<0.01$, *** $p<0.001$. Mean plus standard errors of the means (SEM) are shown

In accordance with K18-hACE2 transgenic mice data, the three vaccinated groups (S-2P, S-21 and S-29) developed similar levels of anti-S and anti-RBD binding IgG (**Fig.27B and C**). Interestingly, the second immunization did not boost vaccine-induced anti-S or anti-RBD IgG antibodies, indicating that a second vaccine dose might not be needed in this animal model. Interestingly, an increase in anti-S IgG levels was observed after viral challenge in both vaccinated and unvaccinated but challenged mice (**Fig.27B**). However, when anti-RBD IgG responses were analyzed, that boosting effect was less evident and only detected in the S-2P and in unvaccinated and challenged groups (**Fig.27C**). These results suggest that viral challenge elicited a rapid humoral response in naïve animals, boosting anti-S IgG responses, but had little effect in vaccinated GSH. Despite that, immunized GSH showed higher levels of anti-S and anti-RBD antibodies than challenged controls (p<0.001 for S-2P and S-29 group, and p<0.01 for S-21 group; Friedman test) (**Fig.27B and C**).
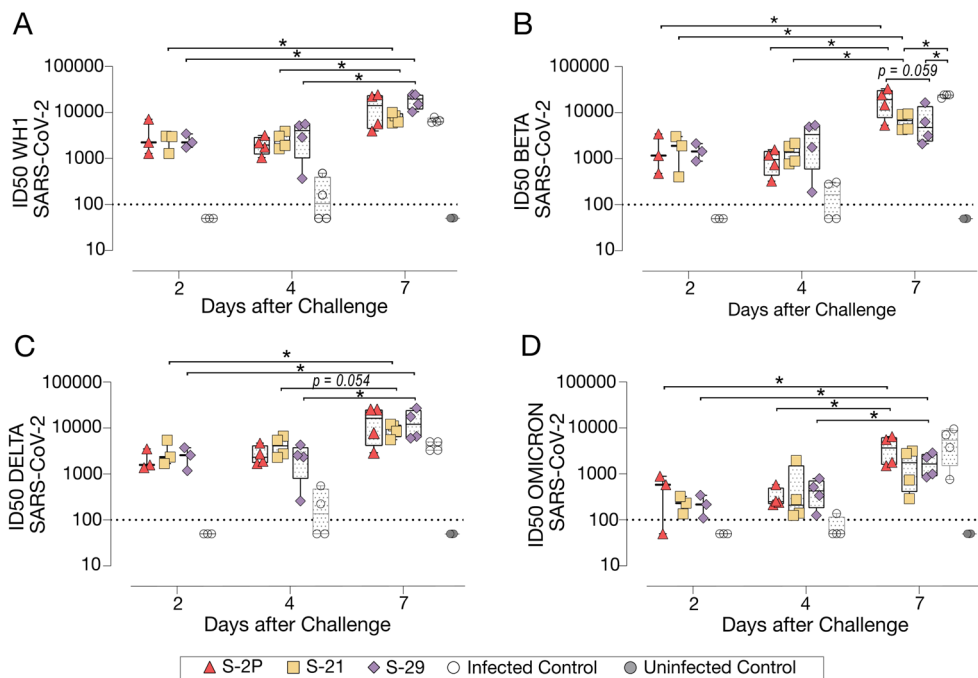
Figure 28. Neutralizing titters elicited by S-21 and S-29 vaccinated GSHs after challenge with SARS-CoV-2 B.1.351 (Beta) variant. Sera neutralizing activity after viral challenge against **(A)** SARS-CoV-2 WH-1, **(B)** B.1.351 (Beta), **(C)** B.1.617.2 (Delta), and **(D)** B.1.1.529 (Omicron) variants. Neutralization data per groups in each time point were analyzed using Kruskal-Wallis and Conover's post-hoc tests with multiple comparison correction by FDR. Differences among animals within a particular group along time were analyzed using the Friedman and Conover's post-hoc tests for paired data with FDR correction. * p<0.05. P values proximal to statistical significance are shown as numbers. Mean plus standard errors of the means (SEM) are shown.

Sera neutralizing activity against SARS-CoV-2 WH1, Beta and Delta, and to a lesser extent, Omicron variants was detected in vaccinated animals at all post-challenge timepoints (**Fig.28A-D**). No differences were identified among immunized groups. Remarkably, and contrarily to K18-hACE2 transgenic mice vaccine study data, sera neutralizing activity against all four SARS-CoV-2 variants were observed in some challenged positive control animals by day 4 after challenge (**Fig.28A-D**). These results indicate that cross-reactive neutralizing antibodies were generated in those individuals. Unexpectedly, the neutralizing activity against the SARS-CoV-2 Beta variant was higher in challenged control animals than in S-21- and S-29-vaccinated GSH by day 7 (**Fig.28B**). According to the binding ELISA data, neutralization titers also increased in immunized GSH by day 7 after viral challenge (p<0.05; Conover´s post-hoc test), indicating that infection boosts vaccine-induced humoral neutralizing responses (**Fig.28A-D**).

To determine whether vaccination protected GSHs from SARS-CoV-2-induced disease, we monitored animal weight over time after viral challenge (**Fig.29A**). Challenged control GSHs showed progressive weight reduction until day 6, which was indicative of disease progression. One animal from this group suffered a weight reduction greater than 20% by day 6 post-inoculation and was euthanized according to humane endpoints (**Fig.29B**). No significant weight loss was observed in vaccinated GSHs, indicating that these animals were protected from disease development (**Fig.29A and B**).
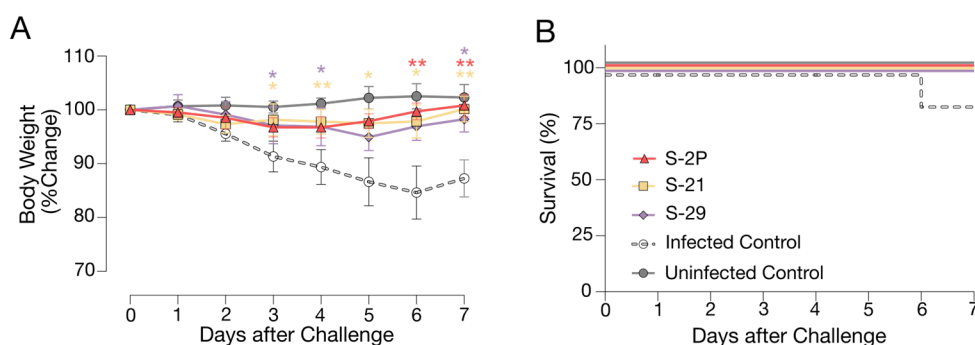
Figure 29. Prophylactic activity of S-21 and S-29 vaccination in GSHs infected with SARS-CoV-B.1.351 (Beta) VoC. (A) Percentage of weight variation in SARS-CoV-2 B.1.351-infected GSH over time. **(B)** Kaplan-Meier plot showing the frequency of disease-free SARS-CoV-2-infected animals at the end of the experiment. Statistical analysis was performed against the unvaccinated group using Kruskal Wallis and Dunn´s post-hoc tests. * p<0.05, ** p<0.01, *** p<0.001. Mean plus standard errors of the means (SEM) are shown.

To evaluate viral replication in tissues, we determined the levels of gRNA by RT-qPCR. We did not identify any differences among study groups in the levels of gRNA in nasal turbinate, lung, in oropharyngeal samples were detected (**Fig. 30**). However, vaccinated animals exhibited a decreasing trend in their nasal turbinate levels of gRNA over time after challenge (p=0.061; Peto & Peto Left-censored k-sample test) (**Fig. 30**). In addition, the analysis of nasal turbinate samples on day 7 post-challenge showed that vaccinated GSH displayed lower gRNA levels tendency compared with unvaccinated-challenged controls (gRNA: p=0.061; Peto & Peto Left-censored k-sample test) (**Fig. 30**).
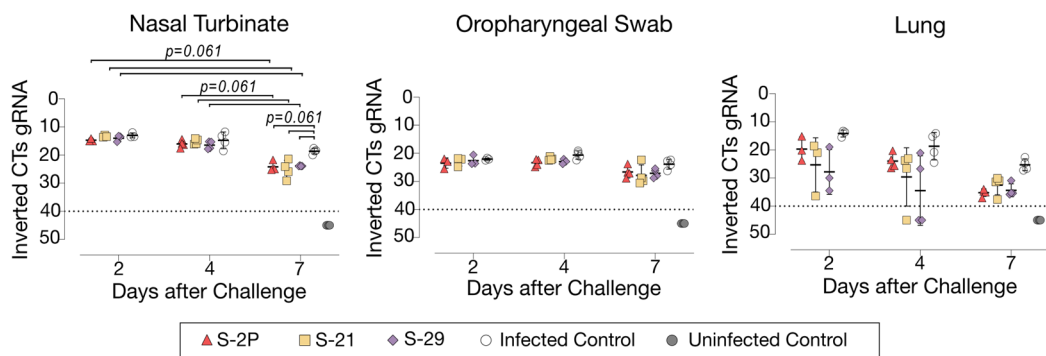
Figure 30. viral loads in tissues from vaccinated GSH after challenge with SARS-CoV-2 Beta variant. Levels of SARS-CoV-2 gRNA, expressed as cycles threshold (CTs), in oropharyngeal swabs, nasal turbinate, and lung during infection. Dotted line indicates limit of positivity (40 CTs). Differences among groups were analyzed using Peto & Peto left-censored k-sample test with FDR correction. P values proximal to statistical significance are shown as numbers.

In order to confirm RT-qPCR data, the presence of N protein was analyzed in nasal turbinate and lung by IHC. N protein was not detected in nasal turbinate samples from immunized animals on day 7 (**Fig. 31A**). These results confirm the decreasing trend observed when gRNA and sgRNA were analyzed over time. Similarly, SARS-CoV-2 replication associated lesions were hardly detected in nasal turbinate samples on day 7 (**Fig. 31B**). However, despite N protein was not detected in lung of vaccinated GSHs on day 7, low levels of tissue lesions were still present (**Fig. 31B**). No significant differences in tissue damage were observed in lung samples among study groups, probably due to the low number of animals per group.

Overall, these results confirm that all three S-2P, S-21 and S-29 immunogens showed an equivalent immunogenicity and prophylactic activity in GSHs, protecting these animals from the development of severe SARS-CoV-2-induced disease.
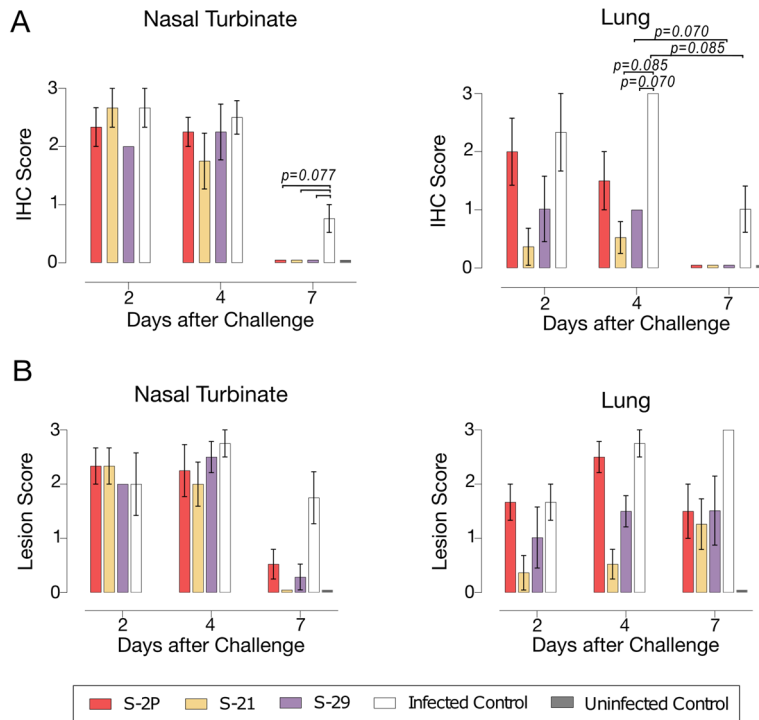
Figure 31. Histopathology of tissues from vaccinated GSH after challenge with SARS-CoV-2 Beta variant. (A) Histopathological analysis of lung and nasal turbinate by hematoxylin and eosin staining. Lesion score: (0) no lesion, (1) mild lesion, (2) moderate lesion, and (3) severe lesion. **(B)** Detection of SARS-CoV-2 N protein in lung and nasal turbinate by IHC. Staining score: (0) no antigen, (1) low, (2) moderate, and (3) high viral antigen. Differences among groups were analyzed using Asymptotic Generalized Pearson Chi-Squared test and FDR. P values proximal to statistical significance are shown as numbers.

DISCUSSION

The rapid development of COVID-19 vaccines has been pivotal for the control of SARS-CoV-2 pandemic. Despite this pathogen has several proteins that play a crucial role in virus life cycle, the S glycoprotein is critical for SARS-CoV-2 infection through its binding to the ACE2 receptor on the target cell surface. The analysis of the SARS-CoV-2 immune response has shown that S induces both humoral and cellular protective immune responses. Indeed, neutralizing antibodies titters against the S protein, and more especially the RBD, correlate with protection[175]. Thus, the S glycoprotein is presented as the main antigen in most available COVID-19 vaccines. However, during the pandemic, the virus has evolved, and several variants emerged acquiring mutations into the S glycoprotein. Thus, novel SARS-CoV-2 variants showed resistance to previously acquired immunity. Moreover, since most COVID-19 vaccines are based on the ancestral SARS-CoV-2 WH1 strain sequence, SARS-CoV variants also showed resistance to vaccine-induced immune responses. The incorporation of additional booster immunizations partially restored the protection against SARS-CoV-2 variants. As alternative, some vaccines were adapted to the new viral variants showing a modest protection improvement against disease development.

The S glycoprotein, as many other viral proteins that are functionally equivalent (e.g. the human immunodeficiency virus (HIV) envelope glycoprotein)[342], is prone to structural rearrangements. Therefore, S is unstable in its prefusion conformation, which limits its immunogenicity and capability for inducing neutralizing protective antibodies. Thus, several strategies for stabilizing the S glycoprotein in its prefusion conformation have been used. A previous study conducted with the S glycoprotein of MERS-CoV showed that the incorporation of two proline mutations in the central helix (V1060 and L1061) increased the stability of the protein in the prefusion conformation and improved its immunogenicity and capacity to induce neutralizing antibodies[65]. Moreover, this study reported that this approach may be a common strategy to the S glycoprotein from other coronaviruses. Thus, the S glycoprotein of SARS-CoV-2 was successfully stabilized by incorporating two prolines substitution at residues K986P and V987P (referred to as S-2P) into a similar region, between the HR1 and the central helix within the S2 subdomain. This modification increases S production and immunogenicity, and was incorporated into several commercial vaccines (e.g. BNT162b2, mRNA-1273, VidPrevtyn Beta, and Ad26.CoV2.S).

However, S-2P yield remains low when it is produced as soluble recombinant protein (about 0.5 mg/L)[61], hampering its use for vaccine development. Importantly, S-2P still shows some structural motility related to RBD exposure[61], which is the major S domain targeted by neutralizing antibodies [165]. Thus, the S-2P´s immunogenicity may still be improved by alternative S glycoprotein stabilization approaches.

Here we screened two different stabilization strategies based on a novel set of non-proline mutations in the (1) absence or the (2) presence of both K986P and V987P mutations. Mutations were designed to reduce the structural motility of the S protein, favoring a (1) close or (2) open state, respectively. Selection of potential mutations were based on Gibbs free energy changes of S variants among the close and open conformation, and prioritizing those mutations which generate well-defined interactions between the RBDs of each S chains. Regarding the first set of mutations, during the screening we found that those mutations that limit RBD exposure had a negative effect on protein yield, suggesting that open conformation may contribute to the protein expression as Xiong et al. mentioned[343]. In contrast, a single V987H mutation presented higher ACE2 receptor recognition, hinting a better RBD exposure, and an increased protein yield by 2.5-fold compared to S-2P. Thus, we evaluated the immunogenicity and prophylactic capability of S-V987H face to S-2P and recombinant monomeric RBD. To this end, we used two different animal models: K18-hACE2 mice and GSHs. While K18-hACE2 mice develops severe disease after SARS-CoV-2 challenge and most mice succumb due to central nervous system affectation[344], GSHs progress to a moderate disease after viral challenge and finally recover spontaneously[337]. In addition, two SARS-CoV-2 variants (D614G and B.1.351/Beta) were used to prove immunogen efficacy. Beta variant was selected since it showed resistance against NAbs[180] and had increased virulence in K18-hACE2[340]. Of note, Omicron VoC was not employed because of reducing virulence in K18-hACE2 mice[340]. As adjuvants and immunization strategy may impact on immunogenicity and vaccines efficacy[345], we applied heterologous (DNA/protein) and homologous (protein) administrations regimens formulated with aluminum or AddaVax (MF59-like), respectively. Despite S-V987H showed higher yields than S-2P, its immunogenicity was equivalent in both animal models and administration regimens. However, the humoral response elicited after the homologous protein regimen with AddaVax was higher and more homogeneous

than after heterologous regimen with DNA plus aluminum. Additionally, vaccination with S trimers induced higher antibodies titters than recombinant monomeric RBD, which correspond with enhancing protection against severe disease. The poor immune response elicited by monomeric RBD might be explained by its small molecular size, as well as, its lower antigen valency in comparison with full S trimer. Indeed, RBD-based vaccines usually use different strategies to enhance its immunogenicity such as increasing antigen size by fusion protein or by RBD multimerization[215,346,347]. All mice immunized with S-V987H were disease free, whereas one mouse from S-2P group developed severe disease after both SARS-CoV-2 D614G and SARS-CoV-2 Beta challenge. Thus, S-V987H protective efficacy might be higher than the one observed with S-2P. According to the protection data, S-V987H showed faster viral clearance in respiratory tissues than S-2P immunized mice, especially in nasal turbinate. In addition, immunogenicity and prophylactic capability of these immunogens were confirmed in GSHs. Overall, S-V987H results suggest that this mutation may be an alternative approach over S-2P, since the incorporation of this mutation increased protein yields and improved protection in animal models.

Besides the two proline (K986P and V987P) strategy, other mutations have been described to increase the S trimer stability and yield. In this sense, Hsieh et al. identified some S single mutations which increased protein yield over 2.5-fold in comparison to S-2P. Indeed, the same authors described that the addition of four proline mutations (F817P, A892P, A899P, A942P) into the S2 subdomain of the S-2P protein (HexaPro-S) increased protein yields by 10-fold[348]. The HexaPro-S protein expression into Newcastle disease virus vector (NDV-HXP-S) have shown protection in GSHs model against SARS-CoV-2 induced disease[349]. Moreover, NDV-HXP-S induced robust immune immunogenicity and was well-tolerated during phase I/II clinical trials[350,351]. A trivalent vaccine NDV-HXP-S vaccine, which implement the HexaPro approach into the S sequence from SARS-CoV-2 Beta, Gamma and Delta variants, provides great cross-protection against phylogenetically distant variants in animal model[352]. Thus, despite the set of mutations in this work were based on the original SARS-CoV-2 WH1 S sequence as S-2P, the trivalent NDV-HXP-S vaccine suggests that our stabilization approaches can be also susceptible to apply to other SARS-CoV-2 VoC S proteins. Apart from the HexaPro-S protein, Juraszek and colleagues identified three regions critical for S protein

stability: the HR1, the SD1 and the SD2 domain[353]. Furthermore, Juraszek et al. described the combination of four mutations (D614N, A892P, A942P, and V987P) that stabilized the S protein increasing its expression by 6.4-fold[353]. Riley et al., showed that chemical cross-linking between the S2 and S1 subunit increase S protein stability[354]. Other stabilization approaches have been described including disulfide bonds (positions Ser383-Asp985 and Gly413-Val987)[343] and mutations that fill linolenic acid-binding pocket in the RBD[355]. However, except for HexaPro-S protein, whether all the rest S variants show an improved immunogenicity or protective capability compare to the S-2P protein remains unknown.

In addition to S-V987H variant, we designed and tested a second set of S mutations in combination with both K986P and V987P. The yield of these novel variants increased between 2 and 5-fold compared to S-2P. According to their production levels and their RBD exposure, we selected two S variants: S-21 showed a moderate increased production but the highest RBD exposure, while S-29 presented the greatest production but a moderate enhanced RBD exposure. We evaluated S-21 and S-29 immunogenicity and protection capability against the virulent SARS-CoV-2 Beta variant in two animal models, K18-hACE2 mice and GSHs, in comparison to S-2P. S-21, S-29, and S-2P showed equivalent immunogenicity and protected both animal models against disease progression, but the degree of protection was different. Only S-29 protein provided 100% of mice protection after challenge with SARS-CoV-2 Beta VoC. On the contrary, one mouse in both S-2P and S-21 groups developed severe disease. In accordance to humoral response data, immunized animals showed lower viral load in lung and brain than control animals and a decrease trend over time in nasal turbinate and oropharyngeal swab samples.These data together with S-V987H results pinpoint that the S stabilization approaches may impact on the protection capacity of the S glycoprotein. Indeed, Lu et al., found that the HexaPro S is more immunogenic and protective than the S-2P expressed into vesicular stomatitis virus vector[356]. Despite both S-V987H and S-29 showed full disease protection, the S-29 protein yield is higher than S-V987H (2-fold) and S-2P (5-fold). Apart from their specific mutations, all S variants described here had in common a T4 foldon trimerization motif and the silenced furin cleavage site as Pallesen et al. used before in S MERS-CoV-2 production[65]. A S recombinant protein-based vaccine developed by Sanofi Pasteur (CoV2 preS dTM) includes these two structure patterns added to 2P substitutions.

The CoV2 preS dTM vaccine have demonstrated to be well-tolerated and immunogenic in humans[357]. Different formulations of CoV2 preS dTM as booster vaccines have shown increased neutralizing titters and enhanced cross-neutralization activity against different SARS-CoV-2 variants, including Omicron variant[358]. Furthermore, Sanofi Pasteur have successfully implemented these approaches to SARS-CoV-2 Beta variant S sequence (Vidprevtyn Beta), which have shown improved boosting capacity against Beta, Delta, and Omicron than either CoV2 preS dTM or BNT162b2 boost dose after complete vaccination with BNT162b2[359]. Recently, the EMA have approved the Vidprevtyn Veta as booster vaccine. Interestingly, our S-29 construct may be a great alternative to the S-2P backbone for the generation of novel SARS-CoV-2 variant-adapted S-based vaccines, since it presented increased protein production and protection in animal models against virulent and neutralization against resistant SARS-CoV-2 variants.

Immunogen conformation directly influences vaccine capacity to trigger an effective immune response. Thus, during the S-ACE2 receptor binding and membrane fusion process, the S glycoprotein suffers several conformational changes that expose many epitopes that are occluded in prefusion conformation. These novel epitopes can be high immunogenic, focusing the immune response, and hampering the development of other specificities particularly neutralizing antibodies. Therefore, preservation of the native S prefusion conformation may be critical for vaccine development. Thus, Bowed et al. showed that stabilized S-based vaccines elicit superior immune response than non-stabilized S-based vaccines, emphasizing the relevance of prefusion stabilized approaches in SARS-CoV-2 S based vaccine development[360]. Several strategies for stabilize class I viral fusion proteins from other viruses, such as HIV[361,362], respiratory syncytial virus (RSV)[363], and Ebola[364], have also resulted in improved immunogenicity, highlighting the importance of stabilizing approaches in viral vaccine development.

In summary, we described a novel set of mutations that stabilized the S glycoprotein in its prefusion conformation, increasing its production *in vitro* and improving its protective capacity against SARS-CoV-2-induced disease *in vivo*. Hence, these new stabilization approaches may be incorporated in future SARS-CoV-2 vaccines and may also contribute to the progress of novel vaccines for other SARS-CoV-2-like respiratory viruses.

CONCLUDING REMARKS

Objective I: To design novel S-stabilizing mutations *in silico.*

In a first step 10 S-stabilizing mutations were designed to favor the close S state. Additionally, 18 S-stabilizing approaches in combination with K986P and V987P mutations were designed to promote the open S conformation.

Objective II: To evaluate the yield and RBD exposure of S-stabilizing trimers.

Stabilizing mutations impact protein yield and RBD exposure. Three S-trimer variants were selected based on their improved yield and RBD exposure: S-V987H, S-21 and S-29.

Objective III: To produce and purify the selected S trimer mutants.

Selected S-trimer mutants were correctly produced in Expi293 cells and purified by IMAC with a purity over 90%

Objective IV: To evaluate the immunogenicity and efficacy of selected mutated S-trimers in animal models upon challenge with different SARS-CoV-2 variants.

S-V987H, S-21, and S-29 immunogenicity was similar to the S-2P protein in K18-hACE2 mice and Golden Syrian hamster, and superior to monomeric RBD. After viral challenge, animal immunized with these proteins showed faster viral clearance than RBD or S-2P vaccinated animals. Only immunization with S-V987H and S-29 coffered full protection against severe disease in both animal models.

Since S-29 has the highest protein yield and full protection capacity, this S-variants may be a promising alternative to S-2P on the next generation of SARS-CoV-2 variant adapted S-based vaccines or future SARS-CoV-2 like coronaviruses vaccines.

SYPHILIS

INTRODUCTION

1. Syphilis Disease

Syphilis is a sexual transmitted infection caused by the spirochete *Treponema pallidum* subspecie *pallidum* (TPA). Although the origin of the syphilis epidemic is unclear, the first cases of the disease were reported in Europe in the late 15th century[365,366]. In 1905, Schaudinn and Hoffmann discovered the bacteria causing this venereal disease, and in 1943, the first cases of syphilis were successfully treated with penicillin[367]. Over half a century later, penicillin remains one of the most efficacious treatments[368].

Syphilis and three nonvenereal treponematoses (yaws, bejel and pinta) were at first believed to be caused by the same agent, despite the fact that their clinical manifestations are different. Since pathogenic treponemes are morphologically and antigenically very similar (> 95% DNA homology), genomic sequencing was needed to identify distinct subspecies of *Treponema pallidum* that cause nonvenereal treponematoses: *Treponema pallidum endemicum* (causative agent of bejel), and *Treponema pallidum pertenue* (causative agent yaws). Pinta is caused by a different species of spirochete bacteria, namely *Treponema carateum*[368,369]. All of them are obligate human pathogens characterized by its invasiveness and immune evasiveness[370–373].

A syphilis infection consists of three main stages[369]. Primary syphilis usually begins approximately 2-3 weeks after contact with the pathogen, and it is characterized by the presence of an ulcerated lesion, called chancre. Typically, this lesion appears on the genital area, or other body parts related to sexual contact, usually accompanied by regional lymphadenopathy[369,374]. In the absence of treatment, primary lesion resolves spontaneously in 3-6 weeks. Secondary syphilis develops as a result of bacteria dissemination[374]. Clinical manifestations include malaise, headache, fever, diffuse lymphadenopathy, and maculopapular rashes with either discrete or widespread body involvement[369,374]. Unless treated, secondary lesions can take up to several months to resolve. The disease then enters in a latent stage without exhibiting clinical manifestations[369,370,374]. It remains unclear how TPA establishes latency, and which tissues or organs act as reservoirs[370]. A relapse of infection from these reservoirs can occur in 25% of untreated patients within two years after secondary syphilis resolution, and present new secondary-like clinical manifestations.[370,374]. After years or even decades, 15-40% of untreated and latently

infected individuals will develop tertiary syphilis. This stage involves serious cardiovascular, neurological, bony and visceral affections that may eventually result on death of infected individuals[369,374]. Remarkably, penicillin administration prevents syphilis progression to its secondary and tertiary stages and cures the infection. However, treated patients remain susceptible to reinfection, because the previous one fails to produce a protective immune response[375–377].

According to WHO data, in 2016, 19.9 million people had syphilis, and there were 6.3 million of new cases per year[378]. The prevalence of congenital syphilis was 0.69% in 2016, with a rate of 473 cases per 100.000 live births[379]. Syphilis is considered the second cause of stillbirths after malaria[380]. A high prevalence of syphilis is observed in low-income countries, and it has been rising in high-middle income states during the last decade[369,378,381,382]. Particularly, this increase has been observed in men who have sex with men (MSM) with multiple sexual partners, as well as sexual networks of heterosexual individuals. In this setting, syphilis is also associated with higher risk of HIV infection[369,381–383].

Importantly, although syphilis can be easily diagnosed, treated with an inexpensive antibiotic, and no animal reservoir has been identified to date, syphilis continues to be a significant global health problem. Therefore, the development of a syphilis vaccine is urgently needed to complement disease control and prevention measures. In this review, we focus on syphilis vaccine development, use of outer membrane proteins (OMPs) as putative immunogens, anti-TPA immune responses, as well as TPA evasion mechanisms, to provide information about potential antigen selection in syphilis vaccine and immunization strategies.

1.1. *Treponema pallidum* subsp. *pallidum*

TPA is a flat-wave spirochete of 5-15 μm and 0.2 μm of diameter[384] that belongs to Spirochaetaceae family, particularly *Treponema* genus (**Fig.32**). Treponemes are usually classified as Gram-negative bacteria due to their double membrane structure[385]. However, the composition of their outer membrane (OM) is noticeably different[386,387]. The TPA OM is characterized by the paucity of surface-exposed proteins[388–390], the presence of phosphatidylcholine, phosphatidylglycerol, phosphatidylserine, and the lack of cardiolipins[387] and lipopolysaccharide (LPS) [391,392]. Interestingly, cardiolipins are present in the cytoplasmic membrane[387], and

represent the main lipid antigen targeted by anti-TPA antibodies of infected individuals[387]. However, other constituents of the OM (e.g. glycolipids) do not present immune reactivity[387,393]. The lipid composition and poor protein content of OM are key features of TPA, and may contribute to the poor immunogenicity of this pathogen[386–388,390].
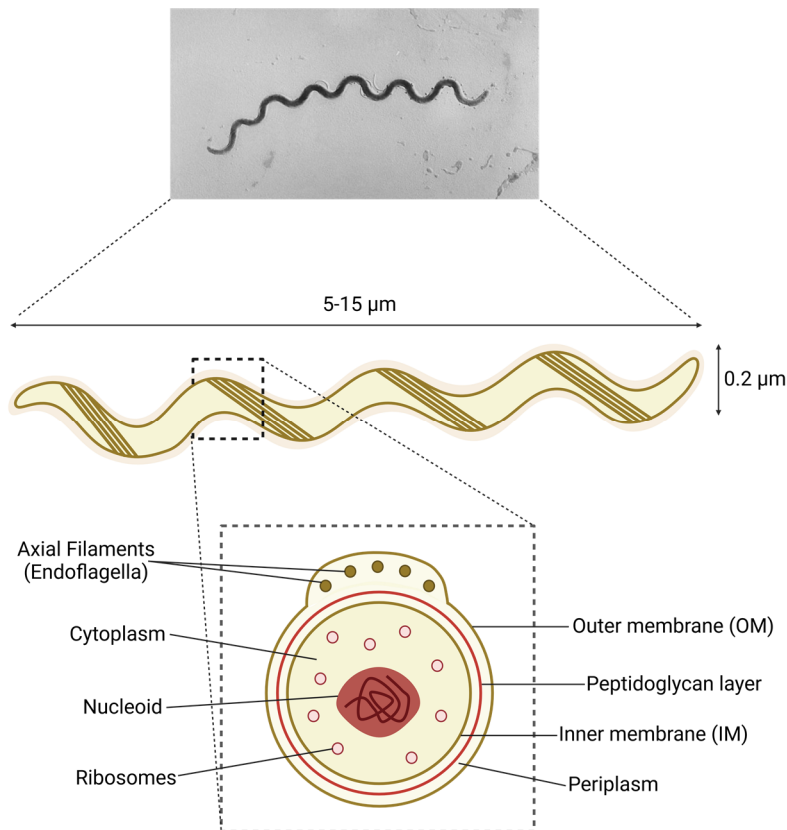
Figure 32. Treponema pallidum. Microscopy image of TPA is provided by Centers for Disease Control and Prevention (1972). A graphical representation of TPA is showed. TPA has a double membrane structure with a peptidoglycan layer among them. TPA is a flat-wave spiroquete crossed by axis filaments along all its body which allow its motility.

TPA is actively motile, although its motile system differs from other flagellar bacteria[394]. Axis filaments (known as endoflagella) are found in the periplasmatic space and extend from cell poles through the entire cell body length[395] (**Fig.32**). These filaments comprise three core proteins (FlaB1, FlaB2, and FlaB3) and an external protein, which surround the filament core (FlaA)[392,395]. When endoflagella rotate in one direction, the cell body moves in the opposite one. This torsion results

in a corkscrew-like motion that, together with the action of metalloprotease and adhesin proteins, allows spirochetes to cross tissues and disseminate through the body[396,397].

Until recently, TPA had not been grown *in vitro*[398], and bacteria propagation in rabbits was the only strategy to obtain sufficient live and infective organisms for experimental investigation[399]. The lack of the tricarboxylic acid cycle and microaerophilic requirements make this bacterium totally dependent on host cells for the acquisition of purines, pyrimidines, and most amino acids[370,372,392]. Therefore, TPA cannot survive outside the host, and loses its infectious capability within few hours[372,400].

Besides humans, rabbits are one of the few mammalians that are susceptible to TPA infection, and has become the reference animal model to study syphilis immune protection. After infection, rabbits develop primary and secondary stage-like clinical signs, and a humoral response similar to the one observed in humans[401–403]. Intradermal TPA inoculation induces dermal lesions that resemble human chancres, and bacteria can disseminate to distal organs, mainly secondary lymphoid organs (i.e. spleen)[396,404]. However, invasion of the central nervous system is not frequently observed and it depends on the utilized TPA strain[405]. In addition to rabbits, there are other species that are also susceptible to TPA (i.e. non-human primates, hamsters, guinea pigs, and mice). While only non-human primates and rabbits develop clinical signs similar to humans[404,406], mice and other rodents may be useful to study bacteria dissemination[407].

The TPA genome is a circular chromosome of approximately 1138 kilobase pairs that contains 1041 predicted ORFs[392]. Its genome is small compared to other pathogenic bacteria[392]. The genome sequence confirms that TPA cannot synthetize *de novo* enzyme cofactors, fatty acids, tricarboxylic pathway enzymes, or nucleotides, even though it contains 57 ORFs encoding transport proteins and is able to use the glycolytic pathway[392]. TPA lacks genes encoding superoxide dismutase, catalase, or peroxidase, which could explain its susceptibility to oxygen. Additionally, several genes have also been identified that are involved in the synthesis of motile proteins and lipoproteins[368,372,392]. Genome comparison among pathogenic *Treponema pallidum* subspecies has shown that they are similar in size and structure, and differ less than 0.2%-0.4% in their genome sequence[408,409].

1.2. Infection Course and Immune Response

Syphilis is generally transmitted through sexual contact or from mother to child. Spirochetes gain access to the host through epidermal micro-abrasions or directly penetrating mucosal membranes[410,411]. Once TPA has entered the body, it adheres to epithelial cells and extracellular matrix and locally multiplies with an estimate rate of once every 30-33 hours[412,413]. *In vitro* binding studies have shown that laminin and fibronectin are among the anchor molecules involved in these interactions[414–417]. Since TPA lacks cytotoxic toxins or other virulence factors[392], tissue destruction and chancre lesions are probably caused by the inflammatory response at the entry site[411]. The initial immune response clears bacteria locally, and the primary stage lesions resolve spontaneously within 3-6 weeks. Meanwhile spirochetes spread throughout the body and the infection rapidly becomes systemic, triggering secondary syphilis. Afterward, spirochetes penetrate deeper tissues and induce the expression of inflammatory signals, promoting the migration of immune cells to the infected tissues[411]. *In vitro* studies have shown that TPA can induce the expression of the adhesion molecules ICAM-1, VCAM-1 and E-selectin in endothelial cells[418–420]. In addition, metalloprotease activity plays a major role in the penetration and dissemination of TPA through extracellular matrix and intercellular junctions[421,422]. In the final stage, infection and the associated immune response damage various organs (e.g. heart and brain), resulting in debilitating health problems[411].

TPA infection triggers a complex immune response that fails to control the spread of the bacteria and the progression of the disease. In primary syphilis, polymorphonuclear leukocytes (PMNs) are the first immune cells to infiltrate the infection site[423] (**Fig.33A**). These cells may contribute to the initial control of the infection by secreting anti-microbial peptides[424] and clearing spirochetes by phagocytosis[423,425]. However, the initial control of the infection is limited as bacteria dissemination occurs in virtually all cases. Besides PMN, dendritic cells (DCs) (**Fig.33A**) can also phagocyte whole or bacteria-derived fragments, thereby stimulating their maturation and antigen-presentation capacity. Thus, DCs increase the production of pro-inflammatory cytokines, such as IL-12, IL-6 and IL-1B, and upregulate the expression of CD54, CD83, CD80, CD86, and HLA-DR[426,427]. Mature DCs migrate to lymph nodes (LNs) where they present treponemal antigens to T cells, inducing antigen-specific T cells responses. These T cells can be detected in secondary lymphoid organs of infected animals three days post-infection and

progressively accumulate at the infection site[428–430], coinciding with maximal TPA burden[431,432]. Rabbits infected with TPA showed a rapid hyperplasia of T cell zones in secondary lymphoid organs (LNs and spleen)[402,430]. Although Th1 CD4^{+} T cells dominate the T cell infiltrate[402,425,433] (**Fig.33A**), cytotoxic T cells (CD8^{+}) can also be found in primary lesions, where their role remains unclear. CD8^{+} T cells may be required for the elimination of TPA reservoir inside non-phagocytic cells in early syphilis lesions[433–435]. In this sense, perforin and granzyme are detected in early lesions, suggesting cytolytic activity[436]. Furthermore, CD8^{+} T cells, as well as NK cells, could contribute to the secretion of interferon-γ (IFN-γ)[373,437]. Th1 cytokines can promote the migration and activation of macrophages (**Fig.33A**), whose number increase rapidly by day 10 after infection at the entry site[432]. Activated macrophages phagocytose and destroy spirochetes[428,438] until they are completely cleared from the infection site. Interestingly, this process can be enhanced by TPA opsonizing antibodies and IFN-γ, particularly through the Fc-Fcγ receptor interaction[437–441]. However, other less efficient mechanisms, such as non-opsonic phagocytosis and active direct invasion, may also participate in TPA-macrophage interplay[442]. In response to TPA infection, macrophages polarize to M1 phenotype and secrete proinflammatory cytokines (i.e. IL-1β, TNF-α, IL-12, and IL-15)[441,443], which can ultimately promote necrosis and ulcer formation typical of primary chancre lesions.

Regarding the humoral response, anti-TPA antibodies can be detected as early as 6 days post-infection[444]. However, the antibody response kinetics vary based on the target protein and TPA strain. For example, antibodies targeting *Treponema pallidum repeat* (Tpr) Subfamily I and II rise between days 10 and 45 after infection[445]. During primary infection, IgM dominates the anti-TPA humoral response, while IgG levels gradually increase[444,446] (**Fig.33A**). Antibodies are not only involved in opsonization processes, they can also block bacteria dissemination and dermal lesions. Furthermore, the complement system is also involved in limiting treponemal activity, specially working in conjunction with antibodies[447–449]. TPA accumulates sialic acid on its surface, making it resistant to complement lysis by the alternative pathway[450–453]. Thus, classical complement activation pathway is key to bacterial clearance. This data suggest that the immune response generated against TPA during primo-infection is a delayed type hypersensitivity (DTH) immune response, where sensitized T cells play a major role. In fact, it has been hypothesized that syphilis prognosis depends on the balance between DTH and

humoral responses. Thus, it has been proposed that a strong DTH immune response may be required to clear the infection, whereas latency may result from intermediate DTH responses. Tertiary disease would be related to a weak DTH and a strong humoral response[432,454]. Despite this, antibodies may be crucial for preventing infection[432,455]. Accordingly, rabbits receiving immune serum showed a delay in the appearance of lesions that were also less severe[456]. Further, patients who have been previously treated for syphilis remain susceptible to reinfection because they do not develop an effective anti-TPA humoral response[432].
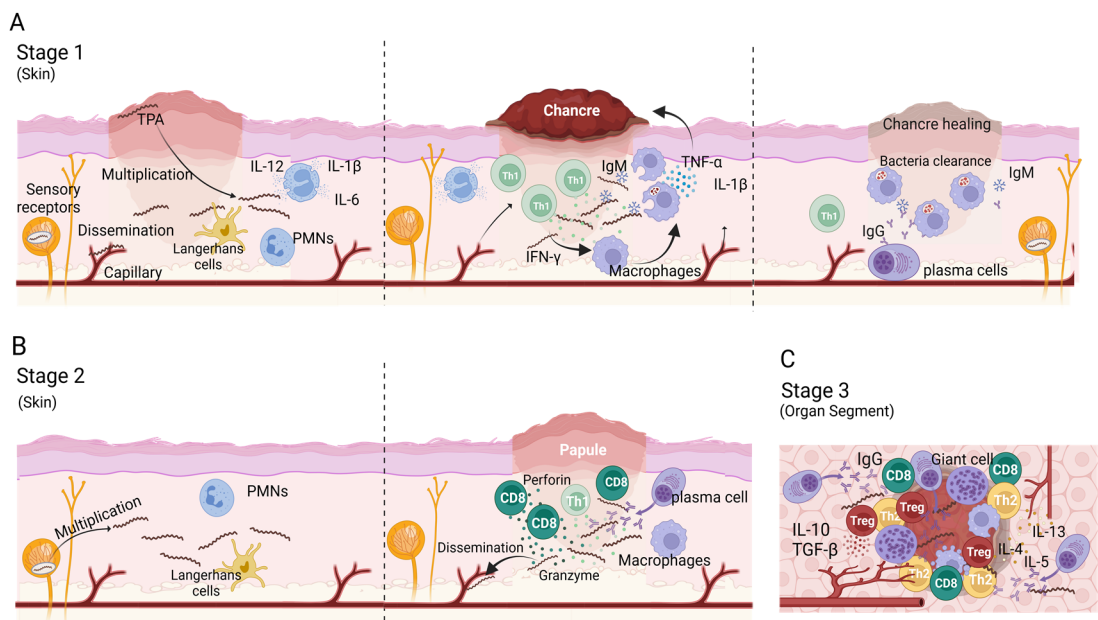
Figure 33. Immune response to TPA infection. (A) During primary syphilis, a local lesion called chancre appear in the site of infection. After bacteria entry, the microorganisms proliferate and disseminate to distal organs. Bacteria are phagocyted by polymorphonuclear cells (PMN) and dendritic cells (Langergans cells) that migrate to draining lymph nodes to activate CD4+ Th cells. Th1 T cells migrate to the bacteria proliferating foci and produce Th1 cytokines (IFN-γ) for recruiting and activating macrophages. M1 macrophages phagocyte bacteria and produce TNF-α and IL-1β that contribute to chancre development and eventually necrosis. IgM antibodies and complement contribute to bacteria opsonization favoring their removal by macrophages. **(B)** During secondary syphilis, TPA expands from reservoirs with systematic affectation. A typical rash appears in most cases. Anti-TPA humoral responses are mainly IgGs and plasma cells are visible in the infiltrate of secondary cutaneous lesions. CD8+ T-cells are more represented than CD4+ T cells in lesion infiltrates. **(C)** Tertiary syphilis affects deep organs like brain and heart. A Th1/Th2 switch progressively occur and the immune response is down regulated by the presence of regulatory T cells. Plasma cells are well represented. Gummas can be developed in different locations (i.e., liver, skin, brain). Gummas are a granuloma-like structure characterized by a necrotic hyaline nucleus surrounded by immune cells (i.e. plasma cells, macrophages and giant cells) and fibroblasts.

Both cellular and humoral responses are maintained for months after clearance of primary syphilis lesions[403,457,458], and their magnitude correlate with the persistence of TPA as latent infection[459–462]. From this state, relapse of active infection can occur leading to secondary and tertiary syphilis. Secondary syphilis manifests as inflammatory cutaneous affection that differs in histological appearance from primary syphilis. The histology of secondary syphilis is variable but, in general, lymphocytes, macrophages, and plasma cells are commonly present in secondary lesions whereas polymorphonuclear and eosinophilic infiltrates are found in a smaller proportion[463–465] (**Fig.33B**). Furthermore, CD8$^+$ T cells are highly represented[463] (**Fig.33B**). Contrary to primary syphilis, IgGs dominate the anti-TPA humoral immune response during secondary syphilis[446,466,467] (**Fig.33B**). Moreover, whereas IgG1 is the main IgG subclass in primary syphilis, both IgG1 and IgG3 subclass can be equally found in secondary syphilis[468].

Finally, tertiary syphilis is characterized by a multiorgan affection and the development of gummas in different tissues (such as liver and skin). Gummas are granuloma-like structures characterized by a necrotic nucleus surrounded by macrophages, giant multinucleate cells, lymphocytes, and plasma cells[432] (**Fig.33C**). Neurosyphilis is characterized by an increase in the number of CD8$^+$ T cells in blood[469]. Moreover, a switch in the production of Th1 to Th2 cytokines is observed during the evolution of the disease. While Th1 cytokines are mainly detected during primary syphilis, Th2 cytokines increase in late states of the disease[470] (**Fig.33C**). This correlates with cell depletion in the diffuse cortex, and a follicular hyperplasia in LNs with plasma cells accumulation within the interfollicular areas during tertiary syphilis[432]. These changes in the immune response during syphilis are closely related with disease progression.

2. Immunization Studies: Challenges and Controversies

Despite public health campaigns and the availability of efficacious treatment, syphilis prevalence has increased worldwide in the last decade381, suggesting the need for additional measures to control the transmission of the infection. The development of a syphilis vaccine could be a valuable tool. However, after several decades of research, an effective vaccine for syphilis remains elusive. A variety of strategies have been tested, including inactivated bacteria and subunit recombinant proteins, even though with limited success. Interestingly, Miller et al. demonstrated

protection of rabbits against TPA infection following 60 immunizations with γ-irradiated bacteria for 37 weeks[471]. Although this experimental strategy is far from being applicable to humans, it serves as a proof of concept that a syphilis vaccine is feasible. In addition, human challenge studies performed in the 50's showed that latently infected patients were resistant to reinfection with a heterologous TPA strain[472]. Accordingly, Marra and colleagues reported that previous syphilis infection may attenuate the manifestation of subsequent TPA infection[473]. Thus, those individuals that experimented three or more episodes of syphilis were more likely to develop latent early syphilis after subsequent infections. These studies indicate that it will take a long time to establish a protective immunity against TPA, further emphasizing the low immunogenicity of this pathogen.

Until 2018, one of the main handicaps in the development of a syphilis vaccine was the inability to grow the bacteria *in vitro*[398]. This technical limitation shifted the focus of most studies towards recombinant OMPs[474]. Although none of these proteins provided complete protection against *in vivo* TPA challenge, promising results were observed; namely, the induction of a strong humoral response, less ulcerative lesions, faster recovery of lesions, or inhibition of bacterial dissemination to distal organs. These studies provided meaningful knowledge about OMPs, immunization regimens, and potential vaccine targets. The advancement of bioinformatic tools allowed the identification of additional putative OMPs, as well as the prediction of structure models and B cell epitopes[475,476]. The employment of newly-developed approaches (e.g. genetic engineering), and refined bioinformatic tools enable to delve further into OMPs knowledge, benefiting future vaccine studies[477,478].

2.1. The Outer Membrane Proteins

One of the major features that differentiate TPA from other bacteria is the paucity of surface-exposed OMPs[388–390]. It has been calculated that the density of OMPs in TPA is approximately 100-fold less than that in *E. coli*[386]. The identification and characterization of TPA OMPs has been challenging due to the inability to genetically manipulate and cultivate TPA *in vitro* (until recently)[398], and the fragility of its OM, which generated a strong controversy in some studies. The intrinsic properties of the OM (i.e lack of LPS and low density of proteins) makes it can be easily damaged by common experimental manipulations (e.g. centrifugation, resuspension, or using low concentration of non-ionic detergent)[386,390]. OM

disruption leads to potential exposure of lipoproteins that are normally present in the periplasmic space and cytoplasmic membrane, and could erroneously pinpoint proteins as OMPs. Due to these technical limitations, the identification of OMPs was often based on prediction of their sequence and structure or by comparison with functional orthologs from other species[475]. Thus, OMPs can be classified in three main groups according to their putative functions (**Fig.34**).
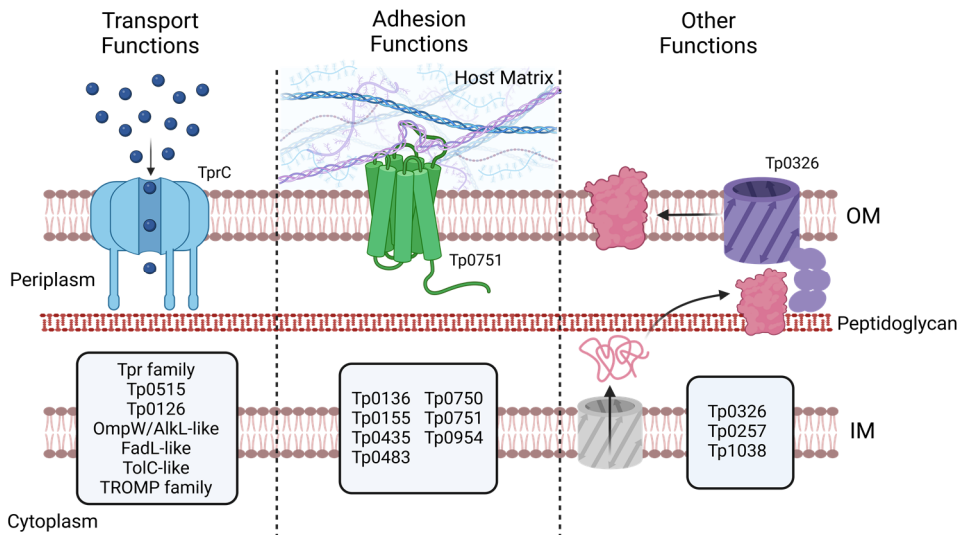
Figure 34. OMPs functions. Overview of TPA membrane arquitecture showing the three main function of OMPs: (1) transport of nutrients and toxic substances (e.g. TprC), (2) adhesion and bacteria dissemination (e.g. Tp00751), (3) and other functions related to cellular homeostasis as protein translocation (e.g, Tp0326). (OM) Outer membrane. (IM) Inner membrane. Gray squares include the OMPs involved in each function.

Transport Function

Since nutrient import and toxics efflux are crucial for bacteria surveillance, several TPA OMPs have been involved in transport function.

Tpr protein family

The Tpr family of proteins include 12 members that are divided into three subfamilies according to their amino acid composition: subfamily I (TprC, D, F, I), subfamily II (TprE, G, J) and subfamily III (TprA, B, H, K, L). Among them, subfamily I and TprK (subfamily III) are the most widely studied. Regarding Tpr protein location, sequence analysis predicted that TprB, TprC, TprD, TprE, TprG, TprH, TprI, TprJ, TprK and TprL could be located in the OM[386]. Supporting this prediction, a putative cleavable signal peptide was identified in most of the Tprs superfamily members, including TprC, D, F, I, E, G, J, A, B and TprK proteins[475,479].

The Tpr family is related to the major outer sheath protein (MOSP) of *Treponema denticola* [479], a surface-exposed protein with adhesive and porin function[480–482]. Most Tprs include three main domains: 1) a N-terminal domain related to the N-terminal domain of *Treponema denticola* MOSP, 2) a central region, and 3) a C-terminal domain related to the C-terminal domain of *Treponema dentiola* MOSP, that is lacking in TprF and TprA proteins. Recently, the presence of short molecular recognition features (MoRFs) was predicted in most Tprs. These motifs may interact with specific proteins and undergo disorder-to-order transition upon binding[475]. Sequence analysis has shown that the N- and C-terminal domains of the Tpr proteins from subfamilies I and II are relatively conserved, whereas central domains are variable in length and sequence[370]. Terminal domains present amphipathic regions and flank hydrophilic regions of the central domains. According to Hawley et al., the N- and C-terminal domains from all Tprs adopt a β-stranded structure, while the central regions may be mostly α-helices[475].

Structural analysis of the subfamily I has shown that these proteins form a β-barrel trimeric channel. However, unlike classical porins, in which the entire polypeptide forms a β-barrel, Tpr subfamily I possesses bipartite topology. The C-terminal domain forms a β-barrel structure and is surface-exposed, while the N-terminal and central domains anchor the β-barrel into the peptidoglycan sacculus of the periplasmatic region[483,484]. Accordingly, while the expression of TprC/D in *E. coli* is surface-exposed, TprF lacks the C-terminal domain, and therefore, it is entirely periplasmatic[386]. The immunodetection of Tpr proteins by electron microscopy using purified rabbit anti-Tpr I immunoglobulins, confirmed the presence of Tpr proteins in OM and periplasmic spaces, which could be due to the bipartite structure previously described or because the anti-Tpr I antibody recognized proteins with distinct location[485]. More recently, Hawley et al., confirmed that the bipartite membrane topology identified in subfamily I is common to all Tprs with three full domains[475]. Based on sequence and structure analysis, it has been shown that the Tpr family may be involved in the import of small soluble molecules. In this sense, the integration of some Tpr proteins in liposomes increased their permeability[483,484]. Therefore, changes in protein expression and/or variation of their channel-forming β-barrel region could be used to adapt TPA nutritional requirements to the environment. Accordingly, the expression of Tpr proteins can vary among strains, and in the same strain overtime[486], which may explain why the anti-Tpr humoral

response differ among TPA isolates[445]. This observation suggests the existence of mechanisms that can regulate the expression of these genes. Thus, a hypervariable homopolymeric guanosine (poly-G) tract and a cAMP receptor protein (CRP) binding motif have been identified upstream of the transcription start site of the Tpr subfamily II and III[487–489]. In fact, Tp0262 (a TPA CRP homologue) can bind to these promoters and regulate the surface expression of these proteins during infection[487]. As a result, the specificity of the humoral response elicited against Tpr proteins differ among TPA isolates[445].

Of the Tpr superfamily, TprK is one of the best characterized proteins. It has been previously shown that recombinant TprK is a monomeric porin by negative-staining electron microscopy[490]. Anti-TprK antibodies can be detected early during infection[445]. However, TprK exhibits sequence variation that contributes to immune escape. Thus, several alleles have been identified among TPA strains[491,492]. Moreover, this protein shows seven variable domains whose sequence changes by non-reciprocal recombination, mainly with regions downstream of the TprD gene[491,492], a mechanism that is enhanced under immune pressure[493,494]. The existence of this mechanism could explain why TprK variability was higher in TPA isolates from patients affected with secondary syphilis than those with primary syphilis[492]. However, TprK genetic variation can also occur in the absence of immune pressure[495]. Interestingly, it has been reported that humoral response *in vivo* targets variable regions, while cellular response recognizes conserved TprK epitopes[496,497]. Moreover, animal challenges using TPA with TprK homologous to the one used in immunization regimen show better protection than those animals challenged with a strain expressing heterologous TprK[496]. Despite that, there are controversies on the role of anti-TprK antibodies, and TprK protective efficacy as immunogen and its location. Centurion-Lara and colleagues described that TprK is located on the OM, and TprK-specific antibodies had opsonization capacity[479]. Interestingly, rabbits immunized with this protein did not develop ulcerative lesions. These lesions healed faster than those observed in unvaccinated control animals and contained fewer spirochetes, when analyzed by darkfield microscopy[479]. Additionally, Morgan et al. identified the N-terminal region of TprK (37-273 amino acids) and, to a lesser extent, the C-terminal portion (349-478 amino acids), as the parts of the protein that induced the previously-described protective immune response[498]. Conversely, Hazlett and colleagues described that TprK was located in the periplasmic space, anti-TprK antibodies lacked opsonization activity, and

immunization with recombinant TprK did not induce a protective immune response nor TprK sequence variation[499]. Further investigation would be needed to clarify these discrepancies.

Regarding the immunity elicited against other Tprs members, anti-TprI antibodies were detected in 98% of syphilis-affected individuals. These antibodies mainly targeted the conserved N-terminal region. The lack of reactivity was associated with early infection[485]. Remarkably, experiments performed in rabbits showed that TprI immunization did not protect rabbits from infection[500]. However, cutaneous lesions did not ulcerate and healed faster than those generated in unvaccinated animals. This protein elicited strong humoral and cellular responses mainly targeting the conserved N-terminal region of the protein during TPA infection[445,500]. Not surprisingly, immunization with the conserved N-terminal region of TrpF, which is also common to all subfamily I members, did not protect rabbits from TPA infection after challenge. However, TprF vaccination attenuated lesion development, prevented ulceration, and reduced bacterial burden in skin lesions[500]. In regard to TprC and TprD, epitope mapping has shown that the humoral response detected in rabbit sera is directed against exposed loops[476]. Moreover, the N- and C- terminal regions contain the most reactive epitopes. Surprisingly, Anand et al. showed that sera from infected individuals do not recognize TprC, while TPA-infected rabbits develop antibodies with opsonization activity[483]. One explanation could be the low expression of TprC and the different magnitude of the humoral response found among various syphilis strains and subspecies.

Tp0515

Tp0515 is a structural ortholog of LptD protein, which is part of a multiprotein complex involved in LPS trafficking to the OM in Gram-negative bacteria[386]. Thus, since LptD is embedded in the OM, Tp0515 is inferred to be an OMP. However, sequence analysis of TPA genome failed to identify LPS biosynthetic pathway[392]. Notably, orthologous proteins for several components of the LPS transport pathway have been found in TPA[475], suggesting that even without LPS, these proteins could be involved in translocation of other cellular products to the OM, as glycolipids[386]. Tp0515 structural modelling found that this protein is a 26-stranded β-barrel embedded in OM with exposed extracellular loops[475]. Moreover, Hawley et al. identified B cells epitopes inside these extracellular loops using bioinformatic analysis[475]. However, the immunogenicity and capacity of this protein to induce protective immune response still need to be empirically demonstrated.

Tp0126 and other OmpW/AlkL orthologs

Four proteins that are orthologs of OmpW (Tp0126 and Tp0733) and OprG (Tp0479 and Tp0698) have been identified in TPA[475]. Both *E. coli* OmpW and *Pseudomonas aeruginosa* OprG proteins are members of the OmpW/AlkL family of proteins, which have been suggested to be involved in bacterial adaption to environment stress and nutrient acquisition[501,502]. OmpW and OprG have an eight-stranded β-barrel architecture and form a peculiar hydrophobic channel, which allows the transport of hydrophobic molecules directly to the membrane, bypassing the hydrophilic periplasmatic space[475,503]. Thus, Tp0126 could be involved in fatty acid transport (unable to be synthesized by TPA alone)[504]. Interestingly, this protein is highly conserved among TPA strains. Its transcription is regulated by the presence of guanidine homopolymers of various lengths located upstream of its promoter, which is consistent with phase variation[505].

Remarkably, Tp0126 may show low immunogenicity. Anti-Tp0126 antibody levels in serum samples from patients with latent syphilis were lower than those targeting Tp0574, a highly expressed and immunogenic TPA protein[505]. In addition, anti-Tp0126 antibodies were detected in Tp0126-immunized rabbits only after the third boost, highlighting the potentially low immunogenicity of this protein[505]. Interestingly, these antibodies targeted Tp0126-external loops and were able to opsonize TPA. However, immunization with Tp0126 showed poor protective capacity, if any, in rabbits. In fact, treponemes isolates from lesions of immunized and challenged rabbits showed lower transcription levels of Tp0126, which was associated with a longer polyG region ($\geq$ 9 G's), when compared to treponemes obtained from the challenge inoculum[505]. These results suggest that the expression of Tp0126 may be reduced during infection, which could explain the absence of protection observed in immunization and challenge experiments.

Like Tp0126, other members of the TPA OmpW/AlkL ortholog group (Tp0733, Tp0479, and Tp0698)[475] are predicted to form a membrane-channel and be involved in transport of small molecules. Hawley et al. predicted multiple surface-exposed B cell epitopes in their extracellular loops, although the density of these epitopes differs from one to another protein[475]. Future experimental studies with these OMPs are envisaged to confirm their *in silico* predictions, and to inform about potential immunogenicity and capacity of inducing protective immune responses.

FadL-like proteins

Due to the low OM permeability of Gram-negative bacteria, these bacteria have an OM protein machinery involved in the uptake of long-chain fatty acids, such as FadL protein. TPA is unable to synthesize long-chain fatty acids[392]. However, since TPA OM is more permeable to fatty acids than other Gram-negative bacteria[506], membrane diffusion may be one of the mechanisms that this microorganism uses to uptake these molecules. Nevertheless, five FadL orthologs (Tp0548, Tp0856, Tp0858, Tp0859, and Tp0865) have been identified in TPA, suggesting that passive diffusion of fatty acids is not the only mechanism[475]. Structural modelling of these orthologs predicted that all TPA FadL-like proteins form a 14-stranded β-barrel with N-terminal in the barrel lumen[475]. Moreover, all five proteins contain one or more predicted B cell epitopes[475]. Interestingly, Delgado et al. recently described the presence of IgG antibodies and IgG⁺ B cells in TPA-infected rabbits that recognized the extracellular loops 2 and 4 from Tp0856 and Tp0858[507], indicating that these proteins could be useful in vaccine design.

TolC-like proteins

TolC is an OM protein from *E. coli*, which is part of an efflux pump complex involved in the removal of toxic substances[508]. To date, four TolC orthologs (Tp0966, Tp0967, Tp0968, and Tp0969) have been described in TPA[509]. Structural modelling of these proteins identified that they have a TolC-like topology based on four β-strands with two large extracellular loops and six α-helices[475]. Furthermore, Hawley et al. predicted that all four TolC-like TPA proteins, particularly Tp0969, enclose surface-exposed B cells epitopes[475]. Thus, these predicted OMPs could be targeted by the immune system. However, further *in vivo* analysis of their immunogenicity is required to determine their potential in vaccine development.

Treponema rare outer membrane proteins (TROMPs)

TROMP family includes three proteins: TROMP-1 (31 kDa), TROMP-2 (28 kDa) and TROMP-3 (65 kDa)[510]. TROMP-1 (also called TroA or Tp0163) was firstly described as a surface-exposed protein with porin-like properties[511]. However, it was later identified to be a periplasmatic metalloprotein anchored to the cytoplasmatic membrane[512–514]. TROMP-2 (also called Tp0663) was localized on the OM when it was expressed as recombinant protein in *E. coli*. However, the isolation of TROMP-2 from *E. coli* OM showed low porin insertional events, casting doubts on its porin

function[393]. Interestingly, both TROMP-1 and TROMP-2 were targeted by antibodies present in sera from infected rabbits and humans[510]. In fact, TROMP-2 could be a potential candidate for serodiagnosis of all syphilis stages[515]. TPA challenge experiments performed in Tp0663-immunized rabbits showed partial protection, with high titers of anti-Tp0663 antibodies. The authors observed attenuated lesions with an increased cellular infiltration. Importantly, no bacteria dissemination to distal organs was detected in immunized animals[516]. Of note, TROMP-3 is expressed at a lower concentration than the other two members of this family, and its function and structure remain unknown[393]

Adhesion Function

Adhesion to cells and extracellular matrix is crucial to the establishment of infection and the dissemination of TPA.

Tp0136

Tp0136 has been identified as a fibronectin-binding TPA OMP that binds more efficiently to cellular than plasma fibronectin[414,415]. This selective binding involves different domains of this protein. Thus, the conserved N-terminal region is mainly responsible for binding to plasma fibronectin. Residues in the C-terminal end, and also in the central portion of the protein, participate in binding to the cellular form of fibronectin[415]. Interestingly, Tp0136 shows sequence variability among TPA strains, and its transcription is regulated during infection[414,415]. The interaction of Tp0136 with fibronectin expressed on cell surface can promote bacteria attachment to tissues, facilitating body dissemination and favoring the colonization of distal endothelial tissues, central nervous system, or placenta[517].

In addition to its adhesion function, Tp0136 may also play an important role in chancre healing by promoting fibroblast and microvascular endothelial cell migration, and the activation and aggregation of platelets[518]. Immunization and challenge experiments performed in rabbits using recombinant Tp0136 produced in *E. coli* showed a delay in lesion ulceration but not in their development, indicating no protection against infection[414]. Remarkably, sera obtained from immunized animals reduced the attachment of the bacteria to fibronectin, although at lower levels than sera obtained from infected rabbits[414]. Interestingly, Xu et al. showed that rabbits immunized with Tp0136 elicited high levels of antigen-specific

antibodies, attenuated lesion development with increased cellular infiltration, and limited treponemal dissemination to distant organs[516]. Although there are discrepancies between both studies that could be explained by differences in adjuvant, immunization schedule, and the amount of live inoculated bacteria, these results suggest that antibodies developed against Tp0136 might be protective. However, the fact that antibodies elicited during experimental infection blocked more efficiently TPA binding to fibronectin than vaccine-induced antibodies elicited against Tp0136, suggest that, during vaccine design, other specificities should be also targeted to block bacteria more efficiently from binding to the extracellular matrix[415].

Tp0155

It has been described that Tp0155 preferably binds to fibronectin matrix and, therefore, it might be involved in the dissemination of TPA[519]. Tp0155 shows two lysin motifs (LysM) domains in its N-terminal portion that can play a major role in binding to fibronectin and peptidoglycans, and a M23 peptidase domain in the C-terminal region, which might show peptidoglycan lytic activities[520].

There is some controversy regarding Tp0155 surface location. Inhibition assays showed that recombinant Tp0155 reduced live TPA binding to fibronectin-coated slides, suggesting that Tp0155 is expressed on the OM[519]. This result was in line with the fact that TDE2318, a fibronectin-binding protein with high homology to Tp0155, was found in the surface of *T. denticola* according to immunofluorescence microscopy data[520]. However, immunofluorescence studies using agarose microencapsulated treponemes showed that Tp0155 is not exposed on the OM of TPA[521]. According to this observation, Tp0155-immunized rabbits, which elicited high antigen-specific antibody titers, were not protected against an intradermal challenge with live treponemes[521]. Thus, further investigation will be needed to determine whether Tp0155 would be a bona fide OMP or not. Remarkably, studies performed with human sera showed that approximately 70% of syphilis patients did not show antibodies against Tp0155, indicating that the expression of this protein or its immunogenicity may be low in natural infection[521,522].

Tp0435

Tp0435 is a highly immunogenic 14 kDa lipoprotein with adhesin function, also known as Tp17. To identify the location of Tp0435 in TPA, Chan and colleagues performed a study that analyzed the Tp0435 surface expression in TPA and Tp0435-transformed *B. burgdorferi* cells[523]. The authors concluded that Tp0435 may be post-translationally modified, generating several variants that can be differentially located between the surface and the periplasmic space. Contrarily, Cox et al., did not find Tp0435 surface-exposure evidences[524]. Structurally, Tp0435 encompasses eight-stranded anti-parallel β-barrel with a basin-like domain located at one end[525]. According to Chan et al., Tp0435 favors the attachment of the spirochetes to mammalian cell lines[523]. Interestingly, human sera from infected patients are reactive against Tp0435[522], and immunization of rabbits with a Tp0435-expressing *B. burgdorferi* strain induced a strong immune response against Tp0435[526]. However, this immune response failed to protect from infection or lesion development after experimental challenge[526]. Thus, further studies may be needed to determine the location of Tp0435 and its potential as vaccine candidate.

Tp0483

Tp0483 can bind both extracellular matrix and soluble fibronectin[519]. The C-terminal portion of Tp0483 (179-374 amino acids) also showed reactivity against laminin[527]. Little is known about the structure of Tp0483. However, a peptide encompassing 316-333 amino acids inhibited binding of Tp0483 to fibronectin, suggesting that this peptide, or a near region, should be responsible for binding to adhesive glycoprotein[528]. Similar to Tp0155, Cameron et al. indirectly suggested that Tp0483 was an OMP[519]. Contrarily, Tomson and colleagues did not find evidences of the Tp0483 OM location. Even though rabbits immunized with this protein elicited high antibody titers, the authors did not detect protection after challenge[521].

Tp0750

Tp0750 binds to fibrinogen and the fibrinolytic receptor complex protein Annexin A2. Tp0750 shows serine metalloprotease activity, and it is able to degrade fibrinogen and fibronectin, inhibiting the coagulation cascade, but cannot degrade fibrin clots[421]. Structurally, Tp0750 shows metal ion-dependent adhesion site (MIDAS)-containing von Willebrand Factor type A (vWA) domains (region V29-T147). The MIDAS domains bind to primary calcium. This protein, as well as Tp0751 (see

next section), are co-transcribed and might coexist as heterodimeric complex. However, unlike Tp0751, Tp0750 shows a limited laminin binding capacity[421]. Sequence analyses of both proteins have shown that Tp0750 is highly conserved among pathogenic treponemes species, whereas Tp0751 is less conserved, except for the most invasive treponemes species. Interestingly, Tp0750 and Tp0751 orthologs from the less invasive treponemes species do not bind or degrade host proteins, which strengthen the idea that both adhesion function as well as degradative capabilities are important to syphilis progression[529].

Tp0751

While there is a degree of agreement in regard to the structure of Tp0751, there are discrepancies regarding its function, location, and the relevance of the immune response elicited against this protein. From the structural point of view, Tp0751 presents a bipartite topology with a disorganized N-terminal region that is joined through an α-helix domain to a C-terminal portion arranged in eight anti-parallel β-sheets[416,530].

It has been previously described that Tp0751 binds to different forms of laminin in a dose-dependent manner, and can work as vascular adhesin, promoting bacterial dissemination[417,531]. Additionally, Tp0751 showed metalloprotease activity, and can degrade fibrinogen and laminin, promoting clot dissolution, and favoring bacterial dissemination[422]. However, Luthra and colleagues showed that Tp0751 is located in the periplasmic space and its main role is binding to small molecules along the barrel rim, such as hemes[530].

While Cameron and colleagues described that Tp0751 is recognized by antibodies in patient and infected rabbit sera[527], and these antibodies can opsonize the bacterium, Luthra et al. observed opposite results. In their study, Tp0751 induced a weak antibody response in infected human and challenged rabbits, and anti-Tp0751 antibodies lack opsonization capacity, probably due to the low levels of Tp0751 expression on the OM[530]. Immunization and challenge experiment in rabbits also provided contradictory results. Lithgow and colleagues showed that Tp0751-immunized animals showed attenuated lesions with low bacteria burden. Although immunization did not prevent infection, it successfully inhibited bacteria dissemination[532]. Conversely, Luthra et al. showed no protection against local or disseminated infection following intradermal TPA challenge in Tp0751-immunized animals[530]. Therefore, further research will be needed to clarify these discrepancies.

Tp0954

Tp0954 has been recently described as a surface lipoprotein, and may have a major role in congenital syphilis[533]. According to its structure, this protein is predicted to have a tetratricopeptide repeat structural motif with tandem α-helices. Moreover, Tp0954 sequence is conserved among several TPA strains (e.g. Nichols, Chicago, Mexico A and Amoy)[533]. Primus et al. also described that Tp0954-transformed *B. burgdorferi* B314 bacteria, which is known to be a poorly adherent strain, gained binding to mammalian epithelial cell lines, including a human placental cell line [i.e. BeWo (CCL-98)][533]. Unlike other TPA adhesins, Tp0954 can mediate adhesion and bacteria dissemination through binding to glycosaminoglycans present in human placenta, such as dermatan sulfate, heparin, and heparan sulfate, which are components of the extracellular matrix[533]. Dermatan sulfate is associated with fetal blood vessels and syncytial surface, whereas heparan sulfate is located in trophoblast layers[534–537]. Thus, it is possible that Tp0954 might facilitate congenital infection through binding to placental glycosaminoglycans.

Other Function

A number of proteins in the OM of TPA are not involved in neither transport or adhesion function and they are involved in other bacterial functions related to cellular homeostasis.

Tp0326

Tp0326 (or Tp92) shows homology with BamA orthologs from other Gram-negative bacteria. BamA-like proteins are characterized by a bipartite structure with a β-barrel domain located in the C-terminal portion, and at least one polypeptide-transport-associated (POTRA) domain in the N-terminal end. Particularly, Tp0326 was predicted to contain five N-terminal POTRA and one C-terminal β-barrel domains[538,539]. According to Desrosiers et al., the N-terminal POTRA domains are periplasmic, whereas the C-terminal β-barrel is embedded in the OM forming a pore[539]. The N-terminal end can bind to multiple periplasmatic proteins through POTRA domains, establishing a protein complex that is crucial for membrane synthesis. As other BamA-like proteins, Tp0326 is suggested to be part of a protein machinery involved in the translocation and insertion of proteins from the periplasmatic space to the TPA OM[539]. Interestingly, human antibodies are mainly directed against the Tp0326 periplasmic segment, while rabbit antibodies target

both N-terminal and C-terminal regions[539]. Indeed, Luthra et al. found that POTRA domains are immunodominant over the β-barrel domains in both rabbits and humans[538]. In addition, these authors described that the Tp0326 central pore exposes eight loops to the extracellular space. Among them, loop 4 is specially targeted by antibodies with opsonizing capabilities from infected rabbits and humans with secondary syphilis[538]. By contrast, Tomson and colleges failed to detect the expression of Tp0326 on the OM of treponemes encapsulated within agarose gel microdroplets using indirect immunofluorescence[521]. In addition, they did not observe protection in Tp0326-immunized animals after TPA challenge. Conversely, Cameron et al. showed that, although all Tp0326-immunized rabbits were infected after challenge, there was some degree of protection in the vaccinated animals that had high antigen-specific antibody titers[540].

Tp0257

Tp0257 (or GpD) was identified using a treponema genetic expression library and opsonized rabbit immune sera. This protein presents homology with *H. influenzae* GplQ protein, a glycerolphosphodiester phosphodiesterase protein, which is partially expressed on the surface[541]. Thus, it is possible that Tp0257 may be an OM protein. Accordingly, Cameron et al. reported indirect evidence of its surface location by immunoblot analysis of TPA lysates. The authors observed positive staining in the preparation that included the OM, but not in the OM-removed TPA lysate fraction[542]. Moreover, GpD was isolated from OM preparations[543]. Interestingly, rabbits immunized with recombinant Tp0257 exhibited a reduction in lesions development and bacterial proliferation after TPA challenge[542]. Contrarily, Shevchenko et al., showed that Tp0257 could be a periplasmic protein, since they did not identify surface-exposed evidences by multiple assays, and Tp0257-immunization failed to protect rabbits from TPA challenge[544]. More recently, a DNA vaccine encoding a Tp0257-IL-2 fusion protein showed a decrease in ulcerative lesions, as well as, in the number of lesions containing TPA[545]. The inclusion of IL-2 in the vaccine enhanced anti-GpD humoral responses and the levels of IFN-γ. Remarkably, rabbits immunized with a Tp0257-IL2 DNA prime and intranasal boost with recombinant protein adjuvanted with CpG-ODN induced mucosal and systemic immunity, and showed a faster lesion recover after TPA inoculation[546].

Interestingly, Tp0257 is conserved among TPA strains, as well as in *Treponema pallidum endemicum* and *Treponema pallidum pertenue* [547]. These results make this protein an attractive immunogen candidate for vaccine design.

Tp1038

Tp1038, also known as TpF1 or antigen 4D, is a bacterioferritin with ferroxidase activity playing a major role in iron uptake[548]. Radolf et al. showed that Tp1038 is surface-exposed since sera from Tp1038-immunized rabbits was reactive to immobilized TPA in the presence of complement[549].

Tp1038 is able to induce diverse immune responses. For example, this protein might be involved in the proinflammatory response during primary syphilis, since it can activate the inflammasome complex in monocytes, and thereby, induces the release of IL-1β, IL-6, and TNF-α[550,551], which could result in tissue damage associated with this stage. However, Babolin et al. described that Tp1038 may also drive a T regulatory response[550]. CD4+ CD25+ Foxp3+ T cells from patients with secondary syphilis produce TGF-β under Tp1038 stimulation, and Tp1038-stimulated monocytes produce IL-10 and TGF-β, two cytokines linked to Treg cell differentiation[550]. Therefore, TpF1 might be a virulence factor involves in the persistence of TPA infection through the downregulation of the immune response[550]. Regarding the humoral response, anti-Tp1038 antibodies are detectable in all syphilis stages[550,552]. Finally, Pozzobon and colleagues identified that patients with tertiary syphilis have Tp1038-specific T cells, which stimulate monocyte and human umbilical vein endothelial cells to produce tissue factor, IL-8, and CCL-20[553]. These cytokines are involved in angiogenesis, thus Tp1038 may also be implicated in tertiary syphilis, in which vascular inflammation and angiogenesis characterize the lesions of this stage[553]. Thus, Tp1038 is an interesting target for vaccine development since it is engaged in all syphilis stage.

2.2. Immune Evasion Mechanisms

While an immune response is triggered against TPA, it does not protect against bacterial dissemination and disease progression to the second or third stage. In addition, reinfections are quite common, with an incidence around 5-22%[554–556], indicating that TPA has developed some mechanisms to evade the immune system (**Fig.35).**
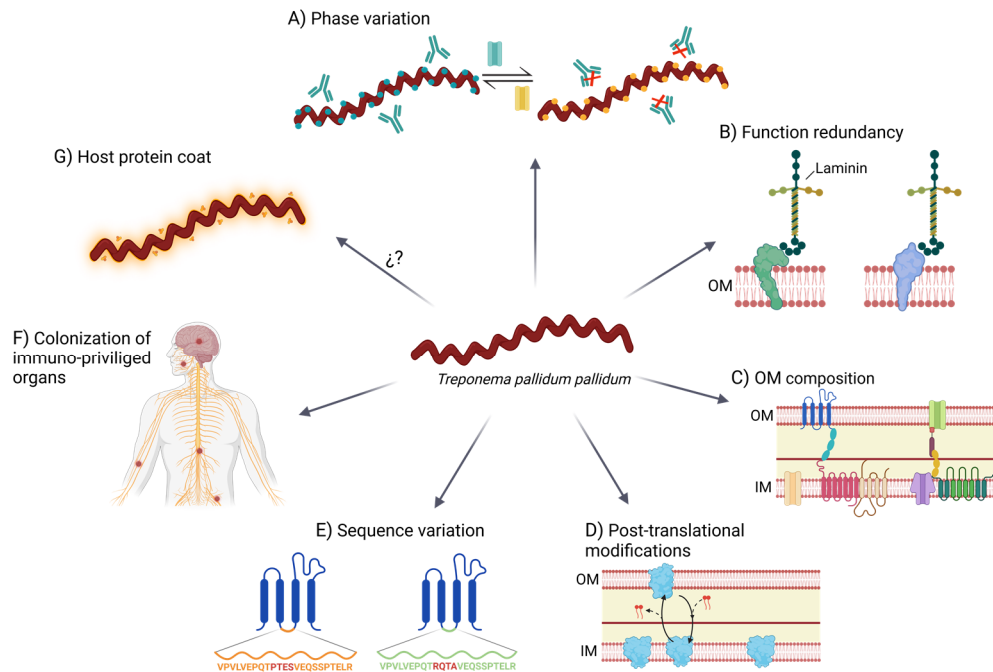
Figure 35. Immune evasions mechanisms used by TPA. (A) During its adaptation to environmental changes, including the immune system pressure, TPA modulates the expression of certain genes by a switch on/off mechanism. **(B)** Linked with the prior mechanism; function redundancy ensure that bacterial homeostasis is not compromised by changing the expression of proteins with vital functions. **(C)** OM of TPA is characterized by a paucity of protein compared with the inner membrane (IM), the lack of LPS and the presence of anti-inflammatory phospholipids (i.e., phosphatidylserine and phosphatidylcholine). **(D)** Some proteins experience post-translational modifications that result in variants with different location preference. **(E)** Proteins can accumulate sequence variations by point mutation, gene conversion or recombination. **(F)** TPA can persist in immune privileged organs, such as central nervous system or nerve fibers, and prolong their survival by remaining hidden to the immune system. **(G)** TPA may be coated by host serum proteins, reducing its immunogenicity.

Phase variation or switch on/off

TPA can modulate the expression of several OMPs during its life cycle[486]. However, the mechanisms controlling the expression of those proteins are not well characterized. In the case of subfamilies I and II of Tpr proteins, guanosine homopolymer (polyG) repeats have been identified upstream of the transcriptional start site. The length of the polyG sequences differ among treponemal isolates and modulate the expression of Tpr proteins at transcriptional level[488]. PolyG signals have also been found in other OMPs, such as the Tp0126 protein[504]. Phase variation based on hypervariable homopolymeric repeats have been previously reported in

several other bacteria such as *Neisseria meningitidis*, *Helicobacter pylori*, or *Haemophilus influenzae*, and it is crucial for the survival of pathogens facing host immunity[557–559]. Moreover, other transcriptional regulatory mechanisms have been identified, such as the G4FS cis-acting DNA elements, which form guanine-quadruplexes and induce recombination and gene conversion of Tp0136 gene[560]. Using these mechanisms, TPA can modify its OMP repertoire to adapt to the environment conditions and evade the immune response. Consequently, the specificity of the humoral response against Tpr proteins may vary between animals or humans that are infected with the same or different TPA strain, thereby supporting the existence of a variable repertoire of OMPs[446].

Functional redundancy

Several OMPs present similar functions in transport or cell adhesion. Functional redundancy may be advantageous since the replacement of one protein by a functional homologous can guarantee that phase variation and post-translational modifications will not adversely affect cell homeostasis[386]. As an example, *Salmonella* has been reported to have two distinct flagellin genes, fliC and fliB, with the same function but different structure. By switching their expression from one flagellin protein to the other, the immune system becomes ineffective against assembled flagella[561].

Outer membrane composition

TPA is characterized by a low number of OMPs, which may encompass an advantage by limiting the number of exposed antigens to the immune system. Moreover, the spacing distribution of these proteins may promote that antibodies bind to them just with one arm, reducing the avidity of the interaction. This mechanism has been previously described in HIV infection[562], which also presents low density of Envelope glycoprotein on the virion surface. In HIV, polyreactivity of neutralizing antibodies may increase binding avidity by heteroligation with membrane components[562]. However, the development of these antibodies could be limited by tolerance mechanisms[563]. Whether this phenomenon is also related to TPA immunity requires further investigation, but it could partially explain the low antibody efficacy at controlling infection. Since the OM lacks LPS[391,392], and it is enriched in anti-inflammatory phospholipids (e.g. phosphatidylserine and phosphatidylcholine), these characteristics may also hamper the development of an efficient immune response[564,565].

Post-translational modifications

Post-translational protein modifications play a crucial role in different processes of prokaryote cells, including persistence and virulence[566]. These modifications have been found in the TPA proteome. For example, there are several variants of Tp0435 that may coexist and were generated by palmitoylation[523]. Palmitoylation consists in the addition of lipid chains to terminal cysteine residues. This process has been previously reported in other bacteria and contributes to their infectivity and recognition of the immune system[567]. Tp0435 variants may be located on the surface or into periplasmatic spaces, being the latter one the most abundant[523], which could explain why there is no consensus about the Tp0435 location. In fact, this protein has been the first description of post-translationally modified protein variants in TPA. However, other OMPs could be also susceptible to post-translational modifications.

Sequence variation

Genetic variation of several OMPs has been described in TPA, including laboratory-adapted or primary isolated strains[491,493,568]. Some of these variations have been reported in the Tpr family, including TprC, TprD, TprG and TprK proteins[491,568,569]. Interestingly, TprK accumulates sequence variation in variable regions (particularly in V6) by non-reciprocal recombination with silent cassettes, which is enhanced under immune pressure[493,494]. Additionally, several *tprk* alleles have been identified in different TPA strains[491], which contribute to increase the variability of this protein. Besides Tpr proteins, others OMPs, such as Tp0326 (BamA), also show genetic variants[568,569]. This protein has accumulated mutations on the extracellular hydrophilic loops predicted to contain B cell epitopes[568]. Sequence variation was also confirmed in FadL orthologs proteins ranging from fully conserved Tp0856 to deeply variable Tp0548, as well as in Tp0136, Tp0868, Tp0966 and Tp0967[570–572].

Colonization of immune privileged organs

TPA can colonize distal immune privileged organs, such as the central nervous system, placenta, or eyes. In these tissues, the action of the immune system may be limited, contributing to the persistence of this pathogen[573–575]. In fact, studies performed using the rabbit model showed that TPA can be detected in nerves early after infection[432].

Similarly to other bacteria; for example, some streptococcal species[576], TPA immune evasion may be associated with host proteins forming a surface coat, also known as antigenic disguise. Alderete and Baseman described that both rabbit and human albumins, as well as other host proteins, could be adsorbed on the surface of TPA[577]. Egesten et al. showed that Group G streptococci express protein G on their surface, and it is able to bind human albumin, and therefore, inhibit anti-microbial action of CXCL9[578]. Accordingly, it has been proposed that the capacity of Tp0483 to bind soluble fibronectin could be related to the evasion of the humoral response[528]. However, Cox and colleagues did not detect serum proteins on the surface of TPA by immunoelectron microscopy[390], stating that the low density of OMPs might be the main immune evasion mechanism of TPA.

3. Vaccine Strategy

Nowadays an effective syphilis vaccine remains elusive. Despite several decades of research, the impossibility to genetically manipulate and grow TPA *in vitro*, the paucity of OMPs, the OM fragility, and the lack of an appropriate animal model that recapitulates all stages of human syphilis have hampered the field progress. In addition, many controversies remain unresolved with respect to OMPs identification, location, function, the potential of these proteins to induce protective immune responses, or the characteristics of these responses. Researchers have hypothesized that a DTH immune response is essential to control and clear TPA infection, but it is also responsible for the development of tissue damage, including an ulcerative lesion that forms chancres. As DTH is primarily mediated by Th1 CD4$^+$ T cells, the presentation of antigens by DCs, macrophages, or other professional antigen-presenting cells is crucial. Of note, this process is independent of antigen location, and both intracellular and surface-exposed antigens can be indistinctly processed and presented to T cells. Therefore, both antigens might generate protective Th1 CD4$^+$ T cell responses. Thus, rabbits immunized with intracellular endoflagellar antigens that have been directly isolated from TPA showed faster development of lesions[579]. However, bacteria were not detected in these lesions, which may be explained by an accelerated memory DTH response. In contrast,

rabbits immunized with a plasmid coding for FlaB3 showed attenuated lesion development that was associated with an enhanced cellular infiltration, and an inhibition of bacteria dissemination to distal organs[580]. In line with this observation, rabbits immunized with TprF, a periplasmic protein, displayed attenuated skin lesions with reduced bacteria burden[500]. The reasons behind these different outcomes are not completely understood, but differences in vaccine formulation and delivery routes, the magnitude of vaccine-induced T cell responses, and the relative representation of antigens (flagellin and TprF) within the whole TPA proteome could be involved. Similar results to TprF immunization were also observed when OMPs were used as antigens. Therefore, DTH could be a protective immune response that modifies lesion development and clears bacteria from infection sites. However, none of TPA proteins tested as immunogens to date protected against infection, indicating that additional immune responses are likely to be required.

Despite some controversy[432], strong evidence supports a protective role of antibodies, facilitating bacteria opsonization and killing by innate immune cells, as well as blocking their interaction with components of the extracellular matrix, such as laminin and fibronectin. These functions strictly depend on the exposure of antigens on the OM and, in some cases (e.g. bacteria phagocytosis), the interaction with Fcγ receptors expressed on the surface of innate immune cells, such as macrophages. IgG-FcγR interaction may also improve antigen presentation by antigen-presenting cells and the generation of Th1 cellular responses[581]. Therefore, to develop a protective TPA vaccine, it is crucial to define which types of antigens can induce synergic anti-TPA immune responses. It is also essential to considerer immune evasion strategies developed by TPA, such as functional redundancy and phase variation. In this sense, targeting several proteins with two or more functions, such as transport and adhesion, could increase vaccine efficacy, as it was previously observed[582,583].

The ideal syphilis vaccine should provide protection against TPA infection. However, even if the vaccine is unable to completely prevent infection, it could still worth considering as a mean of limiting bacteria dissemination and tissue invasiveness, blocking the establishment of latency, or preventing the disease from progressing

to secondary and tertiary stages[477]. Additionally, a vaccine that reduces bacterial persistence or prevents TPA transplacental invasion might also reduce the number of congenital syphilis in endemic areas, where the number of non-diagnosed infected individuals may be high, and the access to health care is limited. Moreover, a syphilis vaccine has to be effective against possible reinfections with similar or different TPA strains or isolates, indicating the importance of using conserved antigens. Recently, there has been evidence that TPA can be cultured *in vitro* and that genetic manipulation of this pathogen can be accomplished[478,584,585]. These scientific advances are likely to open the gateway to new research lines that can shed light on the current controversies.

HYPOTHESIS AND OBJECTIVES

Hypothesis

Although syphilis can be successfully treated using unexpensive antibiotics, its incidence is increasing and remains a global health problem. A syphilis vaccine may represent an inflexion point in the control of this disease. The TPA´s OMPs are ideal antigens for syphilis vaccine formulation since they are exposed on the surface of the bacteria and can be targeted by both antibodies and T cells. However, the development of a syphilis vaccine remains challenging since TPA has developed multiple mechanisms which can modify its OM protein content. Thus, OMPs expression is controlled by phase variation, and post-transcriptional modification, and they can also accumulate mutations, which make that TPA can adapt its OMP profile to the environment, including the immune system pressure. These immune evasion mechanisms are supported by a high degree of functional redundancy among OMPs and may explain why rabbit immunization studies using single or just few antigens have failed protection. Therefore, we hypothesized that a vaccine that includes multiple OMPs expressed in different phases of pathogen growth, and cover the functional diversity of the OM, it will generate a strong and protective immune response from which TPA will not escape. This vaccine-induced immune response will prevent infection or bacterial dissemination and protect from disease development and progression.

Objectives

The main aim of this project is to generate a multiple-antigen vaccine against TPA infection.

The specific objectives to fulfill this aim are:

Objective I: To identify the OMPs candidates to be included in the multi-antigen vaccine.

Objective II: To express and purify the selected recombinant OMPs.

Objective III: To characterize the binding activity of produced OMPs to extracellular matrix proteins.

Objetive IV: To evaluate the immunogenicity of recombinant OMPs in a murine model.

MATERIAL AND METHODS

1. DNA construct design

Two different types of DNA constructs were designed for the expression of the thirteen selected OMPs. Briefly, the first design (V1) (**Fig.36A**) consist of 8xHis tag followed by the OMP sequence, a Flag tag, and the Strep tag II tag on the C-terminal side. In addition, we added two HRV3C protease cleavage sites flanking the OMP sequence for tag removal. The second design (V2) (**Fig. 36B**) consists of an 8xHis tag located at the N-terminal end, followed by the OMP sequence and a Flag tag at C-terminal. Flag tag can be removed by enzyme restriction and ligation. Additionally, a TEV protease site up-stream OMP sequence was added to remove 8xHis tag.

All DNA sequences were synthetized at GeneArt (ThermoFisher Scientific) and cloned into pET21d (+) vector (Novagen) using Nhe I and Xho I restriction enzymes (ThermoFisher Scientific) for V1 design and Nco I and Blp I restriction enzymes (ThermoFisher Scientific) for V2 design. V1 cloning was performed using T4 DNA ligase (ThermoFisher Scientific) while V2 cloning was made by homologous recombination using Gibson Assembly Hifi (ThermoFisher Scientific). Plasmids were transformed in One Shot TOP10 Chemically Competent *E. coli* (Invitrogen) and in BL21 (DE3) Competent *E.coli* (New England Biolabs) for plasmid amplification and protein production, respectively. ZymoPure II Plasmid Maxiprep Kit (Zymo Research) was used for plasmid purification. Nucleic acid concentration was measured by NanoDrop (ThermoFisher Scientific) at 260 nm.
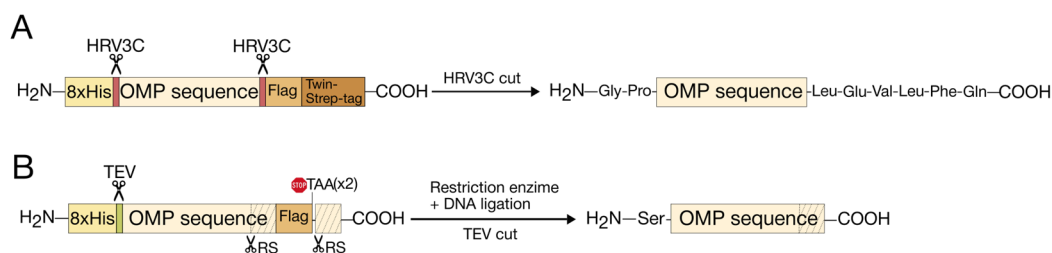
Figure 36. Schematic representation of recombinant OMPs constructs designs. (A) V1 OMPs construct. Protein sequence was flanked by an 8xHis tag at the N-terminal part, and Flag and Twin-Strep tags at the C-terminal part. Two HRV3C protease cleavage sites were added flanking protein sequence to remove tags. The action of HRV3C leave two extra amino acids at the N-terminal extreme, and six additional amino acids at the C-terminal extreme, which do not belong to the protein sequence. **(B)** V2 OMPs construct. Protein sequence contains an 8xHis tag and a Flag tag at the extremes. A TEV protease cleavage site was added between the 8xHis tag and protein sequence. Additionally, an extra sequence about 60-100 amino acids (dotted sequence) was copied from the protein, and localized behind a double stop codon (TAA) after Flag. Through restriction enzyme and DNA ligation Flag can be removed without adding extra amino acids. Scissors point the protease sites (i.e. HRV3C and TEV) and restriction enzymes sites (RS).

2. Cell Culture and Protein Extraction

Transformed BL21 (DE3) Competent *E.coli* (New England Biolabs) were grown in LB medium overnight at 37°C or 27°C, with agitation at 225 rpm. Next day, cells were induced with Isopropyl-β-D-1-thiogalactopyranoside (IPTG) during 2 hours. Different concentrations of IPTG (from 0.1 to 2 mM) were tested. After induction, cell cultures were centrifuged at 3220xg for 30 minutes. Supernatants were discarded and cellular pellets were resuspended in Lysis Buffer (50 mM Tris buffer, 100 mM NaCl, 5 mg/ml Lysozyme (ThermoFisher Scientific), pH 8.0) (**Table 3**) and incubated 30 minutes at room temperature with end-over-end mixing. Then, cells were disrupted by freezing at -80°C for 1 hour. After thawing, 1% of Triton X-114 (Thermo Fisher), 1% protease inhibitor cocktail (P8849, Merck Millipore), 10 µg/mL DNAse (DN25, Merck Millipore) and 10 mM of MgCl2 were added to cells suspension and incubated 20 min with end-over-end mixing at 4°C. Cells were centrifugated at 15000xg for 30 minutes at 4°C. From this centrifugation two fractions were obtained, the supernatant or lysis fraction, and the pellet which contain inclusion bodies (white pellet) among other cellular debris. Inclusion bodies were resuspended in Buffer IB (100mM phosphate buffer, 500 mM NaCl, 8M Urea, pH 8.0) (**Table 3**) and incubated for one hour at room temperature with end-over-end mixing. Finally, they were centrifuged at 15000xg for 30 minutes at 4°C. Supernatants containing solubilized inclusion bodies were collected and the pellets were discarded.

3. Protein Purification and dialysis

3.1. Immobilized Metal Affinity Chromatography (IMAC)

Proteins from both fractions, lysis and inclusion bodies, were purified by IMAC using Ni Sepharose 6 fast Flow resin (Cytiva). Resin was equilibrated by two washing steps with equilibrium buffer according to protein preparation (**Table 3**). Additionally, NaCl was adjusted until 1M in each protein fraction and 30 mM of Imidazole was added. Resin was incubated with proteins during 2 hours at room temperature with end-over-end mixing. Purification was performed by gravity into Poly-Prep® chromatography columns (Bio-Rad). After recover resin into Poly-Prep columns, two wash steps were done before elution. The formulation of washing and elution buffers depended on fraction used as starting material, and is described in **Table 3**. After elution proteins were concentrated and buffer exchanged to remove imidazole by ultrafiltration using Amicon-Ultra Centrifugal Filter Units (Merk Milipore). Purified products were quantified at 280 nm and stored at -80°C until use.

Buffers / Starting Material	Extraction Buffer	Equilibrium Buffer	Wash 1 Buffer	Wash 2 Buffer	Elution Buffer	Concentration Buffer
Soluble Fraction	Tris 50mM, 100mM NaCl, 5 mg/mL Lysozyme, pH: 8.0	Phosphate 30 mM, 1 M NaCl, 30 mM Imidazole, pH: 7.0-8.0	Phosphate 30 mM, 1 M NaCl, 30 mM Imidazole, 1% Triton X-114, pH: 6.0-7.0	Phosphate 30 mM, 1 M NaCl, 50 mM Imidazole, pH: 6.0-7.0	Phosphate 30 mM, 1 M NaCl, 500 mM Imidazole, pH: 6.0-7.0	Phosphate 30 mM, 0,5 M NaCl, pH: 6.0-7.0
Inclusion Bodies	Phosphate 100 mM, 0,5 M NaCl, 8 M Urea, pH: 8.0	Phosphate 100 mM, 1M NaCl, 8 M Urea, 30 mM Imidazole, pH: 8.0	Phosphate 100 mM, 1 M NaCl, 8 M Urea, 30 mM Imidazole, 1% Triton X-114, pH: 8.0	Phosphate 100 mM, 1 M NaCl, 8 M Urea, 50 mM Imidazole, pH: 8.0	Phosphate 100 mM, 1 M NaCl, 8 M Urea, 500 mM Imidazole, pH: 8.0	Phosphate 100 mM, 0,5 M NaCl, 8 M Urea, pH: 8.0

Table 3. Summary of buffers used during protein extraction and purification. Buffer used in soluble and inclusion bodies recombinant protein extraction are indicated. Sequential buffers used during purification protocol from soluble and inclusion bodies are described, including buffer for column equilibration, wash, elution, and concentration and buffer exchanged on ultrafiltration devises.

3.2. Dialysis

Buffer exchange for protein refolding and formulation was performed by sequential dialysis steps in Slide-A-Lyzer MINI dialysis devices (ThermoFisher Scientific). Several buffers were investigated (**Table 6,** see results section). All proteins were tested at 0.1-0.25 mg/mL. Particularly, for Tp0435, Tp0750, and Tp0633, a two-step dialysis approach (firstly against Buffer T1 and then against Buffer T2, see **Table 6**) was used. Protein concentration was performed in Amicon-Ultra Centrifugal Filter Units (Merk Milipore). Dialyzed products were stored at -80°C until use.

3.3. Affinity Chromatography by Twin-Strep-Tag.

After IMAC purification, a second affinity chromatography using Strep-Tactin resin (Iba-LifeSicence) was performed with V1 proteins. As the binding of Twin-Strep-tag to Strep-Tactin resin is not possible in the presence of high urea concentration, proteins purified from inclusion bodies were first dialyzed to 1 M urea. After that, protein solutions were incubated with Step-Tactin resin for 1 hour at room temperature. Purification was performed by gravity into Poly-Prep® chromatography columns (Bio-Rad). Column was washed twice with Buffer W supplied by Iba-LifeScience. Elution of columns was made with Buffer E supplied by Iba-LifeScience.

4. Analysis of Protein Production

Integrity and purity of purified proteins were analyzed by sodium dodecyl sulfate polyacrylamide gel electrophoresis (SDS-PAGE) and Coomassie G-250 staining (ThermoFisher Scientific). Specific detection of purified protein was performed by Western Blot. Proteins were transferred onto PVDF membrane (Bio-Rad) using Trans-Blot Turbo Transfer System (Bio-Rad). Then, membranes were blocked with Blocking buffer (PBS 1x, 0.05% Tween20, 5% non-fat milk powder) for 1 hour at room temperature. After that, they were incubated with the primary antibody 6xHis tag monoclonal antibody (His.H8) (1:2000, ThermoFischer Scientific) overnight at 4°C in Blocking buffer. The next day, membranes were washed twice by 20 minutes and incubated with secondary antibody, HRP-conjugated AffiniPure Donkey anti-mouse IgG (H+L) (1:10000, Jackson ImmunoResearch) during 1 hour in Blocking buffer at room temperature. Finally, after washing, membranes were developed using SuperSignal West Pico PLUS Chemiluminescent Substrate (ThermoFisher Scientific).

Image Lab Software from Bio-Rad was used to analyze purity of proteins from Coomassie blue stained gel imagen.

5. *In vitro* protein binding

Binding of purified recombinant OMPs (Tp0155, Tp0751, Tp0435, Tp0750, Tp0633) to murine laminin (ThermoFisher Scientific), human fibrinogen (ThermoFisher Scientific), and human fibronectin (Merk Milipore) was determined in duplicates by ELISA in the same plate to allow comparisons among them. In addition, all plates were run in parallel to reduce inter-assay variability. Nunc MaxiSorp ELISA plate was coated with 10 µg/mL of laminin, fibrinogen, and fibronectin in PBS 1x. Coating was made overnight at 4°C. After that, plates were blocked using PBS 1x with 1% of bovine serum albumin (BSA, Miltenyi Biotech) and 0.05% Tween20 (ThermoFisher Scientific) in Tp0155, Tp0751 and Tp0633 plates; or using PBS 1x with 1% of casein enzymatic hydrolysate (Sigma Aldrich) and 0.05% Tween20 (ThermoFisher Scientific) in Tp0750 and Tp0435 plates, during 2 hours at room temperature. Then, 50 µL of recombinant OMP was added on laminin, fibrinogen and fibronectin lane at eight 1/2 dilution starting at 30 µg/mL in blocking buffer and incubated overnight

at 4°C. OMPs were confronted also against a lane with only 1%BSA in duplicate. The following day, bound OMP was detected using an anti-6xHis antibody HIS.H8 (ThermoFisher Scientific) (1/1000) and HRP conjugated (Fab)2 Goat anti-mouse IgG (Fc specific) (1/10.000) (Jackson Immuno Research) during two and one hours, respectively, at room temperature. Plates were revealed with o-Phenylenediamine dihydrochloride (OPD) (Sigma-Aldrich) and stopped using 4N of H_2SO_4 (Sigma-Aldrich). The signal was analyzed as the optical density (OD) at 492 nm with noise correction at 620 nm. Data is shown as OD at 492 nm minus OD at 620 nm.

6. *In vivo* Immunization

All animal procedures were performed according to the approval of the Committee on the Ethics of Animal Experimentation of the IGTP and the authorization of Generalitat de Catalunya (Code: 11881). Immunogenicity of recombinant Tp0155, Tp0751, Tp0435, Tp0750 and Tp0633 protein was evaluated in eight BALB/c mice (50% males, 50% females, 7 weeks old) which received 75 µg of a mix of all proteins (15 µg of each protein) adjuvanted with aluminum hydroxide gel (Alhydrogel® adjuvant 2%, Invivogen) at 1:1 related volume (100 µL maximum per animal corresponding with 800 µg of aluminum approximately). Animals were immunized following a prime-boost regimen with a gap of three weeks among doses. Vaccine preparation was administered subdermically in the hock from both hindlegs (50 µL maximum in each on) and in the back (100 µL). Two control animals (one male, one female) were immunized equally with sterile PBS1x plus aluminum hydroxide gel. One month after second immunization, animals received a third dose via the intraperitoneal route (250 µL). Mice weight was monitored during all immunization experiment. Animals were finally euthanized at day 67 according to the end of the assay. Blood samples were collected before first (day 0) and second immunization (day 21), two weeks after second immunization (day 37) and at euthanasia point (day 67). Blood was left at room temperature for two hours for clotting and serum was recovered after centrifugation (10 minutes at 5000xg) and stored at -80°C until use.

7. Quantification of anti-OMPs Antibodies

Specific IgG antibodies elicited against Tp0155, Tp0751, Tp0435, Tp0750 and Tp0633 proteins were detected individually using an in-house ELISA. Humoral response was evaluated in serum samples from immunized and control mice obtained at day 0, 21, 37 and 67. One half of a Nunc MaxiSorp ELISA plate was coated overnight at 4°C with 1 µg/mL of one of the five proteins in PBS 1x. The other half was incubated only with PBS. The following day, the plate was blocked using PBS 1x plus 1% of bovine serum albumin (BSA, Miltenyi Biotech) and 0.05% Tween20 (ThermoFisher Scientific) for two hours at room temperature. A standard was prepared in blocking buffer using anti-6xHis antibody HIS.H8 (ThermoFisher Scientific) at eight 1/3 dilutions, stating at 1µg/mL. Serum samples were prepared in blocking buffer at different dilutions. After blocking step, 50 µL of each standard and samples were added to each half plate in duplicates and incubated at 4°C overnight. Each plate contained two serum samples as controls. Plates were run in parallel to reduce inter-assay variability. Bound mouse antibodies were detected by HRP conjugated (Fab)2 Goat anti-mouse IgG (Fc specific) (1/10.000) (Jackson Immuno Research) that was incubated for two hours at room temperature. Plates were revealed with o-Phenylenediamine dihydrochloride (OPD) (Sigma-Aldrich) and stopped using 4N of H_2SO_4 (Sigma-Aldrich). The signal was analyzed as the optical density (OD) at 492 nm with noise correction at 620 nm.

To calculate the specific signal of each serum sample, the background signal from antigen-free wells was subtracted to the one obtained from antigen coated wells. Data is shown as arbitrary units (AU) according to the standard curve used.

8. Binding Blocking-Antibodies Assay

The blocking capability of vaccine-induced antibodies was evaluated by ELISA. Nunc MaxiSorp ELISA plates were coated overnight at 4°C with 10 µg/mL of laminin, fibrinogen or fibronectin in PBS 1x. Six well were incubated only with PBS 1x. Next day, Tp0155and Tp0633 plates were blocked using PBS/1%BSA (Miltenyi Biotech) and 0.05% Tween20 (ThermoFisher Scientific), and Tp0750 and Tp0435 plates were blocked using PBS/1% of casein enzymatic hydrolysate (Sigma Aldrich) and 0.05% Tween20 (ThermoFisher Scientific). Plates were incubated with blocking buffer for 2

hours at room temperature. Recombinant OMPs were diluted in blocking buffer (Tp0155 and Tp0633) or PBS with 0.05% Tween20 (Tp435 and Tp0750) at different concentration depending on the coated protein. Thus, Tp0155 was prepared at 4 µg/mL for fibronectin and fibrinogen, and at 5 µg/mL for laminin. Tp0435, Tp0750 and Tp0633 were used at 8, 5 and 4 µg/mL for all three coated proteins, respectively. Serum samples from immunized mice obtained at different time points: basal (day 0), prime (day 21), boost (day 37), and second boost (day 67); samples were diluted at 1/200 in each OMPs preparation and incubated for 2 hours at room temperature. After incubation, 50 µL of OMPs + serum samples were added in duplicate to plate wells. Additionally, 50 µL of OMPs preparation without serum was confronted against six coated wells and six not coated wells to measure normal binding and background signal against blocking buffer, respectively. Samples were incubated overnight at 4°C. Then, OMPs binding was detected using 6x-His tag antibody HIS.H8-Biotin (ThermoFisher Scientific) (1/1000) for two hours and HRP-Streptavidin (ThermoFisher Scientific) (1/6000) for half hours at room temperature. Finally, plates were revealed with o-Phenylenediamine dihydrochloride (OPD) (Sigma-Aldrich) and stopped using 4N of H_2SO_4 (Sigma-Aldrich). The signal was analyzed as the optical density (OD) at 492 nm with noise correction at 620 nm. The background signal from coated protein-free wells was subtracted from protein coated wells. Data is shown as OD at 492 nm minus OD at 620 nm.

9. Statistical analysis

Differences in antibody levels between male and female immunized mice were analyzed using Mann-Whitney test, while comparison among vaccination timeline (i.e. basal, prime, boost, and second boost) was performed by Wilcoxon signed-rank test. This test was also applied to analyze the results from blocking binding assay. Correlation between antibody levels and binding blockade was performed using nonparametric Spearman test. P values are indicated as follows: * $p < 0.05$, ** $p < 0.01$, *** $p < 0.001$, **** $p < 0.0001$. Not significance differences are not shown in graphs. Statistical analyses were conducted using GraphPad Prism v8.0.

RESULTS

1. Selection of Outer Membrane Proteins

The low density of OMPs and the fragility of the OM have hampered the identification and characterization of bona fide TPA´s OMPs. In addition, there is a strong controversy on the location of some proteins, since some studies identified them on the OM, whereas other showed they may be located in periplasmic space. To identify and select the OMPs that will be incorporated into the multi-antigen vaccine, we performed an extensive bibliographic search[586] based on their function, their potential location in the OM, and the existence of previous immunogenicity data in human or animal models. A total of thirty-nine proteins (**Table 4**) with any evidences of being an OMP were compiled from this literature search. Besides their location, we focused on those proteins for which *in vivo* immunogenicity data (in human or animal model) supported a protective role. Thus, we selected twelve OMPs for the generation of a multi-antigen vaccine against syphilis. OMPs with a huge sequencing variation like Tpr family and those based on *in silico* predictions (e.g., Tp0515 and Tp0856) were not considered, excepting Tp0733 that was included to test the performance of *in silico* predictions. Selected OMPs included three transport proteins (Tp0126, Tp0733 and Tp0633), six adhesion proteins (Tp0136, Tp0155, Tp0483, Tp0750, Tp0751, Tp0435), and three involved in other functions related to cellular homeostasis like membrane synthesis, protein translocation to the OM, and iron storage (Tp0326, Tp0257, Tp1038).

2. Generation of Recombinant Outer Membrane Proteins

For recombinant protein production, the sequences of the selected OMPs were modified as follows: 1) we removed the hydrophobic signal peptide for all proteins sequence to favor its expression as soluble proteins, and 2) we eliminated the periplasmic region in those putative OMPs that presented this domain (e.g Tp0326). Thus, we only expressed the region located in the OM. In addition, in the case of Tp0126, for which the extracellular loops are well defined, we synthetized a short version of this protein which only included the four extracellular loops (Tp0126_L). Thus, we designed a total of 13 proteins (the twelve selected OMPs and the loop version of Tp0126). Protein sequences were flanked by an 8xHis tag in the N-terminal part, and a Flag and a Strep tag II in the C-terminal part (**Fig.35A**).

Proteins	Function	Cellular Location	Location Evidence	Immunization Data	Sera Reactivity
TprC (Tp0117)	Porin proteins	OM	*In vivo /* *In silico*	-	Yes
TprD (Tp0131)				-	Yes
TprI (Tp0620)				Yes	Yes
TprE (Tp0313)				-	-
TprG (Tp0317)				-	-
TprJ (Tp0621)				-	-
TprA (Tp0009)				-	-
TprB (Tp0011)				-	-
TprK (Tp0897)				Yes	Yes
TprF (Tp0316)				Yes	-
TprH (Tp0610)		Periplasmic		-	-
TprL (Tp1031)				-	-
TROMP1 (Tp0163)	Porin proteins	Periplasmic	*In vivo*	-	Yes
* TROMP2 (Tp0633)		OM		Yes	Yes
TROMP3		-		-	-
* Tp0126	Fatty acid transport	OM	*In vivo*	Yes	Yes
* Tp0733	Small molecules transport		*In silico*	-	-
Tp0479				-	-
Tp0698				-	-
Tp0548	Long-chain fatty acid transport	OM	*In silico*	-	-
Tp0856					-
Tp0858					-
Tp0859					-
Tp0865					-
Tp0966	Efflux pump complex	OM	*In silico*	-	-
Tp0967					
Tp0968					
Tp0969					
Tp0515	LPS trafficking	OM	*In silico*	-	-
* Tp0136	Adhesin	OM	*In vivo*	Yes	-
* Tp0155	Adhesin	Discrepancies	*In vivo*	Yes	Yes
* Tp0435	Adhesin	Discrepancies	*In vivo*	Yes	Yes
* Tp0483	Adhesin	Discrepancies	*In vivo*	Yes	-
* Tp0750	Adhesin / Metalloprotease	OM	*In vivo*	-	-
* Tp0751	Adhesin/ Metalloprotease	Discrepancies	*In vivo*	Yes	Yes
Tp0954	Adhesin	OM	*In vivo*	-	-
* Tp0326	Protein trafficking	Discrepancies	*In vivo*	Yes	Yes
* Tp0257	Glycrolphosphodiester phosphodiesterase	Discrepancies	*In vivo*	Yes	Yes
* Tp1038	Bacterioferritin	OM	*In vivo*	-	Yes

Table 4. List of OMPs. Information about function, cellular location, location evidence (description based on *in vitro* or *in vivo* evidences), immunization data, and sera reactivity are included for each protein. (-) Unknown, (*) Proteins selected to develop a multiple-antigen vaccine.

This plasmid design allows us to confirm that the protein was produced correctly by specifically targeting both ends and to use a purification strategy based on a double affinity chromatography. Moreover, between tags and protein sequence, we introduced two HRV3C cleavage site for tags removing. We referred to this protein design as V1 constructs.

DNA constructs for recombinant protein production were synthetized by GeneART and cloned into a pET-21d (+) vector. Recombinant proteins were produced in BL21 (DE3) *E. coli*. Protein expression in soluble fractions or forming inclusion bodies was evaluated in 6 mL cell culture. Moreover, the effect of two different temperatures (27°C and 37 °C) duringIPTG-induced protein expression was screened. The detection of protein in each fraction was carried out by Western Blot using an anti-6xHis antibody. Results showed that Tp0733, Tp0751, Tp0257, Tp0435, and Tp0750 expressed all in the soluble fraction and with the correct molecular weight at both temperatures (**Fig.36A**). However, the intensity of the signal was lower at 27°C than 37°C, indicating a higher protein production in the last condition, except for Tp0257, that was equally low at both temperatures. Additional bands were detected in the case of Tp0733, Tp0435 and Tp0750, mainly when the proteins were expressed at 37°C, likely corresponding to truncated forms of the proteins (low molecular weight) or protein aggregates (high molecular weight). In the case of Tp0136 and Tp1038, a single band with a lower molecular weight than expected was observed indicating that the protein is not properly produced or partially degraded. Low level of production was observed for Tp0633 at 27°C, whileTp0155, Tp0326, Tp0483, Tp0126, and Tp0126_L were not detected in the soluble fraction. Nonetheless, we found Tp0155, and low Tp0326, Tp483 and Tp126_L expression in inclusion bodies (**Fig.36B**). Additionally, Tp0733, Tp0751, Tp0257, Tp0435, Tp0750 and Tp0633 were also produced in inclusion bodies with a higher signal intensity than in soluble fractions, suggesting that these proteins were produced mainly as inclusion bodies. Notably, Tp1038 and Tp0136 were detected in inclusion bodies at the correct molecular weight, although for Tp0136 only when the protein is expressed at 27°C. Although these results are qualitative, the low band intensity observed with Tp0326, Tp0136, Tp0483 and Tp0126_L suggested that these proteins were poorly expressed in both cellular fractions. Finally, higher amount of proteins but also truncated forms were observed at 37°C. A summary of V1 protein expression can be found in **Table 5**.

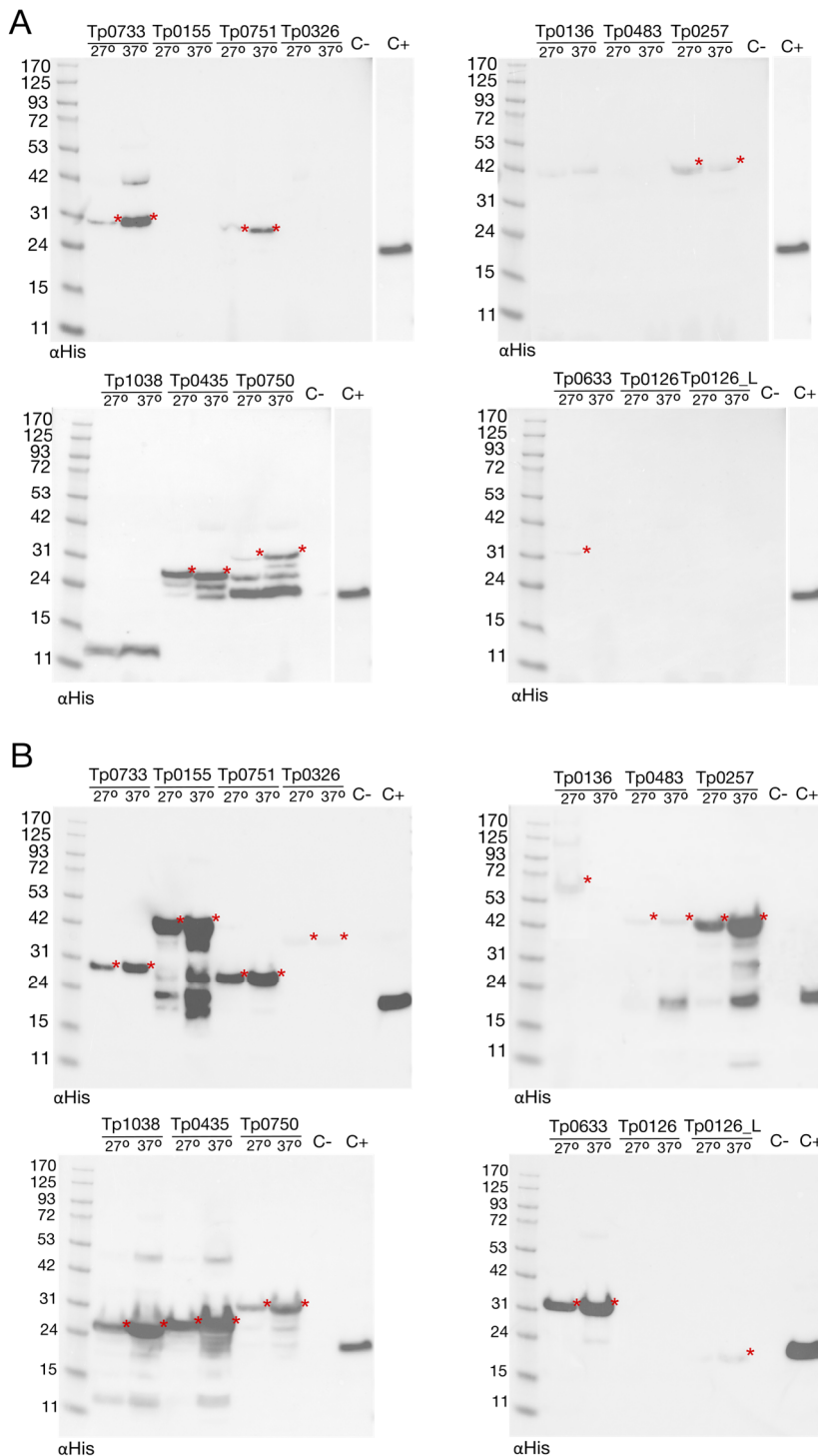**Figure 36. Analysis of V1 recombinant OMPs expression.** The expression of the 13 OMPs (V1 construct) in **(A)** lysis/soluble fraction and **(B)** inclusion bodies obtained from bacteria cultures at two temperatures 27° vs 37° (in Celsius scale) was analyzed by Western Blot using anti-His antibody. Red asterisk pinpoints the expected molecular weight. C+ and C- mark the positive and negative control, respectively.

	MW (kDa)	PI	Soluble Fraction 27°C	Soluble Fraction 37°C	Inclusion Bodies 27°C	Inclusion Bodies 37°C
Tp0733	28.10	6.66	Very Low	High	Low	High
Tp0155	43.47	9.50	No Expression	No expression	High**	Very High**
Tp0751	25.53	6.49	Very Low	Low	High	Very High
Tp0326	37.83	7.99	No expression	No expression	Very Low	Very Low
Tp0136	53.90	6.56	Very Low*	Very Low*	Very Low**	No expression
Tp0483	46.72	8.99	No expression	No expression	Very Low**	Very Low**
Tp0257	45.56	8.60	Very Low	Very Low	Low**	High**
Tp1038	24.82	5.61	Low*	Low*	Low**	High**
Tp0435	21.95	6.93	Very Low**	Low**	Low**	High**
Tp0750	31.06	7.08	Very Low**	Low**	Very Low	Low
Tp0633	32.50	6.31	Very Low	No expression	Low	High
Tp0126	29.26	6.61	No expression	No expression	No expression	No expression
Tp0126_L	16.86	6.15	No expression	No expression	No expression	Very Low

Table 5. Summary of V1 recombinant OMPs expression. Molecular weight (MW) and isoelectric point (PI) of the thirteen selected proteins are indicated. Protein expression levels in soluble or inclusion bodies fractions at 27°C and 37°C are indicated. Qualitative quantification was based on band intensity from Western Blots results (Fig.36). One asterisk points proteins that were produced with erroneous MW. Two asterisks indicate presence of multiple truncated forms.

Then, we expressed Tp0733, TP0751, Tp0257, Tp0435 and Tp0750 in 250 mL cell culture at 27°C and purified them from soluble fractions by Immobilized-Metal Affinity Chromatography (IMAC). We chose these conditions since these proteins were produced in this fraction at the correct molecular weight and with the lowest amount of contaminants. However, after purification, multiple bands were observed in all protein preparations (**Fig.37A**). We performed a Western Blot analysis (**Fig.37B**) for the detection of truncated forms, which were present in Tp0435, Tp0750, Tp0751, but not in Tp0733 and Tp00257. Overall, we obtained protein preparations with low purity from soluble fraction. As these five proteins were also expressed in inclusion bodies, we tried to purify them, and the remaining proteins, from this cellular fraction. In this case, we obtained between 0.5-1 mg of total proteins after purification. Nonetheless, several contaminant bands co-purified with our proteins (**Fig.37C**). When, we analyzed purified products by Western Blot (**Fig.37D**), we observed that most of the bands correspond to truncated forms. Some bands were observed in Tp1038 and Tp0435 protein preparations by Western Blot, despite they were barely detected by Coomassie staining. Moreover, we noticed a high degree

of truncated forms in some samples, such as Tp0751 andTp1038, that we did not detect before in inclusion bodies obtained from 6 mL culture (**Fig.36B**); which could indicate that cell culture scalation may be challenging. Notably, Tp0136, Tp0126, and Tp0126_L were hardly detected (**Fig.37D**).

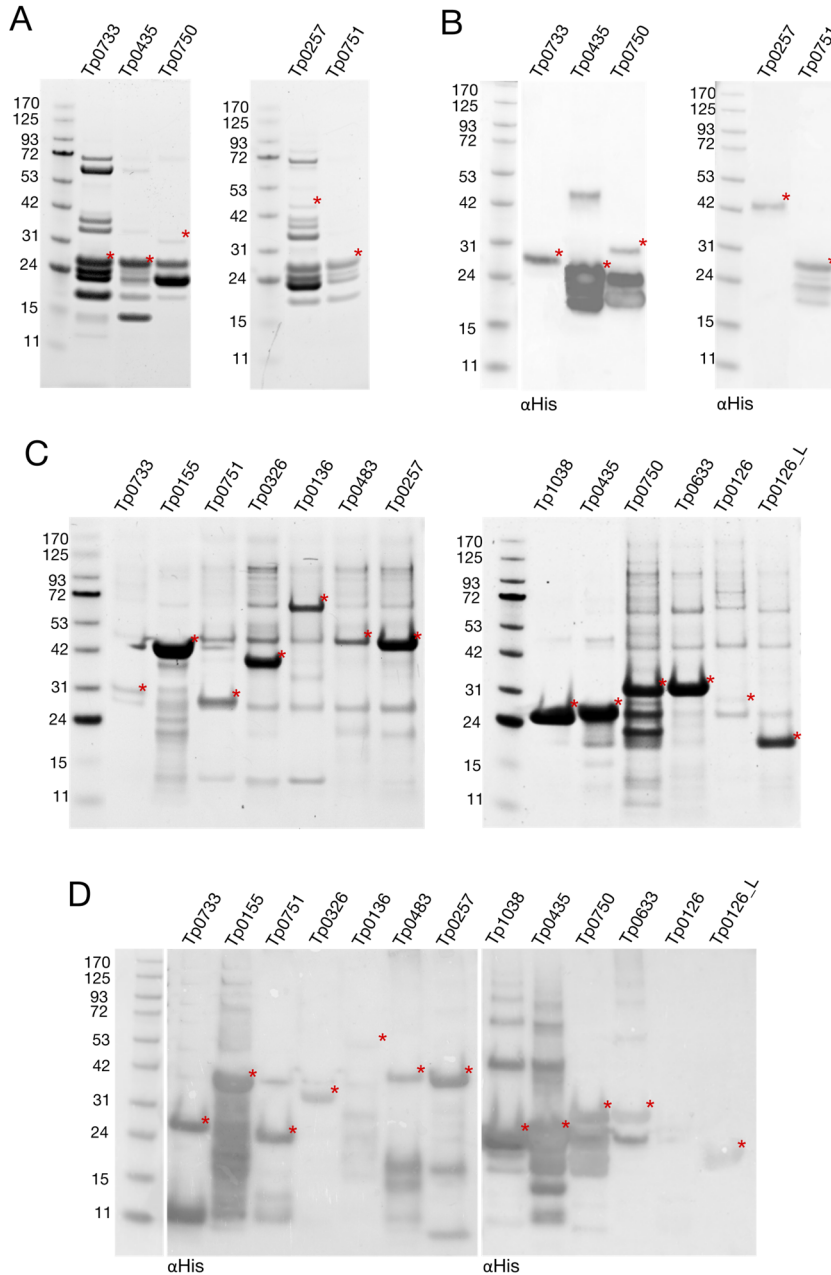**Figure 37. Purification of V1 recombinant OMPs by IMAC.** V1 proteins purified from lysis fractions were analyzed by **(A)** Coomassie blue staining and **(B)** Western Blot using anti-His antibody. V1 proteins purified from inclusion bodies were analyzed by **(C)** Coomassie blue staining, and **(D)** Western Blot using anti-His antibody. Red asterisk pinpoints the expected molecular weight.

The purity results highlighted that additional purification step would be needed to improve the purification process. For that reason, we introduced the Twin-Strep-tag. Thus, a second step of affinity chromatography could be performed to increase the purity of the recombinant proteins. However, inclusion bodies are solubilized using urea at 8M, which is not compatible with Strep-Tactin resin. Therefore, the urea concentration should be reduced to less than 1M, which imply the use of different additives to allow protein refolding and solubility in the absence of urea. Buffer exchange was performed by step-wise dialysis. We found that when the urea concentration was below 1M, most of the proteins precipitated even in the presence of arginine, mannitol, or other stabilizing agents. In addition, we tested the addition of reduced and oxidized glutathione to improve protein refolding and solubility. Protein solubility and re-folding are protein-dependent and we did not find a common strategy for all proteins (**Table 6**). Thus, glutathione only worked for Tp0435 and Tp0750, and mannitol increased the solubility of Tp0136. Despite that, a small amount of protein precipitated even with fitting conditions, with a loss of almost 20% of protein. As a complete urea removal was not suitable for all proteins, we tested the efficiency of protein purification using Strep-Tactin resin in presence of 1M urea. We tested three different proteins Tp0155, Tp1038 and Tp0633. Results show that Tp1038 and Tp0633 were purified with a very low yield (10% for Tp1038 and 4% for Tp0633); while no protein was recovered in the Tp0155 elution fraction (**Fig.38A**). Additionally, we proved Tp0136 in absence of urea, with an efficiency of 14,5% (**Fig.38B**). Therefore, the strategy of protein purification using a sequential affinity chromatography (IMAC + Strep-Tactin) did not work properly and the purification process needed further optimization.

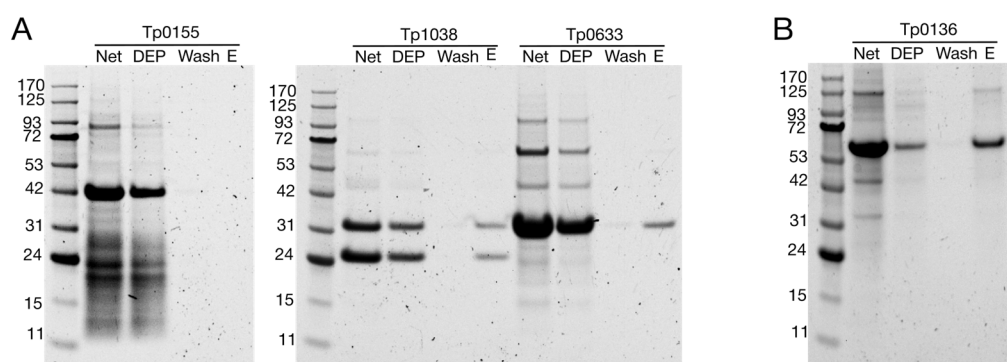**Figure 38. Evaluation of the Twin-Strep-tag affinity chromatography as a second purification step. (A)** Analysis of purification products from Strep-Tactin chromatography of protein preparation containing 1M urea. **(B)** Strep-Tactin purification of Tp0136 dialyzed sample in absence of urea. Net, depleted (DEP), wash, and elution (E) samples are shown in Coomassie blue staining gels.

	Dialysis Buffer	Sequential Order	Protein Construct	Soluble	Precipitate
Buffer A [1]	Phosphate 100 mM, 130 mM NaCl, 1M Urea,1M Arginine, 0.1% Tween20, pH: 7.0-8.0	First dialysis step	V1	Tp0733,Tp0751, Tp0326,Tp0136, Tp1038,Tp0435, Tp0750,Tp0633, and Tp0126	Tp0155,Tp0483, and Tp0257
Buffer G [1]	Phosphate 100 mM, 130 mM NaCl, 0.5M Arginine, 0.01% Tween20, 2mM reduced GSH, 0.4 mM oxided GSH, pH: 7.0-8.0	Second dialysis step	V1	Tp0435 and Tp0750	Tp0733,Tp0751, Tp0326,Tp0136, Tp1038,Tp0633, and Tp0126
Buffer M [1]	Phosphate 100 mM, 130 mM NaCl, 0.5 M Arginine, 0.01% Tween20, 200 mM Mannitol, pH: 7.0-8.0	Second dialysis step	V1	Tp0136	Tp0733,Tp0751, Tp0326,Tp0136, Tp1038,Tp0633, and Tp0126
Buffer T1 [2]	Phosphate 100 mM, 500 mM NaCl, 1M Urea, 1M Arginine, 5% Trehaloxe, 0.1% Tween 20, pH: 7.0-8.0	First dialysis step	V2	Tp0733,Tp0751, Tp0326,Tp0136, Tp1038,Tp0435, Tp0750,Tp0633, and Tp0126	Tp0155,Tp0483, and Tp0257
Buffer T2 [2]	Phosphate 100 mM, 500 mM NaCl, 0.5 M Arginine, 5% Trehaloxe, 0.05% Tween20, pH: 7.0-8.0	Second dialysis step	V2	Tp0435,Tp0750, and Tp0633	Tp0733,Tp0751, Tp0326,Tp0136, Tp1038, and Tp126
Buffer T3 [2]	Phosphate 100 mM, 500 mM NaCl, 0.1 M Arginine, 5% Trehaloxe, 0.01% Tween20, ph: 7.0-8.0	Third dialysis step	V2	None of the testes proteins was soluble	Tp0435,Tp0750, and Tp0633

Table 6. List of evaluated buffers during step-wise dialysis of recombinant OMPs. Composition of each buffer and the order used during the step-wise dialysis protocol is shown. The protein state in each buffer is indicated as soluble or precipate. Buffers which belong to the same step-wise protocol are pointed under (1) or (2). The version of the recombinant protein (V1 or V2) tested is specified.

Previously in our group, a recombinant form of Tp0751 was produced and purified from lysis fraction with higher yield and purity than the Tp0751 designed in this work (Tp0751_V1). This preceding Tp0751 (pre_Tp0751) was also cloned into the pET-21d(+) plasmid. However, its design was different, presenting a Flag tag in the N-terminal part, following by a Tobacco Etch virus (TEV) protease cleavage site, the protein sequence, and a 6xHis tag in the C-terminal end. Since pre_Tp0751 expressed better in the soluble fraction than our Tp0751_V1, we compared both designs to find differences in the aggregation and solubility profile between both recombinant proteins. We used Protein-Sol and ccSOL omics webservers to predict protein solubility from sequence in *E. coli* expression system. Both softwares returned a similar solubility score/probability when we faced pre_Tp0751 and Tp0751_v1 sequences, 0.450 versus 0.446 for Protein-Sol, and 51% versus 50% for ccSOL omics. Moreover, when we compared the solubility profile between both proteins, it looks quite similar along all sequence (**Fig.39A**). Contrary, when we studied the aggregation profile of each protein using the webserver Aggrescan, they differed in the number of aggregation-prone domains (hot spots) (**Fig.39B**). While pre_Tp0751 has six regions, Tp0751_V1 has two additional ones, that localize in the protein extremes and correspond specifically to the HRV3C protease cleavage sequence. These two hot spots were present in the rest of V1 recombinant protein. Therefore, we wondered if the removal of HRV3C protease sites could favor the expression of the recombinant OMPs into the soluble fraction. Thus, we created a new version of our constructs according to the pre_Tp0751 design, in which the HRV3C cleavage sites were absent. This new protein constructs were named as V2 (**Fig.36B**). Apart from that, we maintained the position of 8xHis and Flag tags, while we removed the Twin-Strep-tag. To eliminate tags for future immunization studies we introduced a TEV protease cleavage site in the N-terminal end among 8xHis tag and protein sequence. However, this method cannot be used in the C-terminal part to remove Flag, since TEV protease cut would leave six extra amino acid residues, which could be immunogenic. To avoid that, we arranged a new set of flag-tag free constructs that were generated from V2 versions by introducing a unique restriction site that allow eliminating Flag by single digestion with a restriction enzyme and following re-ligation with a T4 DNA ligase. When we analyzed *in silico* the solubility of the Tp0751 into the V2 plasmid, same solubility and aggregation profile than pre_Tp0751 was obtained (data not shown), indicating that Flag tag was not impacting the solubility of the protein.

A

B
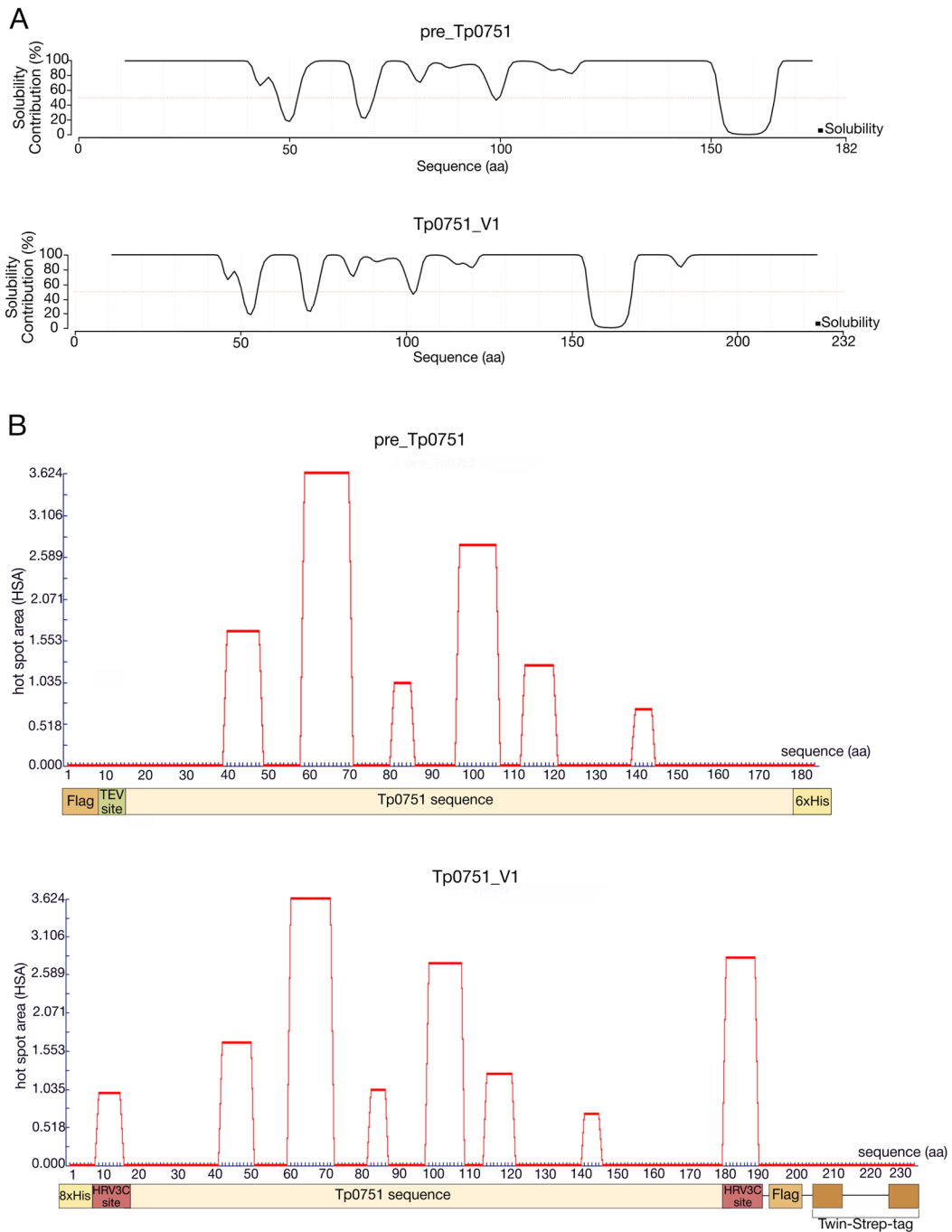
Figure 39. Predicted solubility and aggregation profile of pre_Tp0751 and Tp0751_V1 recombinant proteins. (A) Comparison of the solubility profile between pre_Tp0751 and Tp0751_V1 sequence obtained by ccSOL omics web-software. Solubility is indicated as percentage, a low % correspond to low contribution to solubility in the region and vice versa. **(B)** Aggregation profile of pre_Tp0751 and Tp0751_V1 from Aggrescan webserver. Protein diagram appears under X axis. Regions prone to aggregation have associated a hot spot area value superior to 0 (line red).

We evaluated the expression of the 13 OMPs_V2 in 6 mL culture of transformed BL21 (DE3) *E.coli*, at two different temperatures 27°C and 37°C and in lysis and inclusion bodies fractions. Protein expression was induced using IPTG. Protein detection in each fraction was made by Western Blot using the anti-6xHis antibody. The recombinant Tp0733, Tp0155, Tp0751, Tp0326, Tp136, Tp0257, Tp1038, Tp0435, Tp0750, Tp0633, and Tp0126 proteins were expressed in the lysis fraction from bacteria at the correct molecular weight (**Fig.40A**). Only two proteins, Tp0483 and Tp126_loop were not expressed in the soluble fraction. Notoriously, Tp0155, Tp0326 and Tp0136 were only found when protein was expressed at 37°C, while the rest of proteins were detected using both temperatures. In general, no important differences in band intensity were observed between 27°C and 37°C, except for Tp1038 and Tp126, which were expressed better at 37°C. Some truncated forms were observed in the case of Tp0751, Tp0257, Tp0435, Tp750 and Tp0633. Despite that, the integrity and yield in soluble fraction of V2 proteins were higher than the one observed in V1 at both expression temperatures. Protein expression in each bacterial fraction is summarized in **Table 7**. Since the production of Tp0155, Tp0326, Tp0136, Tp0483 and Tp0126_loop was still low in soluble fraction, we tested other growing conditions. Firstly, high IPTG concentration was tested (1 mM and 2 mM) resulting in a suppression of protein expression (data not shown). As our expression system shows some leaky protein expression in the absence of IPTG, we wondered if low IPTG concentration might improve protein expression. Thus, we checked the expression of these proteins in the lysis fraction using no IPTG or 0.1 mM of IPTG at 37°C. However, no improvement in production was detected in any of these conditions (data not shown).

Besides the analysis of the soluble samples, we also examined the protein expression in inclusion bodies. We observed that all proteins expressed at the correct molecular weight, excluding Tp0126_loop which was not detected (**Fig40B**). Nevertheless, the expression of some proteins, such as, Tp0326, Tp0136, Tp0483, and Tp0126 was very low. Furthermore, Tp0136 appeared only under 37°C condition. Interestingly, these proteins were also barely found in the soluble fraction, except for Tp0126 at 37°C. Regarding these results, Tp0326, Tp0136 and Tp0483 were the most difficult to produce, and Tp0155 was mainly produced as inclusion bodies. Notably, truncated forms were more abundant in inclusion bodies than in soluble lysis fractions.

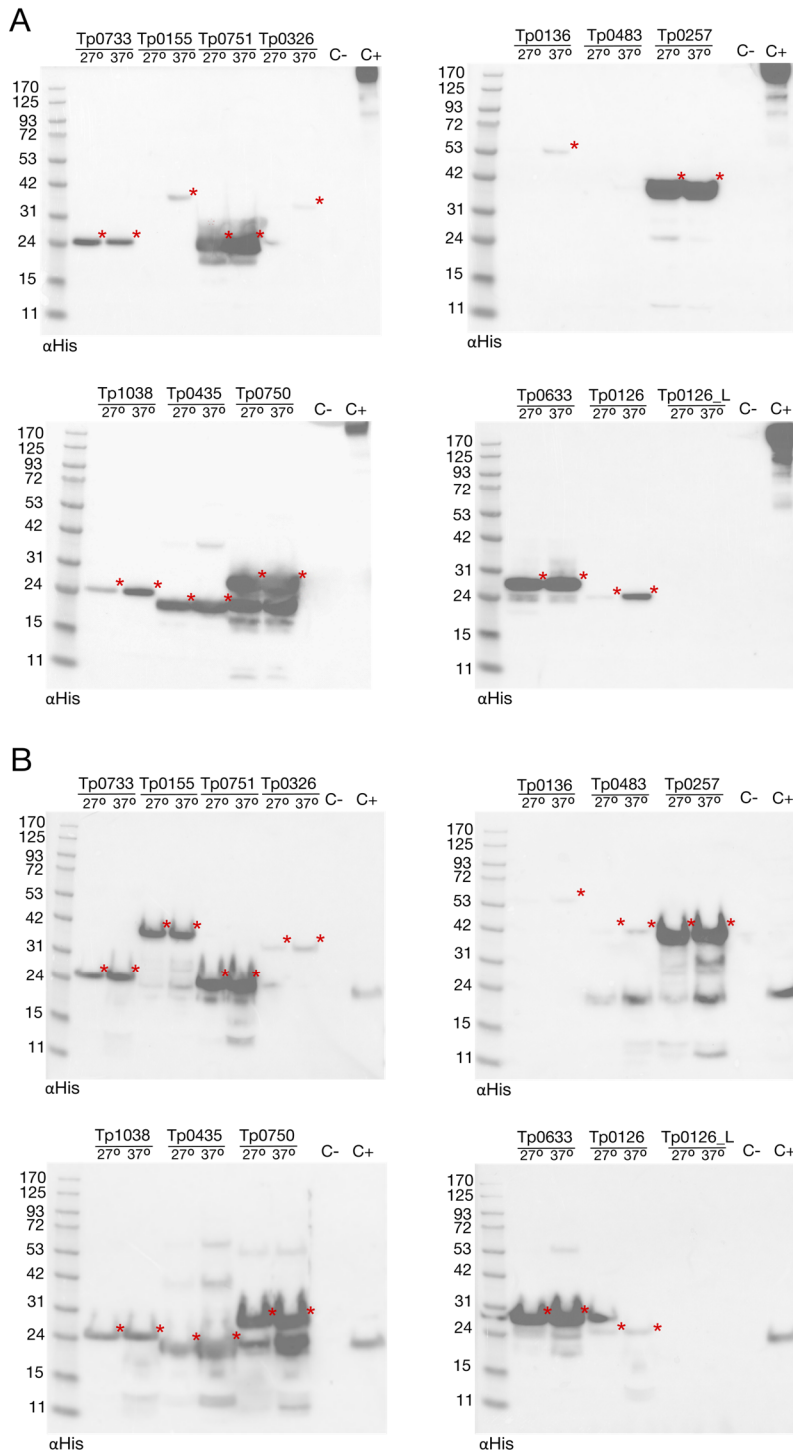**Figure 40. Analysis of V2 recombinant OMPs expression.** The expression of the 13 OMPs (V2 construct) in **(A)** lysis/soluble fraction and **(B)** inclusion bodies fraction at two temperatures 27° vs 37° (in Celsius scale) was analyzed by Western Blot using anti-His antibody. Red asterisk pinpoints the expected molecular weight. C+ and C- mark the positive and negative control, respectively.

	MW (kDa)	PI	Soluble Fraction 27°C	Soluble Fraction 37°C	Inclusion Bodies 27°C	Inclusion Bodies 37°C
Tp0733	23.78	6.53	Low	Low	Low	High
Tp0155	39.15	9.52	No expression	Very Low	High**	High**
Tp0751	20.96	6.53	Very High**	Very High**	High**	High**
Tp0326	33.50	7.87	No expression	Very low	Very low	Very low
Tp0136	49.58	6.48	No expression	Very low	No expression	Very low
Tp0483	42.30	9.00	No expression	No expression	Very low**	Very low**
Tp0257	41.26	8.59	Very High**	Very High**	High**	High**
Tp1038	20.41	5.43	Very Low	Low	Low	Low**
Tp0435	17.62	6.79	High	High	Low**	High**
Tp0750	26.74	6.96	Very High**	Very High**	High**	High**
Tp0633	28.18	6.21	Very High**	Very High**	High**	High**
Tp0126	24.93	6.51	Very low	Low	Low	Low**
Tp0126_L	12.53	6.99	No expression	No expression	No expression	Very Low

Table 7. Summary of V2 recombinant OMPs expression. Features of the 13 recombinant OMPs into V2 design are described, including molecular weight (MW) and isoelectric point (PI). Protein production in soluble or inclusion bodies fractions at 27°C and 37°C are shown according to band intensity from Western Blots results (Fig.40). Two asterisks point presence of multiple truncated forms.

Once we evaluated the production of V2 proteins, the next step was to purify them from cellular fractions. According to the previous results, we purified Tp0733, Tp0751, Tp0257, Tp1038, Tp0435, Tp0750, Tp0633 and Tp0126 from soluble fraction of 250 mL cell cultures growth at 37°C. From these eight proteins only three were purified in an amount higher than 0.1 mg: Tp0751, Tp0435 and Tp0750 (**Fig.41A**). We obtained 0,9 mg of Tp0751, 0,78 mg of Tp0435 and 1,35 mg of Tp0750. An extra band of about 15 kDa co-purified with Tp0435 that was not detected by Western Blot targeting the His-tag, contrary to Tp0751 and Tp0750 preparations, in which low molecular weight bands presented signal (**Fig.41B**). Low levels of Tp0733, Tp0257, Tp1038, Tp0633 and Tp0126 were purified (**Fig.41A**). Tp0257 precipitated during filtration and concentration of elution fraction, which justify the small amount of protein recovered. Interestingly, Tp0733, Tp0257, Tp1038, Tp0633 and Tp0126 showed low expression levels, while they were well detected in 6 mL culture (**Fig.40A**), indicating again that the scale-up process may be challenging.
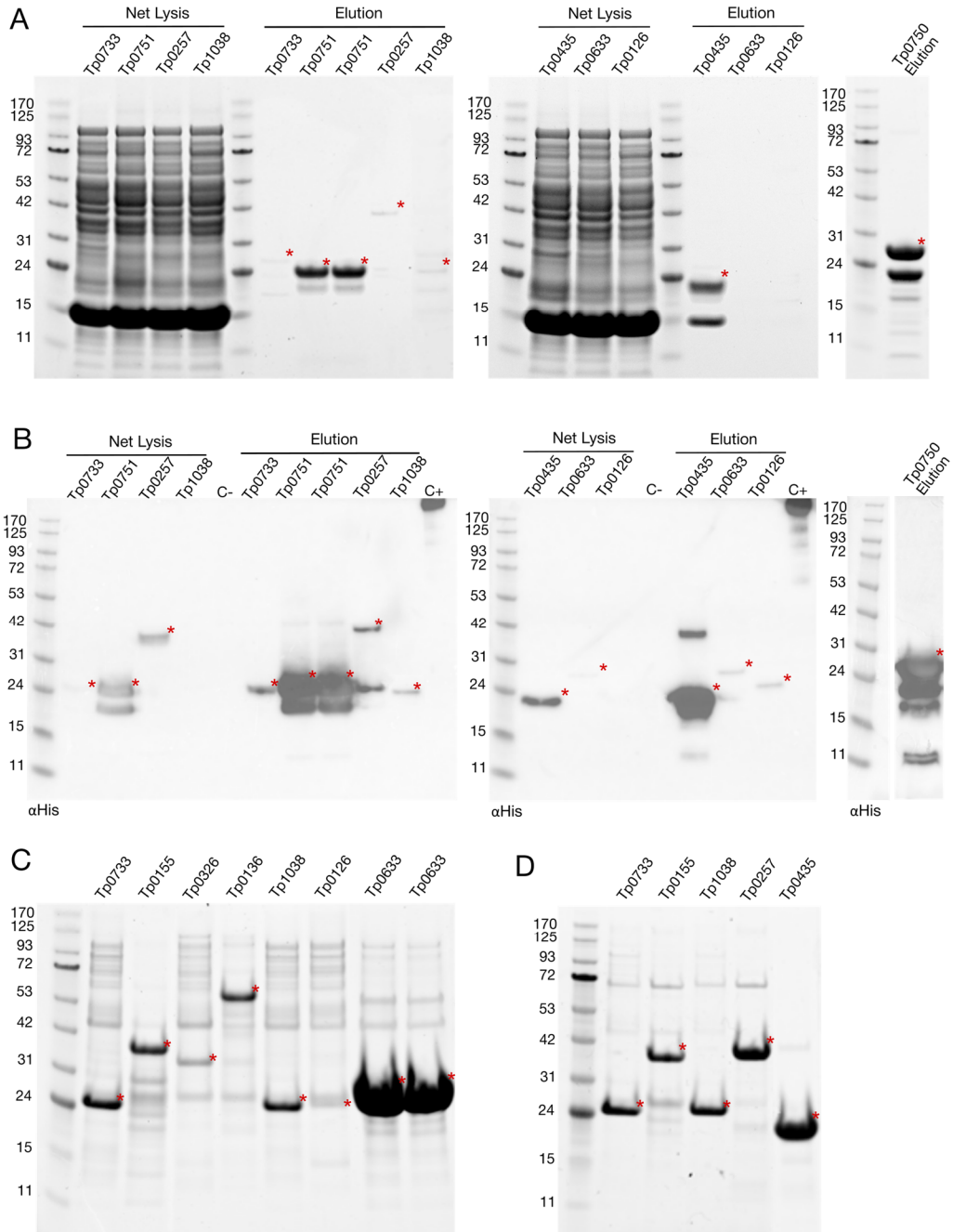
Figure 41. Purification of recombinant OMPs (V2) by IMAC. Analysis of protein purified from lysis fractions by **(A)** Coomassie blue staining and **(B)** Western Blot using anti-His antibody. **(C)** Analysis of purified proteins from inclusion bodies by Coomassie blue staining. **(D)** Purity analysis of recombinant proteins isolated from inclusion bodies after incorporating a washing step at pH:6.0. Proteins were discriminated by SDS-PAGE and stained with Coomassie blue. Red asterisk pinpoints the expected molecular weight.

In parallel, purification from inclusion bodies was performed for those proteins with low yield and truncated forms in soluble fractions, as well as those with purification issues associated (e.g. Tp0257). We obtained between 0.5-1.5 mg of each protein, except for Tp0633, which was purified with high yield (8,7 mg). However, purification products had low purity (**Fig.41C**). To increase the purity of final preparation of Tp0733, Tp0155 Tp1038, Tp0257 and Tp0435, we repeated the purification process adding a washing step at acid pH (pH=6). As it is shown in **Fig.41D**, the purity of purified Tp0733, Tp0155, and Tp1038 vary overall from ~54%(Fig.S5c) to ~75% (Fig.S5d). However, contaminants were not totally removed with this extra washing step and purity strongly depended on the degree of truncated form of each protein. Thus, Tp0733 (80.5%) and Tp1038 (83.5%) had higher purity than Tp0155 (60,5%), the later one showing the highest amount of truncated forms among the three proteins (**Fig.40B**). Additionally, we obtained 0.82 mg of Tp0257 (purity 77.9%) and 1.5 mg of Tp0435 (purity 88.9%) (**Fig.41D**).

Since proteins from inclusion bodies were purified using denaturing condition, we evaluated new approaches for urea removal and protein refolding (**Table 6**). In a first step, we used a phosphate buffer with 1 M urea, 1 M arginine, 5% trehalose and 0,1% tween20. Three proteins precipitate during this buffer exchange, Tp0155, Tp0483 and Tp0257. However, Tp0435, Tp0750, Tp0633, Tp0733, Tp0326, and Tp01038 remained soluble. After that, we completely removed urea and decrease the amount of arginine and tween 20 to 0.5 M and 0.05%, respectively; keeping the amount of trehalose fixed. Only three proteins, Tp0435, Tp0750 and Tp0633, were soluble under this condition. Proteins precipitated when the concentration of arginine was reduced below 0.5M.

Therefore, further investigation is still needed to stablish the refolding protocols for each protein, and to determine the formulation of the buffer that will maintain protein solubility and stability.

3. Binding to extracellular matrix proteins

As recombinant OMPs were hardly produced and purified, we could not proceed with the thirteen OMPs to the next step. Thus, we only moved forward with those proteins that were purified at enough amount and purity to perform immunization experiments in mice. Specifically, there were five recombinant OMPs expressed into the V2 construct: Tp0751, Tp0155, Tp0435, Tp0633, and Tp0750. Notably, Tp0751 was extracted from bacterial soluble fraction with an 87.4 % of purity and at 0.45 mg/mL. In contrast, Tp0155, Tp0435, Tp0633, and Tp0750 were obtained from inclusion bodies fractions. Tp0435, Tp0633, and Tp0750 were solubilized by dialysis in buffer T2 (**Table 6**) with an 83.4%, 88.3%, and 81% purity and at 0.51 mg/mL, 0.82 mg/mL and 0.76 mg/mL, respectively. In contrast, Tp0155 was purified at 0.74 mg/mL with 85.3% purity, but we did not have success reducing the concentration of urea below 8M by step-wise dialysis. Thus, we worked with Tp0155 diluted preparations in which urea was decreased up to 60-80 mM. Prior to immunization, biological activity of purified OMPs were evaluated by ELISA. The biological activity of proteins purified from inclusion bodies depends on extraction and refolding protocol.

Since four out of five OMPs (i.e. Tp0751, Tp0155, Tp0435, and Tp0750) have adhesin function, we tested their binding to components of the extracellular matrix such as laminin, fibrinogen, and fibronectin by ELISA. The results showed that Tp0155 bound to fibronectin > fibrinogen > laminin (**Fig.42A**). In contrast Tp0751 presented weak binding to all three proteins and some binding was only observed at high protein concentration. Surprisingly, Tp0633, which was described as a protein with porin function, bound to fibrinogen, fibronectin and laminin. Interestingly, Tp0435 and Tp0750 bound to the extracellular matrix proteins, but also to bovine serum albumin (BSA). Because BSA is used as blocking reagent in ELISA, we replaced it by casein (CAS) into the blocking buffer to confirm the biological activity of Tp0435 and Tp0750. Both recombinant OMPs barely bound to CAS, so it worked properly as blocking reagent. Thus, we confirmed that Tp0750 binds to laminin and more potently to fibrinogen and fibronectin, while Tp0435 binds mainly to fibrinogen and to a lesser extent to fibronectin and laminin (**Fig.42B**). Overall, all proteins showed binding to extracellular and/or plasma proteins in a dose-response manner.
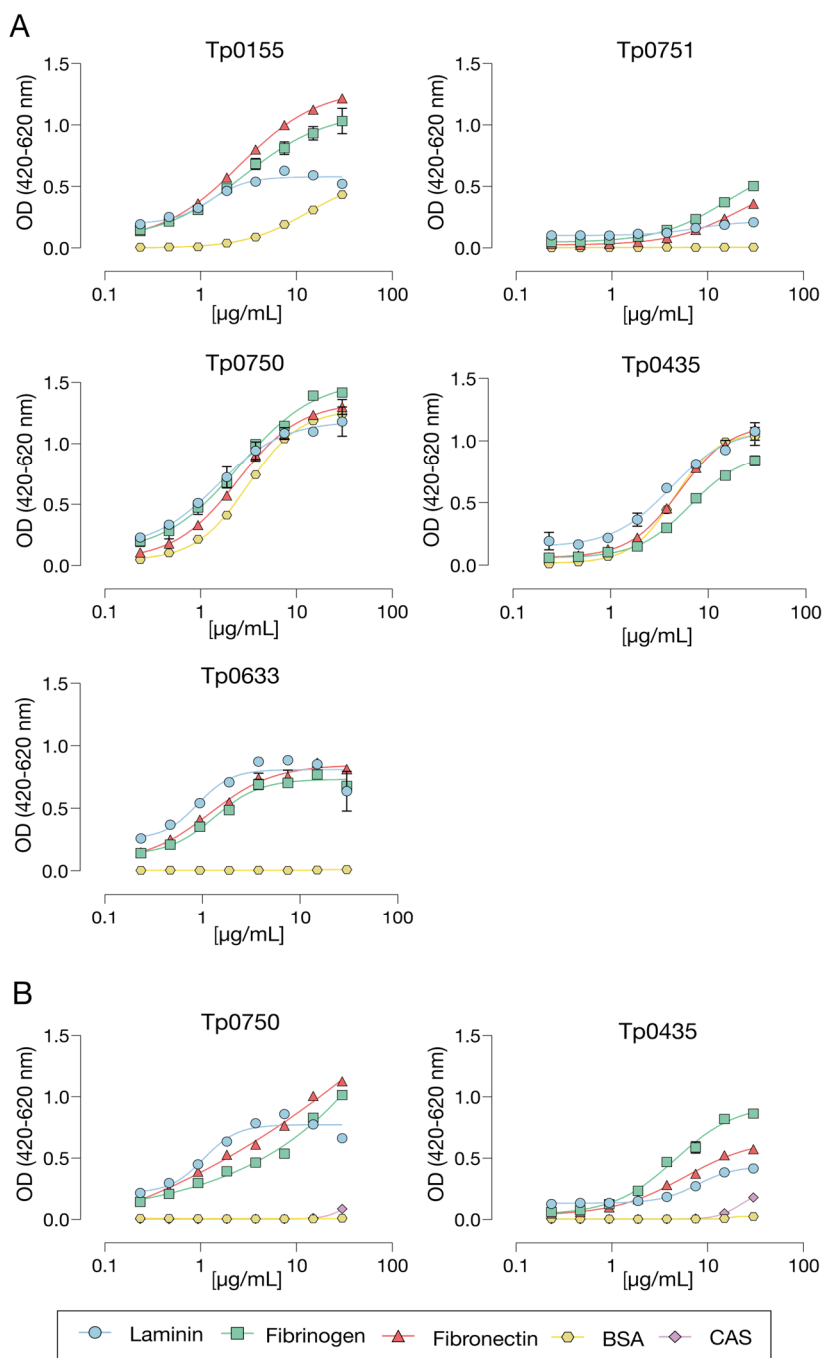
Figure 42. Binding of recombinant OMPs to extracellular proteins. (A) Binding of purified Tp0155, Tp0751, Tp0435, Tp0750, and Tp0633 to laminin, fibrinogen, fibronectin and bovine serum albumin (BSA). BSA blocking buffer was used. **(B)** Binding of Tp0750 and Tp0435 to laminin, fibrinogen, fibronenctin, BSA and casein (CAS). CAS blocking buffer was employed. Blue circle, green square, red triangle, yellow hexagone, and purple diamond showed binding measures to laminin, fibrinogen, fibronectin, BSA, and CAS, respectively. Proteins were assayed in a concentration range of 30 µg/mL to 0,2 µg/mL. Binding is displayed as optical density (OD) at 420 nm minus noise correction at 620 nm.

4. Immunogenicity of recombinant OMPs

After biological activity validation, we evaluated the immunogenicity of the five OMPs. Firstly, we tested the adsorption of Tp0155, Tp0751, Tp0435, Tp0750, and Tp0633 to aluminum hydroxide gel adjuvant by mixing the recombinant OMPs (15 ug of each one) with aluminum hydroxide gel at 1:1 volume ratio. Since, Lyer et al.[587] reported that aluminum hydroxide gel adjuvant can adsorb proteins in the presence of 2M urea, Tp0155 was diluted and mixed with aluminum hydroxide and protein-adjuvant preparation was progressively dialyzed against a urea free PBS buffer. All proteins were effectively adsorbed to aluminum hydroxide gel and protein adsorption was confirmed by spectroscopy at 280nm (90% of protein was adsorbed).
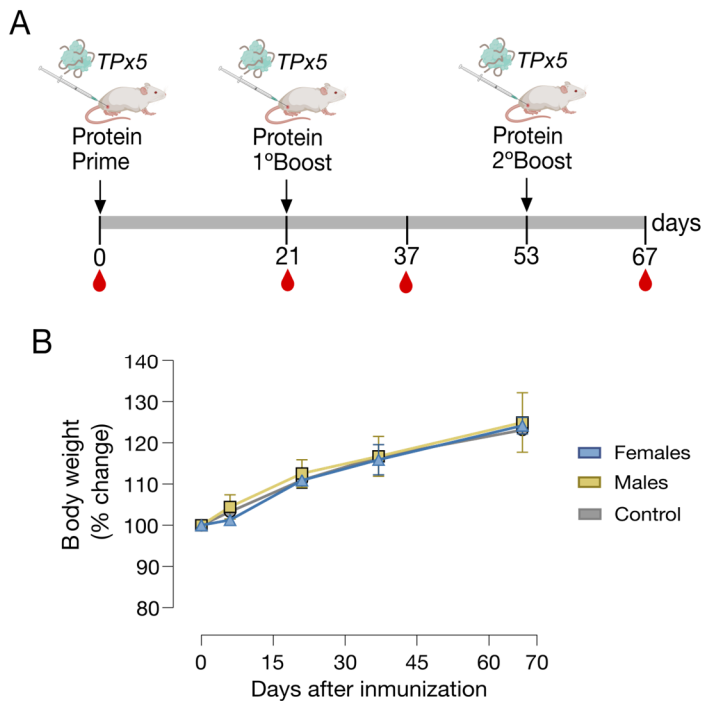
Figure 43. TPx5 vaccination outline and tolerance. (A) Overview of vaccination strategy. Mice were immunized three time with a preparation of five recombinant OMPs with aluminum hydroxide gel referred as TPx5, which included Tp0155, Tp0751, Tp0435, Tp0750, and Tp0633. Red drops point days in which blood sample collection was performed. **(B)** Percentage of weight variation in males (n=4) and females (n=4) immunized animals, as well as, free-antigen immunized control animals (n=2). Mean plus standard errors of the means (SEM) are shown.

Eight BALB/c mice (four males and four females) were immunized using a homologous prime-boost regimen strategy (**Fig.43A**). Mice were vaccinated with a pentavalent preparation (TPx5) including 15 ug of Tp0155, Tp0751, Tp0435, Tp0750, and Tp0633 formulated with aluminum hydroxide gel adjuvant (800 µg per

animal). Two extra mice were used as controls and received PBS with aluminum hydroxide gel adjuvant. Animals were monitored along all the experiment. Weight increased in both animal groups, without significance difference, pointing that protein preparation was well-tolerated (**Fig.43B**). Blood samples were collected from each animal prior to prime dose (day 0) and boost dose (day 21), and also two weeks after the second (day 37) and the third inoculation (day 67) to evaluate the response against the protein preparation. Humoral responses were individually analyzed against each protein (**Fig.44**). Overall, antigen-specific IgGs were detected in all immunized animals against the five tested proteins, without an apparently immunodominance of any antigen over the rest. Moreover, levels of specific antibodies increased after all three immunizations for each protein ($p < 0.01$, Wilcoxon test). No significant differences were found among females and males at any time point (Mann Whitney test), indicating that TP5x preparation induces a similar immune response in both male and female.
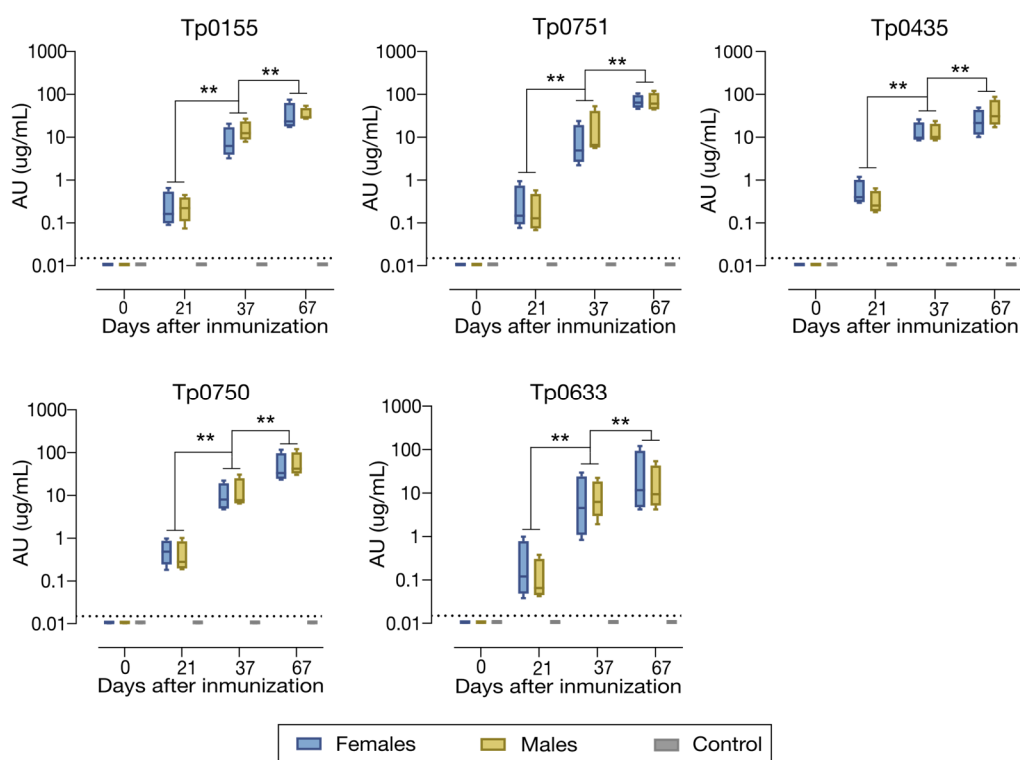
Figure 44. Humoral response elicited by TPx5 immunized mice. Kinetics of specific IgG antibodies in serum samples against each protein individually. Amount of IgG is expressed as arbitrary unit (AU) per mL. Immunized female mice are showed in blue, and immunized male mice in yellow. Immunized control group is displayed in grey. Minimal to maximal values are represented in box and whiskers graph. Groups in each time point were analysed using Wilcoxon signed-rank test. ** p <0.01.
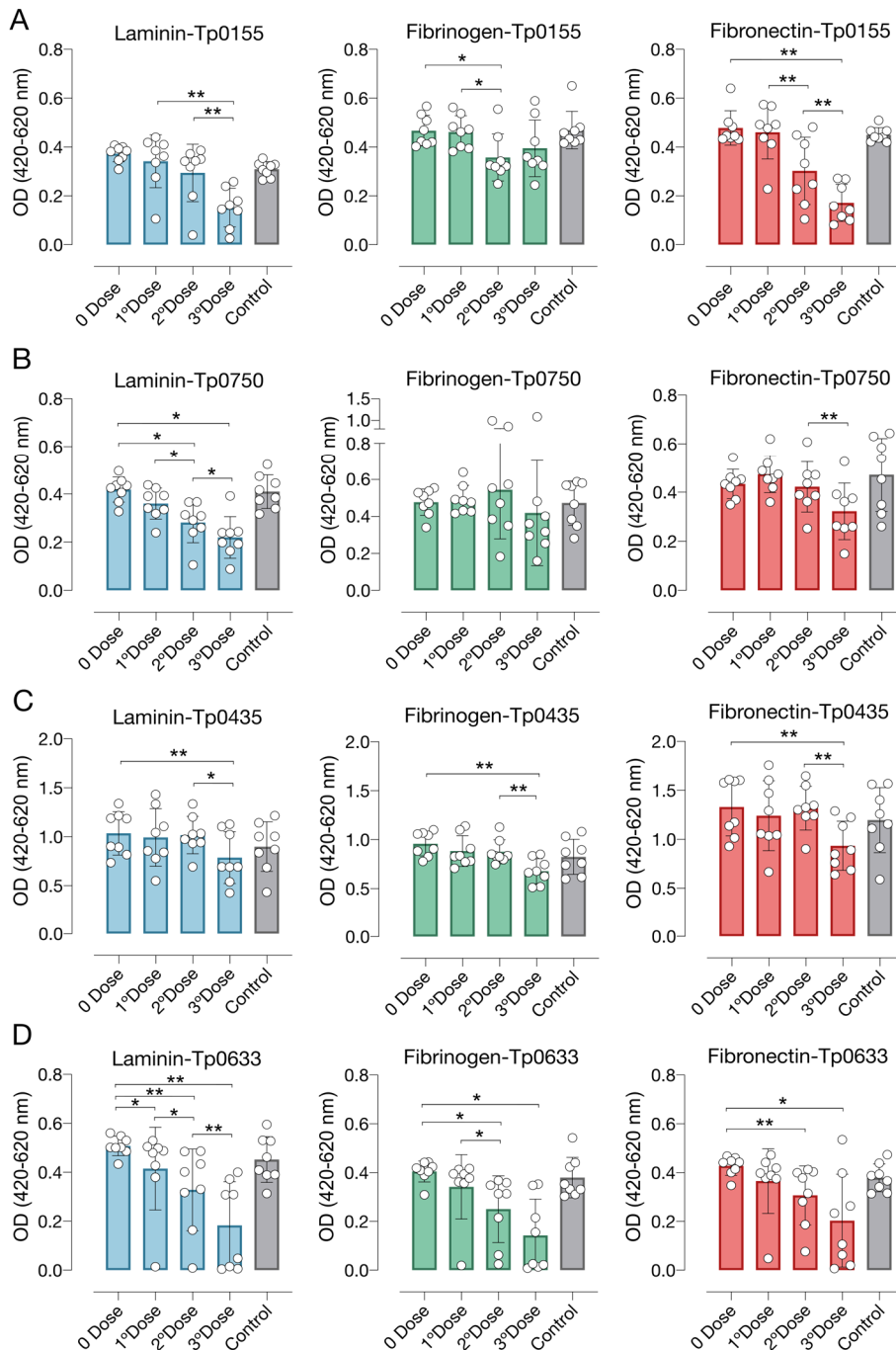
Figure 45. Sera from immunized mice block OMP binding to laminin, fibronectin and fibrinogen. (A) Tp0155, **(B)** Tp0750, **(C)** Tp0435, **(D)** Tp0633 binding assay to laminin (blue), fibrinogen (green) and fibronectin (red) in presence of serums. Blocking activity of immune sera from several time points were tested: 0 Dose (day 0), 1 ° Dose (day 21), 2 ° Dose (day 37), and 3 ° Dose (day 67). Binding blockade corresponding to sera from non-vaccinated mice (all time point grouped) is indicated as Control in grey. Differences between OD after serum incubation at each immunization timepoint was performed using Wilcoxon signed-rank test. * p <0.05, ** p <0.01. Mean plus standard errors of the means (SEM) are shown.

Since OMPs used in vaccination demonstrated *in vitro* binding to laminin, fibrinogen and fibronectin, we wondered whether elicited antibodies from immunized animals would reduce the OMPs binding to extracellular matrix proteins. Thus, a binding blocking assay was performed for Tp0155, Tp0435, Tp0750 and Tp0633, in which each recombinant OMP was incubated with serum from immunized animals and confronted to laminin, fibrinogen and fibronectin. Tp0751 was discarded since binding was only observed at high protein concentration. A decreased binding to extracellular proteins was observed for all four OMPs preincubated with sera form immunized mice (**Fig.45**). Particularly, the highest inhibition was observed for Tp0155/fibronectin (**Fig.45A**), Tp0750/laminin (**Fig.45B**), and Tp0633/laminin, fibrinogen, and fibronectin (**Fig.45D**). Similar inhibition capacity of anti-Tp0435 serum was found for the three extracellular proteins evaluated (**Fig.45C**). No binding inhibition was observed with serum from control mice neither with pre-immune sera
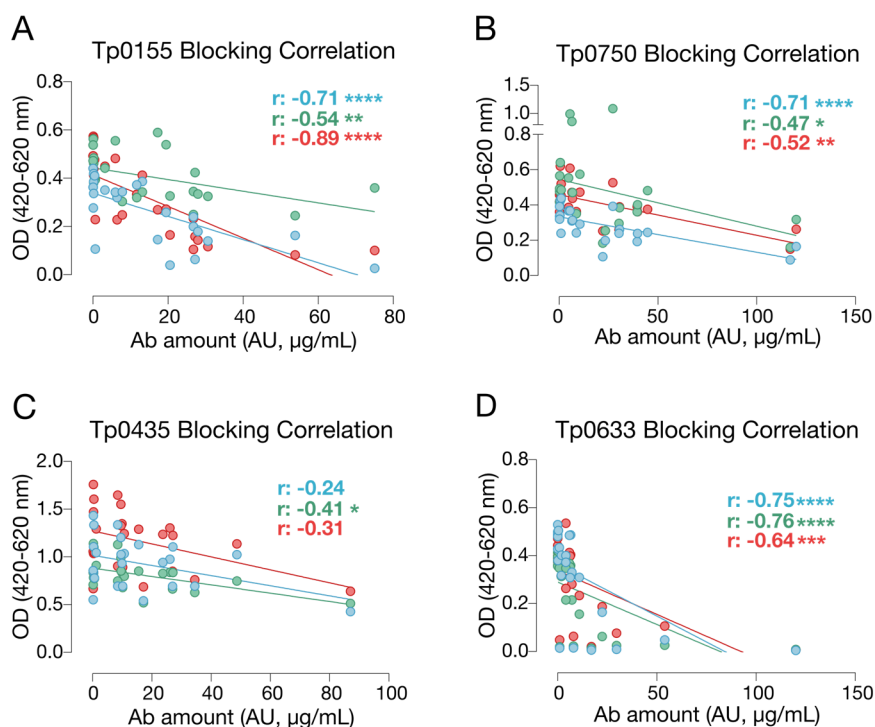
Figure 46. Correlation among binding blockade and specific antibody levels. Correlation analysis between **(A)** anti-Tp0155, **(B)** anti-Tp0750, **(C)** anti-Tp0435, and **(D)** anti-Tp0633 antibodies levels in sera from immunized mice (day 21, day 37, and day 67) and Tp0155, Tp0750, Tp0435, and anti-Tp0633 binding blockade to laminin, fibrinogen and fibronectin, in blue, green and red, respectively. Analysis was performed by nonparametric Sperman test. * $p <0.05$, ** $p <0.01$, *** $p <0.001$, **** $p < 0.0001$.

from basal time point (**Fig.45**). Therefore, the observed blocking effect of immune sera may be related to the generation of specific blocking antibodies. Accordingly, a negative correlation was found among the levels of specific antibodies and the binding capacity of Tp0155 (**Fig.46A**), Tp0750 (**Fig.46B**), and Tp0633 (**Fig.46D**) suggesting a relation among binding blockade and vaccine elicited antibodies. Immune sera poorly blocked the binding of Tp0155 (**Fig.45A and Fig.46A**) and Tp0750 (**Fig.45B and Fig.46B**) to fibrinogen. No correlation was observed for Tp0435 binding blockade and Tp0435 IgG levels, excepting for binding to fibrinogen (**Fig.46C**).

In summary, the five recombinant OMPs evaluated here (i.e. Tp0155, Tp0751, Tp0435, Tp0750, and Tp0633) induced specific antibodies without a clear immunodominance. Furthermore, immunization elicited antibodies that blocked the binding of the recombinant OMPs to extracellular and plasma proteins *in vitro*. Both, levels of specific antibodies and blocking capacity were related and increased after the third immunization.

DISCUSSION

Syphilis is an infectious venereal disease caused by TPA. Despite its etiological agent is known from more than a century ago, there is still no vaccine available. Nowadays, the only effective treatment against TPA infection is penicillin. However, antibiotic treatment and clinical surveillance have not been successful in eradicate syphilis disease and 7 million of new cases are estimated per year[588]. Thus, besides additional preventive health measures, a syphilis vaccine may be crucial for disease control. Nonetheless, none experimental immunization study has reported full protection against infection yet[586]. Among TPA antigens, OMPs are the most widely studied as immunogens. However, TPA can change its OM protein composition to adapt to the host environment. Therefore, this OMP profile modification can be used by the bacteria as an immune evasion mechanism[586]. Moreover, the OM is characterized by a low OMPs density, which reduces its immunogenicity. OMPs showed a high plasticity and functional redundancy, involving two main functions: adhesion and molecular transport. TPA cannot survive outside the organism and, therefore, it is an obligate pathogen. Therefore, a multiple antigen vaccine which covers the OMPs spectrum and targets its essential function may be more effective hampering TPA survival and dissemination than a single antigen vaccine. With this hypothesis in mind, we selected twelve OMPs which are comprised in transport (Tp0126, Tp0733, and Tp0633), adhesion (Tp0136, Tp0155, Tp0483, Tp0750, Tp0751, and Tp0435) and other cellular functions as membrane synthesis, protein translocation to the OM, and iron uptake (Tp0326, Tp0257, and Tp1038). All of them will be include in a multi-antigen vaccine. For each protein, we designed two different constructs based on the pET21d (+) vector, and proteins were expressed using the *E.coli* BL21(DE3) expression system. Overall, we found that most of the OMPs expressed preferably in inclusion bodies and at low amount. According to the literature, the expression of recombinant OMPs after signal peptide removing usually derives into inclusion bodies formation[589]. Indeed, some of the selected proteins (e.g. Tp0136[414], Tp0155[527], Tp0483[527], Tp0126[505], and Tp0257[542]) have been isolated and purified previously from this cellular fraction. Inclusion bodies are cytoplasmic or periplasmic macro-molecules aggregates, mostly proteins, which develop in response to disequilibrium in protein homeostasis[590]. This process can be driven by different situations which are usually associated with foreign protein expression, such as high expression rate, unsuitable post-translational

modifications, and/or misfolding issues inherent to the physicochemical features of the proteins[590]. In order to decrease inclusion bodies formation, many strategies have been proposed in literature to shift protein balance toward soluble forms[590]. Here we explored the effect of modifying bacterial culture conditions, specifically growth temperature and IPTG concentration. One of the major problems of heterologous protein expression in *E. coli* occurs when the amount of protein exceeds the processing capacity of the cellular machinery. Under this situation, protein expression results toxic for normal cellular function and inclusion bodies production is promoted. High rate of recombinant protein is usually related with strong promoter and plasmids with high copy numbers, as T7 promoter used in this work. According to several studies, suboptimal culture temperatures below 37°C slow down bacterial metabolism reducing protein synthesis and increasing their recovery from soluble fraction[591,592]. Thus, we evaluated protein production at two different temperatures: 37°C and 27°C. We did not find any improvement in the level of expression of soluble proteins at 27°C condition; however, protein integrity was better preserved since lower number of truncated protein forms were detected in inclusion bodies. Protein expression rate can be also modulated by decreasing the concentration of IPTG[593]. However, by reducing levels of IPTG, we did not observe an increase in the production of soluble proteins. Besides growth temperature and inducer concentration, inclusion of chemical additives, such as osmolytes or chemical chaperones[594] and control of culture pH have been reported to affect also protein expression rate and processing[595]. We will explore these parameters in the near future to improve soluble protein expression. Since protein sequence strongly determines protein folding and solubility, we analyzed the solubility profile of our constructs using different bioinformatic tools (i.e. ccSOL omics and Aggrescan web software). We found that HRV3C protease cleave sites were predicted as common aggregation prone sequences to our twelve constructs and, therefore, we decided to remove them in a second-generation plasmid design. HRV3C replacement resulted in a raise of protein expression rate in soluble fraction. However, these results were not maintained after culture scalation and an extensive study and monitoring of growth conditions are needed to clarify the reasons behind this disagreement. Additional strategies have been described to overcome inclusion bodies formation such as co-expression of chaperones, use of engineered strains more suitable for post-translational modification, or reducing transcriptional activity

by using a weaker promoter[590]. Nevertheless, the success of all these approaches cannot be generalized to all proteins, since it is most likely dependent of protein characteristics.

Beside expression system optimization, inclusion bodies suppose a major complication for industrial scale up of recombinant protein production since they require extensive procedures including isolation, solubilization, refolding and purification to finally obtain biological active proteins. Inclusion bodies were originally thought to be inactive protein aggregates. However, they can include intermediate folded proteins and even active protein forms[596,597]. Thus, according to previous studies the recovery of biological active proteins from inclusion bodies is possible[598–600], but its success depends mainly on the isolation, solubilization, and refolding methods used[601]. Overall, less or mild aggressive isolation processes are preferable as integrity and protein quality is less altered. Both lysozyme and freeze-thawing methods have been tested to isolate inclusion bodies and they are considered non-harsh processes preserving inclusion bodies integrity[602,603]. However, both techniques are less effective in bacterial wall disruption. Thus, we performed a combination of both methods. Then, inclusion bodies were solubilized using strong denaturing conditions, 8M urea, which has the advantage of solubilizing almost all type of inclusion bodies. In contrast, the use of high urea concentration has several disadvantages and it is related with a lower recovery of bioactive protein. Urea can induce carbamylation of amino acids[604] and denatures folded protein intermediates, which make aggregates more prone during refolding step[605]. Thus, solubilization step will require further optimization by exploring different mild-denaturing methods, which overall have greater preservation of folded protein intermediates[601]. Despite using strong denaturing condition, recovery of folded and bioactive protein is still possible, as it was demonstrated in previous works with OMPs[519,527,606]. According to Anfinsen's dogma, protein amino acid sequence contain itself the information to fold into its three-dimensional structure from denatured state[607]. Hence, *in vitro* refolding of denatured proteins can be accomplished by gradually removing denaturing agents. The efficiency of protein refolding would depend on the solubilization process, the concentration of the protein, the refolding buffer and the refolding method chosen. Here, we used a step-wise dialysis protocol to eliminate urea in the presence of different chemical additives to minimize interactions among folding intermediates which may lead to

aggregates nucleation. Both, arginine and trehalose are widely used aggregation suppressors[608–612] and three proteins were found soluble in their presence (Tp0435, Tp0750, and Tp0633). However, these two additives were not useful for all proteins. Further aggregation suppressors, which were reported to favor refolding, were explored, including glutathione redox environment[613–615] and mannitol[612], without any improvement in solubilization during refolding step. Thus, extra optimization process is required in order to find a protocol which fit to each protein. This includes the evaluation of further additives (e.g. detergents, glycine betaine, proline, glycerol, amphipols, glutamic acid, etc.)[590,616,617], as well as other refolding techniques, such as column-based chromatography methods[618,619] which have previously been demonstrated effective in membrane protein refolding.

Given the difficulties associated with inclusion bodies isolation, purification, and refolding; we could only move forward with five of the thirteen recombinant OMPs while we continue working on the production and purification of the remaining OMPs. Tp0751 was purified from soluble fraction, while Tp0155, Tp0435, Tp0750, and Tp0633 were obtained from inclusion bodies. Regarding their biological activity, recombinant Tp0155, Tp0435, and Tp0750 preserved their adhesion capability to different extracellular and plasma proteins, including fibronectin, fibrinogen, and laminin. As Cameron et al. described, we found that Tp0155 bound to fibronectin[519]. In addition, we showed that Tp0155 can also react with fibrinogen and weakly with laminin. Similarly, Tp0750 bound to laminin, fibronectin and fibrinogen as Houston and colleagues reported[421]. Notably, Tp0435 interacted with all three matrix proteins and showed higher affinity against fibrinogen than fibronectin and laminin. According to literature, Tp0435 was described to bind to mammalian cell lines[523], but its adherence to extracellular matrix components has not been reported before. Interestingly, Tp0155, and more specially Tp0435 and Tp0750, also bound to BSA. Specifically, BSA and human serum albumin (HSA) have a 75.6% sequence homology and show similar structure and binding pockets[620]. In this sense, Alderete and Baseman showed that both rabbit and human albumin adsorbed on the surface of TPA[577]. A host protein coat is a well-known bacteria evasion mechanism[390] and it supposes an advantage to the pathogen since antigens are masked from immune recognition. Although this immune evasion mechanism is controverted in the case of TPA[390], Tp0155, Tp0435, and Tp0750 may be involved in the HSA adsorption observed by Alderete and Baseman. Thus, further investigation is still needed to

confirm the role of Tp0155, Tp0435, and Tp0750 as host cell binding protein and their role escaping from the immune system. Moreover, we found that Tp0663, which was described as a porin-like protein, bound to laminin, fibronectin and fibrinogen. According to Blanco et al., recombinant Tp0663 barely formed porin insertional events on *E.coli* surface in comparison to Tromp1 and consequently its porin function remains unclear[393]. Remarkably, an immunization study performed in rabbits with Tp0633 showed a comparable decrease of TPA dissemination than rabbits immunized with Tp0136, a well-known TPA adhesin[516]. Thus, our results suggest that Tp0663 have adhesin function. Finally, recombinant Tp0751 only showed binding to extracellular proteins at high protein concentration. While various studies highlighted Tp0751 role in bacterial adhesion and dissemination[417,531], Luthra and colleagues described Tp0751 as a periplasmic protein which binds small molecules like retinol and hemes[530]. Thus, the low Tp0751 binding capacity found in this work could be in accordance with this last study. However, loss of adhesion function may be also due to the lack of a correct protein folding and further characterization is needed.

The immunogenicity of the combined recombinant Tp0155, Tp0751, Tp0435, Tp0750, and Tp0633 was evaluated in mice. Protein mix was well tolerated since no loss of weight was observed among vaccinated mice and control group. In general, all OMPs induced homogeneous humoral responses. However, Tp0633 elicited a more heterogenous IgG response among mice. Despite that, the antibody kinetic was similar among antigens and increased after each immunization without immunodominance of any single OMP. Notably, among the second and the third booster dose the increment was similar to the one observed between the first and second dose, indicating that the antibody response can still be improved with a third dose. Moreover, no differences in seroconversion rate or antibody levels were found between immunized female and male mice. This is an important finding since syphilis is the second most common infectious disease cause of stillbirth[621], with more than 200000 estimated cases per year and the number of congenital syphilis have been rising in the last years (i.e United States and Canada)[622,623]. Interestingly, vaccine-elicited antibodies showed the capacity of blocking the binding of OMPs to laminin, fibrinogen, and fibronectin. Moreover, the blocking effect increased with each vaccine doses and, in some cases, it was only observed after the third immunization. *In vitro* adhesion interference by vaccine elicited antibodies have not

been previously reported for any of the tested recombinant OMPs. However, antibody induction has been previously reported after immunization with Tp0155[521], Tp0435[526], Tp0751[532] and Tp0633[516], and accompanied in some cases by decrease in TPA dissemination to distal tissues[516,532]. Here, we showed inhibition of adhesion at protein level using the same recombinant proteins used during vaccination, but we do not know how serum anti-OMPs antibodies will behave against TPA. In this sense, to confirm the results of the present work, it would be interesting to evaluate the *in vitro* inhibition of TPA attachment by serum, as Ke and colleagues made with anti-Tp0136 serum from immunized rabbits[415].

Overall, here we found that Tp0155, Tp0751, Tp0435, Tp0750 and Tp0633 induced specific humoral response and can be administrated in combination. Moreover, specific antibodies were able to interfere with the binding of this recombinant proteins to different matrix and plasma proteins. A third dose regimen induced broad potent antibody response over a second dose regimen. Thus, this study represents a first approach for a multi-antigen protein vaccine against syphilis. Further studies will be required to evaluate its protective role *in vivo* in an infection animal model as rabbits.

CONCLUDING REMARKS

Objective I: To identify the OMPs candidates to be included in the multi-antigen vaccine.

Among thirty-nine syphilis proteins, a total of twelve OMPs were selected to multi-antigen vaccine development.

Objective II: To express and purify the selected recombinant OMPs.

Most recombinant OMPs were expressed forming insoluble cellular inclusion bodies and were purified by IMAC using denaturant conditions. A common refolding protocol was not stablished but a two step-dialysis protocol yield the higher recovery of soluble OMPs.

Objective III: To characterize de binding activity of produced OMPs to extracellular matrix proteins

Tp0155, Tp0435, Tp0750, Tp0633 and, to a lesser extent Tp0751 bind to different matrix and plasma proteins including laminin, fibrinogen, fibronectin and BSA after purification.

Objective IV: To evaluate the immunogenicity of recombinant OMPs in a murine model.

Mice immunized with a combination of Tp0155, Tp0751, Tp0435, Tp0750, and Tp0633 in the presence of aluminum hydroxide as adjuvant developed specific antibodies against all antigens with similar kinetics. Adittionally, serum from immunized animals interfered with the binding of recombinant Tp0155, Tp0435, Tp0750, and Tp0633 to laminin, fibrinogen, and fibronectin; and this blocking effect correlated with the quantity of specific antibodies against each OMPs, supporting antibody involvement.

RECAPITULATION

Although vaccines are designed according to each pathogen, there have been several common steps during preclinical SARS-CoV-2 and syphilis vaccine development.

Objective I: To select and design antigens to be included in the vaccine.

Vaccine antigens should be selected based on their role in the life cycle of the pathogens and their capability for inducing protective immune responses. In addition, it is crucial to consider their structure, yield, and purification complexity. Whereas for SARS-CoV-2, a single trimeric S glycoprotein confers protection to severe disease, a subunit vaccine for bacteria, such as *T.pallidum*, might need the combination of several defined antigens.

Objective II: To produce and purify selected antigens.

The production platform used will be according to the final properties of the antigen. S-stabilizing trimers were produced in mammalian cells to preserve a proper glycosylation profile. Moreover, the transmembrane region was replaced by a trimerization domain to facilitate the soluble expression of trimeric S protein. In contrast, selected T. pallidum antigens were produced in *a prokaryotic* expression system (*E.coli BL21 DE3)* to mimic their bacteria origin.

Objective III: To characterize the produced antigens.

After purification, antigens must be characterized in terms of integrity, purity, and antigenicity. In addition, functional properties of protein should also be determined. Accordingly, SARS-CoV-2 S-variants showed improved yield and RBD exposure, which could also improve its immunogenicity. While, binding capability of *T.pallidum* antigens to components of the extracellular matrix was confirmed *in vitro* after purification.

Objective IV: To evaluate the immunogenicity of antigens and their efficacy against infection *in vivo* or *in vitro.*

The evaluation of immunogenicity and vaccine efficacy should be adapted to each pathogen. Specifically, this evaluation should be performed in the appropriate animal model. Immunogenicity and efficacy of SARS-CoV-2 vaccine was tested in two animal models susceptible to viral infection and the vaccine efficacy was evaluated by antibody levels and protection against severe disease. Thus, one S-variant was identified as promising SARS-CoV-2 vaccine candidate.

In the case of syphilis vaccine, as first approach, only immunogenicity was tested in mice and a functional assay was developed to analyzed the *in vitro* capability of antibodies to block OMP binding to matrix proteins. Our data support to move forward the project and to perform efficacy studies in rabbits to determine vaccine protection.

REFERENCES

1. WHO. Novel Coronavirus – China. Accessed August 1, 2023. https://www.who.int/emergencies/disease-outbreak-news/item/2020-DON233

2. Kumar A, Singh R, Kaur J, et al. Wuhan to World: The COVID-19 Pandemic. *Front Cell Infect Microbiol*. (2021); 11: 596201. doi:10.3389/fcimb.2021.596201

3. Huang C, Wang Y, Li X, et al. Clinical features of patients infected with 2019 novel coronavirus in Wuhan, China. *Lancet*. 2020;395(10223):497-506. doi:10.1016/S0140-6736(20)30183-5

4. Li Q, Guan X, Wu P, et al. Early Transmission Dynamics in Wuhan, China, of Novel Coronavirus–Infected Pneumonia. *New England Journal of Medicine*. 2020;382(13):1199-1207. doi:10.1056/NEJMoa2001316

5. Lu R, Zhao X, Li J, et al. Genomic characterization and epidemiology of 2019 novel coronavirus: implications for virus origins and receptor binding. *Lancet*. 2020;395(10224):565-574. doi:10.1016/S0140-6736(20)30251-8

6. Coronaviridae Study Group of the International Committee on Taxonomy of Viruses. The species Severe acute respiratory syndrome-related coronavirus: classifying 2019-nCoV and naming it SARS-CoV-2. *Nature Microbiology*. (2020) ;5(4):536-544. doi:10.1038/s41564-020-0695-z

7. WHO. Coronavirus Disease (COVID-19) Situation Reports. Accessed September 1, 2023. https://www.who.int/emergencies/diseases/novel-coronavirus-2019/situation-reports

8. Hu B, Guo H, Zhou P, Shi ZL. Characteristics of SARS-CoV-2 and COVID-19. *Nature Reviews Microbiology*. (2020); 19(3):141-154. doi:10.1038/s41579-020-00459-7

9. Wu Z, McGoogan JM. Characteristics of and Important Lessons from the Coronavirus Disease 2019 (COVID-19) Outbreak in China: Summary of a Report of 72 314 Cases from the Chinese Center for Disease Control and Prevention. *JAMA*. (2020); 323(13):1239-1242. doi:10.1001/jama.2020.2648

10. Gao YD, Ding M, Dong X, et al. Risk factors for severe and critically ill COVID-19 patients: A review. *Allergy*. (2021); 76(2):428-455. doi:10.1111/all.14657

11. Dessie ZG, Zewotir T. Mortality-related risk factors of COVID-19: a systematic review and meta-analysis of 42 studies and 423,117 patients. *BMC Infect Dis*. (2021); 21(1):855. doi:10.1186/S12879-021-06536-3

12. Luo G, Zhang X, Zheng H, He D. Infection fatality ratio and case fatality ratio of COVID-19. *International Journal of Infectious Diseases*. (2021); 113:43-46. doi:10.1016/j.ijid.2021.10.004

13. Talukder H, Debnath K, Raquib A, Uddin MM, Hussain S. Estimation of Basic Reproduction Number (Ro) of Novel Coronavirus (COVID-19) from SEIR Model in Perspective of Bangladesh. *Journal of Infectious Diseases and Epidemiology*. (2020); 6:144. doi:10.23937/2474-3658/1510144

14. Buowari DY, Ogundipe HD. Severe Acute Respiratory Syndrome coronavirus-2 (SARS-COV-2) Infection: An Epidemiological Review. *Ann Ib Postgrad Med.* 2021;19(Suppl 1):S68-S76.

15. Liu Y, Rocklöv J. The effective reproductive number of the Omicron variant of SARS-CoV-2 is several times relative to Delta. *J Travel Med.* (2022); 29(3). doi:10.1093/jtm/taac037

16. Kang SJ, Jung SI. Age-Related Morbidity and Mortality among Patients with COVID-19. *Infect Chemother.* (2020); 52(2):154-164. doi:10.3947/ic.2020.52.2.154

17. Mehta V, Goel S, Kabarriti R, et al. Case fatality rate of cancer patients with COVID-19 in a New York Hospital system. *Cancer Discov.* (2020); 10(7):935-941. doi:10.1158/2159-8290.CD-20-0516

18. Vahey GM, McDonald E, Marshall K, et al. Risk factors for hospitalization among persons with COVID-19—Colorado. *PLoS One.* (2021); 16(9):e0256917. doi:10.1371/journal.pone.0256917

19. Korneta P, Rostek K. The Impact of the SARS-CoV-19 Pandemic on the Global Gross Domestic Product. *Int J Environ Res Public Health.* (2021); 18(10):5246. doi:10.3390/ijerph18105246

20. de Miquel C, Domènech-Abella J, Felez-Nobrega M, et al. The Mental Health of Employees with Job Loss and Income Loss during the COVID-19 Pandemic: The Mediating Role of Perceived Financial Stress. *Int J Environ Res Public Health.* (2022);19(6):3158. doi:10.3390/IJERPH19063158

21. WHO. Essential health services face continued disruption during COVID-19 pandemic. Accessed January 17, 2023. https://www.who.int/news/item/07-02-2022-essential-health-services-face-continued-disruption-during-covid-19-pandemic

22. Hoofman J, Secord E. The Effect of COVID-19 on Education. *Pediatr Clin North Am.* (2021); 68(5):1071-1079. doi:10.1016/j.pcl.2021.05.009

23. Long E, Patterson S, Maxwell K, et al. COVID-19 pandemic and its impact on social relationships and health. *J Epidemiol Community Health.* 2022;76(2):128-132. doi:10.1136/JECH-2021-216690

24. Xiong J, Lipsitz O, Nasri F, et al. Impact of COVID-19 pandemic on mental health in the general population: A systematic review. *J Affect Disord.* (2020); 277:55-64. doi:10.1016/j.jad.2020.08.001

25. Jacob Machado D, Scott R, Guirales S, Janies DA. Fundamental evolution of all Orthocoronavirinae including three deadly lineages descendent from Chiroptera-hosted coronaviruses: SARS-CoV, MERS-CoV and SARS-CoV-2. *Cladistics.* (2021); 37(5):461. doi:10.1111/cla.12454

26. Kesheh MM, Hosseini P, Soltani S, Zandi M. An overview on the seven pathogenic human coronaviruses. *Rev Med Virol.* (2022); 32(2):e2282. doi:10.1002/rmv.2282

27. Körner RW, Majjouti M, Alcazar MAA, Mahabir E. Of Mice and Men: The Coronavirus MHV and Mouse Models as a Translational Approach to Understand SARS-CoV-2. *Viruses*. (2020); 12(8). doi:10.3390/v12080880

28. Cavanagh D. Coronavirus avian infectious bronchitis virus. *Vet Res*. (2007); 38(2):281-297. doi:10.1051/vetres:2006055

29. Erles K, Toomey C, Brooks HW, Brownlie J. Detection of a group 2 coronavirus in dogs with canine infectious respiratory disease. *Virology*. (2003); 310(2):216-223. doi:10.1016/S0042-6822(03)00160-0

30. Durham PJ, Stevenson BJ, Farquharson BC. Rotavirus and coronavirus associated diarrhoea in domestic animals. *N Z Vet J*. (1979); 27(3):30-32. doi:10.1080/00480169.1979.34595

31. Singh D, Yi S V. On the origin and evolution of SARS-CoV-2. *Experimental & Molecular Medicine* (2021); 53(4):537-547. doi:10.1038/s12276-021-00604-z

32. Chan-Yeung M, Xu RH. SARS: epidemiology. *Respirology*. (2003); 8(Suppl 1):S9-14. doi:10.1046/J.1440-1843.2003.00518.X

33. WHO. Middle East Respiratory Syndrome Coronavirus –Saudi Arabia. Accessed January 3, 2023. https://www.who.int/emergencies/disease-outbreak-news/item/2022-DON422

34. Su S, Wong G, Shi W, et al. Epidemiology, Genetic Recombination, and Pathogenesis of Coronaviruses. *Trends Microbiol*. (2016); 24(6):490-502. doi:10.1016/j.tim.2016.03.003

35. Lau SK, Woo PC, Li KS, et al. Discovery of a Novel Coronavirus, China Rattus Coronavirus HKU24, from Norway Rats Supports the Murine Origin of Betacoronavirus 1 and Has Implications for the Ancestor of Betacoronavirus Lineage A. *J Virol*. (2015); 89(6):3076. doi:10.1128/jvi.02420-14

36. Holmes EC, Goldstein SA, Rasmussen AL, et al. The origins of SARS-CoV-2: A critical review. *Cell*. (2021); 184(19):4848-4856. doi:10.1016/j.cell.2021.08.017

37. Zhou P, Yang X Lou, Wang XG, et al. A pneumonia outbreak associated with a new coronavirus of probable bat origin. *Nature*. (2020); 579(7798):270-273. doi:10.1038/s41586-020-2012-7

38. Nie J, Li Q, Zhang L, et al. Functional comparison of SARS-CoV-2 with closely related pangolin and bat coronaviruses. (2021); 7(1):21. doi:10.1038/s41421-021-00256-3

39. Ye ZW, Yuan S, Yuen KS, Fung SY, Chan CP, Jin DY. Zoonotic origins of human coronaviruses. *Int J Biol Sci*. (2020); 16(10):1686-1697. doi:10.7150/ijbs.45472

40. Turakhia Y, Thornlow B, Hinrichs A, et al. Pandemic-scale phylogenomics reveals the SARS-CoV-2 recombination landscape. *Nature*. (2022); 609(7929):994-997. doi:10.1038/s41586-022-05189-9

41.   Wu F, Zhao S, Yu B, et al. A new coronavirus associated with human respiratory disease in China. *Nature*. (2020); 579(7798):265-269. doi:10.1038/s41586-020-2008-3

42.   Masters PS. The molecular biology of coronaviruses. *Adv Virus Res*. (2006); 66:193-292. doi:10.1016/S0065-3527(06)66005-3

43.   Redondo N, Zaldívar-López S, Garrido JJ, Montoya M. SARS-CoV-2 Accessory Proteins in Viral Pathogenesis: Knowns and Unknowns. *Front Immunol*. (2021); 12:708264. doi:10.3389/fimmu.2021.708264

44.   Liu DX, Fung TS, Chong KK, Shukla A, Hilgenfeld R. Accessory proteins of SARS-CoV and other coronaviruses. *Antiviral Res*. (2014); 109(1):97-109. doi:10.1016/j.antiviral.2014.06.013

45.   Li X, Hou P, Ma W, et al. SARS-CoV-2 ORF10 suppresses the antiviral innate immune response by degrading MAVS through mitophagy. *Cellular & Molecular Immunology*. (2021); 19(1):67-78. doi:10.1038/s41423-021-00807-4

46.   Low ZY, Zabidi NZ, Yip AJW, Puniyamurti A, Chow VTK, Lal SK. SARS-CoV-2 Non-Structural Proteins and Their Roles in Host Immune Evasion. *Viruses*. (2022); 14(9):1991. doi:10.3390/V14091991

47.   Gao Y, Yan L, Huang Y, et al. Structure of the RNA-dependent RNA polymerase from COVID-19 virus. *Science*. (2020); 368(6492):779-782. doi:10.1126/science.abb7498

48.   Liu C, Mendonça L, Yang Y, et al. The Architecture of Inactivated SARS-CoV-2 with Postfusion Spikes Revealed by Cryo-EM and Cryo-ET. *Structure*. (2020); 28(11):1218-1224.e4. doi:10.1016/j.str.2020.10.001

49.   Mariano G, Farthing RJ, Lale-Farjat SLM, Bergeron JRC. Structural Characterization of SARS-CoV-2: Where We Are, and Where We Need to Be. *Front Mol Biosci*. (2020); 7: 605236. doi:10.3389/fmolb.2020.605236

50.   Kuo L, Hurst-Hess KR, Koetzner CA, Masters PS. Analyses of Coronavirus Assembly Interactions with Interspecies Membrane and Nucleocapsid Protein Chimeras. *J Virol*. (2016); 90(9):4357-4368. doi: 10.1128/jvi.03212-15

51.   Cong Y, Ulasli M, Schepers H, et al. Nucleocapsid Protein Recruitment to Replication-Transcription Complexes Plays a Crucial Role in Coronaviral Life Cycle. *J Virol*. (2020); 94(4):e01925-19. doi:10.1128/jvi.01925-19

52.   Stertz S, Reichelt M, Spiegel M, et al. The intracellular sites of early replication and budding of SARS-coronavirus. *Virology*. (2007); 361(2):304-315. doi:10.1016/j.virol.2006.11.027

53.   Schoeman D, Fielding BC. Coronavirus envelope protein: current knowledge. *Virol J*. (2019); 16(1). doi:10.1186/S12985-019-1182-0

54.   Mortola E, Roy P. Efficient assembly and release of SARS coronavirus-like particles by a heterologous expression system. *FEBS Lett*. (2004); 576(1-2):174. doi:10.1016/j.febslet.2004.09.009

55. Ruch TR, Machamer CE. The Hydrophobic Domain of Infectious Bronchitis Virus E Protein Alters the Host Secretory Pathway and Is Important for Release of Infectious Virus. *J Virol*. (2011); 85(2):675-685. doi:10.1128/jvi.01570-10

56. Collins AR, Knobler RL, Powell H, Buchmeier MJ. Monoclonal antibodies to murine hepatitis virus-4 (strain JHM) define the viral glycoprotein responsible for attachment and cell-cell fusion. *Virology*. (1982); 119(2):358-371. doi:10.1016/0042-6822(82)90095-2

57. Qian Z, Dominguez SR, Holmes K V. Role of the Spike Glycoprotein of Human Middle East Respiratory Syndrome Coronavirus (MERS-CoV) in Virus Entry and Syncytia Formation. *PLoS One*. (2013); 8(10):76469. doi:10.1371/journal.pone.0076469

58. Buchholz UJ, Bukreyev A, Yang L, et al. Contributions of the structural proteins of severe acute respiratory syndrome coronavirus to protective immunity. *Proc Natl Acad Sci U S A*. (2004); 101(26):9804-9809. doi:10.1073/pnas.0403492101

59. Xia S, Zhu Y, Liu M, et al. Fusion mechanism of 2019-nCoV and fusion inhibitors targeting HR1 domain in spike protein. *Cell Mol Immunol*. (2020); 17(7):765-767. doi:10.1038/S41423-020-0374-2

60. Hoffmann M, Kleine-Weber H, Schroeder S, et al. SARS-CoV-2 Cell Entry Depends on ACE2 and TMPRSS2 and Is Blocked by a Clinically Proven Protease Inhibitor. *Cell*. (2020); 181(2):271-280.e8. doi:10.1016/j.cell.2020.02.052

61. Wrapp D, Wang N, Corbett KS, et al. Cryo-EM structure of the 2019-nCoV spike in the prefusion conformation. *Science*. (2020); 367(6483):1260-1263. doi: 10.1126/science.abb2507

62. Premkumar L, Segovia-Chumbez B, Jadi R, et al. The receptor-binding domain of the viral spike protein is an immunodominant and highly specific target of antibodies in SARS-CoV-2 patients. *Sci Immunol*. (2020); 5(48): eabc8413. doi:10.1126/sciimmunol.abc8413

63. Song W, Gui M, Wang X, Xiang Y. Cryo-EM structure of the SARS coronavirus spike glycoprotein in complex with its host cell receptor ACE2. *PLoS Pathog*. (2018);14(8):e1007236. doi:10.1371/journal.ppat.1007236

64. Gui M, Song W, Zhou H, et al. Cryo-electron microscopy structures of the SARS-CoV spike glycoprotein reveal a prerequisite conformational state for receptor binding. *Cell Res*. (2017); 27(1):119-129. doi:10.1038/cr.2016.152

65. Pallesen J, Wang N, Corbett KS, et al. Immunogenicity and structures of a rationally designed prefusion MERS-CoV spike antigen. *Proc Natl Acad Sci U S A*. (2017); 114(35):E7348-E7357. doi: 10.1073/pnas.1707304114

66. Peng C, Zhu Z, Shi Y, et al. Computational Insights into the Conformational Accessibility and Binding Strength of SARS-CoV-2 Spike Protein to Human Angiotensin-Converting Enzyme 2. *Journal of Physical Chemistry Letters*. 2020;11(24):10482-10488. doi: 10.1021/acs.jpclett.0c02958

67.	Takeda M. Proteolytic activation of SARS-CoV-2 spike protein. *Microbiol Immunol.* (2022); 66(1):15-23. doi:10.1111/1348-0421.12945

68.	Yu S, Zheng X, Zhou B, et al. SARS-CoV-2 spike engagement of ACE2 primes S2′ site cleavage and fusion initiation. *Proc Natl Acad Sci U S A.* (2022); 119(1):e2111199119. doi:10.1073/pnas.2111199119

69.	Tai L, Zhu G, Yang M, et al. Nanometer-resolution in situ structure of the SARS-CoV-2 postfusion spike protein. *Proc Natl Acad Sci U S A.* (2021); 118(48):e2112703118. doi: 10.1073/pnas.2112703118

70.	Fuentes-Prior P. Priming of SARS-CoV-2 S protein by several membrane-bound serine proteinases could explain enhanced viral infectivity and systemic COVID-19 infection. *Journal of Biological Chemistry.* (2021); 296:100135. doi:10.1074/jbc.rev120.015980

71.	Kishimoto M, Uemura K, Sanaki T, et al. TMPRSS11D and TMPRSS13 Activate the SARS-CoV-2 Spike Protein. *Viruses.* (2021); 13(3):384. doi:10.3390/v13030384

72.	Zang R, Castro MFG, McCune BT, et al. TMPRSS2 and TMPRSS4 promote SARS-CoV-2 infection of human small intestinal enterocytes. *Sci Immunol.* (2020); 5(47). doi:10.1126/sciimmunol.abc3582

73.	Bayati A, Kumar R, Francis V, McPherson PS. SARS-CoV-2 infects cells after viral entry via clathrin-mediated endocytosis. *Journal of Biological Chemistry.* (2021); 296:100306. doi:10.1016/j.jbc.2021.100306

74.	Zhao MM, Yang WL, Yang FY, et al. Cathepsin L plays a key role in SARS-CoV-2 infection in humans and humanized mice and is a promising target for new drug development. *Signal Transduct and Targeted Ther.* (2021); 6(1):134. doi:10.1038/s41392-021-00558-8

75.	V'kovski P, Kratzel A, Steiner S, Stalder H, Thiel V. Coronavirus biology and replication: implications for SARS-CoV-2. *Nature Reviews Microbiology.* (2020);19(3):155-170. doi:10.1038/s41579-020-00468-6

76.	Snijder EJ, Decroly E, Ziebuhr J. The Nonstructural Proteins Directing Coronavirus RNA Synthesis and Processing. *Adv Virus Res.* (2016); 96:59-126. doi:10.1016/bs.aivir.2016.08.008

77.	Emrani J, Ahmed M, Jeffers-Francis L, et al. SARS-COV-2, infection, transmission, transcription, translation, proteins, and treatment: A review. *Int J Biol Macromol.* (2021); 193(Pt B):1249-1273. doi:10.1016/j.ijbiomac.2021.10.172

78.	Knoops K, Kikkert M, Van Den Worm SHE, et al. SARS-coronavirus replication is supported by a reticulovesicular network of modified endoplasmic reticulum. *PLoS Biol.* (2008); 6(9):1957-1974. doi:10.1371/journal.pbio.0060226

79.	Lebeau G, Vagner D, Frumence É, et al. Deciphering SARS-CoV-2 Virologic and Immunologic Features. *International Journal of Molecular Sciences.* (2020); 21(16):5932. doi:10.3390/ijms21165932

80. Coutard B, Valle C, de Lamballerie X, Canard B, Seidah NG, Decroly E. The spike glycoprotein of the new coronavirus 2019-nCoV contains a furin-like cleavage site absent in CoV of the same clade. *Antiviral Res*. (2020); 176:104742. doi:10.1016/j.antiviral.2020.104742

81. Benton DJ, Wrobel AG, Xu P, et al. Receptor binding and priming of the spike protein of SARS-CoV-2 for membrane fusion. *Nature* (2020); 588(7837):327-330. doi:10.1038/s41586-020-2772-0

82. Johnson BA, Xie X, Bailey AL, et al. Loss of Furin Cleavage Site Attenuates SARS-CoV-2 Pathogenesis. *Nature*. (2021); 591(7849):293-299. doi:10.1038/S41586-021-03237-4

83. Bar-On YM, Flamholz A, Phillips R, Milo R. Sars-cov-2 (Covid-19) by the numbers. *Elife*. (2020); 9:e57309. doi:10.7554/eLife.57309

84. Yewdell JW. Antigenic drift: Understanding COVID-19. *Immunity*. (2021); 54(12):2681-2687. doi:10.1016/j.immuni.2021.11.016

85. Sui J, Aird DR, Tamin A, et al. Broadening of Neutralization Activity to Directly Block a Dominant Antibody-Driven SARS-Coronavirus Evolution Pathway. *PLoS Pathog*. (2008); 4(11):e1000197. doi:10.1371/journal.ppat.1000197

86. WHO. Tracking SARS-CoV-2 variants. Accessed January 14, 2023. https://www.who.int/en/activities/tracking-SARS-CoV-2-variants/

87. Choi JY, Smith DM. SARS-CoV-2 Variants of Concern. *Yonsei Med J*. (2021); 62(11):961-968. doi:10.3349/ymj.2021.62.11.961

88. Zhao Z, Zhou J, Tian M, et al. Omicron SARS-CoV-2 mutations stabilize spike up-RBD conformation and lead to a non-RBM-binding monoclonal antibody escape. *Nature Communications*. (2022); 13(1):4958. doi:10.1038/s41467-022-32665-7

89. Wölfel R, Corman VM, Guggemos W, et al. Virological assessment of hospitalized patients with COVID-2019. *Nature*. (2020); 581(7809):465-469. doi:10.1038/s41586-020-2196-x

90. Ziegler CGK, Allon SJ, Nyquist SK, Shalek AK. SARS-CoV-2 Receptor ACE2 Is an Interferon-Stimulated Gene in Human Airway Epithelial Cells and Is Detected in Specific Cell Subsets across Tissues. *Cell*. (2020); 81(5):1016-1035.e19. doi:10.1016/j.cell.2020.04.035

91. Liu J, Li Y, Liu Q, et al. SARS-CoV-2 cell tropism and multiorgan infection. *Cell Discovery*. (2021); 7(1):17. doi:10.1038/s41421-021-00249-2

92. Ackermann M, Verleden SE, Kuehnel M, et al. Pulmonary Vascular Endothelialitis, Thrombosis, and Angiogenesis in Covid-19. *New England Journal of Medicine*. (2020); 383(2):120-128. doi: 10.1056/NEJMoa2015432

93. Robayo-Amortegui H, Forero-Delgadillo A, Pérez-Garzón M, et al. Severe gastrointestinal injury associated with SARS-CoV-2 infection: Thrombosis or Inflammation?: A retrospective case series study. *Medicine*. (2022); 101(42):e31188. doi:10.1097/MD.0000000000031188

94. Gabarre P, Dumas G, Dupont T, Darmon M, Azoulay E, Zafrani L. Acute kidney injury in critically ill patients with COVID-19. *Intensive Care Med.* (2020); 46(7):1339-1348. doi:10.1007/S00134-020-06153-9

95. Petersen EL, Goßling A, Adam G, et al. Multi-organ assessment in mainly non-hospitalized individuals after SARS-CoV-2 infection: The Hamburg City Health Study COVID programme. *Eur Heart J.* (2022); 43(11):1124-1137. doi:10.1093/eurheartj/ehab914

96. Zaim S, Chong JH, Sankaranarayanan V, Harky A. COVID-19 and Multiorgan Response. *Curr Probl Cardiol.* (2020); 45(8):100618. doi:10.1016/j.cpcardiol.2020.100618

97. Diamond MS, Kanneganti TD. Innate immunity: the first line of defense against SARS-CoV-2. *Nature Immunology.* (2022); 23(2):165-176. doi:10.1038/s41590-021-01091-0

98. Li D, Wu M. Pattern recognition receptors in health and diseases. *Signal Transduction and Targeted Therapy.* (2021); 6(1):1-24. doi:10.1038/s41392-021-00687-0

99. Zheng M, Karki R, Williams EP, et al. TLR2 senses the SARS-CoV-2 envelope protein to produce inflammatory cytokines. *Nature Immunology.* (2021); 22(7):829-838. doi:10.1038/s41590-021-00937-x

100. Khan S, Shafiei MS, Longoria C, Schoggins JW, Savani RC, Zaki H. SARS-CoV-2 spike protein induces inflammation via TLR2-dependent activation of the NF-κB pathway. *Elife.* (2021); 10:e68563. doi: 10.7554/eLife.68563

101. Qian Y, Lei T, Patel PS, et al. Direct Activation of Endothelial Cells by SARS-CoV-2 Nucleocapsid Protein Is Blocked by Simvastatin. *J Virol.* (2021); 95(23):e0139621. doi:10.1128/JVI.01396-21

102. Shirato K, Kizaki T. SARS-CoV-2 spike protein S1 subunit induces pro-inflammatory responses via toll-like receptor 4 signaling in murine and human macrophages. *Heliyon.* (2021); 7(2):e06187. doi:10.1016/j.heliyon.2021.e06187

103. Totura AL, Whitmore A, Agnihothram S, et al. Toll-like receptor 3 signaling via TRIF contributes to a protective innate immune response to severe acute respiratory syndrome coronavirus infection. *mBio.* (2015); 6(3):e00638-15. doi: 10.1128/mBio.00638-15

104. Bortolotti D, Gentili V, Rizzo S, et al. Tlr3 and tlr7 rna sensor activation during sars-cov-2 infection. *Microorganisms.* (2021);9(9):1820. doi:10.3390/microorganisms9091820

105. Yin X, Riva L, Pu Y, et al. MDA5 Governs the Innate Immune Response to SARS-CoV-2 in Lung Epithelial Cells. *Cell Rep.* (2021); 34(2):108628. doi:10.1016/j.celrep.2020.108628

106. Thorne LG, Reuschl A, Zuliani-Alvarez L, et al. SARS-CoV-2 sensing by RIG-I and MDA5 links epithelial infection to macrophage inflammation. *EMBO J.* (2021); 40(15):e107826. doi:10.15252/embj.2021107826

107. Yamada T, Sato S, Sotoyama Y, et al. RIG-I triggers a signaling-abortive anti-SARS-CoV-2 defense in human lung cells. *Nature Immunology*. (2021); 22(7):820-828. doi:10.1038/s41590-021-00942-0

108. Franchi L, Warner N, Viani K, Nuñez G. Function of Nod-like Receptors in Microbial Recognition and Host Defense. *Immunol Rev*. (2009); 227(1):106-128. doi:10.1111/J.1600-065x.2008.00734.x

109. Kelley N, Jeltema D, Duan Y, He Y. The NLRP3 Inflammasome: An Overview of Mechanisms of Activation and Regulation. *Int J Mol Sci*. (2019); 20(13):3328. doi:10.3390/ijms20133328

110. Campbell GR, To RK, Hanna J, Spector SA. SARS-CoV-2, SARS-CoV-1, and HIV-1 derived ssRNA sequences activate the NLRP3 inflammasome in human macrophages through a non-classical pathway. *iScience*. (2021); 24(4):102295. doi:10.1016/j.isci.2021.102295

111. Xu H, Akinyemi IA, Chitre SA, et al. SARS-CoV-2 viroporin encoded by ORF3a triggers the NLRP3 inflammatory pathway. *Virology*. (2022); 568:13-22. doi: 10.1016/j.virol.2022.01.003

112. Pan P, Shen M, Yu Z, et al. SARS-CoV-2 N protein promotes NLRP3 inflammasome activation to induce hyperinflammation. *Nature Communications*. 2021;12(1):4664. doi:10.1038/s41467-021-25015-6

113. Callaway E. Scientists deliberately gave people COVID-here's what they learnt. *Nature*. (2022);602(7896):191-192. doi:10.1038/d41586-022-00319-9

114. Zhu Z, Cai T, Fan L, et al. Clinical value of immune-inflammatory parameters to assess the severity of coronavirus disease 2019. *Int J Infect Dis*. (2020); 95:332-339. doi:10.1016/j.ijid.2020.04.041

115. Liu Y, Zhang C, Huang F, et al. Elevated plasma levels of selective cytokines in COVID-19 patients reflect viral load and lung injury. *Natl Sci Rev*. (2020); 7(6):1003-1011. doi:10.1093/nsr/nwaa037

116. Chen K, Xiao F, Hu D, et al. SARS-CoV-2 Nucleocapsid Protein Interacts with RIG-I and Represses RIG-Mediated IFN-β Production. *Viruses*. (2020); 13(1):47. doi:10.3390/v13010047

117. Han L, Zhuang MW, Deng J, et al. SARS-CoV-2 ORF9b antagonizes type I and III interferons by targeting multiple components of the RIG-I/MDA-5–MAVS, TLR3–TRIF, and cGAS–STING signaling pathways. *J Med Virol*. (2021); 93(9):5376-5389. doi:10.1002/jmv.27050

118. Konno Y, Kimura I, Uriu K, et al. SARS-CoV-2 ORF3b Is a Potent Interferon Antagonist Whose Activity Is Increased by a Naturally Occurring Elongation Variant. *Cell Rep*. (2020); 32(12):108185. doi:10.1016/j.celrep.2020.108185

119. Blanco-Melo D, Nilsson-Payant BE, Liu WC, et al. Imbalanced Host Response to SARS-CoV-2 Drives Development of COVID-19. *Cell*. (2020); 181(5):1036-1045.e9. doi:10.1016/j.cell.2020.04.026

120. Karki R, Sharma BR, Tuladhar S, et al. Synergism of TNF-α and IFN-γ Triggers Inflammatory Cell Death, Tissue Damage, and Mortality in SARS-CoV-2 Infection and Cytokine Shock Syndromes. *Cell.* (2021); 184(1):149-168.e17. doi:10.1016/j.cell.2020.11.025

121. Ting JPY, Trowsdale J. Genetic Control of MHC Class II Expression. *Cell.* (2002); 109(2):S21-S33. doi:10.1016/S0092-8674(02)00696-7

122. Zhou F. Molecular Mechanisms of IFN-γ to Up-Regulate MHC Class I Antigen Processing and Presentation *Int Rev Immunol.* (2009); 28(3-4):239-260. doi:10.1080/08830180902978120

123. Sallusto F, Lanzavecchia A. The instructive role of dendritic cells on T-cell responses. *Arthritis Res.* (2002); 4(Suppl 3):S127-132. doi:10.1186/ar567

124. Rydyznski Moderbacher C, Ramirez SI, Dan JM, et al. Antigen-Specific Adaptive Immunity to SARS-CoV-2 in Acute COVID-19 and Associations with Age and Disease Severity. *Cell.* (2020); 183(4):996-1012.e19. doi:10.1016/j.cell.2020.09.038

125. Grifoni A, Weiskopf D, Ramirez SI, et al. Targets of T Cell Responses to SARS-CoV-2 Coronavirus in Humans with COVID-19 Disease and Unexposed Individuals. *Cell.* (2020); 181(7):1489-1501.e15. doi:10.1016/j.cell.2020.05.015

126. Weiskopf D, Schmitz KS, Raadsen MP, et al. Phenotype and kinetics of SARS-CoV-2-specific T cells in COVID-19 patients with acute respiratory distress syndrome. *Sci Immunol.* (2020); 5(48):eabd2071. doi:10.1126/sciimmunol.abd2071

127. Sekine T, Perez-Potti A, Rivera-Ballesteros O, et al. Robust T Cell Immunity in Convalescent Individuals with Asymptomatic or Mild COVID-19. *Cell.* (2020); 183(1):158-168.e14. doi:10.1016/j.cell.2020.08.017

128. Peng Y, Mentzer AJ, Liu G, et al. Broad and strong memory CD4+ and CD8+ T cells induced by SARS-CoV-2 in UK convalescent individuals following COVID-19. *Nature Immunology.* (2020); 21(11):1336-1345. doi:10.1038/s41590-020-0782-6

129. Le Bert N, Tan AT, Kunasegaran K, et al. SARS-CoV-2-specific T cell immunity in cases of COVID-19 and SARS, and uninfected controls. *Nature.* (2020); 584(7821):457-462. doi:10.1038/s41586-020-2550-z

130. Nelde A, Bilich T, Heitmann JS, et al. SARS-CoV-2-derived peptides define heterologous and COVID-19-induced T cell recognition. *Nature Immunology 2020 22:1.* (2020); 22(1):74-85. doi:10.1038/s41590-020-00808-x

131. Guo L, Wang G, Wang Y, et al. SARS-CoV-2-specific antibody and T-cell responses 1 year after infection in people recovered from COVID-19: a longitudinal cohort study. *Lancet Microbe.* (2022); 3(5):e348-e356. doi:10.1016/S2666-5247(22)00036-2

132. Le Bert N, Clapham HE, Tan AT, et al. Highly functional virus-specific cellular immune response in asymptomatic SARS-CoV-2 infection. *Journal of Experimental Medicine.* (2021); 218(5):e20202617. doi:10.1084/jem.20202617/211835

133. Dan JM, Mateus J, Kato Y, et al. Immunological memory to SARS-CoV-2 assessed for up to 8 months after infection. *Science.* (2021); 371(6529):eabf4063. doi:10.1126/science.abf4063

134. Poon MML, Rybkina K, Kato Y, et al. SARS-CoV-2 infection generates tissue-localized immunological memory in humans. *Sci Immunol.* (2021); 6(65):eabl9105. doi:10.1126/sciimmunol.abl9105

135. Gao Y, Cai C, Grifoni A, et al. Ancestral SARS-CoV-2-specific T cells cross-recognize the Omicron variant. *Nature Medicine.* (2022); 28(3):472-476. doi:10.1038/s41591-022-01700-x

136. Keeton R, Tincho MB, Ngomti A, et al. T cell responses to SARS-CoV-2 spike cross-recognize Omicron. *Nature.* (2022); 603(7901):488-492. doi:10.1038/s41586-022-04460-3

137. Cyster JG, Allen CDC. B Cell Responses: Cell Interaction Dynamics and Decisions. *Cell.* (2019); 177(3):524-540. doi:10.1016/j.cell.2019.03.016

138. Hoffman W, Lakkis FG, Chalasani G. B Cells, Antibodies, and More. *Clin J Am Soc Nephrol.* (2016); 11(1):137-154. doi:10.2215/cjn.09430915

139. Roco JA, Mesin L, Binder SC, et al. Class-Switch Recombination Occurs Infrequently in Germinal Centers. *Immunity.* (2019); 51(2):337-350.e7. doi:10.1016/j.immuni.2019.07.001

140. Akkaya M, Kwak K, Pierce SK. B cell memory: building two walls of protection against pathogens. *Nature Reviews Immunology.* (2019); 20(4):229-238. doi:10.1038/s41577-019-0244-2

141. Long QX, Liu BZ, Deng HJ, et al. Antibody responses to SARS-CoV-2 in patients with COVID-19. *Nat Med.* (2020); 26(6):845-848. doi:10.1038/s41591-020-0897-1

142. Zheng J, Deng Y, Zhao Z, et al. Characterization of SARS-CoV-2-specific humoral immunity and its potential applications and therapeutic prospects. *Cellular & Molecular Immunology.* (2021); 19(2):150-157. doi:10.1038/s41423-021-00774-w

143. Ma H, Zeng W, He H, et al. Serum IgA, IgM, and IgG responses in COVID-19. *Cell Mol Immunol.* (2020); 17(7):773-775. doi:10.1038/s41423-020-0474-z

144. Cervia C, Nilsson J, Zurbuchen Y, et al. Systemic and mucosal antibody responses specific to SARS-CoV-2 during mild versus severe COVID-19. *Journal of Allergy and Clinical Immunology.* (2021); 147(2):545-557.e9. doi:10.1016/j.jaci.2020.10.040

145. Yu HQ, Sun BQ, Fang ZF, et al. Distinct features of SARS-CoV-2-specific IgA response in COVID-19 patients. *European Respiratory Journal.* (2020); 56(2):2001526. doi:10.1183/13993003.01526-2020

146. Lynch KL, Whitman JD, Lacanienta NP, et al. Magnitude and Kinetics of Anti–Severe Acute Respiratory Syndrome Coronavirus 2 Antibody Responses and Their Relationship to Disease Severity. *Clinical Infectious Diseases.* (2021); 72(2):301-308. doi:10.1093/cid/ciaa979

147. Wang Y, Zhang L, Sang L, et al. Kinetics of viral load and antibody response in relation to COVID-19 severity. *J Clin Invest.* (2020); 130(10):5235-5244. doi:10.1172/jci138759

148. Liu Y, Yan LM, Wan L, et al. Viral dynamics in mild and severe cases of COVID-19. *Lancet Infect Dis.* (2020); 20(6):656-657. doi:10.1016/S1473-3099(20)30232-2

149. Pradenas E, Ubals M, Urrea V, et al. Virological and Clinical Determinants of the Magnitude of Humoral Responses to SARS-CoV-2 in Mild-Symptomatic Individuals. *Front Immunol.* (2022);13:860215. doi:10.3389/fimmu.2022.860215

150. Carsetti R, Zaffina S, Piano Mortari E, et al. Different Innate and Adaptive Immune Responses to SARS-CoV-2 Infection of Asymptomatic, Mild, and Severe Cases. *Front Immunol.* (2020); 11:610300. doi:10.3389/fimmu.2020.610300

151. Tang J, Ravichandran S, Lee Y, et al. Antibody affinity maturation and plasma IgA associate with clinical outcome in hospitalized COVID-19 patients. *Nature Communications.* (2021); 12(1):1221. doi:10.1038/s41467-021-21463-2

152. Henry C, Zheng NY, Huang M, et al. Influenza Virus Vaccination Elicits Poorly Adapted B Cell Responses in Elderly Individuals. *Cell Host Microbe.* (2019); 25(3):357-366.e6. doi:10.1016/j.chom.2019.01.002

153. Sherina N, Piralla A, Du L, et al. Persistence of SARS-CoV-2-specific B and T cell responses in convalescent COVID-19 patients 6–8 months after the infection. *Med.* (2021); 2(3):281-295.e4. doi:10.1016/j.medj.2021.02.001

154. Ortega N, Ribes M, Vidal M, et al. Seven-month kinetics of SARS-CoV-2 antibodies and role of pre-existing antibodies to human coronaviruses. *Nat Commun.* 2021;12(1):4740. doi:10.1038/S41467-021-24979-9

155. L'Huillier AG, Meyer B, Andrey DO, et al. Antibody persistence in the first 6 months following SARS-CoV-2 infection among hospital workers: a prospective longitudinal study. *Clinical Microbiology and Infection.* (2021); 27(5):784.e1. doi:10.1016/J.CMI.2021.01.005

156. Sarjomaa M, Diep LM, Zhang C, et al. SARS-CoV-2 antibody persistence after five and twelve months: A cohort study from South-Eastern Norway. *PLoS One.* (2022); 17(8):e0264667. doi:10.1371/journal.pone.0264667

157. Petersen MS, Hansen CB, Kristiansen MF, et al. SARS-CoV-2 Natural Antibody Response Persists for at Least 12 Months in a Nationwide Study From the Faroe Islands. *Open Forum Infect Dis.* (2021); 8(8):ofab378. doi:10.1093/ofid/ofab378

158. Marcotte H, Piralla A, Zuo F, et al. Immunity to SARS-CoV-2 up to 15 months after infection. *iScience.* (2022); 25(2):103743. doi:10.1016/j.isci.2022.103743

159. Pušnik J, König J, Mai K, et al. Persistent Maintenance of Intermediate Memory B Cells Following SARS-CoV-2 Infection and Vaccination Recall Response. *J Virol.* (2022); 96(15):e0076022. doi:10.1128/jvi.00760-22

160. Pribanić Matešić M, Kučan Brlić P, Lenac Roviš T, et al. Collection of Monoclonal Antibodies Targeting SARS-CoV-2 Proteins. *Viruses*. (2022); 14(2):443. doi:10.3390/v14020443

161. Szymczak A, Jędruchniewicz N, Torelli A, et al. Antibodies specific to SARS-CoV-2 proteins N, S and E in COVID-19 patients in the normal population and in historical samples. *J Gen Virol*. (2021);102(11):1692. doi:10.1099/jgv.0.001692

162. Liu W, Liu L, Kou G, et al. Evaluation of nucleocapsid and spike protein-based enzyme-linked immunosorbent assays for detecting antibodies against SARS-CoV-2. *J Clin Microbiol*. (2020); 58(6):e00461-20. doi: 10.1128/JCM.00461-20

163. Sanghavi DK, Bhakta S, Wadei HM, et al. Low antispike antibody levels correlate with poor outcomes in COVID-19 breakthrough hospitalizations. *J Intern Med*. (2022); 292(1):127-135. doi:10.1111/joim.13471

164. Liao B, Chen Z, Zheng P, et al. Detection of Anti-SARS-CoV-2-S2 IgG Is More Sensitive Than Anti-RBD IgG in Identifying Asymptomatic COVID-19 Patients. *Front Immunol*. (2021); 12:3365. doi:10.3389/fimmu.2021.724763

165. Piccoli L, Park YJ, Tortorici MA, et al. Mapping Neutralizing and Immunodominant Sites on the SARS-CoV-2 Spike Receptor-Binding Domain by Structure-Guided High-Resolution Serology. *Cell*. (2020); 183(4):1024-1042.e21. doi: 10.1016/j.cell.2020.09.037

166. Chi X, Yan R, Zhang J, et al. A neutralizing human antibody binds to the N-terminal domain of the Spike protein of SARS-CoV-2. *Science*. (2020); 369(6504):650-655. doi:10.1126/science.abc6952

167. Liu L, Wang P, Nair MS, et al. Potent neutralizing antibodies against multiple epitopes on SARS-CoV-2 spike. *Nature*. (2020); 584(7821):450-456. doi:10.1038/s41586-020-2571-7

168. Pinto D, Sauer MM, Czudnochowski N, et al. Broad betacoronavirus neutralization by a stem helix–specific human antibody. *Science*. (2021); 373(6559):1109-1116. doi: 10.1126/science.abj3321

169. Dacon C, Tucker C, Peng L, et al. Broadly neutralizing antibodies target the coronavirus fusion peptide. *Science.* (2022); 377(6607):728-735. doi: 10.1126/science.abq3773.

170. Mittal A, Khattri A, Verma V. Structural and antigenic variations in the spike protein of emerging SARS-CoV-2 variants. *PLoS Pathog*. (2022); 18(2):e1010260. doi:10.1371/journal.ppat.1010260

171. Moriyama S, Adachi Y, Sato T, et al. Temporal maturation of neutralizing antibodies in COVID-19 convalescent individuals improve potency and breadth to circulating SARS-CoV-2 variants. *Immunity*. (2021); 54(8):1841-1852.e4. doi:10.1016/j.immuni.2021.06.015

172. Muecksch F, Weisblum Y, Barnes CO, et al. Affinity maturation of SARS-CoV-2 neutralizing antibodies confers potency, breadth, and resilience to viral escape mutations. *Immunity*. (2021); 54(8):1853-1868.e7. doi:10.1016/j.immuni.2021.07.008

173. Pauvolid-Corrêa A, Costa Caetano B, Beatriz Machado A, et al. Sera of patients infected by earlier lineages of SARS-CoV-2 are capable to neutralize later emerged variants of concern. *Biol Methods Protoc.* (2022); 7(1). doi:10.1093/biomethods/bpac021

174. Winklmeier S, Eisenhut K, Taskin D, et al. Persistence of functional memory B cells recognizing SARS-CoV-2 variants despite loss of specific IgG. *iScience.* (2022); 25(1):103659. doi:10.1016/j.isci.2021.103659

175. Garcia-Beltran WF, Lam EC, Astudillo MG, et al. COVID-19-neutralizing antibodies predict disease severity and survival. *Cell.* (2021);184(2):476-488.e11. doi:10.1016/j.cell.2020.12.015

176. Trinité B, Tarrés-Freixas F, Rodon J, et al. SARS-CoV-2 infection elicits a rapid neutralizing antibody response that correlates with disease severity. *Scientific Reports.* (2021);11(1):2608. doi:10.1038/s41598-021-81862-9

177. Suthar MS, Zimmerman MG, Kauffman RC, et al. Rapid Generation of Neutralizing Antibody Responses in COVID-19 Patients. *Cell Rep Med.* (2020); 1(3):100040. doi:10.1016/j.xcrm.2020.100040

178. Seow J, Graham C, Merrick B, et al. Longitudinal observation and decline of neutralizing antibody responses in the three months following SARS-CoV-2 infection in humans. *Nature Microbiology.* (2020); 5(12):1598-1607. doi:10.1038/s41564-020-00813-8

179. Gaebler C, Wang Z, Lorenzi JCC, et al. Evolution of antibody immunity to SARS-CoV-2. *Nature.* (2021); 591(7851):639-644. doi:10.1038/s41586-021-03207-w

180. Pradenas E, Trinité B, Urrea V, et al. Clinical course impacts early kinetics,magnitude, and amplitude of SARS-CoV-2 neutralizing antibodies beyond 1 year after infection. *Cell Rep Med.* (2022); 3(2):100523. doi:10.1016/j.xcrm.2022.100523

181. Pradenas E, Trinité B, Urrea V, et al. Stable neutralizing antibody levels 6 months after mild and severe COVID-19 episodes. *Med.* (2021); 2(3):313-320.e4. doi:10.1016/j.medj.2021.01.005

182. Bergwerk M, Gonen T, Lustig Y, et al. Covid-19 Breakthrough Infections in Vaccinated Health Care Workers. *New England Journal of Medicine.* (2021); 385(16):1474-1484. doi:10.1056/nejmoa2109072

183. Addetia A, Crawford KHD, Dingens A, et al. Neutralizing Antibodies Correlate with Protection from SARS-CoV-2 in Humans during a Fishery Vessel Outbreak with a High Attack Rate. *J Clin Microbiol.* (2020); 58(11): e02107-20. doi:10.1128/jcm.02107-20

184. Lopez-Munoz AD, Kosik I, Holly J, Yewdell JW. Cell surface SARS-CoV-2 nucleocapsid protein modulates innate and adaptive immunity. *Sci Adv.* (2022); 8(31):9770. doi:10.1126/sciadv.abp9770

185. Dufloo J, Grzelak L, Staropoli I, et al. Asymptomatic and symptomatic SARS-CoV-2 infections elicit polyfunctional antibodies. *Cell Rep Med*. (2021); 2(5):100275. doi:10.1016/j.xcrm.2021.100275

186. Chen X, Rostad CA, Anderson LJ, et al. The development and kinetics of functional antibody-dependent cell-mediated cytotoxicity (ADCC) to SARS-CoV-2 spike protein. *Virology*. (2021); 559:1-9. doi:10.1016/j.virol.2021.03.009

187. Vangeti S, Periasamy S, Sun P, et al. Serum Fc-Mediated Monocyte Phagocytosis Activity Is Stable for Several Months after SARS-CoV-2 Asymptomatic and Mildly Symptomatic Infection. *Microbiol Spectr*. (2022); 10(6):e0183722. doi: 10.1128/spectrum.01837-22

188. Adom D, Dillon SR, Yang J, et al. Immune responses to SARS-CoV-2 infection in hospitalized pediatric and adult patients. *Sci Transl Med*. (2020); 12(564):eabd5487. doi:10.1126/scitranslmed.abd5487

189. Lin JT, Zhang JS, Su N, et al. Safety and Immunogenicity from a Phase I Trial of Inactivated Severe Acute Respiratory Syndrome Coronavirus *Vaccine*. (2007); 12(7):1107-1113.

190. Martin JE, Louder MK, Holman LSA, et al. A SARS DNA vaccine induces neutralizing antibody and cellular immune responses in healthy adults in a Phase I clinical trial. *Vaccine*. 2008;26(50):6338-6343. doi:10.1016/j.vaccine.2008.09.026

191. Khan S, El Morabet R, Khan RA, et al. Where we missed? Middle East Respiratory Syndrome (MERS-CoV) epidemiology in Saudi Arabia; 2012–2019. *Sci Total Environ*. (2020); 747:141369. doi:10.1016/j.scitotenv.2020.141369

192. Modjarrad K, Roberts CC, Mills KT, et al. Safety and immunogenicity of an anti-Middle East respiratory syndrome coronavirus DNA vaccine: a phase 1, open-label, single-arm, dose-escalation trial. *Lancet Infect Dis*. (2019); 19(9):1013-1022. doi:10.1016/S1473-3099(19)30266-X

193. Bosaeed M, Balkhy HH, Almaziad S, et al. Safety and immunogenicity of ChAdOx1 MERS vaccine candidate in healthy Middle Eastern adults (MERS002): an open-label, non-randomised, dose-escalation, phase 1b trial. *Lancet Microbe*. (2022); 3(1):e11-e20. doi:10.1016/S2666-5247(21)00193-2

194. Koch T, Dahlke C, Fathi A, et al. Safety and immunogenicity of a modified vaccinia virus Ankara vector vaccine candidate for Middle East respiratory syndrome: an open-label, phase 1 trial. *Lancet Infect Dis*. (2020); 20(7):827-838. doi:10.1016/S1473-3099(20)30248-6

195. Cao Z, Liu L, Du L, et al. Potent and persistent antibody responses against the receptor-binding domain of SARS-CoV spike protein in recovered patients. *Virol J*. (2010); 7:299. doi:10.1186/1743-422X-7-299

196. Gierer S, Bertram S, Kaup F, et al. The Spike Protein of the Emerging Betacoronavirus EMC Uses a Novel Coronavirus Receptor for Entry, Can Be Activated by TMPRSS2, and Is Targeted by Neutralizing Antibodies. *J Virol*. (2013); 87(10):5502-11. doi:10.1128/jvi.00128-13

197. Jiang L, Wang N, Zuo T, et al. Potent neutralization of MERS-CoV by human neutralizing monoclonal antibodies to the viral spike glycoprotein. *Sci Transl Med*. (2014); 6(234): 234ra59. doi:10.1126/scitranslmed.3008140

198. Vetter V, Denizer G, Friedland LR, Krishnan J, Shapiro M. Understanding modern-day vaccines: what you need to know. *Ann Med*. (2018); 50(2):110-120. doi:10.1080/07853890.2017.1407035

199. Dhere R, Yeolekar L, Kulkarni P, et al. A pandemic influenza vaccine in India: from strain to sale within 12 months. *Vaccine*. (2011); 29 (Suppl 1):A16-21. doi: 10.1016/j.vaccine.2011.04.119

200. Agrawal AS, Tao X, Algaissi A, et al. Immunization with inactivated Middle East Respiratory Syndrome coronavirus vaccine leads to lung immunopathology on challenge with live virus. *Hum Vaccin Immunother*. (2016); 12(9):2351-2356. doi:10.1080/21645515.2016.1177688

201. Qu D, Zheng B, Yao X, et al. Intranasal immunization with inactivated SARS-CoV (SARS-associated coronavirus) induced local and serum antibodies in mice. *Vaccine*. (2005); 23(7):924-931. doi:10.1016/j.vaccine.2004.07.031

202. Takasuka N, Fujii H, Takahashi Y, et al. A subcutaneously injected UV-inactivated SARS coronavirus vaccine elicits systemic humoral immunity in mice. *Int Immunol*. (2004); 16(10):1423-1430. doi:10.1093/intimm/dxh143

203. Bolles M, Deming D, Long K, et al. A Double-Inactivated Severe Acute Respiratory Syndrome Coronavirus Vaccine Provides Incomplete Protection in Mice and Induces Increased Eosinophilic Proinflammatory Pulmonary Response upon Challenge. *J Virol*. (2011); 85(23):12201-12215. doi: 10.1128/JVI.06048-11

204. Fett C, DeDiego ML, Regla-Nava JA, Enjuanes L, Perlman S. Complete protection against severe acute respiratory syndrome coronavirus-mediated lethal respiratory disease in aged mice by immunization with a mouse-adapted virus lacking E protein. *J Virol*. (2013); 87(12):6551-6559. doi:10.1128/jvi.00087-13

205. Lamirande EW, DeDiego ML, Roberts A, et al. A live attenuated severe acute respiratory syndrome coronavirus is immunogenic and efficacious in golden Syrian hamsters. *J Virol*. (2008); 82(15):7721-7724. doi:10.1128/jvi.00304-08

206. Menachery VD, Gralinski LE, Mitchell HD, et al. Middle East Respiratory Syndrome Coronavirus Nonstructural Protein 16 Is Necessary for Interferon Resistance and Viral Pathogenesis. *mSphere*. (2017); 2(6): e00346-17. doi:10.1128/msphere.00346-17

207. Menachery VD, Gralinski LE, Mitchell HD, et al. Combination Attenuation Offers Strategy for Live Attenuated Coronavirus Vaccines. *J Virol*. 2018;92(17): :e00710-18. doi:10.1128/jvi.00710-18

208. Graham RL, Becker MM, Eckerle LD, Bolles M, Denison MR, Baric RS. A live, impaired-fidelity coronavirus vaccine protects in an aged, immunocompromised mouse model of lethal disease. *Nat Med*. (2012); 18(12):1820-1826. doi:10.1038/nm.2972

209. Skwarczynski M, Toth I. Peptide-based synthetic vaccines. *Chem Sci*. (2016); 7(2):842-854. doi:10.1039/C5SC03892H

210. Li J, Ulitzky L, Silberstein E, Taylor DR, Viscidi R. Immunogenicity and protection efficacy of monomeric and trimeric recombinant SARS coronavirus spike protein subunit vaccine candidates. *Viral Immunol*. (2013); 26(2):126-132. doi:10.1089/vim.2012.0076

211. He Y, Li J, Heck S, Lustigman S, Jiang S. Antigenic and Immunogenic Characterization of Recombinant Baculovirus-Expressed Severe Acute Respiratory Syndrome Coronavirus Spike Protein: Implication for Vaccine Design. *J Virol*. (2006); 80(12):5757-67. doi:10.1128/jvi.00083-06

212. Kam YW, Kien F, Roberts A, et al. Antibodies against trimeric S glycoprotein protect hamsters against SARS-CoV challenge despite their capacity to mediate FcγRII-dependent entry into B cells in vitro. *Vaccine*. (2007); 25(4):729-740. doi:10.1016/j.vaccine.2006.08.011

213. Du L, Zhao G, Chan CC, et al. A 219-mer CHO-expressing receptor-binding domain of SARS-CoV S protein induces potent immune responses and protective immunity. *Viral Immunol*. (2010); 23(2):211-219. doi:10.1089/vim.2009.0090

214. Du L, Zhao G, Chan CCS, et al. Recombinant receptor-binding domain of SARS-CoV spike protein expressed in mammalian, insect and E. coli cells elicits potent neutralizing antibody and protective immunity. *Virology*. (2009); 393(1):144-150. doi:10.1016 j.virol.2009/.07.018

215. Du L, Zhao G, He Y, et al. Receptor-binding domain of SARS-CoV spike protein induces long-term protective immunity in an animal model. *Vaccine*. (2007); 25(15):2832-2838. doi:10.1016/j.vaccine.2006.10.031

216. He Y, Zhou Y, Siddiqui P, Niu J, Jiang S. Identification of immunodominant epitopes on the membrane protein of the severe acute respiratory syndrome-associated coronavirus. *J Clin Microbiol*. (2005); 43(8):3718-3726. doi:10.1128/jcm.43.8.3718-3726.2005

217. Liu SJ, Leng CH, Lien SP, et al. Immunological characterizations of the nucleocapsid protein based SARS vaccine candidates. *Vaccine*. (2006); 24(16):3100-3108. doi:10.1016/j.vaccine.2006.01.058

218. Guo Y, Sun S, Wang K, Zhang S, Zhu W, Chen Z. Elicitation of immunity in mice after immunization with the S2 subunit of the severe acute respiratory syndrome coronavirus. *DNA Cell Biol*. (2005); 24(8):510-515. doi:10.1089/dna.2005.24.510

219. Tai W, Wang Y, Fett CA, et al. Recombinant Receptor-Binding Domains of Multiple Middle East Respiratory Syndrome Coronaviruses (MERS-CoVs) Induce Cross-Neutralizing Antibodies against Divergent Human and Camel MERS-CoVs and Antibody Escape Mutants. *J Virol*. (2016); 91(1):e01651-16. doi:10.1128/jvi.01651-16

220. Wang Y, Tai W, Yang J, et al. Receptor-binding domain of MERS-CoV with optimal immunogen dosage and immunization interval protects human transgenic mice from MERS-CoV infection. *Hum Vaccin Immunother*. (2017); 13(7):1615-1624. doi:10.1080/21645515.2017.1296994

221. Tai W, Zhao G, Sun S, et al. A recombinant receptor-binding domain of MERS-CoV in trimeric form protects human dipeptidyl peptidase 4 (hDPP4) transgenic mice from MERS-CoV infection. *Virology*. (2016); 499:375-382. doi:10.1016/j.virol.2016.10.005

222. Adney DR, Wang L, Van Doremalen N, et al. Efficacy of an Adjuvanted Middle East Respiratory Syndrome Coronavirus Spike Protein Vaccine in Dromedary Camels and Alpacas. *Viruses*. 2019;11(3):212. doi:10.3390/v11030212

223. Jiaming L, Yanfeng Y, Yao D, et al. The recombinant N-terminal domain of spike proteins is a potential vaccine against Middle East respiratory syndrome coronavirus (MERS-CoV) infection. *Vaccine*. 2017;35(1):10-18. doi:10.1016/j.vaccine.2016.11.064

224. Wang L, Shi W, Joyce MG, et al. Evaluation of candidate vaccine approaches for MERS-CoV. *Nature Communications 2015 6:1*. (2015); 6:7712. doi:10.1038/ncomms8712

225. Tian JH, Patel N, Haupt R, et al. SARS-CoV-2 spike glycoprotein vaccine candidate NVX-CoV2373 immunogenicity in baboons and protection in mice. *Nat Commun*. 2021;12(1):372. doi:10.1038/s41467-020-20653-8

226. Curley SM, Putnam D. Biological Nanoparticles in Vaccine Development. *Front Bioeng Biotechnol*. (2022); 10:867119. doi:10.3389/fbioe.2022.867119

227. Liu Y V., Massare MJ, Barnard DL, et al. Chimeric severe acute respiratory syndrome coronavirus (SARS-CoV) S glycoprotein and influenza matrix 1 efficiently form virus-like particles (VLPs) that protect mice against challenge with SARS-CoV. *Vaccine*. (2011); 29(38):6606-6613. doi:10.1016/j.vaccine.2011.06.111

228. Lokugamage KG, Yoshikawa-Iwata N, Ito N, et al. Chimeric coronavirus-like particles carrying severe acute respiratory syndrome coronavirus (SCoV) S protein protect mice against challenge with SCoV. *Vaccine*. (2008); 26(6):797-808. doi:10.1016/j.vaccine.2007.11.092

229. Wang C, Zheng X, Gai W, et al. Novel chimeric virus-like particles vaccine displaying MERS-CoV receptor-binding domain induce specific humoral and cellular immune response in mice. *Antiviral Res*. (2017); 140:55-61. doi:10.1016/j.antiviral.2016.12.019

230. Wang C, Zheng X, Gai W, et al. MERS-CoV virus-like particles produced in insect cells induce specific humoural and cellular imminity in rhesus macaques. *Oncotarget.* (2016); 8(8):12686-12694. doi:10.18632/oncotarget.8475

231. Rauch S, Jasny E, Schmidt KE, Petsch B. New vaccine technologies to combat outbreak situations. *Front Immunol.* (2018); 9:1963. doi:10.3389/fimmu.2018.01963

232. Fausther-Bovendo H, Kobinger GP. Pre-existing immunity against Ad vectors: humoral, cellular, and innate response, what's important? *Hum Vaccin Immunother.* (2014); 10(10):2875-84. doi:10.4161/hv.29594.

233. Knuchel MC, Marty RR, Morin TN, Ilter O, Zuniga A, Naim HY. Relevance of a pre-existing measles immunity prior immunization with a recombinant measles virus vector. *Hum Vaccin Immunother.* (2013); 9(3):599-606. doi:10.4161/hv.23241

234. Gao W, Tamin A, Soloff A, et al. Effects of a SARS-associated coronavirus vaccine in monkeys. *Lancet.* (2003); 362(9399):1895-1896. doi:10.1016/S0140-6736(03)14962-8

235. Jung SY, Kang KW, Lee EY, et al. Heterologous prime-boost vaccination with adenoviral vector and protein nanoparticles induces both Th1 and Th2 responses against Middle East respiratory syndrome coronavirus. *Vaccine.* (2018); 36(24):3468-3476. doi:10.1016/j.vaccine.2018.04.082

236. Guo X, Deng Y, Chen H, et al. Systemic and mucosal immunity in mice elicited by a single immunization with human adenovirus type 5 or 41 vector-based vaccines carrying the spike protein of Middle East respiratory syndrome coronavirus. *Immunology.* (2015); 145(4):476-484. doi:10.1111/imm.12462

237. Kim E, Okada K, Kenniston T, et al. Immunogenicity of an adenoviral-based Middle East Respiratory Syndrome coronavirus vaccine in BALB/c mice. *Vaccine.* (2014); 32(45):5975-5982. doi:10.1016/j.vaccine.2014.08.058

238. Kobinger GP, Figueredo JM, Rowe T, et al. Adenovirus-based vaccine prevents pneumonia in ferrets challenged with the SARS coronavirus and stimulates robust immune responses in macaques. *Vaccine.* (2007); 25(28):5220-5231. doi:10.1016/j.vaccine.2007.04.065

239. Alharbi NK, Padron-Regalado E, Thompson CP, et al. ChAdOx1 and MVA based vaccine candidates against MERS-CoV elicit neutralising antibodies and cellular immune responses in mice. *Vaccine.* (2017); 35(30):3780-3788. doi:10.1016/j.vaccine.2017.05.032

240. Munster VJ, Wells D, Lambe T, et al. Protective efficacy of a novel simian adenovirus vaccine against lethal MERS-CoV challenge in a transgenic human DPP4 mouse model. *NPJ Vaccines.* (2017); 2(1):28. doi:10.1038/S41541-017-0029-1

241. Alharbi NK, Qasim I, Almasoud A, et al. Humoral Immunogenicity and Efficacy of a Single Dose of ChAdOx1 MERS Vaccine Candidate in Dromedary Camels. *Sci Rep.* (2019); 9(1):16292. doi:10.1038/S41598-019-52730-4

242. van Doremalen N, Haddock E, Feldmann F, et al. A single dose of ChAdOx1 MERS provides protective immunity in rhesus macaques. *Sci Adv*. 2020;6(24):eaba8399. doi:10.1126/sciadv.aba8399

243. Chen Z, Zhang L, Qin C, et al. Recombinant modified vaccinia virus Ankara expressing the spike glycoprotein of severe acute respiratory syndrome coronavirus induces protective neutralizing antibodies primarily targeting the receptor binding region. *J Virol*. (2005); 79(5):2678-2688. doi:10.1128/jvi.79.5.2678-2688.2005

244. Czub M, Weingartl H, Czub S, He R, Cao J. Evaluation of modified vaccinia virus Ankara based recombinant SARS vaccine in ferrets. *Vaccine*. (2005); 23(17-18):2273-2279. doi:10.1016/j.vaccine.2005.01.033

245. Agnihothram S, Gopal R, Yount BL, et al. Evaluation of serologic and antigenic relationships between middle eastern respiratory syndrome coronavirus and other coronaviruses to develop vaccine platforms for the rapid response to emerging coronaviruses. *J Infect Dis*. (2014); 209(7):995-1006. doi:10.1093/infdis/jit609

246. Kapadia SU, Rose JK, Lamirande E, Vogel L, Subbarao K, Roberts A. Long-term protection from SARS coronavirus infection conferred by a single immunization with an attenuated VSV-based vaccine. *Virology*. (2005); 340(2):174-182. doi:10.1016/j.virol.2005.06.016

247. Liu MA. A Comparison of Plasmid DNA and mRNA as Vaccine Technologies. *Vaccines*. (2019); 7(2):37. doi:10.3390/vaccines7020037

248. Yang ZY, Kong WP, Huang Y, et al. A DNA vaccine induces SARS coronavirus neutralization and protective immunity in mice. *Nature*. (2004); 428(6982):561-564. doi:10.1038/nature02463

249. Muthumani K, Falzarano D, Reuschel EL, et al. A synthetic consensus anti-spike protein DNA vaccine induces protective immunity against Middle East respiratory syndrome coronavirus in nonhuman primates. *Sci Transl Med*. (2015); 7(301):301ra132. doi:10.1126/scitranslmed.aac7462

250. Al-Amri SS, Abbas AT, Siddiq LA, et al. Immunogenicity of Candidate MERS-CoV DNA Vaccines Based on the Spike Protein. *Sci Rep*. (2017); 7:44875. doi:10.1038/srep44875

251. Wang Z, Yuan Z, Matsumoto M, Hengge UR, Chang YF. Immune responses with DNA vaccines encoded different gene fragments of severe acute respiratory syndrome coronavirus in BALB/c mice. *Biochem Biophys Res Commun*. (2005); 327(1):130-135. doi:10.1016/j.bbrc.2004.11.147

252. Okada M, Takemoto Y, Okuno Y, Hashimoto S, et al. Development of vaccines and passive immunotherapy against SARS corona virus using SCID-PBL/hu mouse models. *Vaccine*. (2007); 25(16):3038-3040. doi:10.1016/j.vaccine.2007.01.032

253. Zhao P, Cao J, Zhao LJ, et al. Immune responses against SARS-coronavirus nucleocapsid protein induced by DNA vaccine. *Virology*. (2005); 331(1):128-135. doi:10.1016/j.virol.2004.10.016

254. Kim TW, Lee JH, Hung CF, et al. Generation and characterization of DNA vaccines targeting the nucleocapsid protein of severe acute respiratory syndrome coronavirus. *J Virol.* (2004); 78(9):4638-4645. doi:10.1128/jvi.78.9.4638-4645.2004

255. Woo PC, Lau SK, Tsoi HW, et al. SARS coronavirus spike polypeptide DNA vaccine priming with recombinant spike polypeptide from Escherichia coli as booster induces high titer of neutralizing antibody against SARS coronavirus. *Vaccine.* (2005); 23(42):4959-4968. doi:10.1016/j.vaccine.2005.05.023

256. Zakhartchouk AN, Liu Q, Petric M, Babiuk LA. Augmentation of immune responses to SARS coronavirus by a combination of DNA and whole killed virus vaccines. *Vaccine.* (2005); 23(35):4385-4391. doi:10.1016/j.vaccine.2005.04.011

257. Krammer F. SARS-CoV-2 vaccines in development. *Nature.* (2020); 586(7830):516-527. doi:10.1038/s41586-020-2798-3

258. Umscheid CA, Margolis DJ, Grossman CE. Key Concepts of Clinical Trials: A Narrative Review. *Postgrad Med.* (2011); 123(5):194-204. doi:10.3810/pgm.2011.09.2475

259. El-Hagrassy MM, Duarte D, Thibaut A, Lucena MFG, Fregni F. Principles of designing a clinical trial: optimizing chances of trial success. *Curr Behav Neurosci Rep.* (2018); 5(2):143-152. doi:10.1007/S40473-018-0152-Y

260. Lurie N, Saville M, Hatchett R, Halton J. Developing Covid-19 Vaccines at Pandemic Speed. *New England Journal of Medicine.* (2020); 382(21):1969-1973. doi:10.1056/NEJMP2005630

261. Kashte S, Gulbake A, El-Amin SF, Gupta A. COVID-19 vaccines: rapid development, implications, challenges and future prospects. *Hum Cell.* (2021); 34(3):711. doi:10.1007/s13577-021-00512-4

262. WHO.Statement on the fifteenth meeting of the IHR (2005) Emergency Committee on the COVID-19 pandemic. Accessed May 15, 2023. https://www.who.int/news/item/05-05-2023-statement-on-the-fifteenth-meeting-of-the-international-health-regulations-(2005)-emergency-committee-regarding-the-coronavirus-disease-(covid-19)-pandemic

263. WHO. COVID-19 vaccine tracker and landscape. Accessed May 15, 2023. https://www.who.int/publications/m/item/draft-landscape-of-covid-19-candidate-vaccines

264. VIPER Group COVID19 Vaccine Development and Approvals Tracker Team. Vaccines – COVID19 Vaccine Tracker. Accessed May 16, 2023. https://covid19.trackvaccines.org/vaccines/approved/

265. WHO. Regulation and Prequalification. Accessed May 17, 2023. https://www.who.int/teams/regulation-prequalification/eul/covid-19

266. European Medicines Agency .COVID-19 vaccines: authorised. Accessed May 16, 2023. https://www.ema.europa.eu/en/human-regulatory/overview/public-health-threats/coronavirus-disease-covid-19/treatments-vaccines/vaccines-covid-19/covid-19-vaccines-authorised

267. Tasker S, Bendel D, Bevan M, et al. 584. Phase 1 Placebo-Controlled Trial of COVI-VAC™, an Intranasal, Live Attenuated COVID-19 Vaccine. *Open Forum Infect Dis.* (2021); 8(Suppl 1):S394. doi:10.1093/ofid/ofab466.782

268. Khoshnood S, Arshadi M, Akrami S, et al. An overview on inactivated and live-attenuated SARS-CoV-2 vaccines. *J Clin Lab Anal.* (2022); 36(5):e24418. doi:10.1002/jcla.24418

269. Mahase E. Covid-19: Valneva's vaccine produces stronger immune response than AstraZeneca's, company reports. *BMJ.* (2021); 375:n2551. doi:10.1136/bmj.n2551

270. Vályi-Nagy I, Matula Z, Gönczi M, et al. Comparison of antibody and T cell responses elicited by BBIBP-CorV (Sinopharm) and BNT162b2 (Pfizer-BioNTech) vaccines against SARS-CoV-2 in healthy adult humans. *Geroscience.* (2021); 43(5):2321-2331. doi:10.1007/s11357-021-00471-6

271. Chi WY, Li YD, Huang HC, et al. COVID-19 vaccine update: vaccine effectiveness, SARS-CoV-2 variants, boosters, adverse effects, and immune correlates of protection. *Journal of Biomedical Science.* (2022); 29(1):1-27. doi:10.1186/s12929-022-00853-8

272. Mousa M, Albreiki M, Alshehhi F, et al. Similar effectiveness of the inactivated vaccine BBIBP-CorV (Sinopharm) and the mRNA vaccine BNT162b2 (Pfizer-BioNTech) against COVID-19 related hospitalizations during the Delta outbreak in the UAE. *J Travel Med.* (2022); 29(6). doi:10.1093/jtm/taac036

273. Keech C, Albert G, Cho I, et al. Phase 1–2 Trial of a SARS-CoV-2 Recombinant Spike Protein Nanoparticle Vaccine. *New England Journal of Medicine.* (2020); 383(24):2320-2332. doi:10.1056/nejmoa2026920

274. Heath PT, Galiza EP, Baxter DN, et al. Safety and Efficacy of NVX-CoV2373 Covid-19 Vaccine. *New England Journal of Medicine.* (2021); 385(13):1172-1183. doi:10.1056/nejmoa2107659

275. Dunkle LM, Kotloff KL, Gay CL, et al. Efficacy and Safety of NVX-CoV2373 in Adults in the United States and Mexico. *New England Journal of Medicine.* (2022); 386(6):531-543. doi:10.1056/NEJMoa2116185

276. Shinde V, Bhikha S, Hoosain Z, et al. Efficacy of the NVX-CoV2373 Covid-19 Vaccine Against the B.1.351 Variant. *New England Journal of Medicine.* (2021); 384(20):1899. doi:10.1056/nejmoa2103055

277. Pavot V, Berry C, Kishko M, et al. Protein-based SARS-CoV-2 spike vaccine booster increases cross-neutralization against SARS-CoV-2 variants of concern in non-human primates. *Nat Commun.* (2022); 13(1): 1699. doi:10.1038/s41467-022-29219-2

278. Barreiro A, Prenafeta A, Bech-Sabat G, et al. Preclinical evaluation of a COVID-19 vaccine candidate based on a recombinant RBD fusion heterodimer of SARS-CoV-2. *iScience.* (2023); 26(3):106126. doi:10.1016/j.isci.2023.106126

279. Immunogenicity and Reactogenicity Following a Booster Dose of COVID-19 mRNA Vaccine (Pfizer-BioNtech) and Two Adjuvanted Sub-unit Vaccines (SP/GSK) Administered in Adults Who Received 2 Doses of Pfizer-BioNTech mRNA Vaccine as a Primary Vaccination. Identifier: NCT05124171. ClinicalTrials.gov. Accessed May 21, 2023. https://www.clinicaltrials.gov/ct2/show/nct05124171

280. Study of Recombinant Protein Vaccines With Adjuvant as a Primary Series and as a Booster Dose Against COVID-19 in Adults 18 Years of Age and Older. Identifier: NCT04762680. ClinicalTrials.gov. Accessed May 21, 2023. https://clinicaltrials.gov/ct2/show/nct04762680

281. Corominas J, Garriga C, Prenafeta A, et al. Safety and immunogenicity of the protein-based PHH-1V compared to BNT162b2 as a heterologous SARS-CoV-2 booster vaccine in adults vaccinated against COVID-19: a multicentre, randomised, double-blind, non-inferiority phase IIb trial. *The Lancet Regional Health – Europe*. (2023); 28:100613. doi:10.1016/j.lanepe.2023.100613

282. Ramasamy MN, Minassian AM, Ewer KJ, et al. Safety and immunogenicity of ChAdOx1 nCoV-19 vaccine administered in a prime-boost regimen in young and old adults (COV002): a single-blind, randomised, controlled, phase 2/3 trial. *Lancet*. (2021); 396(10267):1979-1993. doi:10.1016/S0140-6736(20)32466-1

283. Folegatti PM, Ewer KJ, Aley PK, et al. Safety and immunogenicity of the ChAdOx1 nCoV-19 vaccine against SARS-CoV-2: a preliminary report of a phase 1/2, single-blind, randomised controlled trial. *Lancet*. (2020); 396(10249):467-478. doi:10.1016/S0140-6736(20)31604-4

284. Thiruvengadam R, Awasthi A, Medigeshi G, et al. Effectiveness of ChAdOx1 nCoV-19 vaccine against SARS-CoV-2 infection during the delta (B.1.617.2) variant surge in India: a test-negative, case-control study and a mechanistic study of post-vaccination immune responses. *Lancet Infect Dis*. (2022); 22(4):473. doi:10.1016/S1473-3099(21)00680-0

285. Kirsebom FCM, Andrews N, Sachdeva R, Stowe J, Ramsay M, Lopez Bernal J. Effectiveness of ChAdOx1-S COVID-19 booster vaccination against the Omicron and Delta variants in England. *Nature Communications*. (2022); 13(1):7688. doi:10.1038/s41467-022-35168-7

286. Tobaiqy M, Maclure K, Elkout H, Stewart D. Thrombotic Adverse Events Reported for Moderna, Pfizer and Oxford-AstraZeneca COVID-19 Vaccines: Comparison of Occurrence and Clinical Outcomes in the EudraVigilance Database. *Vaccines (Basel)*. (2021); 9(11):1326. doi:10.3390/vaccines9111326

287. European Medicines Agency. Vaxzevria (previously COVID-19 Vaccine AstraZeneca). Accessed May 22, 2023. https://www.ema.europa.eu/en/medicines/human/EPAR/vaxzevria

288. Mercado NB, Zahn R, Wegmann F, et al. Single-Shot Ad26 Vaccine Protects Against SARS-CoV-2 in Rhesus Macaques. *Nature*. (2020); 586(7830):583-588. doi:10.1038/s41586-020-2607-Z

289. Sadoff J, Le Gars M, Shukarev G, et al. Interim Results of a Phase 1-2a Trial of Ad26.COV2.S Covid-19 Vaccine. *New England of Journal Medicine*. (2021); 384(19):1824-1835. doi:10.1056/nejmoa2034201

290. Alter G, Yu J, Liu J, et al. Immunogenicity of Ad26.COV2.S vaccine against SARS-CoV-2 variants in humans. *Nature*. (2021); 596(7871):268-272. doi:10.1038/s41586-021-03681-2

291. GeurtsvanKessel CH, Geers D, Schmitz KS, et al. Divergent SARS-CoV-2 Omicron-reactive T and B cell responses in COVID-19 vaccine recipients. *Sci Immunol*. (2022); 7(69):eabo2202. doi:10.1126/SCIIMMUNOL.ABO2202

292. Accorsi EK, Britton A, Shang N, et al. Effectiveness of Homologous and Heterologous Covid-19 Boosters against Omicron. *New England Journal of Medicine*. (2022); 386(25):2433-2435. doi:10.1056/nejmc2203165

293. Muir KL, Kallam A, Koepsell SA, Gundabolu K. Thrombotic Thrombocytopenia after Ad26.COV2.S Vaccination. *New England Journal of Medicine*. (2021); 384(20):1964-1965. doi:10.1056/nejmc2105869

294. Baden LR, El Sahly HM, Essink B, et al. Efficacy and Safety of the mRNA-1273 SARS-CoV-2 Vaccine. *New England Journal of Medicine*. (2021); 384(5):403-416. doi:10.1056/NEJMOA2035389

295. Gutiérrez-Bautista JF, López-Nevot MÁ, Gómez-Vicente E, et al. Study of humoral and cellular immunity in vaccinated with mRNA-1273. *Apmis*. (2022); 130(5):261-269. doi:10.1111/apm.13215

296. El Sahly HM, Baden LR, Essink B, et al. Efficacy of the mRNA-1273 SARS-CoV-2 Vaccine at Completion of Blinded Phase. *New England Journal of Medicine*. (2021); 385(19):1774-1785. doi:10.1056/nejmoa2113017

297. Berec L, Šmíd M, Přibylová L, et al. Protection provided by vaccination, booster doses and previous infection against covid-19 infection, hospitalisation or death over time in Czechia. *PLoS One*. (2022); 17(7):e0270801. doi:10.1371/journal.pone.0270801

298. Chalkias S, Harper C, Vrbicky K, et al. A Bivalent Omicron-Containing Booster Vaccine against Covid-19. *New England Journal of Medicine*. (2022); 387(14):1279-1291. doi:10.1056/nejmoa2208343

299. Scheaffer SM, Lee D, Whitener B, et al. Bivalent SARS-CoV-2 mRNA vaccines increase breadth of neutralization and protect against the BA.5 Omicron variant in mice. *Nature Medicine*. (2022); 29(1):247-257. doi:10.1038/s41591-022-02092-8

300. Chalkias S, Whatley J, Eder F, et al. Safety and Immunogenicity of Omicron BA.4/BA.5 Bivalent Vaccine Against Covid-19. *medRxiv*. (2022); 5:2022.12.11.22283166. doi:10.1101/2022.12.11.22283166

301. Polack FP, Thomas SJ, Kitchin N, et al. Safety and Efficacy of the BNT162b2 mRNA Covid-19 Vaccine. *New England Journal of Medicine*. (2020); 383(27):2603-2615. doi:10.1056/nejmoa2034577

302. Bonnet B, Chabrolles H, Archimbaud C, et al. Decline of Humoral and Cellular Immune Responses Against SARS-CoV-2 6 Months After Full BNT162b2 Vaccination in Hospital Healthcare Workers. *Front Immunol*. (2022); 13:842912. doi:10.3389/fimmu.2022.842912

303. Jiménez-Sepúlveda N, Chico-Sánchez P, Castro-García JM, et al. The Waning of BNT162b2 Vaccine Effectiveness for SARS-CoV-2 Infection Prevention over Time: A Test-Negative Study in Health Care Professionals of a Health Department from January 2021 to December 2021. *Int J Environ Res Public Health*. (2022);19(21):13884. doi:10.3390/ijerph192113884

304. Zeng B, Gao L, Zhou Q, Yu K, Sun F. Effectiveness of COVID-19 vaccines against SARS-CoV-2 variants of concern: a systematic review and meta-analysis. *BMC Med.* 2022;20(1):200. doi: 10.1186/s12916-022-02397-y

305. Winokur P, Gayed J, Fitz-Patrick D, et al. Bivalent Omicron BA.1–Adapted BNT162b2 Booster in Adults Older than 55 Years. *New England Journal of Medicine*. (2023); 388(3):214-227. doi:10.1056/nejmoa2213082

306. Zou J, Kurhade C, Patel S, et al. Neutralization of BA.4–BA.5, BA.4.6, BA.2.75.2, BQ.1.1, and XBB.1 with Bivalent Vaccine. *New England Journal of Medicine*. (2023); 388(9):854-857. doi:10.1056/nejmc2214916

307. Dey A, Chozhavel Rajanathan TM, Chandra H, et al. Immunogenic potential of DNA vaccine candidate, ZyCoV-D against SARS-CoV-2 in animal models. *Vaccine*. (2021); 39(30):4108-4116. doi:10.1016/j.vaccine.2021.05.098

308. Khobragade A, Bhate S, Ramaiah V, et al. Efficacy, safety, and immunogenicity of the DNA SARS-CoV-2 vaccine (ZyCoV-D): the interim efficacy results of a phase 3, randomised, double-blind, placebo-controlled study in India. *Lancet*. (2022); 399(10332):1313-1321. doi:10.1016/S0140-6736(22)00151-9

309. Renegar KB, Small PA, Boykins LG, Wright PF. Role of IgA versus IgG in the control of influenza viral infection in the murine respiratory tract. *J Immunol*. (2004); 173(3):1978-1986. doi:10.4049/jimmunol.173.3.1978

310. Su F, Patel GB, Hu S, Chen W. Induction of mucosal immunity through systemic immunization: Phantom or reality? *Hum Vaccin Immunother*. (2016); 12(4):1070-1079. doi:10.1080/21645515.2015.1114195

311. Focosi D, Maggi F, Casadevall A. Mucosal Vaccines, Sterilizing Immunity, and the Future of SARS-CoV-2 Virulence. *Viruses*. (2022); 14(2):187. doi:10.3390/V14020187

312. Dhama K, Dhawan M, Tiwari R, et al. COVID-19 intranasal vaccines: current progress, advantages, prospects, and challenges. *Hum Vaccin Immunother*. (2022); 18(5):2045853. doi:10.1080/21645515.2022.2045853

313. Waltz E. China and India approve nasal COVID vaccines - are they a game changer? *Nature*. (2022); 609(7927):450. doi:10.1038/D41586-022-02851-0

314. Feikin DR, Higdon MM, Abu-Raddad LJ, et al. Duration of effectiveness of vaccines against SARS-CoV-2 infection and COVID-19 disease: results of a systematic review and meta-regression. *Lancet*. (2022); 399(10328):924-944. doi:10.1016/S0140-6736(22)00152-0

315. Wu N, Joyal-Desmarais K, Ribeiro PAB, et al. Long-term effectiveness of COVID-19 vaccines against infections, hospitalisations, and mortality in adults: findings from a rapid living systematic evidence synthesis and meta-analysis up to December, 2022. *Lancet Respir Med*. (2023); 11(5):439-452. doi:10.1016/S2213-2600(23)00015-2

316. WHO. Weekly epidemiological update on COVID-19 - 13 July 2023. Accessed August 2, 2023.https://www.who.int/publications/m/item/weekly-epidemiological-update-on-covid-19---13-july-2023

317. Martín Sánchez FJ, Martínez-Sellés M, Molero García JM, et al. Insights for COVID-19 in 2023. *Revi Esp Quimioter*. (2023); 36(2):114-124. doi:10.37201/req/122.2022

318. Jaroszewski L, Iyer M, Alisoltani A, Sedova M, Godzik A. The interplay of SARS-CoV-2 evolution and constraints imposed by the structure and functionality of its proteins. *PLoS Comput Biol*. (2021); 17(7):e1009147. doi:10.1371/journal.pcbi.1009147

319. Amoutzias GD, Nikolaidis M, Tryfonopoulou E, Chlichlia K, Markoulatos P, Oliver SG. The Remarkable Evolutionary Plasticity of Coronaviruses by Mutation and Recombination: Insights for the COVID-19 Pandemic and the Future Evolutionary Paths of SARS-CoV-2. *Viruses*. (2022); 14(1):78. doi:10.3390/v14010078

320. Nikolaidis M, Markoulatos P, Van De Peer Y, Oliver SG, Amoutzias GD. The Neighborhood of the Spike Gene Is a Hotspot for Modular Intertypic Homologous and Nonhomologous Recombination in Coronavirus Genomes. *Mol Biol Evol*. (2022); 39(1):msab292. doi:10.1093/molbev/msab292

321. Banerjee A, Doxey AC, Benjamin JMT, et al. Predicting the recombination potential of severe acute respiratory syndrome coronavirus 2 and Middle East respiratory syndrome coronavirus. *J Gen Virol*. (2020); 101(12):1251-1260. doi:10.1099/jgv.0.001491

322. Boni MF, Lemey P, Jiang X, et al. Evolutionary origins of the SARS-CoV-2 sarbecovirus lineage responsible for the COVID-19 pandemic. *Nat Microbiol*. (2020); 5(11):1408-1417. doi:10.1038/S41564-020-0771-4

323. Murray SM, Ansari AM, Frater J, et al. The impact of pre-existing cross-reactive immunity on SARS-CoV-2 infection and vaccine responses. *Nature Reviews Immunology*. (2022); 23(5):304-316. doi:10.1038/s41577-022-00809-x

324. Walls AC, Park YJ, Tortorici MA, Wall A, McGuire AT, Veesler D. Structure, Function, and Antigenicity of the SARS-CoV-2 Spike Glycoprotein. *Cell*. (2020); 181(2):281-292.e6. doi:10.1016/j.cell.2020.02.058

325. Waterhouse A, Bertoni M, Bienert S, et al. SWISS-MODEL: homology modelling of protein structures and complexes. *Nucleic Acids Res.* 2018;46(W1):W296-W303. doi:10.1093/nar/gky427

326. Schymkowitz J, Borg J, Stricher F, Nys R, Rousseau F, Serrano L. The FoldX web server: an online force field. *Nucleic Acids Res.* 2005;33(Web Server issue):W382-388. doi:10.1093/nar/gki387

327. Perez-Zsolt D, Muñoz-Basagoiti J, Rodon J, et al. SARS-CoV-2 interaction with Siglec-1 mediates trans-infection by dendritic cells. *Cellular & Molecular Immunology*. (2021); 18(12):2676-2678. doi:10.1038/s41423-021-00794-6

328. Rodon J, Muñoz-Basagoiti J, Perez-Zsolt D, et al. Identification of Plitidepsin as Potent Inhibitor of SARS-CoV-2-Induced Cytopathic Effect After a Drug Repurposing Screen. *Front Pharmacol.* 2021;12:646676. doi:10.3389/fphar.2021.646676

329. Kamala T. Hock immunization: A humane alternative to mouse footpad injections. *J Immunol Methods*. (2007); 328(1-2):204-214. doi:10.1016/j.jim.2007.08.004

330. Pradenas E, Trinité B, Urrea V, et al. Stable neutralizing antibody levels 6 months after mild and severe COVID-19 episodes. *Med.* (2021); 2(3):313-320.e4. doi:10.1016/j.medj.2021.01.005

331. Connor RI, Chen BK, Choe S, Landau NR. Vpr is required for efficient replication of human immunodeficiency virus type-1 in mononuclear phagocytes. *Virology*. (1995); 206(2):935-944. doi:10.1006/viro.1995.1016

332. Corman VM, Landt O, Kaiser M, et al. Detection of 2019 novel coronavirus (2019-nCoV) by real-time RT-PCR. *Eurosurveillance*. (2020); 25(3):2000045. doi:10.2807/1560-7917.ES.2020.25.3.2000045

333. Vidal E, López-Figueroa C, Rodon J, et al. Chronological brain lesions after SARS-CoV-2 infection in hACE2-transgenic mice. *Vet Pathol*. (2022); 59(4):613-626. doi:10.1177/03009858211066841

334. Brustolin M, Rodon J, Rodríguez de la Concepción ML, et al. Protection against reinfection with D614- or G614-SARS-CoV-2 isolates in golden Syrian hamster. *Emerg Microbes Infect*. (2021); 10(1):797-809. doi:10.1080/22221751.2021.1913974

335. Cai Y, Zhang J, Xiao T, et al. Distinct conformational states of SARS-CoV-2 spike protein. *Science*. 2020; 369(6511):1586-1592. doi:10.1126/science.abd4251

336. Corbett KS, Edwards DK, Leist SR, et al. SARS-CoV-2 mRNA vaccine design enabled by prototype pathogen preparedness. *Nature*. (2020); 586(7830):567-571. doi:10.1038/s41586-020-2622-0

337. Sia SF, Yan LM, Chin AWH, et al. Pathogenesis and transmission of SARS-CoV-2 in golden hamsters. *Nature*. (2020); 583(7818):834-838. doi:10.1038/s41586-020-2342-5

338. Muñoz-Fontela C, Dowling WE, Funnell SGP, et al. Animal models for COVID-19. *Nature*. (2020); 586(7830):509-515. doi:10.1038/s41586-020-2787-6

339. Salehi-Vaziri M, Fazlalipour M, Seyed Khorrami SM, et al. The ins and outs of SARS-CoV-2 variants of concern (VOCs). *Arch Virol*. (2022); 167(2):327-344. doi:10.1007/s00705-022-05365-2

340. Tarrés-Freixas F, Trinité B, Pons-Grífols A, et al. Heterogeneous Infectivity and Pathogenesis of SARS-CoV-2 Variants Beta, Delta and Omicron in Transgenic K18-hACE2 and Wildtype Mice. *Front Microbiol*. (2022); 13:840757. doi:10.3389/fmicb.2022.840757

341. Mrabet NT, Van den Broeck A, Van den brande I, et al. Arginine Residues as Stabilizing Elements in Proteins. *Biochemistry*. (1992); 31(8):2239-2253. doi:10.1021/bi00123A005

342. Rutten L, Lai YT, Blokland S, et al. A Universal Approach to Optimize the Folding and Stability of Prefusion-Closed HIV-1 Envelope Trimers. *Cell Rep*. (2018); 23(2):584-595. doi:10.1016/j.celrep.2018.03.061

343. Xiong X, Qu K, Ciazynska KA, et al. A thermostable, closed SARS-CoV-2 spike protein trimer. *Nat Struct Mol Biol*. (2020); 27(10):934-941. doi:10.1038/s41594-020-0478-5

344. McCray PB, Pewe L, Wohlford-Lenane C, et al. Lethal infection of K18-hACE2 mice infected with severe acute respiratory syndrome coronavirus. *J Virol*. (2007); 81(2):813-821. doi:10.1128/jvi.02012-06

345. Vaccari M, Gordon SN, Fourati S, et al. Adjuvant-dependent innate and adaptive immune signatures of risk of SIVmac251 acquisition. *Nature Medicine*. (2016); 22(7):762-770. doi:10.1038/nm.4105

346. Wang W, Huang B, Zhu Y, Tan W, Zhu M. Ferritin nanoparticle-based SARS-CoV-2 RBD vaccine induces a persistent antibody response and long-term memory in mice. *Cellular & Molecular Immunology*. (2021); 18(3):749-751. doi:10.1038/s41423-021-00643-6

347. Dai L, Zheng T, Xu K, et al. A Universal Design of Betacoronavirus Vaccines against COVID-19, MERS, and SARS. *Cell*. (2020); 182(3):722-733.e11. doi:10.1016/j.cell.2020.06.035

348. Hsieh CL, Goldsmith JA, Schaub JM, et al. Structure-based design of prefusion-stabilized SARS-CoV-2 spikes. *Science*. (2020); 369(6509):1501-1505. doi:10.1126/science.abd0826

349. Sun W, Liu Y, Amanat F, et al. A Newcastle disease virus expressing a stabilized spike protein of SARS-CoV-2 induces protective immune responses. *Nat Commun*. (2021);12(1):6197-6197. doi:10.1038/s41467-021-26499-y

350. Pitisuttithum P, Luvira V, Lawpoolsri S, et al. Safety and Immunogenicity of an Inactivated Recombinant Newcastle Disease Virus Vaccine Expressing SARS-CoV-2 Spike: Interim Results of a Randomised, Placebo-Controlled, Phase 1/2 Trial. *EClinicalMedicine*. (2022); 45:101323. doi:10.1016/j.eclinm.2022.101323

351. Duc Dang A, Dinh Vu T, Hai Vu H, et al. Safety and immunogenicity of an egg-based inactivated Newcastle disease virus vaccine expressing SARS-CoV-2 spike: Interim results of a randomized, placebo-controlled, phase 1/2 trial in Vietnam. *Vaccine*. (2022); 40(26):3621-3632. doi:10.1016/j.vaccine.2022.04.078

352. González-Domínguez I, Martínez JL, Slamanig S, et al. Trivalent NDV-HXP-S Vaccine Protects against Phylogenetically Distant SARS-CoV-2 Variants of Concern in Mice. *Microbiol Spectr*. (2022); 10(3):e0153822. doi:10.1128/spectrum.01538-22

353. Juraszek J, Rutten L, Blokland S, et al. Stabilizing the closed SARS-CoV-2 spike trimer. *Nature Communications*. 2021;12(1):244. doi:10.1038/s41467-020-20321-x

354. Riley TP, Chou HT, Hu R, et al. Enhancing the Prefusion Conformational Stability of SARS-CoV-2 Spike Protein Through Structure-Guided Design. *Front Immunol*. (2021); 12:660198. doi:10.3389/fimmu.2021.660198

355. Ellis D, Brunette N, Crawford KHD, et al. Stabilization of the SARS-CoV-2 Spike Receptor-Binding Domain Using Deep Mutational Scanning and Structure-Based Design. *Front Immunol*. (2021); 12:710263. doi:10.3389/fimmu.2021.710263

356. Lu M, Chamblee M, Zhang Y, et al. SARS-CoV-2 prefusion spike protein stabilized by six rather than two prolines is more potent for inducing antibodies that neutralize viral variants of concern. *Proc Natl Acad Sci U S A*. (2022); 119(35):e2110105119. doi:10.1073/pnas.2110105119

357. Sridhar S, Joaquin A, Bonaparte MI, et al. Safety and immunogenicity of an AS03-adjuvanted SARS-CoV-2 recombinant protein vaccine (CoV2 preS dTM) in healthy adults: interim findings from a phase 2, randomised, dose-finding, multicentre study. *Lancet Infect Dis*. (2022); 22(5):636-648. doi:10.1016/s1473-3099(21)00764-7

358. Bruyn G de, Wang J, Purvis A, et al. Safety and immunogenicity of a variant-adapted SARS-CoV-2 recombinant protein vaccine with AS03 adjuvant as a booster in adults primed with authorized vaccines: a phase 3, parallel-group study. *EClinicalMedicine*. (2023); 62:102109. doi: 10.1016/j.eclinm.2023.102109.

359. Launay O, Cachanado M, Luong Nguyen LB, et al. Immunogenicity and Safety of Beta-Adjuvanted Recombinant Booster Vaccine. *New England Journal of Medicine*. (2022); 387(4):374-376. doi:10.1056/nejmc2206711

360. Bowen JE, Park YJ, Stewart C, et al. SARS-CoV-2 spike conformation determines plasma neutralizing activity elicited by a wide panel of human vaccines. *Sci Immunol*. 2022;7(78):eadf1421. doi:10.1126/sciimmunol.adf1421

361. Kong L, He L, De Val N, et al. Uncleaved prefusion-optimized gp140 trimers derived from analysis of HIV-1 envelope metastability. *Nat Commun*. (2016); 7:12040. doi:10.1038/NCOMMS12040

362. Sanders RW, Vesanen M, Schuelke N, et al. Stabilization of the soluble, cleaved, trimeric form of the envelope glycoprotein complex of human

immunodeficiency virus type 1. *J Virol*. (2002); 76(17):8875-8889. doi:10.1128/jvi.76.17.8875-8889.2002

363. McLellan JS, Chen M, Leung S, et al. Structure of RSV fusion glycoprotein trimer bound to a prefusion-specific neutralizing antibody. *Science*. (2013); (6136):1113-1117. doi:10.1126/science.1234914

364. Rutten L, Gilman MSA, Blokland S, Juraszek J, McLellan JS, Langedijk JPM. Structure-Based Design of Prefusion-Stabilized Filovirus Glycoprotein Trimers. *Cell Rep*. (2020); 30(13):4540-4550.e3. doi:10.1016/j.celrep.2020.03.025

365. Harper KN, Zuckerman MK, Harper ML, Kingston JD, Armelagos GJ. The origin and antiquity of syphilis revisited: An Appraisal of Old World pre-Columbian evidence for treponemal infection. *Am J Phys Anthropol*. (2011); 146(S53):99-133. doi:10.1002/AJPA.21613

366. De Melo FL, De Mello JC, Fraga AM, Nunes K, Eggers S. Syphilis at the Crossroad of Phylogenetics and Paleopathology. *PLoS Negl Trop Dis*. (2010); 4(1):e575. doi:10.1371/journal.pntd.0000575

367. Mahoney JF, Arnold RC, Harris A. Penicillin Treatment of Early Syphilis-A Preliminary Report. *Am J Public Health Nations Health*. (1943); 33(12):1387-1391. doi:10.2105/ajph.33.12.1387

368. Singh AE, Romanowski B. Syphilis: Review with Emphasis on Clinical, Epidemiologic, and Some Biologic Features. *Clin Microbiol Rev*. (1999); 12(2):187-209. doi: 10.1128/cmr.12.2.187

369. Peeling RW, Mabey D, Kamb ML, Chen XS, Radolf JD, Benzaken AS. Syphilis. *Nat Rev Dis Primers*. (2017); 3:17073. doi:10.1038/nrdp.2017.73

370. Radolf JD, Deka RK, Anand A, Šmajs D, Norgard M V., Yang XF. Treponema pallidum, the syphilis spirochete: Making a living as a stealth pathogen. *Nat Rev Microbiol*. (2016); 14(12):744-759. doi:10.1038/nrmicro.2016.141

371. Denee Thomas D, Navabo M, Haaket DA, Fogelmant AM, Miller JN, Lovett MA. Treponema Pallidum Invades Intercellular Junctions of Endothelial Cell Monolayers. *Proc Natl Acad Sci U S A*. (1988); 85(10):3608-3612. doi:10.1073/pnas.85.10.3608.

372. Lafond RE, Lukehart SA. Biological Basis for Syphilis. *Clin Microbiol Rev*. (2006); 19(1):29-49. doi:10.1128/cmr.19.1.29-49.2006

373. Cruz AR, Ramirez LG, Zuluaga A V., et al. Immune evasion and recognition of the syphilis spirochete in blood and skin of secondary syphilis patients: Two immunologically distinct compartments. *PLoS Negl Trop Dis*. (2012); 6(7). doi:10.1371/journal.pntd.0001717

374. Hook EW. Syphilis. *The Lancet*. (2017); 389(10078):1550-1557. doi:10.1016/s0140-6736(16)32411-4

375. Luo Z, Zhu L, Ding Y, et al. Factors associated with syphilis treatment failure and reinfection: A longitudinal cohort study in Shenzhen, China. *BMC Infect Dis*. (2017); 17(1):1-5. doi:10.1186/s12879-017-2715-z

376. Brewer TH, Peterman TA, Newman DR, Schmitt K. Reinfections during the Florida syphilis epidemic, 2000-2008. *Sex Transm Dis.* (2011); 38(1):12-17. doi:10.1097/olq.0b013e3181e9afc7

377. CDC. STD Facts - Syphilis (Detailed). Accessed March 18, 2020. https://www.cdc.gov/std/syphilis/stdfact-syphilis-detailed.html

378. Rowley J, Hoorn S Vander, Korenromp E, et al. Chlamydia, gonorrhoea, trichomoniasis and syphilis: Global prevalence and incidence estimates, 2016. *Bull World Health Organ.* 2019; 97(8):548-562. doi:10.2471/blt.18.228486

379. Korenromp Id EL, Rowley J, Alonso M, et al. Global burden of maternal and congenital syphilis and associated adverse birth outcomes-Estimates for 2016 and progress since 2012. *PLoS One.* (2019); 14(2):e0211720. doi:10.1371/journal.pone.0211720

380. Lawn JE, Blencowe H, Waiswa P, et al. Stillbirths: Rates, risk factors, and acceleration towards 2030. *The Lancet.* (2016); 387(10018):587-603. doi:10.1016/S0140-6736(15)00837-5

381. Kojima N, Klausner JD. An Update on the Global Epidemiology of Syphilis. *Curr Epidemiol Rep.* (2018); 5(1):24-38. doi:10.1007/s40471-018-0138-z

382. Ghanem KG, Ram S, Rice PA. The Modern Epidemic of Syphilis. *New England Journal of Medicine.* (2020); 382(9):845-854. doi:10.1056/nejmra1901593

383. ECDC. European Centre for Disease Prevention and Control. *Syphilis and Congenital Syphilis in Europe, 2018.* Accessed April 10, 2020. https://www.ecdc.europa.eu/en/publications-data/congenital-syphilis-annual-epidemiological-report-2018

384. Izard J, Renken C, Hsieh CE, et al. Cryo-electron tomography elucidates the molecular architecture of Treponema pallidum, the syphilis spirochete. *J Bacteriol.* (2009); 191(24):7566-7580. doi:10.1128/jb.01031-09

385. Madigan MT, Martinko JM, Parker J. Brock biology of micro-organisms. Published online (2015).

386. Radolf JD, Kumar S. The Treponema pallidum Outer Membrane. *Curr Top Microbiol Immunol.* (2018); 415:1-38. doi:10.1007/82_2017_44

387. Radolf JD, Robinson EJ, Bourell KW, et al. Characterization of outer membranes isolated from Treponema pallidum, the syphilis spirochete. *Infect Immun.* (1995); 63(11):4244-4252. doi:10.1128/iai.63.11.4244-4252.1995

388. Bailey DMJ. The outer membrane of treponema pallidum: Biological significance and biochemical properties. *J Gen Microbiol.* (1985); 131(9):2349–57. doi: 10.1099/00221287-131-9-2349.

389. Radolf JD, Norgardt M V, Schulz WW. Outer membrane ultrastructure explains the limited antigenicity of virulent treponema pallidum. *Proc Natl Acad Sci USA.* (1989); 86(6):2051–5. doi:10.1073/pnas.86.6.2051.

390. Cox DL, Chang P, McDowall AW, Radolf JD. The outer membrane, not a coat of host proteins, limits antigenicity of virulent Treponema pallidum. *Infect Immun.* (1992); 60(3):1076-1083. doi:10.1128/iai.60.3.1076-1083.1992

391. Hardy PH, Levin J. Lack of Endotoxin in Borrelia hispanica and Treponema pallidum1. *Proc Soc Exp Biol Med* (1983) 174(1):47–52. doi:10.3181/00379727-174-41702

392. Fraser CM, Norris SJ, Weinstock GM, et al. Complete genome sequence of Treponema pallidum, the syphilis spirochete. *Science.* (1998); 281(5375):375-388. doi:10.1126/science.281.5375.375

393. Blanco DR, Miller JN, Lovett MA. Surface Antigens of the Syphilis Spirochete and Their Potential as Virulence Determinants. *Emerg Infect Dis.* (1997); 3(1):11-20. doi:10.3201/eid0301.970102

394. Charon NW, Cockburn A, Li C, et al. The unique paradigm of spirochete motility and chemotaxis. *Annu Rev Microbiol.* (2012); 66:349-370. doi:10.1146/annurev-micro-092611-150145

395. Liu J, Howell JK, Bradley SD, Zheng Y, Hong Zhou Z, Norris SJ. Cellular Architecture of Treponema pallidum: Novel Flagellum, Periplasmic Cone, and Cell Envelope as Revealed by Cryo-Electron Tomography. *J Mol Biol.* (2010); 403(4):546–61. doi: 10.1016/j.jmb.2010.09.020

396. Salazar JC, Rathi A, Michael NL, Radolf JD, Jagodzinski LL. Assessment of the kinetics of Treponema pallidum dissemination into blood and tissues in experimental syphilis by real-time quantitative PCR. *Infect Immun.* (2007); 75(6):2954-2958. doi:10.1128/iai.00090-07

397. Harman M, Vig DK, Radolf JD, Wolgemuth CW. Viscous dynamics of Lyme disease and syphilis spirochetes reveal flagellar torque and drag. *Biophys J.* (2013); 105(10):2273-2280. doi:10.1016/j.bpj.2013.10.004

398. Edmondson DG, Hu B, Norris SJ. Long-Term In Vitro Culture of the Syphilis Spirochete Treponema pallidum subsp. pallidum. *mBio.* (2018); 9(3):e01153–18. doi:10.1128/mbio.01153-18

399. Lukehart SA, Marra CM. Isolation and Laboratory Maintenance of Treponema pallidum. *Curr Protoc Microbiol.* (2007); 7(1):12A.1.1-12A.1.18. doi:10.1002/9780471729259.mc12a01s7

400. Willcox RR, Guthe T. Treponema pallidum. A bibliographical review of the morphology, culture and survival of T. pallidum and associated organisms. *Bull World Health Organ.* (1966); 35(1):1–16.

401. Izzat NN, Knox JM, Werth JA, Dacres WG. Evolution of syphilitic chancres with virulent Treponema pallidum in the rabbit. *Brit J vener Dis.* (1970); 47:67. doi:10.1136/sti.47.2.67

402. Baker-Zander S, Sell S. A histopathologic and immunologic study of the course of syphilis in the experimentally infected rabbit. Demonstration of long-lasting cellular immunity. *American Journal of Pathology.* (1980); 101(2):387-413.

403. Hanff PA, Fehniger TE, Miller JN, Lovett MA. Humoral immune response in human syphilis to polypeptides of Treponema pallidum. *J Immunol.* (1982); 129(3):1287-1291.

404. Esteves PJ, Abrantes J, Baldauf HM, et al. The wide utility of rabbits as models of human diseases. *Exp Mol Med.* (2018); 50(5):66. doi:10.1038/s12276-018-0094-1

405. Tantalo LC, Lukehart SA, Marra CM. Treponema pallidum strain-specific differences in neuroinvasion and clinical phenotype in a rabbit model. *J Infect Dis.* (2005);191(1):75-80. doi:10.1086/426510

406. Tansey C, Zhao C, Hopkins A, et al. A Nonhuman Primate Model for Rectally Transmitted Syphilis. *J Infect Dis.* (2018); 217(7):1139-1144. doi:10.1093/infdis/jix669

407. Lu S, Zheng K, Wang J, et al. Characterization of Treponema pallidum Dissemination in C57BL/6 Mice. *Front Immunol.* (2021); 11:577129. doi:10.3389/fimmu.2020.577129

408. Čejková DC, Zobaníková M, Chen L, et al. Whole Genome Sequences of Three Treponema pallidum ssp. pertenue Strains: Yaws and Syphilis Treponemes Differ in Less than 0.2% of the Genome Sequence. *PloS Negl Trop Dis.* (2012); 6(1):e1471. doi: 10.1371/journal.pntd.0001471

409. Mikalová L, Strouhal M, Čejková D, et al. Genome Analysis of Treponema pallidum subsp. pallidum and subsp. pertenue Strains: Most of the Genetic Differences Are Localized in Six Regions. *PLoS One.* (2010); 5(12):15713. doi:10.1371/journal.pone.0015713

410. French P. Syphilis. *Br Med J.* (2007); 334(7585):143-147. doi:10.1136/bmj.39085.518148.be

411. Ho EL, Lukehart SA. Syphilis: using modern approaches to understand an old disease. *J Clin Invest.* (2011); 121(12):4584. doi:10.1172/jci57173

412. Magnuson HJ, Eagle H, Fleischman R. The minimal infectious inoculum of Spirochaeta pallida (Nichols strain) and a consideration of its rate of multiplication in vivo. *Am J Syph Gonorrhea Vener Dis.* (1948) 32(1):1–18.

413. Cumberland MC, Turner TB. The rate of multiplication of Treponema pallidum in normal and immune rabbits. *Am J Syph Gonorrhea Vener Dis.* (1949); 33(3):201–12.

414. Brinkman MB, McGill MA, Pettersson J, et al. A novel Treponema pallidum antigen, TP0136, is an outer membrane protein that binds human fibronectin. *Infect Immun.* (2008);76(5):1848-1857. doi:10.1128/iai.01424-07

415. Ke W, Molini BJ, Lukehart SA, Giacani L. Treponema pallidum subsp. pallidum TP0136 Protein Is Heterogeneous among Isolates and Binds Cellular and Plasma Fibronectin via its NH 2-Terminal End. (2015); 9(3):e0003662. doi:10.1371/journal.pntd.0003662

416. Parker ML, Houston S, Pětrošová H, et al. The Structure of Treponema pallidum Tp0751 (Pallilysin) Reveals a Non-canonical Lipocalin Fold That Mediates Adhesion to Extracellular Matrix Components and Interactions with Host Cells. *PLoS Pathog.* (2016); 12(9):e1005919. doi:10.1371/journal.ppat.1005919

417. Cameron CE, Brouwer NL, Tisch LM, Kuroiwa JMY. Defining the interaction of the Treponema pallidum adhesin Tp0751 with laminin. *Infect Immun.* (2005); 73(11):7485-7494. doi:10.1128/iai.73.11.7485-7494.2005

418. Lee KH, Choi HJ, Lee MG, Lee JB. Virulent Treponema pallidum 47 kDa Antigen Regulates the Expression of Cell Adhesion Molecules and Binding of T-Lymphocytes to Cultured Human Dermal Microvascular Endothelial Cells. *Yonsei Med J.* (2000); 41(5):623-633. doi:10.3349/ymj.2000.41.5.623

419. Riley BS, Oppenheimer-Marks N, Hansen EJ, Radolf JD, Norgard M V. Virulent Treponema pallidum Activates Human Vascular Endothelial Cells. *Journal of Infectious Diseases.* (1992); 165(3):484–93. doi: 10.1093/infdis/165.3.484

420. Zhang RL, Zhang JP, Wang QQ. Recombinant Treponema pallidum Protein Tp0965 Activates Endothelial Cells and Increases the Permeability of Endothelial Cell Monolayer. *PloS One.* (2014); 9(12):e115134. doi: 10.1371/journal.pone.0115134

421. Houston S, Hof R, Francescutti T, Hawkes A, Boulanger MJ, Cameron CE. Bifunctional Role of the Treponema pallidum Extracellular Matrix Binding Adhesin Tp0751. *Infect Immun.* (2011); 79(3):1386-1398. doi:10.1128/IAI.01083-10

422. Houston S, Russell S, Hof R, et al. The Multifunctional Role of the Pallilysin-Associated Treponema pallidum Protein, Tp0750, in Promoting Fibrinolysis and Extracellular Matrix Component Degradation. *Mol Microbiol.* (2014); 91(3):618-634. doi:10.1111/mmi.12482

423. Sell S, Salman J, Norris SJ. Reinfection of Chancre-Immune Rabbits With Treponema Pallidum I. Light and Immunofluorescence Studies. *Am J Pathol* (1985) 118(2):248–55

424. Borenstein LA, Ganz T, Sell S, Lehrer RI, Miller′ AJN. Contribution of Rabbit Leukocyte Defensins to the Host Response in Experimental Syphilis. *Infect Immun.* (1991); 59(4):1368–77. doi: 10.1128/iai.59.4.1368-1377.1991

425. Musher DM, Hague-Park M, Gyorkey F, Anderson DC, Baughn RE. The interaction between treponema pallidum and human polymorphonuclear leukocytes. *Journal of Infectious Diseases.* (1983); 147(1):77–86. doi: 10.1093/infdis/147.1.77

426. Shin JL, Chung KY, Kang JM, Lee TH, Lee MG. The effects of Treponema pallidum on human dendritic cells. *Yonsei Med J.* (2004); 45(3):515-522. doi:10.3349/ymj.2004.45.3.515

427. Bouis DA, Popova TG, Takashima A, Norgard M V. Dendritic Cells Phagocytose and Are Activated by Treponema pallidum. *Infect Immun.* (2001); 69(1):518-528. doi:10.1128/iai.69.1.518-528.2001

428. Sell S, Baker-Zander S, Powell HC. Experimental syphilitic orchitis in rabbits: Ultrastructural appearance of Treponema pallidum during phagocytosis and dissolution by macrophages in vivo. *Laboratory Investigation*. (1982); 46(4):355–64

429. Lukehart SA, Baker-Zander SA, Lloyd RMC, Sell S. Characterization of lymphocyte responsiveness in early experimental syphilis. II. Nature of cellular infiltration and Treponema pallidum distribution in testicular lesions. *Journal of Immunology*. (1980); 124(1):461–7

430. Sell S, Baker-Zander SA, Lloyd CRM. T-cell hyperplasia of lymphoid tissues of rabbits infected with treponema pallidum: Evidence for a vigorous immune response. *Sex Transm Dis*. (1980); 7(2):74-84. doi:10.1097/00007435-198004000-00009

431. Leader BT, Godornes C, VanVoorhis WC, Lukehart SA. CD4+ lymphocytes and gamma interferon predominate in local immune responses in early experimental syphilis. *Infect Immun*. 2007;75(6):3021-3026. doi:10.1128/IAI.01973-06

432. Carlson JA, Dabiri G, Cribier B, Sell S, Physician R. The immunopathobiology of syphilis: the manifestations and course of syphilis are determined by the level of delayed-type hypersensitivity. *Am J Dermatopathol*. (2011); 33(5):433-460. doi:10.1097/dad.0b013e3181e8b587

433. Sykes JA, Kalan J. Intracellular Treponema pallidum in cells of a syphilitic lesion of the uterine cervix. *Am J Obstet Gynecol*. (1975); 122(3):361-367. doi:10.1016/0002-9378(75)90185-4

434. Sykes JA, Miller JN. *Intracellular Location of Treponema Pallidum (Nichols Strain) in the Rabbit Testis. Infect Immun*. (1971); 4(3):307–14. doi: 10.1128/iai.4.3.307-314.1971

435. Sykes JA, Miller JN, Kalan AJ. Treponema pallidum within cells of a primary chancre from a human female. *British Journal of Venereal Diseases*. (1974); 50(1):40-44. doi:10.1136/sti.50.1.40

436. Van Voorhis WC, Barrett LK, Nasio JM, Plummer FA, Lukehart SA. Lesions of primary and secondary syphilis contain activated cytolytic T cells. *Infect Immun*. (1996), 64(3):1048–50. doi: 10.1128/iai.64.3.1048-1050.1996

437. Moore MW, Cruz AR, LaVake CJ, et al. Phagocytosis of Borrelia burgdorferi and Treponema pallidum potentiates innate immune activation and induces gamma interferon production. *Infect Immun*. (2007); 75(4):2046-2062. doi:10.1128/iai.01666-06

438. Lukehart SA, Miller JN. Demonstration of the in vitro phagocytosis of Treponema pallidum by rabbit peritoneal macrophages. *J Immunol*. (1978); 121(5):2014-2024. doi: 10.4049/jimmunol.121.5.2014

439. Baker-Zander SA, Lukehart SA. Macrophage-mediated killing of opsonized treponema pallidum. *Journal of Infectious Diseases. J Infect Dis.* (1992); 165(1):69–74. doi: 10.1093/infdis/165.1.69

440. Baker-Zander SA, Shaffer JM, Lukehart SA. Characterization of the serum requirement for macrophage-mediated killing of Treponema pallidum ssp.

pallidum: Relationship to the development of opsonizing antibodies. *FEMS Immunol Med Microbiol.* (1993); 6(4):273–9. doi: 10.1111/j.1574-695x.1993.tb00339.x

441. Hawley KL, Cruz AR, Benjamin SJ, et al. IFNγ enhances CD64-potentiated phagocytosis of Treponema pallidum opsonized with human syphilitic serum by human macrophages. *Front Immunol.* (2017); 8:1227. doi: 10.3389/fimmu.2017.01227

442. Chen H, Tong ML, Liu LL, Lin LR, Yang TC. The whole process of macrophage-Treponema pallidum interactions: Opsonic phagocytosis, nonopsonic phagocytosis and active invasion. *Int Immunopharmacol.* (2022);107:108657. doi:10.1016/j.intimp.2022.108657

443. Lin LR, Liu W, Zhu XZ, et al. Treponema pallidum promotes macrophage polarization and activates the NLRP3 inflammasome pathway to induce interleukin-1β production. *BMC Immunol.* (2018); 19(1):28. doi: 10.1186/s12865-018-0265-9

444. Lukehart SA, Baker-Zander SA, Sell S. Characterization of the humoral immune response of the rabbit to antigens of treponema pallidum after experimental infection and therapy. *Sex Transm Dis.* (1986); 13(1):9–15. doi: 10.1097/00007435-198601000-00003

445. Leader BT, Hevner K, Molini BJ, Barrett LK, Van Voorhis WC, Lukehart SA. Antibody responses elicited against the Treponema pallidum repeat proteins differ during infection with different isolates of Treponema pallidum subsp. pallidum. *Infect Immun.* (2003); 71(10):6054-6057. doi:10.1128/IAI.71.10.6054-6057.2003

446. Moskophidis M. Analysis of the Humoral Immune Response to Treponema pallidum in the Different Stages of Untreated Human Syphilis. *Zentralblatt fur Bakteriologie.* (1989); 271(2):171-179. doi:10.1016/s0934-8840(89)80070-2

447. Fitzgerald TJ. Activation of the Classical and Alternative Pathways of Complement by Treponema Pallidum Subsp. Pallidum and Treponema Vincentii. *Infection and Immunity.* (1987); 55(9):2066–73. doi: 10.1128/iai.55.9.2066-2073.1987

448. Blanco DR, Walker EM, Haake DA, Champion CI, Miller JN, Lovett MA. Complement activation limits the rate of in vitro treponemicidal activity and correlates with antibody-mediated aggregation of Treponema pallidum rare outer membrane protein. *The Journal of Immunology.* (1990); 144(5):1914-1921. doi: 10.4049/jimmunol.144.5.1914

449. Rice M, Fitzgerald TJ. Immune immobilization of Treponema pallidum: Antibody and complement interactions revisited. *Can J Microbiol.* (1985); 31(12):1147-1151. doi:10.1139/m85-216

450. Fearon DT. Regulation by membrane sialic acid of β1H-dependent decay-dissociation of amplification C3 convertase of the alternative complement pathway. *Proc Natl Acad Sci U S A.* (1978);75(4):1971-1975. doi:10.1073/pnas.75.4.1971

451. Meri S, Pangburnt MK. Discrimination between activators and nonactivators of the alternative pathway of complement: Regulation *via* a sialic acid/polyanion binding site on factor h. *Proc Natl Acad Sci USA*. (1990); 87(10):3982–6. doi: 10.1073/pnas.87.10.3982

452. Ram S, Sharma AK, Simpson SD, et al. A Novel Sialic Acid Binding Site on Factor H Mediates Serum Resistance of Sialylated Neisseria Gonorrhoeae. *J Exp Med*. (1998); 187(5):743–52. doi: 10.1084/jem.187.5.743

453. Jarvis' GA, Vedros2 NA. Sialic acid of group b neisseria meningitidis regulates alternative complement pathway activation. *Infect Immun.* (1987); 55(1):174–80. doi: 10.1128/iai.55.1.174-180.1987

454. Sell S, Hsu PL. Delayed hypersensitivity, immune deviation, antigen processing and T-cell subset selection in syphilis pathogenesis and vaccine design. *Immunol Today*. (1993); 14(12):576-582. doi:10.1016/0167-5699(93)90196-r

455. Bishop NH, Miller JN. Humoral immunity in experimental syphilis. II. The relationship of neutralizing factors in immune serum to acquired resistance. *J Immunol*. (1976); 117(1):197-207.

456. Bishop NH, Miller JN. Humoral Immunity in Experimental Syphilis. *The Journal of Immunology*. (1976); 117(1):191-196.

457. Hanff PA, Bishop NH, Miller JN, Lovett MA. Humoral immune response in experimental syphilis to polypeptides of Treponema pallidum. *J Immunol*. (1983); 131(4):1973-1977. doi: 10.4049/jimmunol.131.4.1973

458. Arroll TW, Centurion-Lara A, Lukehart SA, Van Voorhis WC. T-Cell responses to Treponema pallidum subsp. pallidum antigens during the course of experimental syphilis infection. *Infect Immun*. (1999); 67(9):4757-4763. doi: 10.1128/iai.67.9.4757-4763.1999

459. Sell S, Gamboa D, Baker-Zander SA, Lukehart SA, Miller JN. Host response to Treponema pallidum in intradermally-infected rabbits: Evidence for persistence of infection at local and distant sites. *Journal of Investigative Dermatology*. (1980); 75(6):470-475. doi:10.1111/1523-1747.ep12524230

460. Yogeswari L, Chacko CW. Persistence of t. pallidum and its significance in penicillin-treated seropositive late syphilis. *Br J Vener Dis*. (1971); 47(5):339–47. doi:10.1136/sti.47.5.339

461. Wicher K, Abbruscato F, Wicher V, Collins DN, Auger I, Horowitz HW. Identification of persistent infection in experimental syphilis by PCR. *Infect Immun*. (1998); 66(6):2509-2513. doi: 10.1128/iai.66.6.2509-2513.1998

462. Castro R, Prieto E, Águas MJ, et al. Detection of Treponema pallidum sp pallidum DNA in latent syphilis. *Int J STD AIDS*. (2007);v18(12):842-845. doi:10.1258/095646207782716901

463. Engelkens HJ, Ten Kate FJ, Judanarso J, et al. The localisation of treponemes and characterisation of the inflammatory infiltrate in skin biopsies from patients with primary or secondary syphilis, or early infectious yaws. *Genitourin Med*. (1993); 69(2):102-107. doi:10.1136/sti.69.2.102

464. Singh R, Teranno D. Unusual presentation of a skin rash. *J Clin Pathol.* (2017); 70(12):1088. doi: 10.1136/jclinpath-2016-204007

465. Alessi E, Innocenti M, Ragusa G. Secondary syphilis. Clinical morphology and histopathology. *Am J Dermatopathol.* (1983); 5(1):11-17. doi: 10.1097/00000372-198302000-00004

466. Baker-Zander SA, Roddy RE, Handsfield HH, Lukehart SA. Igg and igm antibody reactivity to antigens of treponema pallidum after treatment of syphilis. *Sex Transm Dis.* (1986); 13(4):214-220. doi:10.1097/00007435-198610000-00002

467. Breeze AC. Infectious diseases of the fetus and newborn infant, 6th edn. *Arch Dis Child Fetal Neonatal Ed* (2007); 92:F156. doi: 10.1136/adc.2006.102566

468. Baughn RE, Jorizzo JL, Adams CB, Musher DM. Ig class and IgG subclass responses to Treponema pallidum in patients with syphilis. *J Clin Immunol.* (1988); 8(2):128-139. doi:10.1007/BF00917901

469. Liu LL, Chao PL, Zhang HL, et al. Analysis of lymphocyte subsets in HIV-negative neurosyphilis patients. *Diagn Microbiol Infect Dis.* (2013); 75(2):165-168. doi:10.1016/j.diagmicrobio.2012.10.007

470. Podwinska J, Lusiak M, Zaba R, Bowszyc J. The pattern and level of cytokines secreted by Th1 and Th2 lymphocytes of syphilitic patients correlate to the progression of the disease. *FEMS Immunol Med Microbiol.* (2000); 28(1):1-14. doi:10.1111/j.1574-695X.2000.tb01451.x

471. Miller JN. Immunity in experimental syphilis. VI. successful vaccination of rabbits with treponema pallidum, nichols strain, attenuated by -irradiation. *J Immunol.* (1973); 110(5):1206–15. doi: 10.4049/jimmunol.110.6.np

472. Magnuson HJ, Thomas EW, Olansky S, Kaplan BI, de Mello L, Cutler JC. Inoculation syphilis in human volunteers. *Medicine.* (1956); 35(1):33-82. doi:10.1097/00005792-195602000-00002

473. Marra CM, Maxwell CL, Sahi SK, Tantalo LC, Dunaway SB, Lukehart SA. Previous Syphilis Alters the Course of Subsequent Episodes of Syphilis. *Clinical Infectious Diseases.* (2022); 74(4):e1-e5. doi:10.1093/cid/ciab287

474. Cullen PA, Haake DA, Adler B. Outer membrane proteins of pathogenic spirochetes. *FEMS Microbiol Rev.* (2004); 28(3):291-318. doi:10.1016/j.femsre.2003.10.004

475. Hawley KL, Montezuma-Rusca JM, Delgado KN, et al. Structural Modeling of the Treponema pallidum Outer Membrane Protein Repertoire: a Road Map for Deconvolution of Syphilis Pathogenesis and Development of a Syphilis Vaccine. *Journal of Bacteriology.* (2021); 203:82-103. doi:10.1128/jb

476. Molini B, Fernandez MC, Godornes C, Vorobieva A, Lukehart SA, Giacani L. B-Cell Epitope Mapping of TprC and TprD Variants of Treponema pallidum

Subspecies Informs Vaccine Development for Human Treponematoses. *Front Immunol.* (2022); 13:862491. doi:10.3389/fimmu.2022.862491

477. Kojima N, Konda KA, Klausner JD. Notes on syphilis vaccine development. *Front Immunol.* (2022);13:952284. doi: 10.3389/fimmu.2022.952284

478. Romeis E, Tantalo L, Lieberman N, Phung Q, Greninger A, Giacani L. Genetic engineering of Treponema pallidum subsp. pallidum, the Syphilis Spirochete. *PLoS Pathog.* (2021); 17(7):e1009612. doi:10.1371/journal.ppat.1009612

479. Centurion-Lara A, Castro C, Barrett L, et al. Treponema pallidum major sheath protein homologue Tpr K is a target of opsonic antibody and the protective immune response. *Journal of Experimental Medicine.* (1999); 189(4):647-656. doi:10.1084/jem.189.4.647

480. Edwards AM, Jenkinson HF, Woodward MJ, Dymock D. Binding properties and adhesion-mediating regions of the major sheath protein of Treponema denticola ATCC 35405. *Infect Immun.* (2005); 73(5):2891-2898. doi:10.1128/iai.73.5.2891-2898.2005

481. Fenno JC, Müller KH, McBride BC. Sequence analysis, expression, and binding activity of recombinant major outer sheath protein (Msp) of Treponema denticola. *J Bacteriol.* (1996); 178(9):2489-2497. doi:10.1128/jb.178.9.2489-2497.1996

482. Mathers DA, Leung WK, Fenno JC, Hong Y, McBride BC. The major surface protein complex of Treponema denticola depolarizes and induces ion channels in HeLa cell membranes. *Infect Immun.* (1996); 64(8):2904-2910. doi: 10.1128/iai.64.8.2904-2910.1996

483. Anand A, Luthra A, Dunham-Ems S, et al. TprC/D (Tp0117/131), a trimeric, pore-forming rare outer membrane protein of Treponema pallidum, has a bipartite domain structure. *J Bacteriol.* (2012); 194(9):2321-2333. doi:10.1128/jb.00101-12

484. Anand A, Ledoyt M, Karanian C, et al. Bipartite topology of treponema pallidum repeat proteins C/D and I: Outer membrane insertion, trimerization, and porin function require a c-Terminal-Barrel domain. *J Biol Chem.* (2015); 290(19):12313–31. doi: 10.1074/jbc.m114.629188

485. Giacani L, Sambri V, Marangoni A, et al. Immunological evaluation and cellular location analysis of the TprI antigen of Treponema pallidum subsp. pallidum. *Infect Immun.* (2005); 73(6):3817-3822. doi:10.1128/iai.73.6.3817-3822.2005

486. Giacani L, Molini B, Godornes C, et al. Quantitative analysis of tpr gene expression in Treponema pallidum isolates: Differences among isolates and correlation with T-cell responsiveness in experimental syphilis. *Infect Immun.* (2007); 75(1):104-112. doi:10.1128/iai.01124-06

487. Giacani L, Godornes C, Puray-Chavez M, et al. TP0262 is a modulator of promoter activity of tpr Subfamily II genes of Treponema pallidum ssp. pallidum. *Mol Microbiol.* (2009); 72(5):1087-1099. doi:10.1111/j.1365-2958.2009.06712.x

488. Giacani L, Lukehart S, Centurion-Lara A. Length of guanosine homopolymeric repeats modulates promoter activity of subfamily II tpr genes of Treponema pallidum ssp. pallidum. *FEMS Immunol Med Microbiol.* (2007); 51(2):289-301. doi:10.1111/j.1574-695X.2007.00303.x

489. Haynes AM, Fernandez M, Romeis E, et al. Transcriptional and immunological analysis of the putative outer membrane protein and vaccine candidate TprL of Treponema pallidum. *PLoS Negl Trop Dis.* (2021); 15(1):e0008812. doi:10.1371/journal.pntd.0008812

490. Lian T, Zhang B, Giacani L, et al. Full-length TprK of Treponema pallidum subsp. pallidum in lipid nanodiscs is a monomeric porin. *Enzyme Microb Technol.* (2022); 153:109897. doi:10.1016/j.enzmictec.2021.109897

491. Centurion-Lara A, Godornes C, Castro C, Van Voorhis WC, Lukehart SA. The tprK gene is heterogeneous among Treponema pallidum strains and has multiple alleles. *Infect Immun.* (2000); 68(2):824-831. doi:10.1128/IAI.68.2.824-831.2000

492. Addetia A, Lin MJ, Phung Q, et al. Estimation of full-length tprk diversity in treponema pallidum subsp. Pallidum. *mBio.* (2020); 11(5):1-19. doi:10.1128/mbio.02726-20

493. Lafond RE, Centurion-lara A, Godornes C, Voorhis WC Van, Lukehart SA. TprK sequence diversity accumulates during infection of rabbits with treponema pallidum subsp. pallidum nichols strain. *Infection and Immunity.* (2006); 74(3):1896–906. doi: 10.1128/iai.74.3.1896

494. Giacani L, Molini BJ, Kim EY, et al. Antigenic variation in Treponema pallidum: TprK sequence diversity accumulates in response to immune pressure during experimental syphilis. *J Immunol.* (2010); 184(7):3822-3829. doi:10.4049/jimmunol.0902788

495. Lin MJ, Haynes AM, Addetia A, et al. Longitudinal TprK profiling of in vivo and in vitro-propagated Treponema pallidum subsp. pallidum reveals accumulation of antigenic variants in absence of immune pressure. *PLoS Negl Trop Dis.* (2021); 15(9):e0009753. doi:10.1371/journal.pntd.0009753

496. Morgan CA, Lukehart SA, Van Voorhis WC. Protection against syphilis correlates with specificity of antibodies to the variable regions of Treponema pallidum repeat protein K. *Infect Immun.* (2003); 71(10):5605-5612. doi:10.1128/iai.71.10.5605-5612.2003

497. Morgan CA, Molini BJ, Lukehart SA, Van Voorhis WC. Segregation of B and T cell epitopes of Treponema pallidum repeat protein K to variable and conserved regions during experimental syphilis infection. *J Immunol.* (2002); 169(2):952-957. doi:10.4049/jimmunol.169.2.952

498. Morgan CA, Lukehart SA, Van Voorhis WC. Immunization with the N-Terminal Portion of Treponema pallidum Repeat Protein K Attenuates Syphilitic Lesion Development in the Rabbit Model. *Infect Immun.* (2002); 70(12):6811. doi:10.1128/iai.70.12.6811-6816.2002

499. Hazlett KRO, Sellati TJ, Nguyen TT, et al. The TprK protein of Treponema pallidum is periplasmic and is not a target of opsonic antibody or protective immunity. *Journal of Experimental Medicine*. (2001); 193(9):1015-1026. doi:10.1084/jem.193.9.1015

500. Sun ES, Molini BJ, Barrett LK, Centurion-Lara A, Lukehart SA, Van Voorhis WC. Subfamily I Treponema pallidum repeat protein family: sequence variation and immunity. *Microbes Infect*. (2004); 6(8):725-737. doi:10.1016/j.micinf.2004.04.001

501. Nandi B, Nandy RK, Sarkar A, Ghose AC. Structural features, properties and regulation of the outer-membrane protein W (OmpW) of Vibrio cholerae. *Microbiology (Reading)*. (2005);151:2975-2986. doi:10.1099/mic.0.27995-0

502. Hu WS, Li PC, Cheng CY. Correlation between ceftriaxone resistance of Salmonella enterica serovar Typhimurium and expression of outer membrane proteins OmpW and Ail/OmpX-like protein, which are regulated by BaeR of a two-component system. *Antimicrob Agents Chemother*. (2005); 49(9):3955-3958. doi:10.1128/aac.49.9.3955-3958.2005

503. Hong H, Patel DR, Tamm LK, Van Den Berg B. The outer membrane protein OmpW forms an eight-stranded beta-barrel with a hydrophobic channel. *J Biol Chem*. (2006); 281(11):7568-7577. doi:10.1074/jbc.m512365200

504. Giacani L, Brandt SL, Ke W, et al. Transcription of TP0126, Treponema pallidum Putative OmpW Homolog, Is Regulated by the Length of a Homopolymeric Guanosine Repeat. *Infect Immun*. (2015); 83(6):2275-2289. doi:10.1128/iai.00360-15

505. Haynes AM, Godornes C, Ke W, Giacani L. Evaluation of the protective ability of the treponema pallidum subsp. pallidum Tp0126 OmpW homolog in the rabbit model of syphilis. *Infect Immun*. (2019); 87(8). doi:10.1128/iai.00323-19

506. Cox DL, Radolf JD. Insertion of fluorescent fatty acid probes into the outer membranes of the pathogenic spirochaetes Treponema pallidum and Borrelia burgdorferi. *Microbiology*. (2001); 147(5):1161-1169. doi:10.1099/00221287-147-5-1161

507. Delgado KN, Montezuma-Rusca JM, Orbe IC, et al. Extracellular Loops of the Treponema pallidum FadL Orthologs TP0856 and TP0858 Elicit IgG Antibodies and IgG+-Specific B-Cells in the Rabbit Model of Experimental Syphilis. *mBio*. (2022); 13(4). doi:10.1128/mbio.01639-22

508. Bleuel C, Große C, Taudte N, et al. TolC is involved in enterobactin efflux across the outer membrane of Escherichia coli. *J Bacteriol*. (2005); 187(19):6701-6707. doi:10.1128/jb.187.19.6701-6707.2005

509. Brautigam CA, Deka RK, Ouyang Z, et al. Biophysical and bioinformatic analyses implicate the treponema pallidum tp34 lipoprotein (tp0971) in transition metal homeostasis. *J Bacteriol*. (2012); 194(24):6771-6781. doi:10.1128/jb.01494-12

510. Kubanov A, Runina A, Deryabin D. Novel Treponema pallidum Recombinant Antigens for Syphilis Diagnostics: Current Status and Future

Prospects*BioMed Res Int.* (2017); 2017:1436080. doi:10.1155/2017/1436080

511. Blanco DR, Champion CI, Exner MM, et al. Recombinant Treponema pallidum rare outer membrane protein 1 (Tromp1) expressed in Escherichia coli has porin activity and surface antigenic exposure. *J Bacteriol.* (1996); 178(23):6685-6692. doi:10.1128/jb.178.23.6685-6692.1996

512. Deka RK, Lee YH, Hagman KE, Shevchenko D, Lingwood CA, Hasemann CA, et al. Physicochemical evidence that treponema pallidum TroA is a zinc-containing metalloprotein that lacks porin-like structure. *J Bacteriol.* (1999);181(14):4420–3. doi: 10.1128/jb.181.14.4420-4423.1999

513. Akins DR, Robinson E, Shevchenko D, Elkins C, Cox DL, Radolf JD. Tromp1, a putative rare outer membrane protein, is anchored by an uncleaved signal sequence to the Treponema pallidum cytoplasmic membrane. *J Bacteriol.* (1997); 179(16):5076-5086. doi:10.1128/JB.179.16.5076-5086.1997

514. Hardham JM, Stamm L V., Porcella SF, et al. Identification and transcriptional analysis of a Treponema pallidum operon encoding a putative ABC transport system, an iron-activated repressor protein homolog, and a glycolytic pathway enzyme homolog. *Gene.* (1997); 197(1-2):47-64. doi:10.1016/S0378-1119(97)00234-5

515. Xu M, Xie Y, Jiang C, et al. A novel ELISA using a recombinant outer membrane protein, rTp0663, as the antigen for serological diagnosis of syphilis. *International Journal of Infectious Diseases.* (2016); 43:51-57. doi:10.1016/j.ijid.2015.12.013

516. Xu M, Xie Y, Zheng K, et al. Two Potential Syphilis Vaccine Candidates Inhibit Dissemination of Treponema pallidum. *Front Immunol.* (2021); 12:759474. doi:10.3389/fimmu.2021.759474

517. Djokic V, Giacani L, Parveen N. Analysis of host cell binding specificity mediated by the Tp0136 adhesin of the syphilis agent Treponema pallidum subsp. pallidum. *PLoS Negl Trop Dis.* (2019); 13(5):e0007401. doi:10.1371/journal.pntd.0007401

518. Xu QY, Wang YJ, Lin LR, Liu LL, Yang TC. The Outer Membrane Lipoprotein Tp0136 Stimulates Human Platelet Activation and Aggregation Through PAR1 to Enhance Gq/Gi Signaling. *Front Immunol.* (2022); 13:818151. doi:10.3389/fimmu.2022.818151

519. Cameron CE, Brown EL, Kuroiwa JMY, Schnapp LM, Brouwer NL. Treponema pallidum Fibronectin-Binding Proteins. *J Bacteriol.* (2004); 186(20):7019-7022. doi:10.1128/jb.186.20.7019-7022.2004

520. Bamford C V., Francescutti T, Cameron CE, Jenkinson HF, Dymock D. Characterization of a novel family of fibronectin-binding proteins with M23 peptidase domains from Treponema denticola. *Mol Oral Microbiol.* (2010); 25(6):369-383. doi:10.1111/J.2041-1014.2010.00584.X

521. Tomson FL, Conley PG, Norgard M V., Hagman KE. Assessment of cell-surface exposure and vaccinogenic potentials of Treponema pallidum

candidate outer membrane proteins. *Microbes Infect.* (2007); 9(11):1267-1275. doi:10.1016/j.micinf.2007.05.018

522.   Van Voorhis WC, Barrett LK, Lukehart SA, Schmidt B, Schriefer M, Cameron CE. Serodiagnosis of Syphilis: Antibodies to Recombinant Tp0453, Tp92, and Gpd Proteins Are Sensitive and Specific Indicators of Infection by Treponema pallidum. *J Clin Microbiol.* (2003); 41(8):3668. doi:10.1128/jcm.41.8.3668-3674.2003

523.   Chan K, Nasereddin T, Alter L, Centurion-Lara A, Giacani L, Parveen N. Treponema pallidum Lipoprotein TP0435 Expressed in Borrelia burgdorferi Produces Multiple Surface/Periplasmic Isoforms and mediates Adherence. *Sci Rep.* (2016); 6:1-13. doi:10.1038/srep25593

524.   Cox DL, Akins DR, Porcella SF, Norgard M V., Radolf JD. Treponema pallidum in gel microdroplets: a novel strategy for investigation of treponemal molecular architecture. *Mol Microbiol.* (1995); 15(6):1151-1164. doi:10.1111/j.1365-2958.1995.tb02288.x

525.   Brautigam CA, Deka RK, Liu WZ, Norgard M V. Insights into the potential function and membrane organization of the TP0435 (Tp17) lipoprotein from Treponema pallidum derived from structural and biophysical analyses. *Protein Science.* (2015); 24(1):11-19. doi:10.1002/pro.2576

526.   Parveen N, Fernandez MC, Haynes AM, et al. Non-pathogenic Borrelia burgdorferi expressing Treponema pallidum TprK and Tp0435 antigens as a novel approach to evaluate syphilis vaccine candidates. *Vaccine.* (2019); 37(13):1807–18. doi: 10.1016/j.vaccine.2019.02.022

527.   Cameron CE. Identification of a Treponema pallidum laminin-binding protein. *Infect Immun.* (2003); 71(5):2525-2533. doi:10.1128/iai.71.5.2525-2533.2003

528.   Dickerson MT, Abney MB, Cameron CE, Knecht M, Bachas LG, Anderson KW. Fibronectin binding to the Treponema pallidum adhesin protein fragment rtp0483 on functionalized self-assembled monolayers. *Bioconjug Chem.* (2012); 23(2):184–95. doi: 10.1021/bc200436x

529.   Houston S, Taylor JS, Denchev Y, Hof R, Zuerner RL, Cameron CE. Conservation of the host-interacting proteins Tp0750 and pallilysin among treponemes and restriction of proteolytic capacity to treponema pallidum. *Infect Immun.* (2015); 83(11):4204-4216. doi:10.1128/iai.00643-15

530.   Luthra A, Montezuma-Rusca JM, la Vake CJ, et al. Evidence that immunization with TP0751, a bipartite Treponema pallidum lipoprotein with an intrinsically disordered region and lipocalin fold, fails to protect in the rabbit model of experimental syphilis. *PLoS Pathog.* (2020); 16(9):e1008871. doi:10.1371/journal.ppat.1008871

531.   Kao WCA, Pětrošová H, Ebady R, et al. Identification of Tp0751 (Pallilysin) as a Treponema pallidum Vascular Adhesin by Heterologous Expression in the Lyme disease Spirochete. *Scientific Reports.* (2017);7(1):1-13. doi:10.1038/s41598-017-01589-4

532. Lithgow K V., Hof R, Wetherell C, Phillips D, Houston S, Cameron CE. A defined syphilis vaccine candidate inhibits dissemination of Treponema pallidum subspecies pallidum. *Nature Communications*. (2017); 8(1):1-10. doi:10.1038/ncomms14273

533. Primus S, Rocha SC, Giacani L, Parveen N. Identification and Functional Assessment of the First Placental Adhesin of Treponema pallidum That May Play Critical Role in Congenital Syphilis. *Front Microbiol*. (2020); 11:621654. doi:10.3389/fmicb.2020.621654

534. Giri TK, Tollefsen DM. Placental dermatan sulfate: isolation, anticoagulant activity, and association with heparin cofactor II. *Blood*. (2006); 107(7):2753. doi:10.1182/blood-2005-09-3755

535. Suga N, Sugimura M, Koshiishi T, Yorifuji T, Makino S, Takeda S. Heparin/heparan sulfate/CD44-v3 enhances cell migration in term placenta-derived immortalized human trophoblast cells. *Biol Reprod*. (2012); 86(5). doi:10.1095/biolreprod.111.093690

536. Lala PK, Nandi P. Mechanisms of trophoblast migration, endometrial angiogenesis in preeclampsia: The role of decorin. *Cell Adh Migr*. (2016); 10(1-2):111-125. doi:10.1080/19336918.2015.1106669

537. de Oliveira GB, do Vale AM, dos Santos AC, de Moura CEB, Rocha HA de O, de Oliveira MF. Composition and significance of glycosaminoglycans in the uterus and placenta of mammals. *Brazilian Archives of Biology and Technology*. (2015); 58(4):512-520. doi:10.1590/s1516-8913201500281

538. Luthra A, Anand A, Hawley KL, et al. A Homology Model Reveals Novel Structural Features and an Immunodominant Surface Loop/Opsonic Target in the Treponema pallidum BamA Ortholog TP_0326. *J Bacteriol*. (2015); 197(11):1906-1920. doi:10.1128/jb.00086-15

539. Desrosiers DC, Anand A, Luthra A, et al. TP0326, a Treponema pallidum β-barrel assembly machinery A (BamA) orthologue and rare outer membrane protein. *Mol Microbiol*. (2011); 80(6):1496-1515. doi:10.1111/j.1365-2958.2011.07662.x

540. Cameron CE, Lukehart SA, Castro C, Molini B, Godornes C, Van Voorhis WC. Opsonic potential, protective capacity, and sequence conservation of the Treponema pallidum subspecies pallidum Tp92. *Journal of Infectious Diseases*. (2000); 181(4):1401-1413. doi:10.1086/315399

541. Stebeck CE, Shaffer JM, Arroll TW, Lukehart SA, Van Voorhis WC. Identification of the Treponema pallidum subsp. pallidum glycerophosphodiester phosphodiesterase homologue. *FEMS Microbiol Lett*. (1997); 154(2):303-310. doi:10.1111/j.1574-6968.1997.tb12660.X

542. Cameron CE, Castro C, Lukehart SA, Voorhis WC. Function and Protective Capacity of Treponema pallidum subsp. pallidum Glycerophosphodiester Phosphodiesterase. *Infection and Immunity*. (1998); 66(12):5763–70. doi: 10.1128/IAI.66.12.5763-5770.1998

543. Shevchenko D V., Akins DR, Robinson EJ, Li M, Shevchenko O V., Radolf JD. Identification of homologs for thioredoxin, peptidyl prolyl cis-trans

isomerase, and glycerophosphodiester phosphodiesterase in outer membrane fractions from Treponema pallidum, the syphilis spirochete. *Infect Immun.* (1997); 65(10):4179-4189. doi:10.1128/iai.65.10.4179-4189.1997

544. Shevchenko D V., Sellati TJ, Cox DL, Shevchenko O V., Robinson EJ, Radolf JD. Membrane Topology and Cellular Location of the Treponema pallidum Glycerophosphodiester Phosphodiesterase (GlpQ) Ortholog. *Infect Immun.* (1999); 67(5):2266. doi:10.1128/iai.67.5.2266-2276.1999

545. Zhao F, Wang S, Zhang X, Gu W, Yu J. Protective efficacy of a Treponema pallidum Gpd DNA vaccine vectored by chitosan nanoparticles and fused with interleukin-2. (2012); 123:117-123. doi:10.1139/w11-115

546. Zhang X, Zhao T, Zeng T, et al. Intramuscular primary immunization by nucleic acid vaccine pcDNA/Gpd-IL-2 and enhanced immunization with mucosal adjuvant CpG-ODN and Gpd-IL-2 recombinant protein effectively induced strong mucosal immune responses and immune protective effects against Treponema pallidum skin infection. *Exp Ther Med.* (2018); 15(3):2533. doi:10.3892/etm.2018.5689

547. Cameron CE, Castro C, Lukehart SA, Van Voorhis WC. Sequence Conservation of Glycerophosphodiester Phosphodiesterase among Treponema pallidum Strains. *Infect Immun.* (1999); 67(6):3168. doi:10.1128/iai.67.6.3168-3170.1999

548. Thumiger A, Polenghi A, Papinutto E, Battistutta R, Montecucco C, Zanotti G. Crystal structure of antigen TpF1 from Treponema pallidum. *Proteins: Structure, Function and Genetics.* (2006); 62(3):827-830. doi:10.1002/prot.20828

549. Radolf JD, Fehniger TE, Silverblatt FJ, Miller JN, Lovett MA. The surface of virulent Treponema pallidum: resistance to antibody binding in the absence of complement and surface association of recombinant antigen 4D. *Infect Immun.* (1986); 52(2):579-585. doi:10.1128/iai.52.2.579-585.1986

550. Babolin C, Amedei A, Ozoliņš D, Žileviča A, D'Elios MM, Bernard M de. TpF1 from Treponema pallidum Activates Inflammasome and Promotes the Development of Regulatory T Cells. *The Journal of Immunology.* (2011); 187(3):1377-1384. doi:10.4049/jimmunol.1100615

551. Lu DP, Jia J, Wei SF, et al. Treponema pallidum (Syphilis) Antigen TpF1 Induces Activation of Macrophages and Accelerates P2X7R-Induced NLRP3-Dependent Release of IL-1β. *Endocr Metab Immune Disord Drug Targets.* (2022); 22(4):425-432. doi:10.2174/1871530321666211015091109

552. McGill MA, Edmondson DG, Carroll JA, Cook RG, Orkiszewski RS, Norris SJ. Characterization and serologic analysis of the treponema pallidum proteome. *Infect Immun.* (2010); 78(6):2631-2643. doi:10.1128/IAI.00173-10

553. Pozzobon T, Facchinello N, Bossi F, et al. Treponema pallidum (syphilis) antigen TpF1 induces angiogenesis through the activation of the IL-8 pathway. *Sci Rep.* (2016); 6:1-14. doi:10.1038/srep18785

554. Cohen SE, Ng RAC, Katz KA, et al. Repeat syphilis among men who have sex with men in California 2002-2006: Implications for syphilis elimination efforts. *Am J Public Health*. (2012); 102(1):2002-2006. doi:10.2105/ajph.2011.300383

555. Almeida VC de, Donalisio MR, Cordeiro R. Factors associated with reinfection of syphilis in reference centers for sexually transmitted infections. *Rev Saude Publica*. (2017); 51:64. doi:10.1590/s1518-8787.2017051006432

556. Jain J, Santos GM, Scheer S, et al. Rates and Correlates of Syphilis Reinfection in Men Who Have Sex with Men. *LGBT Health*. (2017); 4(3):232-236. doi:10.1089/lgbt.2016.0095

557. Van der Ende A, Hopman CTP, Zaat S, Essink BBO, Berkhout B, Dankert J. Variable expression of class 1 outer membrane protein in Neisseria meningitidis is caused by variation in the spacing between the -10 and -35 regions of the promoter. *J Bacteriol*. (1995); 177(9):2475-2480. doi:10.1128/jb.177.9.2475-2480.1995

558. Saunders NJ, Peden JF, Hood DW, Moxon ER. Simple sequence repeats in the Helicobacter pylori genome. *Mol Microbiol*. (1998); 27(6):1091-1098. doi:10.1046/j.1365-2958.1998.00768.x

559. Van Der Woude MW, Bäumler AJ. Phase and antigenic variation in bacteria. *Clin Microbiol Rev*. (2004); 17(3):581-611. doi:10.1128/cmr.17.3.581-611.2004

560. Osbak KK, Houston S, Lithgow K V., et al. Characterizing the Syphilis-Causing Treponema pallidum ssp. pallidum Proteome Using Complementary Mass Spectrometry. *PLoS Negl Trop Dis*. (2016); 10(9):e0004988. doi:10.1371/journal.pntd.0004988

561. Bonifield HR, Hughes KT. Flagellar phase variation in Salmonella enterica is mediated by a posttranscriptional control mechanism. *J Bacteriol*. (2003); 185(12):3567-3574. doi:10.1128/jb.185.12.3567-3574.2003

562. Mouquet H, Scheid JF, Zoller MJ, et al. Polyreactivity increases the apparent affinity of anti-HIV antibodies by heteroligation. *Nature*. (2010); 467(7315):591-595. doi:10.1038/nature09385

563. Wardemann H, Yurasov S, Schaefer A, Young JW, Meffre E, Nussenzweig MC. Predominant autoantibody production by early human B cell precursors. *Science*. (2003); 301(5638):1374-1377. doi:10.1126/science.1086907

564. Birge RB, Boeltz S, Kumar S, et al. Phosphatidylserine is a global immunosuppressive signal in efferocytosis, infectious disease, and cancer. *Cell Death & Differentiation*. (2016); 23(6):962-978. doi:10.1038/cdd.2016.11

565. Treede I, Braun A, Sparla R, et al. Anti-inflammatory effects of phosphatidylcholine. *J Biol Chem*. (2007); 282(37):27155-64. doi:10.1074/jbc.m704408200

566. Macek B, Forchhammer K, Hardouin J, Weber-Ban E, Grangeasse C, Mijakovic I. Protein post-translational modifications in bacteria. *Nat Rev Microbiol.* (2019); 17(11):651-664. doi:10.1038/s41579-019-0243-0

567. Sobocińska J, Roszczenko-Jasińska P, Ciesielska A, Kwiatkowska K. Protein palmitoylation and its role in bacterial and viral infections. *Front Immunol.* (2018); 8:1-19. doi:10.3389/fimmu.2017.02003

568. Kumar S, Caimano MJ, Anand A, et al. Sequence Variation of Rare Outer Membrane Protein β-Barrel Domains in Clinical Strains Provides Insights into the Evolution of Treponema pallidum subsp. pallidum, the Syphilis Spirochete. *mBio.* (2018); 9(3):e01006–18. doi:10.1128/mBio.01006-18

569. Centurion-Lara A, Giacani L, Godornes C, Molini BJ, Brinck Reid T, Lukehart SA. Fine Analysis of Genetic Diversity of the tpr Gene Family among Treponemal Species, Subspecies and Strains. *PLoS Negl Trop Dis.* (2013); 7(5):e2222. doi:10.1371/journal.pntd.0002222

570. Hawley K, Luthra A, Vake C La, et al. O01.2 Genetic, structural, and surface antigenic variation of treponema pallidum's OMPeome: steps towards a global syphilis vaccine. *Sex Transm Infect.* (2019); 95:A37–7. doi:10.1136/sextrans-2019-sti.105

571. Grillová L, Oppelt J, Mikalová L, et al. Directly Sequenced Genomes of Contemporary Strains of Syphilis Reveal Recombination-Driven Diversity in Genes Encoding Predicted Surface-Exposed Antigens. *Front Microbiol.* (2019); 10:1691. doi: 10.3389/fmicb.2019.01691

572. Lieberman NAP, Lin MJ, Xie HI, Shrestha L, Nguyen T, Huang M-L, et al. Treponema pallidum genome sequencing from six continents reveals variability in vaccine candidate genes and dominance of nichols clade strains in Madagascar. *PloS Negl Trop Dis.* (2021); 15(12):e0010063. doi:10.1371/journal.pntd.0010063

573. Ovcinnikov NM, Delektorskij V V. Treponema pallidum in nerve fibres. *British Journal of Venereal Diseases.* (1975); 51(1):10. doi:10.1136/sti.51.1.10

574. Sell S, Salman J. Demonstration of Treponema pallidum in axons of cutaneous nerves in experimental chancres of rabbits. *Sex Transm Dis.* (1992); 19(1):1-6. doi:10.1097/00007435-199201000-00001

575. Medici MA. The immunoprotective niche--a new pathogenic mechanism for syphilis, the systemic mycoses and other infectious diseases. *J Theor Biol.* (1972); 36(3):617-625. doi:10.1016/0022-5193(72)90012-4

576. Kronvall G, Simmons A, Myhre EB, Jonsson S. Specific absorption of human serum albumin, immunoglobulin A, and immunoglobulin G with selected strains of group A and G streptococci. *Infect Immun.* (1979); 25(1):1-10. doi:10.1128/iai.25.1.1-10.1979

577. Alderete JF, Baseman JB. Surface-Associated Host Proteins on Virulent Treponema pallidum. *Infect Immun.* (1979); 26(3):1048-1056. doi:10.1128/iai.26.3.1048-1056.1979

578. Egesten A, Frick IM, Mörgelin M, Olin AI, Björck L. Binding of Albumin Promotes Bacterial Survival at the Epithelial Surface. *J Biol Chem*. (2011); 286(4):2469. doi:10.1074/jbc.m110.148171

579. Champion CI, Miller JN, Borenstein LA, Lovett MA, Blanco DR. Immunization with Treponema pallidum endoflagella alters the course of experimental rabbit syphilis. *Infect Immun*. (1990); 58(9):3158-3161. doi:10.1128/iai.58.9.3158-3161.1990

580. Zheng K, Xu M, Xiao Y, et al. Immunogenicity and protective efficacy against Treponema pallidum in New Zealand rabbits immunized with plasmid DNA encoding flagellin. *Emerg Microbes Infect*. (2018); 7(1):177. doi:10.1038/s41426-018-0176-0

581. Nimmerjahn F, Ravetch J V. Fcγ receptors as regulators of immune responses. *Nature Reviews Immunology*. (2008); 8(1):34-47. doi:10.1038/nri2206

582. Lukehart SA, Molini B, Gomez A, et al. Immunization with a tri-antigen syphilis vaccine significantly attenuates chancre development, reduces bacterial load, and inhibits dissemination of Treponema pallidum. *Vaccine*. (2022); 40(52):7676–92. doi:10.1016/j.vaccine.2022.11.002

583. Haake DA, Mazel MK, Mccoy AM, et al. Leptospiral outer membrane proteins OmpL1 and LipL41 exhibit synergistic immunoprotection. *Infect Immun*. (1999); 67(12):6572-6582. doi:10.1128/iai.67.12.6572-6582.1999

584. Edmondson DG, Norris SJ. In Vitro Cultivation of the Syphilis Spirochete Treponema pallidum. *Curr Protoc*. (2021); 1(2):e44. doi:10.1002/cpz1.44

585. Phan A, Romeis E, Tantalo L, Giacani L. In Vitro Transformation and Selection of Treponema pallidum subsp. pallidum. *Curr Protoc*. (2022); 2(8):e507. doi:10.1002/cpz1.507

586. Ávila-Nieto C, Pedreño-López N, Mitjà O, Clotet B, Blanco J, Carrillo J. Syphilis vaccine: challenges, controversies and opportunities. *Front Immunol*. (2023); 14:1126170. doi:10.3389/fimmu.2023.1126170

587. Iyer V, Hu L, Liyanage MR, et al. Preformulation characterization of an aluminum salt-adjuvanted trivalent recombinant protein-based vaccine candidate against streptococcus pneumoniae. *J Pharm Sci*. (2012); 101(9):3078-3090. doi:10.1002/jps.23175

588. WHO. Global progress report on HIV, viral hepatitis and sexually transmitted infections, 2021. Accessed August 12, 2023. https://www.who.int/publications/i/item/9789240027077

589. Bannwarth M, Schulz GE. The expression of outer membrane proteins for crystallization. *Biochimica et Biophysica*. (2003); 1610(1):37-45. doi:10.1016/s0005-2736(02)00711-3

590. Bhatwa A, Wang W, Hassan YI, Abraham N, Li XZ, Zhou T. Challenges Associated with the Formation of Recombinant Protein Inclusion Bodies in Escherichia coli and Strategies to Address Them for Industrial Applications. *Front Bioeng Biotechnol*. (2021); 9:630551. doi:10.3389/fbioe.2021.630551

591. Shirano Y, Shibata D. Low temperature cultivation of Escherichia coli carrying a rice lipoxygenase L-2 cDNA produces a soluble and active enzyme at a high level. *FEBS Lett.* (1990); 271(1-2):128-130. doi:10.1016/0014-5793(90)80388-y

592. Yang X, Zhang Y. Effect of temperature and sorbitol in improving the solubility of carboxylesterases protein CpCE-1 from Cydia pomonella and biochemical characterization. *Appl Microbiol Biotechnol.* (2013); 97(24):10423-10433. doi:10.1007/s00253-013-5236-8

593. Donovan RS, Robinson CW, Click BR. Review: Optimizing inducer and culture conditions for expression of foreign proteins under the control of the lac promoter. *J Ind Microbiol.* (1996); 16(3):145-154. doi:10.1007/bf01569997/metrics

594. Oganesyan N, Ankoudinova I, Kim SH, Kim R. Effect of osmotic stress and heat shock in recombinant protein overexpression and crystallization. *Protein Expr Purif.* (2007); 52(2):280-285. doi:10.1016/j.pep.2006.09.015

595. Castellanos-Mendoza A, Castro-Acosta RM, Olvera A, et al. Influence of pH control in the formation of inclusion bodies during production of recombinant sphingomyelinase-D in Escherichia coli. *Microbial Cell Factories.* (2014); 13(1):1-14. doi:10.1186/s12934-014-0137-9

596. Worrall DM, Goss NH. The formation of biologically active beta-galactosidase inclusion bodies in Escherichia coli. *Aust J Biotechnol.* 1989;3(1):28-32.

597. Przybycien TM, Dunn JP, Valax P, Georglou G. Secondary structure characterization of beta-lactamase inclusion bodies. *Protein Eng.* (1994); 7(1):131-136. doi:10.1093/protein/7.1.131

598. Maksum IP, Yosua Y, Nabiel A, Pratiwi RD, Sriwidodo S, Soedjanaatmadja UMS. Refolding of bioactive human epidermal growth factor from E. coli BL21(DE3) inclusion bodies & evaluations on its in vitro & in vivo bioactivity. *Heliyon.* 2022;8(4):e09306. doi:10.1016/j.heliyon.2022.e09306

599. Upadhyay V, Singh A, Jha D, Singh A, Panda AK. Recovery of bioactive protein from bacterial inclusion bodies using trifluoroethanol as solubilization agent. *Microb Cell Fact.* (2016); 15(1):1-13. doi:10.1186/s12934-016-0504-9

600. Upadhyay AK, Singh A, Mukherjee KJ, Panda AK. Refolding and purification of recombinant L-asparaginase from inclusion bodies of E. coli into active tetrameric protein. *Front Microbiol.* (2014); 5:486. doi:10.3389/fmicb.2014.00486

601. Singhvi P, Saneja A, Srichandan S, Panda AK. Bacterial Inclusion Bodies: A Treasure Trove of Bioactive Proteins. *Trends Biotechnol.* (2020); 38(5):474-486. doi:10.1016/j.tibtech.2019.12.011

602. Peternel S, Komel R. Isolation of biologically active nanomaterial (inclusion bodies) from bacterial cells. *Microb Cell Fact.* (2010); 9:66. doi:10.1186/1475-2859-9-66

603. Kaveh-Baghbaderani Y, Blank-Shim SA, Koch T, Berensmeier S. Selective release of overexpressed recombinant proteins from E. coli cells facilitates one-step chromatographic purification of peptide-tagged green fluorescent protein variants. *Protein Expr Purif*. (2018); 152:155-160. doi:10.1016/j.pep.2018.07.014

604. Stark GR, Stein WH, Moore S. Reactions of the Cyanate Present in Aqueous Urea with Amino Acids and Proteins. *Journal of Biological Chemistry*. (1960); 235(11):3177-3181. doi:10.1016/s0021-9258(20)81332-5

605. Patra AK, Mukhopadhyay R, Mukhija R, Krishnan A, Garg LC, Panda AK. Optimization of Inclusion Body Solubilization and Renaturation of Recombinant Human Growth Hormone from Escherichia coli. *Protein Expr Purif*. (2000); 18(2):182-192. doi:10.1006/prep.1999.1179

606. Zhang HH, Blanco DR, Exner MM, et al. Renaturation of recombinant Treponema pallidum rare outer membrane protein 1 into a trimeric, hydrophobic, and porin-active conformation. *J Bacteriol*. (1999); 181(23):7168-7175. doi:10.1128/jb.181.23.7168-7175.1999

607. Anfinsen CB. Principles that govern the folding of protein chains. *Science*. 1973;181(4096):223-230. doi:10.1126/science.181.4096.223

608. Tsumoto K, Shinoki K, Kondo H, Uchikawa M, Juji T, Kumagai I. Highly efficient recovery of functional single-chain Fv fragments from inclusion bodies overexpressed in Escherichia coli by controlled introduction of oxidizing reagent—application to a human single-chain Fv fragment. *J Immunol Methods*. (1998); 219(1-2):119-129. doi:10.1016/s0022-1759(98)00127-6

609. Suenaga M, Ohmae H, Tsuji S, Itoh T, Nishimura O. Renaturation of recombinant human neurotrophin-3 from inclusion bodies using a suppressor agent of aggregation. *Biotechnol Appl Biochem*. 1998;28(2):119-124. doi:10.1111/J.1470-8744.1998.TB00521.X

610. Saadati Z, Bordbar AK. Stability of beta-lactoglobulin A in the presence of sugar osmolytes estimated from their guanidinium chloride-induced transition curves. *Protein J*. (2008); 27(7-8):455-460. doi:10.1007/s10930-008-9156-x

611. Singer MA, Lindquist S. Multiple effects of trehalose on protein folding in vitro and in vivo. *Mol Cell*. (1998); 1(5):639-648. doi:10.1016/s1097-2765(00)80064-7

612. Leibly DJ, Nguyen TN, Kao LT, Hewitt SN, Barrett LK, van Voorhis WC. Stabilizing Additives Added during Cell Lysis Aid in the Solubilization of Recombinant Proteins. *PLoS One*. (2012); 7(12):e52482. doi:10.1371/journal.pone.0052482

613. Mirnajd Gerami S, Farajnia S, Mahboudi F, Babaei H. Optimizing refolding condition for recombinant tissue plasminogen activator. *Iran J Biotechnol*. (2011); 9(4):253-259.

614. Lu D, Liu Z. Dynamic Redox Environment-Intensified Disulfide Bond Shuffling for Protein Refolding in Vitro: Molecular Simulation and

Experimental Validation. *Journal of Physical Chemistry B.* (2008); 112(47):15127-15133. doi:10.1021/jp804649g

615. Nelson CA, Lee CA, Fremont DH. Oxidative refolding from inclusion bodies. *Methods in Molecular Biology.* (2014); 1140:145-157. doi:10.1007/978-1-4939-0354-2_11

616. Golovanov AP, Hautbergue GM, Wilson SA, Lian LY. A simple method for improving protein solubility and long-term stability. *J Am Chem Soc.* (2004); 126(29):8933-8939. doi:10.1021/ja049297h

617. Le Bon C, Marconnet A, Masscheleyn S, Popot JL, Zoonens M. Folding and stabilizing membrane proteins in amphipol A8-35. *Methods.* 2018; 147:95-105. doi:10.1016/j.ymeth.2018.04.012

618. Rogl H, Kosemund K, Kühlbrandt W, Collinson I. Refolding of Escherichia coli produced membrane protein inclusion bodies immobilised by nickel chelating chromatography. *FEBS Lett.* (1998); 432(1-2):21-26. doi:10.1016/s0014-5793(98)00825-4

619. Köster S, Van Pee K, Yildiz Ö. Purification, Refolding, and Crystallization of the Outer Membrane Protein OmpG from Escherichia coli. *Methods Enzymol.* (2015); 557:149-166. doi:10.1016/bs.mie.2015.01.018

620. Ketrat S, Japrung D, Pongprayoon P. Exploring how structural and dynamic properties of bovine and canine serum albumins differ from human serum albumin. *J Mol Graph Model.* (2020); 98:107601. doi:10.1016/j.jmgm.2020.107601

621. WHO. Syphilis. Accessed August 13, 2023. https://www.who.int/news-room/fact-sheets/detail/syphilis

622. Fang J, Partridge E, Bautista GM, Sankaran D. Congenital Syphilis Epidemiology, Prevention, and Management in the United States: A 2022 Update. *Cureus.* (2022); 14(12). doi:10.7759/cureus.33009

623. Aho J, Lybeck C, Tetteh A, et al. Rising syphilis rates in Canada, 2011–2020. *Canada Communicable Disease Report.* (2022); 47(2-3):52-60. doi:10.14745/ccdr.v48i23a01

DISSEMINATION

Publications related to this thesis project

Ávila-Nieto C, Vergara-Alert J, Amengual-Rigo P, et al. **Immunization with V987H-stabilized Spike glycoprotein protects K18-hACE2 and golden Syrian hamster upon SARS-CoV-2 infection**. *Research Square*; (2023). doi: 10.21203/rs.3.rs-2846684/v1. - *Under peer review in Nature Communications.*

Ávila-Nieto C, Vergara-Alert J, Amengual-Rigo P, et al. **Novel Spike-stabilized trimers with improved production protect K18-hACE2 mice and golden Syrian hamsters from the highly pathogenic SARS-CoV-2 Beta variant**. *bioRxiv*; (2023). doi: 10.1101/2023.07.07.548077. - *Under submission in Frontier Immunology.*

Ávila-Nieto C, Pedreño-López N, Mitjà O, et al. **Syphilis vaccine: challenges, controversies and opportunities**. *Front Immunol.* (2023); 14:1126170. doi:10.3389/fimmu.2023.1126170

Publications related to other projects

Carrillo J, Izquierdo-Useros N, Ávila-Nieto C, et al. **Humoral immune responses and neutralizing antibodies against SARS-CoV-2; implications in pathogenesis and protective immunity**. *Biochem Biophys Res Commun.* (2021); 538:187-191. doi:10.1016/j.bbrc.2020.10.108

Rodríguez de la Concepción ML, Ainsua-Enrich E, Reynaga E, et al. **High-dose intravenous immunoglobulins might modulate inflammation in COVID-19 patients**. *Life Sci Alliance.* (2021);4(9):e202001009. doi:10.26508/lsa.202001009.

Ainsua-Enrich E, Pedreño-Lopez N, Bracke C, Ávila-Nieto C, et al. **Kinetics of immune responses elicited after three mRNA COVID-19 vaccine doses in predominantly antibody-deficient individuals.** iScience. (2022); 25(11):105455. doi: 10.1016/j.isci.2022.105455

Publications from scientific collaborations

Pradenas E, Ubals M, Urrea V, et al. **Virological and Clinical Determinants of the Magnitude of Humoral Responses to SARS-CoV-2 in Mild-Symptomatic Individuals**. *Front Immunol.* (2022); 13:860215. doi: 10.3389/fimmu.2022.860215

Pradenas E, Trinité B, Urrea V, Marfil S, et al. **Stable neutralizing antibody levels 6 months after mild and severe COVID-19 episodes**. *Med.* (2021); 2(3):313-320.e4. doi:10.1016/j.medj.2021.01.005.

Trinité B, Tarrés-Freixas F, Rodon J, et al. **SARS-CoV-2 infection elicits a rapid neutralizing antibody response that correlates with disease severity**. *Sci Rep.* (2021); 11(1):2608. doi:10.1038/s41598-021-81862-9.

Trigueros M, Pradenas E, Palacín D, Muñoz-López F, et al. **Reduced humoral response 3 months following BNT162b2 vaccination in SARS-CoV-2 uninfected residents of long-term care facilities**. *Age Ageing.* (2022); 51(5):afac101. doi:10.1093/ageing/afac101

Morón-López S, Riveira-Muñoz E, Urrea V, et al. **Comparison of Reverse Transcription (RT)-Quantitative PCR and RT-Droplet Digital PCR for Detection of Genomic and Subgenomic SARS-CoV-2 RNA**. *Microbiol Spectr.* (2023); 11(2):e0415922. doi:10.1128/spectrum.04159-22

Massanella M, Martin-Urda A, Mateu L, et al. **Critical Presentation of a Severe Acute Respiratory Syndrome Coronavirus 2 Reinfection: A Case Report**. *Open Forum Infect Dis.* (2021) ;8(7):ofab329. doi:10.1093/ofid/ofab329.

Tarrés-Freixas F, Trinité B, Pons-Grífols A, et al. **Heterogeneous Infectivity and Pathogenesis of SARS-CoV-2 Variants Beta, Delta and Omicron in Transgenic K18-hACE2 and Wildtype Mice**. *Front Microbiol.* (2022); 13:840757. doi:10.3389/fmicb.2022.840757

Tarrés-Freixas F, Aguilar-Gurrieri C, Rodríguez de la Concepción ML, Urrea V, et al. **An engineered HIV-1 Gag-based VLP displaying high antigen density induces strong antibody-dependent functional immune responses**. *NPJ Vaccines.* (2023) ;8(1):51. doi: 10.1038/s41541-023-00648-4

Brustolin M, Rodon J, Rodríguez de la Concepción ML, Ávila-Nieto C, et al. **Protection against reinfection with D614- or G614-SARS-CoV-2 isolates in golden Syrian hamster**. *Emerg Microbes Infect.* (2021); 10(1):797-809. doi:10.1080/22221751.2021.1913974

Vergara-Alert J, Rodon J, Carrillo J, et al. **Pigs are not susceptible to SARS-CoV-2 infection but are a model for viral immunogenicity studies**. *Transbound Emerg Dis.* (2021); 68(4):1721-1725. doi:10.1111/tbed.13861.

Segalés J, Puig M, Rodon J, Ávila-Nieto C, et al. **Detection of SARS-CoV-2 in a cat owned by a COVID-19-affected patient in Spain**. *Proc Natl Acad Sci U S A.* (2020); 117(40):24790-24793. doi:10.1073/pnas.2010817117.

Publications from scientific societies

Cela C, Roa-Bautista A, Méndez-Pérez A, Ávila-Nieto C, et al. **The first year of young group of the Spanish Immunology Society: Progress, challenges, and next steps**. *Eur J Immunol*. (2023); 53(5):e2350491. doi:10.1002/eji.202350491

Oral communications

Rodríguez de la Concepción ML, Ávila-Nieto C, Vergara-Alert J, et al. Early S2-targeting and rapid development of neutralizing antibodies after SARS-CoV-2 infection. **XIV Congrés de la Societat Catalana d' Immunologia**. Barcelona, 19-20/11/2020

Poster presentations

Ávila-Nieto C, Vergara-Alert J, Amengual-Rigo P, et al. Novel SARS-CoV-2-Stabilized Spike Proteins with Improved Production and Protective Activity Against SARS-CoV-2 Induced Disease in Animal Models. **44 Congreso de la Sociedad Española de Inmunología**. Bilbao, 10-13/07/2023.

Moderated sessions

"Presentación Ofical del Grupo Joven de la SEI". Coordinator: Ávila-Nieto C. **43 Congreso de la Sociedad Española de Inmunología**. León, 22-24/09/2022.

"Cuenta tu movida en 5 min. Sesión annual del Grupo Joven de la SEI". Coordinator: Ávila-Nieto C. **44 Congreso de la Sociedad Española de Inmunología**. Bilbao, 10-13/07/2023.

Informational activities

"¿Qué sabes del VIH/SIDA? Divulgando investigación y fomentando la prevención". **Jornada Divulgación EduCaixa**. CosmoCaixa Sevilla, 20/01/20.

"¿Qué sabes del VIH/SIDA? Divulgando investigación y fomentando la prevención". **Jornada Divulgación EduCaixa**. CosmoCaixa Sevilla, 02/04/22.

ACKNOWLEDGMENTS

Toda historia tiene un comienzo y la mía como científico empieza en primero de primaria con un dictado sobre la reproducción de las estrellas de mar por fragmentación. Aquel dictado me marcó y recuerdo llegar a casa diciéndole a mi madre que quería ser biólogo como el maestro. Así que me gustaría empezar esta sección agradeciendo a **Eduardo** por despertar en mi la curiosidad en el mundo de las ciencias biológicas desde tan pequeño. Y como a Eduardo, a tantos otros maestros y profesores que siguieron cultivándola, en especial a **Maria Dolores** de la Universidad de Sevilla.

Desde *chiquetito* como dirían en mi tierra, siempre he sido muy curioso y preguntón. Tuve la gran suerte de que mis padres siempre estuvieron ahí para responderme cada cuestión que les planteaba de la mejor forma que sabían hasta caer cansados de tantos *¿por qué?*; así como alimentando mi curiosidad con aquellas cintas de *Erase una vez el cuerpo humano*, con aquella colección de DVDs de *National Geographic*, con aquel microscopio de juguete, con las visitas a los Parques de las Ciencias de Granada y Cuenca, con el *MuyInteresante* de cada mes, y un largo etcétera. Pero sobre todo y lo más importante es que siempre me apoyaron con este camino que decidí tomar el día que rellenaba la solicitud de estudios universitarios. Siempre han sido y serán mis dos pilares y sin ellos no estaría dónde estoy ahora. Esta tesis es fruto de muchos, pero también de ellos, de mi padre **Domingo** y mi madre **Manoli**, por brindarme una educación y ayudarme a alcanzar mis metas, gracias. Gracias a mi hermana **Paloma**, por ser mi compañera de vida con quién empecé a explorar este mundo nada más llegar y aunque ahora nos separen varios cientos de kilómetros, siempre estará ahí para apretarme fuerte cuando vuelva a casa. A mi tía **Eva** por ser un gran apoyo y haber estado siguiendo siempre desde cerca mis andaduras por este mundo, por animarme a seguir y nunca olvidarse de llamar en todos estos años preguntando cómo me iba. También a mi tía **Mari**, por seguir toda mi trayectoria de cerca y celebrar cada uno de mis logros. A mis **abuelas** que no han podido estar, pero espero que estén orgullosas de su nieto, ellas que cada vez que me preguntaban qué quería ser de mayor y yo contestaba científico, en la humildad de sus tiempos siempre me decían qué si eso daba dinero, pero siempre acababan por alentarme a estudiar lo que me gustara. A **mis tíos, a mis primos, a mi familia**, que siempre me han querido y se han preocupado por mi y que cada vez que volvía al pueblo desde Barcelona me decían

Estos años de tesis no hubieran sido lo mismo sin ellos, sin los predocs. Ellos que han compartido conmigo el día a día de lo que es una tesis, las alegrías, las frustraciones y los momentos de bajona, que han sido un gran apoyo todo este tiempo y siguen siendolo; y que se han acabado convirtiendo en grandes amigos dentro y fuera de IrsiCaixa. Gracias a **Óscar**, **Edward**, **Lucía**, **Clara**, **Anna**, **Eudald**, **Montse** y **Marina,** por ser compañeros de escritorio y poyata, y por comenzar con la Mazmorra dónde tantos momentos de cotilleos y risas compartimos. También a mi cuarteto esquizo favorito (*hombreBarroco), **Raquel**, **Ana**, **Miguel** y **Amaya**, por alegrarme los días, por todo el support hecho, por tantas terapias afterwork y por hacerme olvidar mis problemas por un ratito. Gracias a **Edurne** y **Ángel** por pensar siempre en todos y ser los mejores organizadores de planes, por incluirme siempre en ellos y conseguir sacarme de casa a despejarme, por ser compañeros de cine, excursiones y viajes donde tan bien me lo he pasado y que siempre recordaré como los mejores momentos de esta estapa de mi vida.

Para terminar, quisiera agradecer a una persona que hizo su aparación en esta historia en el último momento, pero que aun así ha sido muy importante para mi y para esta tesis. A **Manu**, que se interesó verdaderamente por mi investigación, que ha sabido aguantarme en estos últimos meses tan estresantes, que me ha acompañado en el laboratorio y la escritura, que ha estado siempre a mi lado y ha sido el hombro en el que apoyarme, que me ha querido tan bien. Gracias por ser el faro y el puerto de este último tramo del viaje, que de otra forma hubiera sido mucho más oscuro y tormentoso.
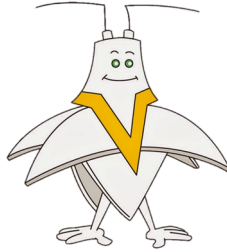
Como empecé viendo a los anticuerpos

Como acabé viéndolos